Volume 68A
Number 2
Mar.-Apr. 1964

Physics and Chemistry

U.S. DEPARTMENT OF COMMERCE

SECTION A

JOURNAL OF RESEARCH

NATIONAL BUREAU OF STANDARDS

Journal of Research

of the

National Bureau of Standards

A. Physics and Chemistry

Mar.–Apr. • 1964

VOLUME • 68A

NUMBER • 2

Editor: C. W. Beckett

Associate Editors: D. D. Wagman
J. M. Richardson

Publication dates:
Feb. 1, Apr. 1, June 1, Aug. 1, Oct. 1, Dec. 1, 1964

JOURNAL OF RESEARCH

The National Bureau of Standards Journal of Research reports research and development in the fields of activity shown at right. Also included from time to time are survey articles on topics closely related to the Bureau's scientific and technical program.

The Journal is published in four separate sections as follows:

A. Physics and Chemistry

Contains papers of interest primarily to scientists working in these fields. Issued six times a year. Annual subscription: domestic, $4.00; foreign, $4.75. Single copy, 70c.

B. Mathematics and Mathematical Physics

Presents studies and compilations designed mainly for the mathematician and the theoretical physicist. Issued quarterly. Annual subscription: domestic, $2.25; foreign, $2.75. Single copy, 75c.

C. Engineering and Instrumentation

Reports research and development results of interest chiefly to the engineer and the applied scientist. Issued quarterly. Annual subscription: domestic, $2.25; foreign, $2.75. Single copy, 75c.

D. Radio Science (formerly Radio Propagation)

Published in cooperation with U.S. National Committee of URSI. Presents papers in radio propagation, communications, and radio science generally. Issued monthly. Annual subscription: domestic, $9.00; foreign, $11.50. Single copy $1.00

The National Bureau of Standards is a principal focal point in the Federal Government for assuring maximum application of the physical and engineering sciences to the advancement of technology in industry and commerce. Its responsibilities include development and maintenance of the national standards of measurement, and the provisions of means for making measurements consistent with those standards; determination of physical constants and properties of materials; development of methods for testing materials, mechanisms, and structures, and making such tests as may be necessary, particularly for government agencies; cooperation in the establishment of standard practices for incorporation in codes and specifications; advisory service to government agencies on scientific and technical problems; invention and development of devices to serve special needs of the Government; assistance to industry, business, and consumers in the development and acceptance of commercial standards and simplified trade practice recommendations; administration of programs in cooperation with U.S. business groups and standards organizations for the development of international standards of practice; and maintenance of a clearinghouse for the collection and dissemination of scientific, technical, and engineering information.

Institute for Basic Standards. Electricity. Metrology. Heat. Radiation Physics. Mechanics. Applied Mathematics. Atomic Physics. Physical Chemistry. Laboratory Astrophysics.* Radio Standards Laboratory: Radio Standards Physics; Radio Standards Engineering.** Office of Standard Reference Data.

Institute for Materials Research. Analytical Chemistry. Polymers. Metallurgy. Inorganic Materials. Reactor Radiations. Cryogenics.** Office of Standard Reference Materials.

Central Radio Propagation Laboratory.** Ionosphere Research and Propagation. Troposphere and Space Communications. Radio Systems. Upper Atmosphere and Space Physics.

Institute for Applied Technology. Textiles and Apparel Technology Center. Building Research. Industrial Equipment. Information Technology. Performance Test Development. Instrumentation. Transport Systems. Office of Technical Services. Office of Weights and Measures. Office of Engineering Standards. Office of Industrial Services.

*NBS Group, Joint Institute for Laboratory Astrophysics at the University of Colorado.
**Located at Boulder, Colo.

U.S. DEPARTMENT OF COMMERCE
Luther H. Hodges, Secretary

NATIONAL BUREAU OF STANDARDS
A. V. Astin, Director

Order all publications from the Superintendent of Documents
U.S. Government Printing Office, Washington, D.C., 20402

Use of funds for printing this publication approved by the Director of the Bureau of the Budget (June 19, 1961).

JOURNAL OF RESEARCH of the National Bureau of Standards—A. Physics and Chemistry
Vol. 68A, No. 2, March–April 1964

Tritium-Labeled Compounds X. Isotope Effects in the Oxidation of Aldoses-*1-t* With Bromine

Horace S. Isbell and Lorna T. Sniegoski

(November 18, 1963)

Tritium isotope effects have been used in bromine oxidation studies of aldoses to evaluate two reaction paths previously postulated by Isbell and Pigman, namely, direct oxidation and oxidation after anomerization. Because the former path involves a primary isotope effect ($k^*/k=0.14$, approximately) and the latter a secondary isotope effect ($k^*/k=0.80$, approximately) it was found possible to evaluate the relative importance of the two reaction paths from the overall isotope effects, which ranged from 0.20 to 0.59.

Under the conditions reported, the direct oxidation for the axial anomers ranges from 38 percent for α-D-galactose to 94 percent for α-D-lyxose. Differences in the proportion of the anomer oxidized by each of the two paths are explained by variations in the free energy required for reaching the respective transition states. Aldoses of high conformational stability having an axial C1-hydroxyl group resist the change in conformation necessary for direct oxidation and react in large measure through a change in configuration (anomerization). Aldoses of lower conformational stability having an axial C1-hydroxyl group react largely through a change in conformation, because this path does not have a high energy barrier.

The equatorial anomers of D-glucose-*1-t* and maltose-*1-t* showed isotope effects of 0.32 and 0.23, respectively in comparison with a value of 0.14 previously found for the oxidation of aldoses-*1-t* with iodine in alkaline solution. The isotope effect in the oxidation of D-glucose-*1-t* with D-glucose oxidase at 30 °C was found to be 0.15. These strong isotope effects are in accord with the rupture of the C1 to H bond in the rate-determining step.

The following reactions gave the values for k^*/k cited in parentheses: D-glucose-*1-t* + NaCN (0.83); D-glucose-*1*-C^{14} + NaCN (1.00); D-glucose-*1-t* + $NaBH_4$ (0.73); D-mannose-*1-t* + phenylhydrazine (0.83); and D-mannose-*1*-C^{14} + phenylhydrazine (0.95). The values of k^*/k are typical of aldose reactions involving rate-determining isomerization of the pyranose structure.

The isotope effects were measured by a double-label method and by a newly developed method based on the radioassay of water evolved in the reaction.

1. Introduction and Discussion

Certain reactions take place by two or more paths having different rate-determining steps which show different isotope effects. Under suitable conditions, the size of the isotope effect can serve as a measure of the relative importance of the paths. This property has now been used in studying the mechanisms of oxidation of aldoses with bromine.

Early work in this laboratory [1, 2][1] showed that the ring forms of aldoses are oxidized by bromine to lactones without cleavage of the ring, and that there are wide differences in the rates of oxidation for the various aldoses and for the α and β anomers of a single aldose. It was found [3, 4] that, in the presence of a large excess of free bromine, "β aldoses" are oxidized rapidly, at a rate proportional to the concentration of free bromine, whereas "α aldoses" are oxidized slowly. Isbell and Pigman [3, p. 349] considered the oxidation of α-D-glucose to consist of "two reactions, namely, the oxidation of the alpha form directly, and the conversion of the alpha to the beta form with the subsequent rapid oxidation thereof." They estimated that about 80 percent of the overall oxidation of α-D-glucose takes place *directly*, in solutions saturated with bromine and buffered with barium carbonate and carbon dioxide. The rate constants which they determined for the overall oxidation of eighteen α and β aldoses [4, 5, pp. 436 and 455] showed a correlation of reaction rate, structure and configuration which Isbell considered to be evidence regarding the conformation of the particular pyranose ring [6, p. 523].

Later, Barker, Overend, and Rees [7] concluded that the rate-determining step in the oxidation of the α aldoses studied by Isbell and Pigman consists very largely of anomerization to the corresponding β aldoses, and that direct oxidation of the α aldoses is of little importance. Thereafter, Isbell reviewed the early work and interpreted the results in the light of present concepts of reaction mechanism and conformation [8, 9].

Because mutarotation and oxidation reactions take place concurrently, quantitative evaluation of the paths by conventional methods is not satisfactory. Hence, an independent method was needed for ascertaining the relative importance of the two paths.

[1] Figures in brackets indicate the literature references at the end of this paper.

Isotope effects [2] provide a powerful means for distinguishing between reaction mechanisms. In general, the isotope effect is large when the isotopic bond is ruptured in the rate-determining step and small when this bond is not involved [10, p. 88]. In the reaction of an aldose with bromine, the C1 to H bond is ruptured in the oxidation step but not in the anomerization step. Hence, it seemed probable that kinetic isotope-effects of tritium could provide a means for distinguishing between direct oxidation and oxidation after anomerization.

Previously, Friedberg and Kaplan [11] had reported isotope effects [3] of 0.2 and 0.25, respectively, for the oxidation of α-D-glucose-*1-t* and β-D-glucose-*1-t* with bromine in solutions buffered with barium carbonate. From the magnitude of the isotope effects, they concluded that the C1 to H bond is ruptured in the rate-determining step. They noted that the oxidation of α-D-glucose is complicated by the anomerization reaction, but did not pursue the subject further.

In the present investigation, isotope effects were measured for the oxidation of a group of aldoses-*1-t* with bromine in solutions buffered with sodium benzoate and benzoic acid.[4] For each aldose, the relative importance of the two reaction paths was estimated from the observed isotope effect as compared with isotope effects characteristic of reactions in which the rate-determining step is known to be (1) cleavage of the C1 to H bond and (2) anomerization. Thus, if k_1^*/k_1 is the isotope effect for path (1) and k_2^*/k_2 for path (2), it follows that the isotope effect for the overall reaction is

$$k^*/k=(k_1^*+k_2^*)/(k_1+k_2) \qquad (1)$$

and that the ratio of the rates of reaction, for the nonisotopic molecules, by the two paths is

$$k_1/k_2=(k_2^*/k_2-k^*/k)/(k^*/k-k_1^*/k_1). \qquad (2)$$

The value used for k_1^*/k_1 (0.14) was obtained from measurements of the oxidation of aldoses-*1-t* with iodine in alkaline solution [12]. This reaction is considered typical of those in which the rate-determining step involves cleavage of the C1 to H bond.

The value used for k_2^*/k_2 (0.80) is the average of the results reported for aldoses-*1-t* in table 1 (starred values). Each of the reactions yields an open-chain product by way of a rate-determining anomerization. By assuming the above values for k_1^*/k_1 and k_2^*/k_2, the ratios of the rates by the two paths, k_1/k_2, were calculated by eq (2) from the observed, overall isotope effects.

[2] An isotope effect can be broadly defined as any difference between the behavior of an isotopically labeled substance and that of the nonlabeled substance. For quantitative evaluation, the effect is defined as k^*/k, where k^* and k are the rates of reaction for the labeled and the nonlabeled molecules, respectively.

[3] The authors actually reported values of k/k^* instead of the values of k^*/k cited here.

[4] In the early work on the oxidation of the anomeric aldoses with bromine, a buffer consisting of solid barium carbonate and carbon dioxide gas was used, because it permits study of the lactones formed. A change was made because this buffer is not suitable for tracer studies that employ small quantities of material. Both buffers maintain a slightly acid solution in which the anomerization reaction is relatively slow.

Table 2 presents a summary of the results obtained for nine of the ten aldoses which Barker, Overend, and Rees had concluded, from the data of Isbell and Pigman, are oxidized by bromine predominantly by way of a rate-determining anomerization. Our results show that the direct oxidation ranges from 38 percent for α-D-galactose to 94 percent for α-D-lyxose.

TABLE 1. *Determinations of* k*/k *for reactions involving rate-determining isomerizations* [a]

Reactant	*f*	*p°*	*p*	*p′*	*k*/k*	*k*/k* (average)
Cyanohydrin reaction						
D-Glucose-*1-t*, *6-C*^{14}	0.5011	9.12	10.56		0.73	
	.5211	9.12	11.09		.79	0.76*
D-Glucose-*1-C*^{14}, *6-t*	.652	0.1144	0.1144		1.00	
	.611	.1144	.1160		0.99	1.00
Sodium borohydride reduction						
D-Glucose-*1-t*, *6-C*^{14}	0.0874	9.12		6.74	0.73	0.73*
D-Mannose phenylhydrazone formation						
D-Mannose-*1-t*, *2-C*^{14}	0.1655	8.65		7.33	0.83	
	.1672	8.65		7.27	.83	
	.2605	8.65		7.44	.84	0.83*
D-Mannose-*1-C*^{14}, *6-t*	.1550	0.0668		0.0637	.95	
	.1572	.0668		.0639	.95	
	.2486	.0668		.0638	.95	.95

[a] Experimental details are given in section 2.4.

TABLE 2. *Oxidation of aldoses with bromine (summary)*

Reactant	Relative rates for overall oxidation [a]		Oxidation of axial anomer of aldose-*1-t* [b]		
	Axial anomer	Equatorial anomer	Isotope effect k^*/k	Reaction paths (ratio) k_1/k_2 [c]	Direct oxidation
					%
D-Galactose	1.3	50	0.55	0.6	37.5
D-Glucose	1.0	39	.53	.7	41.2
D-Mannose	1.6	24	.30	3.1	75.6
D-Talose	2.4	26	.20	10.0	90.9
L-Rhamnose	2.8	24	.25	5.0	83.3
L-Arabinose	3.0	52	.32	2.7	73.0
D-Lyxose	4.9	14	.18	15.5	93.9
D-Ribose	6.1	45	.26	4.5	81.8
D-Xylose	2.8	52	.26	4.5	81.8
Lactose	0.9	30	.46	1.0	50.0

[a] Measurements made at 0 °C with a barium carbonate-carbon dioxide buffer and reported by Isbell [5, pp. 436 and 455]. Based on rate of α-D-glucose as unity.
[b] Measurements made at 0 °C with a sodium benzoate-benzoic acid buffer.
[c] Calculated from eq (2).

In each instance, the extent of the reaction that takes place by way of anomerization parallels the conformational stability of the anomer. Aldoses which have an axial hydroxyl group at C1 in a highly stable conformation (e.g., α-D-glucopyranose-CA [5] and α-D-galactopyranose-CA), resist the change in conformation necessary for direct oxidation, and react largely through anomerization (change in configuration). Aldoses of lower conformational stability (e.g., α-D-lyxopyranose-CA, α-D-talopyranose-

[5] The system for indicating conformation is described in [13].

CA, and α-D-mannopyranose-CA) react chiefly by a change in conformation without a change in configuration.

The rate of the direct reaction depends on the difference in free energy between the reactants in the ground state and in a transition state in which the anomeric oxygen atom lies in the same plane as C1, C2, C5, and the ring oxygen atom [9]. The free energy required in order to reach this transition state depends on the structure and the configuration. With molecules having an axial hydroxyl group at C1 in a highly stable conformation, much energy is required for so changing the conformation as to bring the hydroxyl group into an equatorial position. α-D-Glucopyranose and α-D-galactopyranose have high stability in that chair conformation having an axial hydroxyl group at C1; this fact accounts for the low rates of oxidation and the tendency of these sugars to react through a change in configuration rather than conformation.

The higher reactivity of sugars having the α-D-*manno* structure is in accord with the fact that, in the transition state of the *manno* group, the C1-hydroxyl group is eclipsed by the C2-hydrogen atom (instead of by the larger C2-hydroxyl group, as with α-D-glucopyranose). The high reactivity of the axial anomers of pentopyranoses, in comparison with the axial anomers of hexopyranoses can be explained by a lower energy-requirement for a change in conformation in the pentopyranose series; this arises from the lack of a large substituent group at C5 which, in the transition state of a hexopyranose, must assume an axial position. The high isotope-effect for α-D-lyxopyranose-*1-t*, and the small difference in the rates of reaction for the α and β anomers of this aldose, are in accord with only a small difference in the relative stabilities of the CA and CE conformations of this aldose [14].

Table 3 presents results obtained in the individual measurements summarized in table 2. It includes, in addition, measurements of k^*/k for the bromine oxidation of β-maltose-*1-t*. This sugar was selected for ascertaining the isotope effect in the bromine oxidation of an aldose having an equatorial hydroxyl group, because it is one of the few sugars that crystallize only in this form. The value of k^*/k obtained (0.23) is somewhat high, but is sufficiently close to the expected value for the primary isotope effect (0.14) to indicate cleavage of the C1 to H bond in the rate-determining step.

Interpretation of the reactions of the α and β aldopyranoses depends on the correct assignment of configuration to the anomers. Recent papers by Blom [15] and Christiansen [16] challenged the generally accepted assignments of configuration for the α and β aldoses. This concept has now been shown to be erroneous [17]. One of Blom's reasons for questioning the validity of the assignments is that the aldoses ordinarily considered to have equatorial C1-hydroxyl groups are oxidized more *rapidly* than those having axial C1-hydroxyl groups, whereas cyclohexane derivatives having equatorial hydroxyl groups are oxidized more *slowly* than those having axial hydroxyl groups. As pointed out earlier [9], differences in the relative rates of oxidation of the axial and equatorial derivatives of cyclohexane and of pyranoses can be ascribed to the presence or absence of the ring oxygen atom. With aldopyranoses, the ring oxygen atom provides a low-energy path for the reaction by furnishing electrons in a transition state favored by resonance. This path requires a transition state in which the ring oxygen atom, the hydroxyl oxygen atom, and C1, C2, and C5 lie in one plane. The large differences in the rates of reaction for the α and β aldopyranoses arise from variation in the free energy required in order that the compounds may attain this planar transition state. With a derivative of cyclohexane, there is no resonance stabilization of a planar transition state and, consequently, this path is not favored. The absence of this low-energy path accounts for the lower rates of oxidation of cyclohexane derivatives and the lack of appreciable difference between the rates of reaction of the axial and the equatorial derivatives of 4-*tert*-butylcyclohexanol [18].

TABLE 3. *Experimental data for oxidation of aldoses-1-t with bromine*

Reactant	Reaction time	f	rf	k^*/k	k^*/k (average)
	Min				
α-D-Galactose	40	0.113	0.061	0.53	
	50	.217	.130	.57	0.55
α-D-Glucose	45	.455	.277	.53	
	55	.402	.238	.53	.53
α-D-Mannose	35	.329	.108	.28	
	45	.543	.121	.31	.30
α-D-Talose	25	.210	.046	.20	
	25	.222	.054	.22	
	35	.289	.063	.19	
	35	.309	.073	.20	.20
α-L-Rhamnose H_2O	30	.165	.046	.26	
	40	.235	.061	.24	.25
β-L-Arabinose	20	.151	.049	.31	
	30	.256	.094	.33	.32
α-D-Lyxose	10	.201	.043	.20	
	20	.326	.066	.17	.18
β-D-Ribose	6	.131	.037	.27	
	10	.218	.060	.25	.26
α-D-Xylose	20	.174	.043	.23	
	30	.258	.082	.29	.26
α-Lactose H_2O	40	.454	.241	.46	
	50	.490	.268	.46	.46
β-Maltose H_2O	1	.131	.033	.24	
	2	.201	.052	.24	
	3	.221	.054	.22	
	4	.326	.079	.21	.23

2. Experimental Details

2.1. Materials

The labeled aldoses listed below were prepared by the methods given in the references cited: Aldoses-*1-t* [19], D-glucose-*1*-C^{14} [20], D-glucose-*6*-C^{14} [21], D-glucose-*6-t* [22], D-mannose-*1*-C^{14} [20], D-mannose-*2*-C^{14} [23], and D-mannose-*6-t* [24]. The radioactivity of each tritium-labeled aldose was adjusted, by addition of a carrier, to about 1 μc/mg. The

doubly labeled aldoses, D-glucose-*1-t,6-*C^{14}, D-glucose-*1-*C^{14}*,6-t*, D-mannose-*1-t,2-*C^{14}, and D-mannose-*1-*C^{14}*, 6-t* were prepared by crystallizing mixtures of the singly labeled aldoses containing, respectively, from 1 to 2 μc/mg of tritium and 0.1 to 0.2 μc/mg of carbon 14. The purity of each labeled aldose was checked by paper chromatography.

The buffered bromine solution used for the oxidation measurements contained 0.90 g of benzoic acid, 2.16 g of sodium benzoate, and 3 ml of bromine (an excess) in 100 ml of aqueous solution.

2.2. General Procedures

a. Determination of Aldoses in Reaction Mixtures

The Somogyi method [5, p. 196] was used for determination of the residual aldoses in the reaction mixtures, by selecting suitable heating times and by standardizing with known quantities of the various aldoses. The heating times and factors for converting the titrations to a weight basis are given in table 4. The factors were derived from control measurements run in duplicate with known weights of each aldose.

TABLE 4. *Determination of reducing sugars by the Somogyi method*

Sugar	Heating time	Aldose in sample *
	min	*mg*
L-Arabinose	30	0.133*x*+0.120
D-Galactose	30	.140*x*+.118
D-Glucose	15	.119*x*+.130
Lactose monohydrate	35	.207*x*+.250
D-Lyxose	20	.114*x*+.160
Maltose monohydrate	30	.238*x*+.265
D-Mannose	35	.118*x*+.120
L-Rhamnose monohydrate	35	.152*x*+.182
D-Ribose	25	.147*x*+.156
D-Talose	15	.143*x*+.116
D-Xylose	30	.125*x*+.080

* *x*=titer in ml of 0.005 *N* sodium thiosulfate.

b. Determination of Carbon 14 and Tritium

Carbon-14 and tritium were determined either by counting in solution [25] with a Packard Tri-Carb Liquid Scintillation Spectrometer or by counting in films [26, 27] with a windowless, gas-flow, proportional counter. The solution used for scintillation counting contained, per liter, 7 g of 2,5-diphenyloxazole (PPO, scintillation grade), 0.3 g of 2,2′-*p*-phenylenebis(4-methyl-5-phenyloxazole) (dimethyl-POPOP, scintillation grade), and 100 g of naphthalene, in dioxane (Eastman). The procedure for counting doubly labeled materials in the scintillation counter is described in [12].

The *O*-(carboxymethyl)cellulose (CMC) solution (used for preparing films for the assay of radioactivity with the proportional counter) contained 1.5 g of CMC (medium viscosity CMC, product of Hercules Powder Co.), 0.2 g of phenol, and 1 ml of a red ink (eosin type), dissolved in sufficient water to yield 100 ml of solution. The films were prepared and counted as described in [26, 27].

2.3. Measurements of k^*/k for the Oxidation of Aldoses-*1-t* With Bromine

a. Water-*t* Method [12]

Samples of aldoses-*1-t* of known weight (about 0.05 mmole) were placed in test tubes (20 × 150 mm). Each tube was suspended in an ice-water bath and two ml of ice-cold, buffered bromine solution (sec. 2.1) was added. The tube was stoppered, and mechanically shaken in the bath for the time given in table 3. Then, about 10 ml of ice-cold, distilled water was added, and the excess bromine was removed by bubbling ethylene through the solution for about 1 min. The bromine-free solution was quantitatively transferred to a volumetric flask, the volume was made to 25 ml, and aliquots were taken for determining the reducing sugar (residual reactant) and the water-*t*.

Measurements of reducing sugar were made with two 2-ml and two 4-ml aliquots of the bromine-free solution. Each aliquot was diluted to 5 ml and analyzed by the procedure described in [5, p. 196], using the heating times and factors given in table 5. For each measurement, the results from the 4 aliquots were averaged, and the extent of the oxidation (f of eq (3)) was calculated.

TABLE 5. *Determination of* k*/k *for oxidation of aldoses with bromine (double-label method)*

Reactant	Time	f	p°	p	k^*/k	k^*/k (average)
	min					
α-D-Glucose-*1-t,6-*C^{14}	180	0.495	9.12	11.92	0.61	
	300	.755	9.12	16.79	.57	0.59
α-D-Mannose-*1-t,2-*C^{14}	180	.643	7.72	14.53	.39	
	240	.749	7.72	16.68	.44	
	300	.749	7.72	17.78	.40	.41
β-D-Glucose-*1-t,6-*C^{14}	5	.735	9.12	22.57	.33	
	7	.710	9.12	21.01	.32	.32
α-D-Glucose-*1-*C^{14}*,6-t*	180	.478	0.1144	0.1153	.99	
	300	.647	.1144	.1238	.92	.96
β-D-Glucose-*1-*C^{14}*,6-t*	5	.626	.1144	.1184	.97	
	7	.700	.1144	.1227	.94	.96

For determination of water-*t*, a 2-ml aliquot of the bromine-free solution was transferred to a flask (round-bottomed, standard-tapered, inner-joint) containing about 50 mg of sodium carbonate, and the water-*t* was sublimed by the procedure described in [12]. The water-*t* was analyzed in duplicate with the liquid scintillation counter by use of 100-μl samples and 10-ml aliquots of scintillator solution. Each sample was counted to a total of 10,000 counts, to give a statistical accuracy of ± 1 percent.

The isotope effect, k^*/k, was calculated by the following equation [28, 29]:

$$k^*/k=\log (1-rf)/\log (1-f) \qquad (3)$$

where f is the fraction of initial reactant oxidized, $(1-f)$ is the fraction of initial reactant remaining, and rf is the ratio of the total activity (μc) in the

tritiated water formed to the activity (μc) of tritium in the initial reactant (calculated from the weight and specific activity of the aldose-*1-t* used).

b. Double-Label Method [26]

Measurements of k^*/k were made for the oxidation of α-D-glucose-*1-t* and α-D-mannose-*1-t* by the double-label method, with carbon 14 as the reference isotope (table 5). In each instance, the isotope effect was calculated from the equation:

$$k^*/k = 1 + [\log (p/p^\circ)/\log (1-f)] \quad (4)$$

where p° is the ratio of the functional to the reference isotope in the initial reactant, and p is the ratio of the same isotopes in the residual reactant.

Samples (about 9 mg) of the doubly labeled aldoses were weighed, by means of a semimicro balance, into separate test tubes. Each tube was placed in an ice-water bath, and 2 ml of ice-cold, buffered bromine solution was added. The tube was stoppered, and was mechanically shaken in the bath for a time sufficient for 50 to 90 percent of the aldose to become oxidized. Then, the reaction was stopped by dilution with water containing 100 mg of the nonradioactive aldose (as carrier) and 200 mg of decolorizing carbon. The mixture was filtered, the bromine-free filtrate was passed through 15 ml of mixed anion- and cation-exchange resins, and the salt-free effluent was concentrated. The resulting sirup was diluted with a few drops of methanol, and 2-propanol was added to incipient turbidity. The crystals that formed were separated, and recrystallized twice from water, with addition of methanol and 2-propanol. The purified mixture of the residual reactant and carrier was analyzed for carbon 14 and tritium, and the ratio of tritium to carbon 14 in the residual reactant (p of eq (4)) was calculated.

The ratio of tritium to carbon 14 in the initial reactant (p° of eq (4)) was determined from a sample of the original reactant after dilution with carrier to about the same level of activity as the samples derived from the oxidation mixture.

If w_0 is the weight (in mg) of initial reactant (having s activity of the reference isotope per mg), w_r the weight of residual reactant, w_r' the weight of nonradioactive (reactant) carrier added, and s' the activity of the reference isotope per mg of the residual reactant–carrier mixture, then

$$w_r = s' w_r'/(s-s'), \quad (5)$$

and the fraction of reactant oxidized is

$$f = (w_0 - w_r)/w_0 = [w_0(s-s') - w_r' s']/w_0(s-s'). \quad (6)$$

Table 5 is a résumé of measurements of k^*/k for the oxidation of aldoses-*1-t* (with carbon-14 as the reference isotope) and of aldoses-*1-*C^{14} (with tritium as the reference isotope). The values of k^*/k obtained for the oxidation of α-D-glucose-*1-t,6-*C^{14} and α-D-mannose-*1-t,2-*C^{14} by the double-label method (0.59 and 0.41, respectively) are somewhat higher than the values (0.53 and 0.30) obtained by the water-*t* method. Determinations are based on the first part of the reaction in the water-*t* method and on the last part in the double-label method.

2.4. Measurements of k^*/k for Reactions Involving Rate-Determining Isomerization

a. Reaction of D-Glucose-*1-t,6-*C^{14} With Sodium Cyanide

Samples of about 0.05 mmole of D-glucose-*1-t,6-*C^{14} were weighed into small test tubes. Each sample was dissolved in 100 μl of water, and sufficient 0.47 *M* sodium cyanide in 0.50 *M* sodium hydroxide was added to combine with 50 to 70 percent of the D-glucose-*1-t,6-*C^{14}. The tubes were sealed, and allowed to stand at 25 °C for 24 hr and in the freezer for several days. The tubes were opened, and 100 mg of D-glucose was added to each. After the addition of a few drops of 10-percent, aqueous formic acid, each solution was evaporated to a sirup (to remove excess hydrogen cyanide). The sirup was dissolved in water, and the solution was passed through a column of mixed anion- and cation-exchange resins to remove all ionic substances. The effluent was concentrated, and the D-glucose-*1-t,6-*C^{14} was separated by crystallization. The material was recrystallized twice from water, with addition of methanol and 2-propanol, dried, and radioassayed on planchets for carbon 14 and tritium. The ratio of tritium to carbon 14 (p of eq (4)) was calculated, as well as the extent of reaction (f of eq (6)). The ratio of tritium to carbon 14 in the initial reactant (p° of eq (4)) was determined from a sample of the original reactant after dilution with carrier to about the same level of activity as that of the samples derived from the oxidation mixture. k^*/k was then calculated from eq (4). The results are reported in table 1.

The method was also applied to a study of the reaction of D-glucose-*1-*C^{14}*,6-t* with sodium cyanide. In this instance, tritium was used as the reference isotope for the study of the effect of carbon 14 at C1.

b. Reduction of D-Glucose-*1-t,6-*C^{14} With Sodium Borohydride

A 9-mg sample of D-glucose-*1-t,6-*C^{14} was weighed into a small test tube, and a solution containing 0.5 mg of sodium borohydride in 50 μl of water was added. The reaction mixture was kept in an ice-water bath for 30 to 40 min and at room temperature for 30 min. Then, a drop of glacial acetic acid, 98.2 mg of D-glucitol carrier, and 5 ml of water were added. The solution was passed through several ml of a cation-exchange resin, and the effluent was concentrated under diminished pressure to a sirup. Methanol was added, and the solution was concentrated; this process was repeated several times. The D-glucitol-*1-t,6-*C^{14} in the residue was recrystallized three times from pyridine, with addition of acetone. The pyridine complex was decomposed by heating to constant weight at 85 °C in a vacuum oven. The pure product-carrier mixture and the

initial reactant were assayed in films, on planchets, for carbon 14 and tritium.

The weight of product was calculated from the activity of the product-carrier mixture and that of the initial reactant by the equation:

$$w_p = s' w_p' / (s - s') \tag{7}$$

where w_p is the weight (in mg) of product (having s activity of the reference isotope per mg), w_p' the weight of nonradioactive carrier added, and s' the activity of the reference isotope per mg of product-carrier mixture. Then

$$f = w_p m_r / w_0 m_p = w_p' s' m_r / w_0 (s - s') m_p \tag{8}$$

where m_r and m_p are the equivalent weights of the reactant and product, respectively.

The value of k^*/k was calculated from the eq [26]:

$$k^*/k = \log (1 - f p'/p^\circ) / \log (1 - f) \tag{9}$$

where p° is the ratio of tritium to carbon 14 in the initial reactant, and p' is the ratio in the product.

c. Formation of D-Mannose-*1-t,2-*C^{14} Phenylhydrazone

A 54-mg sample (0.3 mmole) of D-mannose-*1-t,2-*C^{14} was weighed into a small test tube. Then, 0.9 ml of 0.6-percent acetic acid was added, and the solution was allowed to stand for 18 to 20 hr. Sufficient 0.251-*M* phenylhydrazine in 0.6-percent aqueous acetic acid to give a 20- to 30-percent reaction (0.24 to 0.36 ml) was added, and the mixture was allowed to stand at 25 °C for 1 hr with occasional shaking. The resulting labeled D-mannose phenylhydrazone was removed by filtration, successively washed with about 2 ml each of water, ethanol, and ether, and dried overnight in a vacuum desiccator.

D-Mannose-*1-t* phenylhydrazone shows an isotope effect on recrystallization [30]; hence, for analysis, the D-mannose-*1-t,2-*C^{14} phenylhydrazone was reconverted to D-mannose-*1-t,2-*C^{14}. There is no isotope effect in this conversion because the reaction goes to completion. The labeled D-mannose phenylhydrazone was transferred to a 100-ml, standard-tapered flask, and 300 mg of nonradioactive D-mannose phenylhydrazone carrier, a stirring bar, 8 ml of distilled water, and 155.9 μl (1.5 mmole) of benzaldehyde were added. The mixture was heated, with stirring, in a boiling-water bath for 30 min; the appearance of the crystals changed rapidly. Additional water was added to rinse down the sides of the flask. The mixture was cooled, and the benzaldehyde phenylhydrazone was removed by filtration. The filtrate was extracted five times with ether to remove benzaldehyde. The solution was then passed through 10 ml of mixed anion- and cation-exchange resins and concentrated under reduced pressure on a rotary evaporator. Water was added, and the concentration was repeated. The sirup was dissolved in methanol, and the solution was filtered into a test tube and concentrated to a sirup from which D-mannose-*1-t,2-*C^{14} crystallized after addition of methanol and 2-propanol. The material was crystallized three times, dried, and assayed (in films on planchets) for carbon 14 and tritium. w_p was calculated from eq (7) with w_p and w_p' the weights of D-*mannose* in the product and nonradioactive carrier, respectively. Then,

$$f = w_p / w_0. \tag{10}$$

The isotope effect, k^*/k, was then calculated from eq (9).

The results are reported in table 1, and, in addition, those for the isotope effect of carbon 14 in the formation of D-mannose-*1-*C^{14},*6-t* phenylhydrazone from D-mannose-*1-*C^{14},*6-t*, in which reaction tritium was the reference isotope.

2.5. Measurements of k^*/k for the Oxidation of D-Glucose-*1-t* and D-Glucose-*1-*C^{14} With D-Glucose Oxidase by the Double-Label Method

Samples of either D-glucose-*1-t,6-*C^{14} or D-glucose-*1-*C^{14},*6-t* of known weight (about 10 mg) and specific activity were placed in test tubes (20×150 mm). After addition of 2 ml of an aqueous solution containing 430 mg of disodium hydrogen phosphate dodecahydrate, 84 mg of citric acid, and 2 mg of D-glucose oxidase,[6] each tube was stoppered and mechanically shaken in a water bath at 30 °C for the time given in table 6. Then the reaction

TABLE 6. *Determination of* k*/k *for oxidation of* D-*glucose with* D-*glucose oxidase (double-label method)*

Reactant	Time	f	p°	p	k^*/k	k^*/k (average)
	Min					
D-Glucose-*1-t, 6-*C^{14}	55	0.5902	9.12	18.64	0.20	
	65	.7384	9.12	30.37	.10	0.15
D-Glucose-*1-*C^{14},*6-t*	55	.6311	0.1144	0.1211	.94	
	65	.7151	.1144	.1198	.96	.

mixture was cooled in an ice bath, diluted with a solution of 100 mg of D-glucose carrier in 5 ml of water and passed through a column containing 15 ml of mixed anion- and cation-exchange resins. The combined effluent and wash liquors were concentrated in a rotary vacuum still to about 2 ml and filtered after addition of decolorizing carbon. The solution was collected in a test tube and concentrated to a sirup in a stream of dry air. The sirup was diluted with 2 ml of methanol and again concentrated; addition and evaporation of methanol were repeated twice more. The residual sirup was dissolved in 5 drops of methanol, and 2-propanol was added to the point of incipient turbidity; α-D-glucose crystallized from the solution. After one day the mother liquor was removed with a capillary pipet, and the crystals were washed twice with a 1:1 mixture of methanol and 2-propanol. The crystals were recrystallized three times from aqueous meth-

[6] "Dee-O," Takamine Laboratories, Clifton, N.J.

anol as just described. The resulting product was dried to constant weight and analyzed for carbon 14 and tritium by the method previously described [26].

For calculation of k^*/k the isotope at C1 is the functional isotope. The ratio of the functional to the reference isotope in the residual reactant (p of eq (4)) and the extent of reaction (f of eq (6)), were calculated from the analytical data. The ratio of the functional to the reference isotope in the original reactant was determined on a separate sample. The measurements of k^*/k are given in table 6.

The authors express their appreciation to Dr. Harriet L. Frush for many helpful suggestions and to Miss Nancy B. Holt for assistance in the preparation of the labeled sugars and in the analyses.

3. References

[1] H. S. Isbell and C. S. Hudson, BS J. Res. **8,** 327 (1932) RP418.
[2] H. S. Isbell, BS J. Res. **8,** 615 (1932) RP441.
[3] H. S. Isbell and W. W. Pigman, BS J. Res. **10,** 337 (1933) RP534.
[4] H. S. Isbell and W. W. Pigman, J. Res. NBS **18,** 141 (1937) RP969.
[5] F. J. Bates and Associates, Polarimetry, Saccharimetry and the Sugars, NBS Circ. 440, pp. 411 to 456 (1942).
[6] H. S. Isbell, J. Res. NBS **18,** 505 (1937) RP990.
[7] I. R. L. Barker, W. G. Overend, and C. W. Rees, Chem. Ind. (London) **1960,** 1297; **1960,** 1298.
[8] H. S. Isbell, Chem. Ind. (London) **1961,** 593.
[9] H. S. Isbell, J. Res. NBS **66A,** No. 3, 233 (Phys. and Chem.) May–June (1962).
[10] L. Melander, Isotope effects on reaction rates (Ronald Press Co., New York, 1960).
[11] F. Friedberg and L. Kaplan, Abstracts papers Am. Chem. Soc. **131,** 86–o (1957).
[12] H. S. Isbell and L. T. Sniegoski, J. Res. NBS **67A** (Phys. and Chem.), No. 6, 569 (Nov.–Dec. 1963).
[13] H. S. Isbell and R. S. Tipson, Science **130,** 793 (1959); J. Res. NBS **64A** (Phys. and Chem.) No. 2, 171 (Mar.–Apr. 1960).
[14] R. E. Reeves, J. Am. Chem. Soc. **72,** 1499 (1950).
[15] J. Blom, Acta Chem. Scand. **16,** 922 (1962); **17,** 73 (1963).
[16] J. A. Christiansen, Acta Chem. Scand. **16,** 2341 (1962); **17,** 2209 (1963).
[17] S. Furberg and B. Pedersen. Acta Chem. Scand. **17,** 1160 (1963).
[18] I. R. L. Barker, W. G. Overend, and C. W. Rees, Chem. Ind. (London) **1961,** 558.
[19] H. S. Isbell, H. L. Frush, N. B. Holt, and J. D. Moyer, J. Res. NBS **64A** (Phys. and Chem.) No. 2, 177 (Mar.–Apr. 1960).
[20] H. S. Isbell, J. V. Karabinos, H. L. Frush, N. B. Holt, A. Schwebel, and T. T. Galkowski, J. Res. NBS **48,** 163 (1952) RP2301.
[21] R. Schaffer and H. S. Isbell, J. Res. NBS **56,** 191 (1956) RP2667.
[22] H. S. Isbell, H. L. Frush, and J. D. Moyer, J. Res. NBS **64A** (Phys. and Chem.) No. 4, 359 (July–Aug. 1960).
[23] H. S. Isbell, H. L. Frush, and R. Schaffer, J. Res. NBS **54,** 201 (1955) RP2581.
[24] H. S. Isbell, N. B. Holt, and H. L. Frush, unreported synthesis.
[25] Operation Manual, Tri-Carb Liquid Scintillation Spectrometer, Series 314E, Packard Instrument Co., Inc., La Grange, Ill.; F. Newton Hayes, Packard Technical Bulletin, January 1962.
[26] H. S. Isbell, L. T. Sniegoski, and H. L. Frush, Anal. Chem. **34,** 982 (1962).
[27] H. S. Isbell, H. L. Frush, and N. B. Holt, J. Res. NBS **64A,** (Phys. and Chem.) No. 4, 363 (July–Aug. 1960).
[28] W. H. Stevens and R. W. Attree, Can. J. Res. **27B,** 807 (1949).
[29] G. A. Ropp, J. Am. Chem. Soc. **82,** 842 (1960).
[30] F. Weygand, H. Simon, K. D. Keil, H. S. Isbell, and L. T. Sniegoski, Anal. Chem. **34,** 1753 (1962).

(Paper 68A2–262)

JOURNAL OF RESEARCH of the National Bureau of Standards—A. Physics and Chemistry
Vol. 68A, No. 2, March–April 1964

Thermal Degradation of Fractionated High and Low Molecular Weight Polyisobutylene

D. McIntyre, J. H. O'Mara, and S. Straus

(October 30, 1963)

A series of thermal degradation studies on polyisobutylene has been carried out at relatively low degradation temperatures using samples of high purity, both fractionated and unfractionated, and of both high and low molecular weight. Rate curves of the high molecular weight polymer show maximums while those of the low molecular weight polymer show large initial rates which steadily decrease with increased volatilization. Rates of degradation of all samples become similar with increased volatilization. Rate studies indicate strong random initiation with the initial rate of volatilization showing very little dependence on molecular weight. The drop in molecular weight with increased degradation and the lack of broad maximums at moderate values of conversion shows the influence of an appreciable amount of transfer and a low kinetic chain length. The rate of degradation is found to be much faster than that of polypropylene or polyethylene probably because polyisobutylene disproportionates and forms radicals more easily. Equations are suggested for these degradation reactions.

1. Introduction

The thermal degradation of polymers has been extensively studied in recent years. Numerous theoretical and experimental studies have shown that the thermal degradation of some polymers can be described by depolymerization mechanisms involving only random or end initiation. For example, linear polyethylene appears to have a purely random initiation of carbon-carbon bond breaks along the chain backbone, whereas polytetrafluoroethylene has only end-initiated carbon-carbon chain breaks. Different mechanisms for such widely different chemical structures can be explained on the basis of the known differences in the carbon-carbon bond strengths and the relative reactivities of hydrogen and fluorine covalent bonds. However, the degradation experiments and their interpretation become more complicated when the substituents on the carbon-carbon chain exert more subtle chemical effects. In these cases chain transfer reactions must be considered as possible reaction paths, in addition to combined end and random initiation. A very laborious and systematic experimental study may be necessary to sort out their relative contributions to the degradation.

The systematic study of the polyolefin system allows an interesting comparison of the effects of chemical structure. Wall and Straus [1][1] have recently compared the different rates of thermal degradation of linear and branched polyethylene, linear and branched polypropylene, and polyisobutylene. Polyisobutylene shows a significant departure from the degradation results of the other linear polymers in the polyolefin series. It is much more unstable and does not exhibit a maximum in the rate of volatilization. This comparison was based upon earlier kinetic observations of polyisobutylene by Madorsky and Straus [2] over a 20-deg temperature interval and at moderate initial rates of volatilization.

In order to gain greater insight into the mechanism of the polyisobutylene degradation, it is necessary to evaluate initial rates of degradation over a large range of molecular weights, as well as the molecular weight changes during the degradation experiment. For this purpose a series of thermal degradation experiments was carried out at relatively low degradation temperatures using a balance recently utilized by Madorsky [3] for measuring low rates of volatilization, and with polyisobutylene samples of high purity, both fractionated and unfractionated, and of both high and low molecular weight.

2. Materials

High molecular weight polyisobutylene. The high molecular weight polyisobutylene was prepared by Esso Research Company by a BF_3 initiated polymerization of isobutylene. Fractionation of the whole polymer was begun with a 0.4 percent solution in benzene and *n*-heptane (1:2). As the fractionation proceeded the solution was made progressively richer in benzene. A refractionation scheme was

[1] Figures in brackets indicate the literature references at the end of this paper.

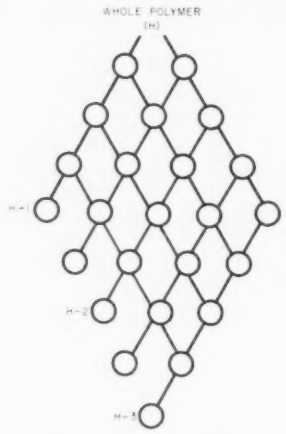

FIGURE 1. *Triangular refractionation scheme.*

used as shown in figure 1. Distilled acetone was used as the precipitant. Six final fractions were obtained. Polymer samples H–1, H–2, and H–3 represent the first, fourth, and sixth fractions.

Low molecular weight polyisobutylene. The low molecular weight whole polymer was a sample of commercially available whole polymer supplied by the Enjay Company of the Esso Standard Oil Company and designated as Vistanex LM, Type MS. Fractionation of the whole polymer was begun with a 1 percent solution in benzene using distilled acetone as a precipitant. Six fractions were obtained, with the first fraction representing about 50 percent of the whole polymer. The remaining fractions were about equal in size. Polymer sample L–3 was the third fraction of this fractionation.

The large first fraction was refractionated using a 1 percent solution in benzene with distilled acetone as the precipitant. Five fractions roughly equal in size were obtained. Polymer sample L–2 was the fourth fraction.

The first fraction of this second fractionation was again refractionated from a 1 percent solution in benzene into three fractions using distilled acetone as the precipitant. Polymer sample L–1 was the first fraction of this fractionation.

TABLE 1. *Degradation of polyisobutylene at 298.5 °C*

Sample	Fraction	Mol. wt (M_v)	Duration	Volatilization
			hr	%
H	Whole polymer	1,800,000	23	71.3
H-1	High fraction	4,800,000	25	83.8
H-2	Middle fraction	1,980,000	23	71.6
H-3	Low fraction	700,000	23	71.8
L	Whole polymer	49,000	23	68.3
L-1	High fraction	234,000	23	70.3
L-2	Middle fraction	44,200	23	69.2
L-3	Low fraction	24,500	23	71.6

Pertinent data on the fractions and whole polymers studied are given in table 1. The molecular weights of these materials were determined by the viscosity method using the relation $[\eta]=1.8\times10^{-4}M^{0.68}$ [4]. The intrinsic viscosities were determined in iso-octane at 40 °C with an Ubbelohde viscometer.

3. Experimental Procedures and Results

3.1. Degradation Procedure

The thermal degradation studies were done using an electronic microbalance that automatically recorded the temperature and loss of weight of the sample and could be operated for long periods of time without attention. Measurements were made at 298.5 °C.

The experimental procedure using this balance has been described in detail [3]. A small platinum crucible containing 4 to 5 mg of polymer was suspended from the arm of the balance enclosed in a glass housing. The system was operated at a pressure of about 10^{-5} mm Hg. The sample was heated by placing a preheated electric furnace around the glass housing. The platinum crucible reached operating temperature in about 15 min, and it was found that very little weight loss occurred during this time. Temperatures were measured by using a chromel-constantan thermocouple directly under the crucible. This thermocouple was precalibrated against a similar thermocouple placed inside the crucible in contact with its bottom. The temperature was kept constant to within $\pm0.2°$ C by means of an electronic thermostat.

3.2. Rates of Degradation

The extents of degradation of the polyisobutylene samples are given in table 1. The rates are plotted in figures 2 and 3 in percent of initial sample volatilized per minute, K_1, as a function of percent volatilized.

The high molecular weight fractions all show, after the establishment of the predetermined temperature, a rapid rise of volatilization in rate to a maximum rate of about 0.06 to 0.07 percent volatilization per minute at about only 4 percent loss (fig. 2). Then the rates decrease slowly to about 0.04 percent volatilization per minute at about 70 percent loss. The whole polymer shows an initial high rate of volatilization which decreases rapidly so that, after about 5 percent loss, the rate of volatilization follows that of the fractions.

The low molecular weight whole polymer shows a very rapid initial degradation rate, over 0.13 percent volatilization per minute, which drops very rapidly to about 0.065 percent loss per minute at only about 4 percent loss of sample (fig. 3). The rate then levels off, decreasing somewhat more rapidly as volatilization proceeds. The two higher fractions of the low molecular weight polymer also show an initial rapid rate of volatilization of much less magnitude than

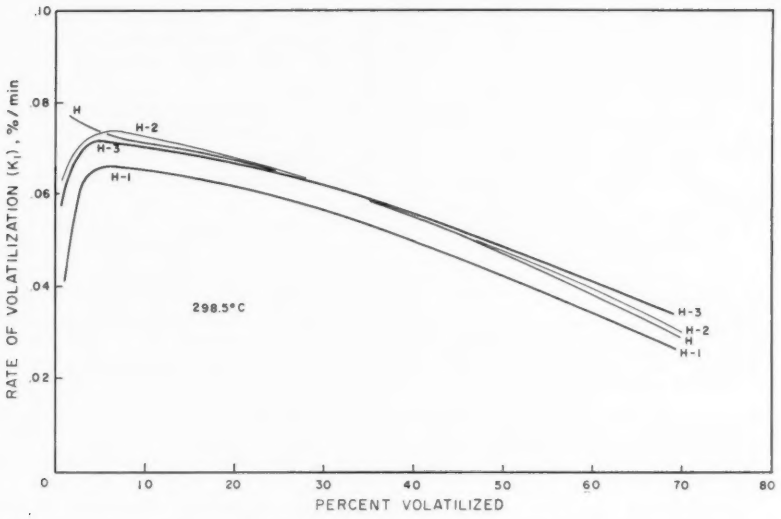

FIGURE 2. *Percent of sample volatilized per minute as a function of percentage volatilized for high molecular weight polyisobutylene.*

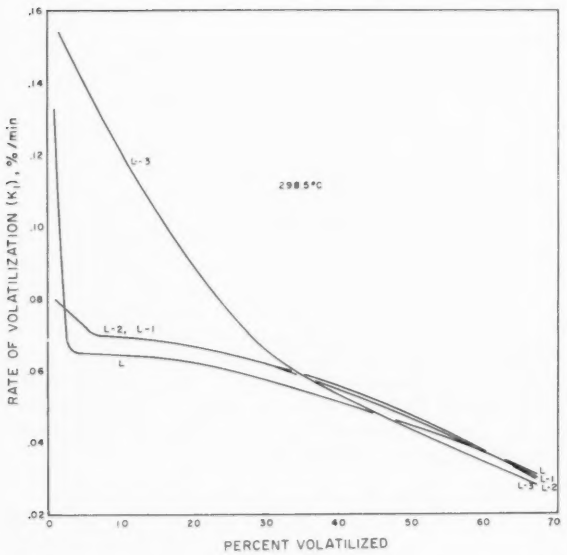

FIGURE 3. *Percent of sample volatilized per minute as a function of percentage volatilized for low molecular weight polyisobutylene.*

that of the whole polymer. After the initial 5 percent loss, these two fractions follow essentially the same rate curve as the whole polymer.

The lowest fraction of the low molecular weight polyisobutylene shows the highest initial rate, over 0.15 percent volatilization per minute. This fraction continues to show a high rate of volatilization which decreases slowly up to about 31 percent loss of sample. At this point the rate becomes essentially that of the other fractions and whole polymer.

3.3 Molecular Weight of Degraded Polymers

Five samples of polyisobutylene fraction H–2 were pyrolized in a vacuum for various periods of time at a temperature of 300 °C.

After pyrolysis, the molecular weights of the residues were determined by viscosity and osmotic pressure methods. The osmotic pressure determinations were made in benezene at 22 °C in a Stabin osmometer fitted with a "never-dried" gel-cellophane No. 600 membrane. All of the measurements were equilibrium osmotic pressures and required about eight days to come to equilibrium for the lower molecular weight samples. Results of these pyrolysis experiments and molecular weight determinations are shown in table 2. In figure 4 the molecular weight of the residue is plotted against the percent volatilized.

TABLE 2. *Molecular weights of degraded polyisobutylene fraction H–2*

Temperature	Duration of pyrolysis	Volatilization	M_v(visc)	M_n(osmotic)	M_v/M_n
°C	*min*	%			
300	24	1.5	95,000	54,800	1.73
300	70	4.2	48,100	33,800	1.42
300	135	9.1	29,000	22,900	1.27
300	260	19.2	19,000		
300	660	42.0	11,400		

Meaningful osmotic pressure measurements could not be made on the last two samples because of solute leakage through the membrane resulting in unstable, drifting osmotic pressures. Small leakage of the smaller molecules in the other samples most probably also accounts for the apparent narrowing of the distribution as given in the last column of table 2. The dotted line is drawn by assuming that the ratio of

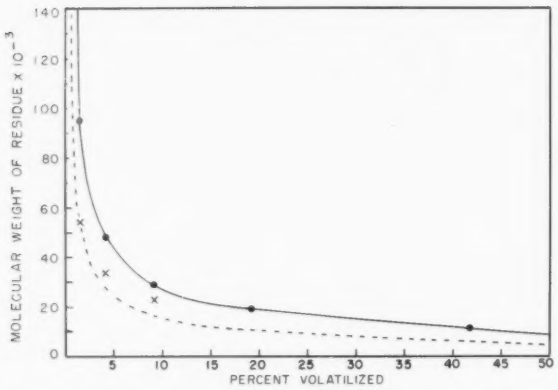

FIGURE 4. *Drop in the molecular weight of polyisobutylene, fraction H–2, molecular weight 1,980,000.*

●, viscosity measurements; x, osmotic pressure measurements; ----, represents calculated curve for a constant ratio of M_v/M_n based on the results from the 1.5 percent volatilized sample.

viscosity average to number-average molecular weight is constant after 1.5 percent volatilization.

The molecular weight measurements indicate a very rapid drop in molecular weight from 1,980,000 to 95,000 with just 1.5 percent loss of weight. The molecular weight drops all the way to 28,000 during the initial 10 percent loss in weight, but then drops less drastically as volatilization proceeds.

4. Discussion

The results of the degradation rate and molecular weight studies very strikingly demonstrate the absence of end initiation and the presence of predominantly random initiation. The rate studies very clearly indicate that over a molecular weight range of 50-fold the initial rate of the volatilization shows very little dependence on molecular weight. There may be some question about the value of the initial rate for the high molecular weight H series, but within the experimental accuracy of the data the curves may be considered to be equivalent. The existence of the maximum in the curves is beyond experimental error and must be explained. The upward curvature for the whole polymer is unquestionably related to the existence of a very broad molecular weight distribution in the whole polymer, the low molecular weight portion of which quickly distills out. Even with the most diligent search for a molecular weight effect in the initial rate, one can only find a doubling of the rate for a molecular weight change of 50 times. What is even more significant is the fact that the extrapolation of the rate curves after only 4 percent volatilization yields values of 0.07 percent/min and deviations no greater than 0.005 from this value.

The drastic upward curvature of the rate of the very low molecular weight fraction (L–3) in figure 3 may indicate a large amount of low molecular weight constituent. When such broadly distributed polymers are fractionated it is extremely difficult to get very narrowly distributed fractions. However the fraction L–3 seems to indicate more low molecular weight material than might be expected from the fractionation. The degradation curve of the fraction does not become coincident with the whole polymer and the other fractions until volatilization reaches 30 percent. This result may indicate a definite change in degradation behavior at very low molecular weight.

The rate data reported here are qualitatively in agreement with the data reported by Madorsky and Straus [2]. However, the rates are about one-half those previously reported after temperature corrections are made. Inoue, Ouchi, and Yasuhira [5] also measured the rates of degradation and reported an activation energy of 41 kcal per mole in contrast to Madorsky's value of 52 kcal per mole. The differences in rates may be due to small differences in the commercial preparation of the polymers. Thus, the chemical analysis of the volatiles from different samples gave 78 percent monomer in one case [6], and 20 percent in another [7]. Another less detailed study [8] indicates even less volatile matter. The preparative details of each of the reported polymers most likely differ from one another. The existence of the maximum in the volatilization rates has not been observed before, although the measurements by Madorsky were not made at such low rates or with as sharply fractionated materials. This maximum may simply be the result of the necessary buildup, in a random degradation, of components that can be distilled out.

The molecular weight study shown in figure 4 also shows the existence of a strong random initiation. The degree of polymerization changes to about 0.03 of the original within 1.5 percent degradation. This is to be compared with polyethylene studies which show a change to 0.002 of the original at the same conversion [9]. This drop in DP for polyisobutylene is not as large as might be expected for random initiation only and indicates the influence of an appreciable amount of transfer. Figure 4 does not extrapolate to low molecular weight volatiles at 100 percent conversion unless a very flat curve is drawn beyond 9 percent volatilization.

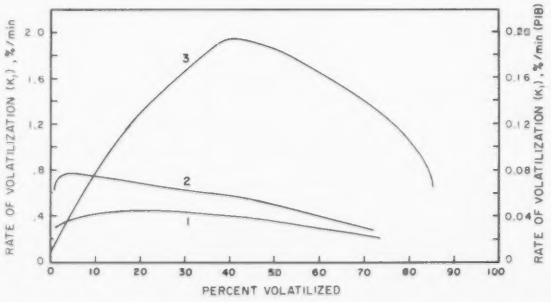

FIGURE 5. *Comparison of the rates of volatilization for linear polymers.*

(1) Polyethylene at 400 °C [1].
(2) Polyisobutylene at 298.5 °C (ordinate at right).
(3) Polypropylene at 375 °C [1].

Figure 5 shows a plot of different degradation rates for linear polyethylene, polypropylene, and polyisobutylene. The ethylene and propylene data are taken from Wall and Straus [1]. By assuming the value of 52 kcal per mole for the polyisobutylene thermal degradation and the rate at 298.5 °C, the polyisobutylene rate is calculated to be about 15 times that of the polypropylene at its maximum at 375 °C and 600 times faster than polyethylene [9]. This increased rate of thermal degradation is probably due to the easy disproportionation and radical formation in polyisobutylene. The lack of the broad maximum at a moderate value of conversion for the polyisobutylene must be explained on the assumption of a very small zip length and prevailing intermolecular and intramolecular transfer soon after the initial random break. This interpretation is in line with the molecular weight studies, and the analysis of volatiles. That only 20 percent of the monomer is distilled off lends support to the transfer reactions.

The reaction for the thermal degradation of polyisobutylene probably consists of thermal breaks of the bonds as shown in eq (1), followed in eq (2) by some rearrangements (intramolecular transfer) of the

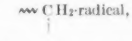

and disproportionation in eq (3) of the

into monomer. Any of the radicals would be able to transfer hydrogen intermolecularly.

(Paper 68A2–263)

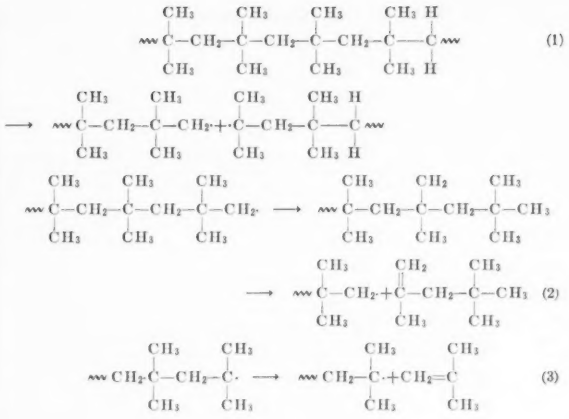

5. References

[1] L. A. Wall and S. Straus, J. Polymer Sci. **44,** 313 (1960).
[2] S. L. Madorsky and S. Straus, J. Res. NBS **53,** 361 (1954) RP2553.
[3] S. L. Madorsky, J. Res. NBS **62,** 219 (1959) RP2957.
[4] 85th Report on Fundamental correlations between physical properties and molecular parameters o synthetic rubber Progress Report, Mellon Institute of Industrial Research, CR3872, December 31, 1955.
[5] R. Inoue, S. Ouchi, and S. Yasuhira, Chem. High Polymers (Japan) **13,** 31 (1956).
[6] L. A. Wall, J. Res. NBS **41,** 315 (1948) RP1928.
[7] S. L. Madorsky, S. Straus, D. Thompson, and L. Williamson, J. Res. NBS **42,** 499 (1949) RP1989; J. Polymer Sci. **4,** 639 (1949).
[8] V. A. Golubtsova, Dokl. Akad. Nauk SSSR **84,** 701 (1952).
[9] L. A. Wall, S. L. Madorsky, D. W. Brown, S. Straus, and R. Simha, J. Am. Chem. Soc. **76,** 3430 (1954).

JOURNAL OF RESEARCH of the National Bureau of Standards—A. Physics and Chemistry
Vol. 68A, No. 2, March–April 1964

Ionization Constants of the Six Dichloroanilines and the Six Dichlorophenols in Aqueous Solution at 25 °C

R. A. Robinson

(October 23, 1963)

The thermodynamic ionization constants of the six dichloroanilines and the six dichlorophenols in aqueous solution at 25 °C have been determined by the spectrophotometric method. The pK values found are recorded in table 3.

An approximately linear relation is found to exist between the pK_A value of a dichloroaniline and the pK_P value of the corresponding dichlorophenol. The relation is

$$pK_A = -9.047 + 1.401\ pK_P.$$

This equation yields pK_A values which differ from the observed by not more than 0.06 pK unit and, on the average, by 0.03 pK unit; it applies even when both substituents are in the ortho position.

1. Introduction

It has been shown [1] [1] that the pK values of the dinitrophenols cannot be predicted with accuracy from data for phenol and the mononitrophenols, if at least one of the nitro groups is in the ortho position with respect to the hydroxyl. The pK values of phenol, *o*-nitrophenol, *m*-nitrophenol, and *p*-nitrophenol at 25 °C are 9.998 [2], 7.230 [3], 8.355 [4], and 7.156 [5], respectively. Thus, the decrement in pK value for *o*-, *m*-, and *p*-nitro substitution is 2.768, 1.643, and 2.842, respectively. If the effects of substitution were strictly additive, a dinitrophenol without ortho substitution, such as 3,5-dinitrophenol, should have a pK value of 6.712; a value of 6.69$_2$ has been found [1], a value not seriously different from that predicted. However, with one ortho substituent, as in 2,4-dinitrophenol, a pK value of 4.388 is predicted, whereas the experimental value is 4.090 [6], a value considerably different from the predicted. But if both substitutents are in the ortho position, as in 2,6-dinitrophenol, the calculated pK value is only 4.462 compared with the observed value of 3.713 [7], the difference being the largest found in the series of dinitrophenols.

It might be expected that additivity relations would have greater validity in the dichlorophenols but there is little data available to confirm this. Judson and Kilpatrick [8] found pK 7.850 for 2,4-dichlorophenol; the values of 8.527 for *o*-chlorophenol [9] and 9.418 for *p*-chlorophenol [10] give a predicted value of 7.947.

The pK values of the six dichloroanilines and the six dichlorophenols have now been measured in order to test this additivity proposition and, further to see if the Hammett relation [11] could be extended to these disubstituted compounds.

[1] Figures in brackets indicate the literature references at the end of this paper.

2. Experimental Procedure

2.1. Materials

The dichloroanilines and dichlorophenols were obtained as commercial products. Details of their recrystallization, melting point, maximum extinction coefficients in alkaline solution (ϵ_2) and in acid solution (ϵ_1) as well as the extinction coefficient at an isosbestic point (ϵ) are as follows: 2,3-Dichloroaniline, three times from heptane, mp 23.5–24°, ϵ_2 2,110 at 292 mμ, ϵ_1 270 at 269 mμ and 220 at 277 mμ. 2,4-Dichloroaniline, three times from petroleum ether, mp 50–50.5°, ϵ_2 2,060 at 297 mμ, ϵ_1 260 at 270 mμ and 200 at 279 mμ. 2,5-Dichloroaniline, three times from petroleum ether, mp 50–50.5°, ϵ_2 2,560 at 294, ϵ_1 400 at 277 mμ and 360 at 280 mμ. 2,6-Dichloroaniline, three times from heptane, mp 38.5–39°, ϵ_2 2,570 at 292 mμ, ϵ_1 280 at 268 mμ and 340 at 277 mμ. 3,4-Dichloroaniline, dissolved in methanol, precipitated by addition of water and recrystallized three times from petroleum ether, mp 72°, ϵ_2 1,680 at 297 mμ, ϵ_1 350 at 271 mμ and 320 at 279 mμ. 3,5-Dichloroaniline, three times from heptane, mp 50–50.5°, ϵ_2 1,760 at 294 mμ, ϵ_1 190 at 272 mμ and 180 at 278 mμ. 2,3-Dichlorophenol, once from heptane and three times from petroleum ether, mp 58°, ϵ_2 3,870 at 297 mμ, ϵ_1 1,840 at 276 mμ and 1,790 at 283 mμ, ϵ 1,140 at 267 mμ and 1,790 at 278 mμ. 2,4-Dichlorophenol, three times from petroleum ether mp 43–43.5°, ϵ_2 3,620 at 307 mμ, ϵ_1 2,120 at 284 mμ, ϵ 850 at 270 mμ and 1,900 at 291 mμ. 2,5-Dichlorophenol, twice from petroleum ether, mp 58.5°, ϵ_2 4,500 at 301 mμ, ϵ_1 2,360 at 280 mμ and 2,160 at 288 mμ, ϵ 650 at 264 mμ and 2,100 at 284 mμ. 2,6-Dichlorophenol, once from methanol-water and then from petroleum ether, mp 66°, ϵ_2 4,950 at 300 mμ, ϵ_1 1,940 at 277 mμ and 1,900 at 283 mμ

ϵ 800 at 265 mμ and 1,750 at 281 mμ. 3,4-Dichlorophenol, three times from petroleum ether, mp 66°, ϵ_2 2,830 at 303 mμ, ϵ_1 1,780 at 284 mμ, ϵ 1,000 at 274 mμ and 1,650 at 288 mμ. 3,5-Dichlorophenol, three times from heptane, mp 67°, ϵ_2 3,220 at 297 mμ, ϵ_1 1,570 at 277 mμ and 1,560 at 284 mμ, ϵ 700 at 267 mμ and 1,420 at 279 mμ.

Absorption spectra were measured either on a Cary or on an Optica instrument. Two typical plots of extinction coefficient versus wavelength are shown in figure 1. It will be noted that the plot for the aniline resembles that of the phenol, the maxima in acid and alkaline solution being found at approximately the same wavelength. Extinction coefficients are, however, much lower for the anilines than for the phenols; moreover, while there are well defined isosbestic points for the phenols, there are none for the anilines in the range of wavelength studied in this paper.

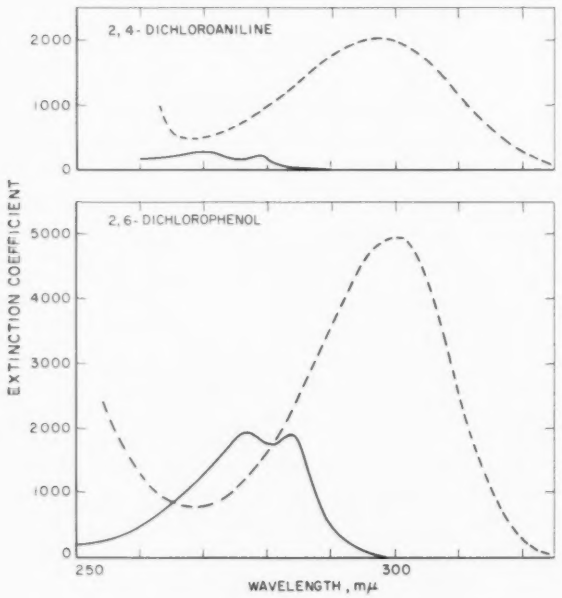

FIGURE 1. *Spectral absorption curves of 2,4-dichloroaniline and 2,6-dichlorophenol in aqueous solution at 25 °C.*

----, With addition of alkali.
——, With addition of acid.

2.2. Determination of *pK* Values

The spectrophotometric method followed in determining the pK values was similar to that used by Bates and Schwarzenbach [12] and by Robinson and Biggs [13]. Since the anilines have pK_A values between 0.4 and 3, solutions were prepared of each aniline in hydrochloric acid solution of concentration comparable with the ionization constant of the aniline so that the concentration ratio of anilinium ion, HR^+, to uncharged aniline, R, lay between 0.2 and 0.8. The pK_A value of the aniline [2] is then given by

$$pK_A = -\log [H^+] - \log \frac{D-D_1}{D_2-D} - \log \frac{\gamma_{H^+}\gamma_R}{\gamma_{HR^+}} \qquad (1)$$

where the symbols have their usual meaning. Thus, D_1 is the optical density of a solution of the aniline to which sufficient concentrated hydrochloric acid has been added to convert the aniline entirely into the positively charged anilinium ion, D_2 the optical density of the solution to which sodium hydroxide has been added and the aniline exists entirely in the uncharged form, and D is the optical density of the solution to which dilute hydrochloric acid has been added and the aniline is present partly in the charged and partly in the uncharged form; in each of the three solutions, the stoichiometric concentration of aniline is the same. γ denotes an activity coefficient and $[H^+]$ the hydrogen ion concentration. The latter was taken as the stoichiometric concentration of hydrochloric acid less the amount of acid required to form the anilinium ion and was expressed on a molarity basis, i.e., in moles per liter; the ionization constant, K_A, is therefore also on the molarity scale. As the ionization constants on the molarity and the molality scale are related by an expression including the density of the solvent, they differ little if the solvent is water. The pK_A values recorded later are on the molarity scale but those on the molality scale would be only 0.001 lower. It is assumed that the last term in eq (1) is negligible; with one exception, this seems justified by the constancy of the pK values obtained over a range of acid concentration; the exception is 2,6-dichloroaniline to which further reference will be made below.

For the phenols, with pK_P values between 6.8 and 8.6, buffer solutions were used. One of these was the equimolal (m) mixture of potassium dihydrogen phosphate and disodium hydrogen phosphate whose total ionic strength is $I=4$ m (this buffer is referred to as phosphate buffer). The other was a mixture of tris-(hydroxymethyl)-aminomethane (m_1) and its hydrochloride (m_2) with $m_1/m_2=1.0157$ and $I=m_2$ (referred to as tris buffer). The pK of the phenol is given by

$$pK_P = -\log (a_{H^+}\gamma_{Cl^-}) - \log \frac{D-D_1}{D_2-D} + \log \frac{\gamma_{HR}\gamma_{Cl^-}}{\gamma_{R^-}}. \qquad (2)$$

Again it is assumed that the last term is negligible and this seemed to be valid for all six phenols, provided that the total ionic strength of the buffer solution did not exceed 0.1. This point was studied in some detail in the case of 2,6-dichlorophenol, measurements being made in eleven phosphate buffer solutions whose ionic strengths lay between

[2] By K_A for an aniline is meant the acidic ionization constant of the corresponding anilinium ion, the equation for whose dissociation is $RH^+ \rightarrow H^+ + R$ and

$$K_A = \frac{C_{H^+}C_R}{C_{HR^+}} \frac{\gamma_{H^+}\gamma_R}{\gamma_{HR^+}}$$

0.01 and 0.20. The results in table 2 for this dichlorophenol indicate that the apparent pK values derived from measurements in solutions of $I>0.10$ are slightly but significantly lower than those derived from measurements in more dilute solutions. Thus, not surprisingly, the final term in eq (2) is not negligible if the ionic strength of the medium exceeds 0.1. In deriving a mean pK value for this dichlorophenol (table 2), the pK values at $I=0.12$, 0.15, and 0.20 were excluded; for the other dichlorophenols no measurements were made at any ionic strength exceeding 0.1. Values of $-\log (a_{H^+}\gamma_{Cl^-})$ were taken from the paper of Bates and Gary [14] as follows:

I	0.01	0.02	0.03	0.04	0.05	0.06	
Phosphate	7.111	7.080	7.058	7.040	7.026	7.013	
Tris	8.176	8.207	8.232	8.251	8.266	8.280	
I	0.07	0.08	0.09	0.10	0.12	0.15	0.20
Phosphate		6.992		6.974	6.959	6.940	6.912
Tris	8.292	8.302	8.312	8.321			

2.3. Results

Table 1 gives data for the six dichloroanilines. The concentration of aniline, the length of the absorption cells, the wavelength at which optical density measurements were made, D_1, and D_2 are recorded first and then values of D and pK_A (calculated by eq (1)) are given for a number of solutions of hydrochloric acid of different concentration.

Table 2 gives similar data for the six dichlorophenols, except that the nature of the buffer mixture is recorded and the first column refers to the total ionic strength of the buffer solution. For 2,6-dichlorophenol, measurements were made at two wavelengths, with concordant results. For 2,3-dichlorophenol, measurements were made with each of the buffer solutions, again with concordant results. Each pK value is corrected for the influence of the phenol on the $\log(a_{H^+}\gamma_{Cl^-})$ value of the buffer solution [15].

TABLE 1. *Ionization constants of dichloroanilines in aqueous solution at 25°*

Conc. of HCl	D	pK	Conc. of HCl	D	pK
2,3-Dichloroaniline 4.36×10^{-4} M 1 cm 292 mμ D_1 0.002, D_2 0.922			2,6-Dichloroaniline 1.167×10^{-4} M 4 cm 202 mμ D_1 0, D_2 1.200		
0.004312	0.743	1.762	0.1748	0.807	0.445
.005854	.697	1.755	.2328	.724	.451
.01004	.591	1.757	.2970	.650	.454
.01560	.490	1.762	.3365	.604	.467
.01723	.467	1.763	.3544	.593	.461
.02001	.430	1.762	.4071	.549	.464
.02479	.385	1.755	.5192	.463	.487
.03003	.340	1.763	.5862	.425	.493
.03993	.280	1.766			
.05005	.237	1.769			
2,4-Dichloroaniline 3.52×10^{-4} M 1 cm 297 mμ D_1 0, D_2 0.725			3,4-Dichloroaniline 4.76×10^{-4} M 1 cm 297 mμ D_1 0, D_2 0.802		
0.002513	0.578	2.010	0.0002023	0.705	2.977
.003518	.535	2.015	.0004938	.598	2.962
.0050?5	.480	2.017	.0006912	.536	2.969
.007035	.424	2.013	.001002	.462	2.964
.008894	.380	2.017	.001248	.411	2.973
.01005	.356	2.023	.001507	.373	2.963
.01158	.332	2.017	.001752	.339	2.966
.01508	.286	2.014	.001977	.311	2.971
.01849	.248	2.022	.002513	.266	2.963
2,5-Dichloroaniline 3.75×10^{-4} M 1 cm 294 mμ D_1 0, D_2 0.959			3,5-Dichloroaniline 1.21×10^{-4} M 4 cm 294 mμ D_1 0, D_2 0.850		
0.007189	0.773	1.529	0.001421	0.634	2.389
.01055	.710	1.526	.001991	.578	2.383
.01524	.633	1.533	.002978	.498	2.382
.01963	.580	1.525	.003341	.474	2.382
.03007	.478	1.528	.003710	.451	2.384
.03994	.409	1.530	.004460	.411	2.386
.04460	.383	1.531	.004972	.391	2.379
.05076	.352	1.532	.005938	.354	2.378
			.007132	.313	2.386
			.007711	.300	2.380

TABLE 2. *Ionization constants of dichlorophenols in aqueous solution at 25°*

I	D	pK (corr.)	I	D	pK (corr.)
2,3-Dichlorophenol 1.03×10^{-4} M 4 cm 297 mμ D_1 0.006, D_2 1.594 Phosphate buffer			2,6-Dichlorophenol 5.32×10^{-5} M 4 cm 240 mμ D_1 0.036, D_2 1.338 Phosphate buffer		
0.01	0.331	7.696	0.01	0.908	6.792
.02	.318	7.689	.02	.889	6.795
.03	.303	7.694	.03	.876	6.793
.04	.292	7.696	.04	.867	6.791
.05	.286	7.694	.05	.858	6.790
.06	.277	7.699	.06	.843	6.799
.08	.270	7.691	.08	.836	6.788
			.10	.823	6.789
4.98×10^{-5} M 4 cm 297 mμ D_1 0.003, D_2 0.769 Tris buffer			5.32×10^{-5} M 4 cm 300 mμ D_1 0.001, D_2 1.053 Phosphate buffer		
0.02	0.590	7.689	0.01	0.705	6.793
.03	.596	7.696	.02	.693	6.790
.04	.602	7.694	.03	.684	6.787
.06	.609	7.702	.04	.675	6.787
.07	.611	7.707	.05	.665	6.791
.09	.617	7.706	.06	.657	6.792
.10	.625	7.687	.08	.646	6.790
			.10	.637	6.789
			.12	.634	6.780
			.15	.627	6.773
			.20	.608	6.777
2,4-Dichlorophenol 6.26×10^{-5} M 4 cm 307 mμ D_1 0.007, D_2 0.907 Tris buffer			3,4-Dichlorophenol 5.90×10^{-5} M 4 cm 303 mμ D_1 0.017, D_2 0.668 Tris buffer		
0.01	0.599	7.889	0.01	0.199	8.587
.02	.611	7.895	.02	.210	8.582
.03	.627	7.886	.03	.221	8.573
.04	.629	7.900	.04	.225	8.579
.05	.640	7.890	.05	.229	8.582
.06	.644	7.895	.06	.232	8.587
.07	.649	7.891	.07	.235	8.590
.08	.654	7.894	.08	.240	8.585
.09	.660	7.890	.09	.241	8.592
.10	.666	7.884	.10	.244	8.592
2,5-Dichlorophenol 4.64×10^{-5} M 4 cm 301 mμ D_1 0.010, D_2 0.835 Phosphate buffer			3,5-Dichlorophenol 2.17×10^{-4} M 1 cm 297 mμ D_1 0.004, D_2 0.699 Tris buffer		
0.01	0.244	7.509	0.01	0.344	8.187
.02	.236	7.501	.02	.359	8.184
.03	.226	7.507	.03	.368	8.184
.04	.220	7.506	.04	.374	8.193
.05	.212	7.514	.05	.385	8.180
.06	.211	7.504	.06	.388	8.188
.08	.200	7.515	.07	.394	8.184
.10	.196	7.510	.08	.397	8.177
			.09	.401	8.186
			.10	.405	8.185

The measurements recorded in these tables were made using specimens of aniline or phenol which showed no change in pK on further recrystallization.

3. Discussion

3.1. 2,6-Dichloroaniline

Inspection of table 1 shows that constant pK_A values are obtained, independent of the hydrochloric acid concentration, except in the case of 2,6-dichloroaniline. The 2,6-dichloroanilinium ion is a comparatively strong acid and considerable amounts of hydrochloric acid had to be added to get favorable optical density readings; it is not surprising that, at such high ionic strengths, the last term of eq (1) is no longer negligible. A similar dependence of apparent pK on hydrochloric acid concentration was found with *o*-nitroaniline [10]. The data were therefore fitted to the equation

$$pK_A \text{ (apparent)} = pK_A + aC_{HCl} \qquad (3)$$

and the true pK_A value obtained as the limiting value of pK_A (apparent) when $C_{HCl}=0$; the method of least squares gave $pK_A=0.422$, $a=0.120$ liter mole^{-1}.

It is worth while considering the reason for this variation in the activity coefficient term of eq (1). For this purpose, we rewrite it as log $(\gamma_{HCl}^2\gamma_R/\gamma_{HRCl}^2)$. Here γ_{HCl} is the mean ionic activity coefficient of hydrochloric acid in the presence of a small amount of dichloroaniline; this can, without serious error, be taken as the activity coefficient in aqueous solution, values of which have been tabulated [16]. γ_{HRCl} is the activity coefficient of the hydrochloride of the dichloroaniline at low concentration in the presence of comparatively large amounts of hydrochloric acid. This has not been measured but we may speculate that the behavior of the activity coefficient of an aniline hydrochloride might be similar to that of ammonium chloride, which is known to resemble that of potassium chloride [17]. The activity coefficient might then be calculated by the equation

$$\log \gamma_{(0)KCl} = \log \gamma_{KCl(0)} - \alpha_2 m, \qquad (4)$$

a relation sometimes known as Harned's rule. Here $\gamma_{(0)KCl}$ is the activity coefficient of potassium chloride present in vanishingly small concentration in a solution of hydrochloric acid of concentration m, $\gamma_{KCl(0)}$ is the activity coefficient of potassium chloride in aqueous solution at the same concentration, m, and α_2 is a parameter which depends on the total ionic strength of the solution. At $m=0.5$, log $\gamma_{KCl(0)}=-0.1876$, $\alpha_2=-0.07$ [18] and hence log $\gamma_{(0)KCl}=-0.1526$. log γ_{HCl} is known to be -0.1209 at $m=0.5$ and hence log $(\gamma_{HCl}^2\gamma_R/\gamma_{HRCl}^2)=0.063$, assuming $\gamma_R=1$. This assumption that the activity coefficient of an uncharged species can be equated to unity is supported by some recent experimental evidence; thus, it has been found [19] that the activity coefficient of mannitol present in very small amount in 0.5 M sodium chloride solution is only 0.993, that of urea in the same solution [20] is 0.983.

Now log $(\gamma_{HCl}^2\gamma_R/\gamma_{HRCl}^2)$, which we have calculated to be 0.063, should by eq (3) represent the difference between the true pK_A which has been found to be 0.422 and the apparent pK_A at $m=0.5$ which, by interpolation in table 1 or by eq (3), is 0.482. The difference in pK_A, 0.060, compares with 0.063 calculated. The agreement is better than one would expect in view of the approximation that had to be made but it does confirm that the variation in apparent pK_A is not unreasonably large.

3.2. pK Values and Comparison With Other Data

Values of pK for the dichloroanilines and the dichlorophenols (with the standard deviations in parentheses) are collected in table 3.

TABLE 3.[a] *Ionization constants* (pK *values*) *of dichloroanilines and dichlorophenols in aqueous solution at 25°*

	pK		$\Delta pK(1)$			$\Delta pK_A(2)$
	Dichloroaniline	Dichlorophenol	Dinitrophenol	Dichlorophenol	Dichloroaniline	
2,3-	1.7_{61}(0.005)	7.69_8(0.006)	0.65	−0.05	0.16	-0.02_8
2,4-	2.01_6(.004)	7.89_2(0.005)	.25	.06	.01	$-.00_6$
2,5-	1.52_9(.003)	7.50$_5$(.005)	.40	.15	.03	$-.05_7$
2,6-	0.42_2(.004)	6.79_1(.003)	.71	.27	.28	$.04_3$
3,4-	2.96_4(.005)	8.58_3(.006)	.13	−.04	−.07	$.01_3$
3,5-	2.38_3(.003)	8.18_5(.004)	.11	.07	.06	$.03_7$

[a] $\Delta pK(1) \equiv pK$ (calc.) $-pK$ (obs.), pK (calc.) being calculated from pK values of the monosubstituted compounds. ΔpK_A (2) $\equiv pK_A$ (calc.) $-pK_A$ (obs.), pK_A (calc.) being calculated by eq (6).

Some previous measurments of these ionization constants have been found in the literature. For 2,5-dichloroaniline Gillois and Rumpf [21] found pK_A 1.57 compared with 1.52_9 in this work. In the case of 2,4-dichloroaniline, whereas the present work gives 2.01_6, Paul [22] gave a tentative value of 2.00. Högfeldt and Bigeleisen [23] found 2.05 at 22 °C and Brønsted et al. [24] found 2.14 at 21°. Judson and Kilpatrick [8] gave 7.85_0 for 2,4-dichlorophenol and quote 7.75 [25] and 7.89 [26] from the literature; the present value is 7.89_2. 2,6-Dichlorophenol has been studied by the same spectrophotometric method [27] but with a succinate-phosphate buffer solution; a pK value of 6.786 was found. Murray and Gordon [25] studied all six of the dichlorophenols by electrometric measurements in a water-methanol solvent and applied a correction to give data in aqueous solution by measuring phenol itself in both solvents and assuming that the difference in pK_P value could be applied to the dichlorophenols. As they found pK_P 9.78 for phenol in aqueous solution, it may be that they overcorrected their data by about pK_P 0.22. If their values are raised by this amount, agreement is found with the values in table 3 to within 0.02 to 0.07 pK_P units, except for 2,6-dichlorophenol for which their adjusted value is 7.01.

Table 3 also contains values of $\Delta pK(1) \equiv pK$ (calc.) $-pK$ (obs.), the calculated values being obtained from pK values for monosubstituted compounds with the assumption of additivity of the effects of substituent groups. Data for the dinitro-

phenols are given for comparison.[3] It will be seen that, as mentioned in the introduction, large deviations from additivity are noticed in the 2,3- and 2,6-dinitrophenols, i.e., if both nitro groups and the hydroxy group are adjacent to one another. The additivity principle holds much better in the dichlorophenols and the dichloroanilines—only in the 2,6- compounds where both substituents are ortho to the hydroxy or amine group is there marked departure from additivity.

3.3. Hammett Relation

This relation can be expressed by the equation

$$\Delta pK = \rho\sigma$$

where ΔpK is the difference between the pK value of a parent acid and that of one of its substituted derivatives, ρ is a characteristic of the parent acid and, by convention, is taken as unity for benzoic acid; σ is a characteristic of the substituent group or groups.

Jaffé [29] has assigned values of 0.600 and 0.746 to the Hammett σ parameter for 3,4- and 3,5-dichloro substitution, respectively. However, more recent determinations [30, 31] of the ionization constants of 3,4- and 3,5-dichlorobenzoic acid give 3.64 and 3.43, respectively; these lead to 0.56 and 0.77 for 3,4- and 3,5-dichloro substitution, respectively.

Biggs and Robinson [10] measured the ionization constants of a number of monosubstituted anilines and phenols; they expressed the Hammett relation for substituted anilines by the equation

$$pK_A = 4.580 - 2.889\sigma \qquad (5)$$

and for substituted phenols by

$$pK_P = 9.919 - 2.229\sigma. \qquad (6)$$

Substituting the above values of σ in these equations, we calculate pK 2.96 and 2.36 for 3,4- and 3,5-dichloroaniline respectively and 8.67 and 8.20 for 3,4- and 3,5-dichlorophenol, respectively. These differ from the observed values by 0.03, 0.02, 0.08, and 0.01, respectively; the agreement between observed and calculated values is comparable to that found in a series of monosubstituted compounds.

3.4. A Linear Relation Between the pK Values of the Dichloroanilines and Those of the Dichlorophenols

A simple rearrangement of eq (5) and eq (6) with elimination of the σ term leads to a relation between the pK_A value of a monosubstituted aniline and the pK_P value of the corresponding monosubstituted phenol; this takes the form

$$pK_A = -8.275 + 1.296\ pK_P. \qquad (7)$$

Figure 2 is a plot of this equation with points for (1) unsubstituted aniline and phenol and (2) some monosubstituted compounds. Equation (7) is merely a restatement of the Hammett relation avoiding direct reference to substituted benzoic acids.

Figure 2 also contains points for the six dichloroanilines and dichlorophenols which form the subject of this study. It will be seen that the points for the dichloro compounds lie close to a straight line whose slope is nearly but not exactly that of the line for the monosubstituted compounds. By the method of least squares, the best equation for the line through the points for the disubstituted compounds was found to be

$$pK_A = -9.047 + 1.401\ pK_P. \qquad (8)$$

Table 3 gives values of $\Delta pK_A(2) \equiv pK_A$ (calc.) $- pK_A$ (obs.) where pK_A (calc.) is obtained by eq (8). The average value of ΔpK_A (2) is 0.032. Thus the linear relation between pK values of dichloroanilines and

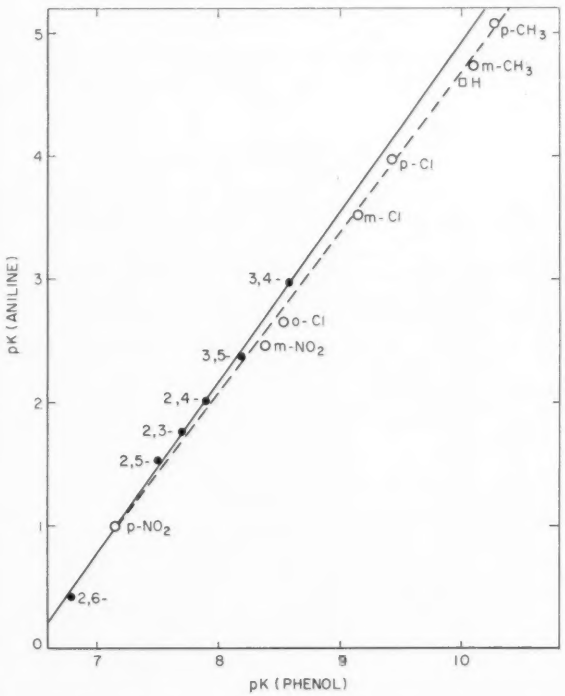

FIGURE 2. pK_A *of an aniline versus* pK_P *of the corresponding phenol.*

□, Aniline-phenol
○, *o*-, *m*-, and *p*- methyl, *o*-, *m*-, *p*- chloro, and *m*- and *p*- nitroanilines and phenols.
●, Dichloroanilines and phenols.
----, Line of the eq (7) $pK_A = -8.275 + 1.296\ pK_P$ for monosubstituted anilines and phenols.
—, Line of the eq (8) $pK_A = -9.047 + 1.401\ pK_P$ for dichloroanilines and phenols.

[3] The $\Delta pK(1)$ values recorded for the dinitrophenols differ slightly from those given previously [1]. The change results from the use of more recent pK determinations of the mononitrophenols. The value now adopted, 7.230 [3], for *o*-nitrophenol is in good agreement with pK 7.234 by Judson and Kilpatrick [8] and 7.229 by Dippy, Hughes, and Laxton [28]. The value of pK 8.355 for *m*-nitrophenol [4] is preferred to the earlier value of 8.399 [10] because the more recent measurements were made in a tris buffer in place of the borax buffer of comparatively low pH used earlier. Judson and Kilpatrick [8] found pK 8.346 for *m*-nitrophenol.

dichlorophenols holds somewhat better than the corresponding linear relation for monosubstituted compounds. What is indeed remarkable is that a linear relation is valid in a series of six dichloro compounds in four of which at least one substituent is in the ortho position. Further study will be needed to ascertain the validity of this linear relation in other disubstituted compounds but there are sufficient data available to show that there are limits. Thus, we have $pK = -1.03$ for 4-chloro-2-nitroaniline [32] and 6.46 for the corresponding phenol [33]; eq (8) predicts $pK = 0$ for this aniline. Again, we have pK 4.57 for 2,5-xylidene [34] and 10.40 for 2,5-xylenol [9]; eq (8) predicts pK 5.52 for 2,5-xylidene. It is clear eq (8) is not valid for 4-chloro-2-nitro substitution nor for the dimethyl compounds, the discrepancy between observed and predicted pK values being 1.03 in the former case and 0.95 in the latter. There is, however, one indication that the validity of eq (8) is not limited to dichloro substitution; Wepster [35] has found pK 1.50 for 4-nitro-*m*-toluidine; pK 7.409 has been found for 4-nitro-*m*-cresol [3] and substitution of this value in eq (8) gives pK 1.33 for 4-nitro-*m*-toluidine, a value only 0.17 below the observed. Further work will be necessary to reveal the applicability of eq (8) to compounds other than the dichloroanilines and phenols.

My sincere thanks are expressed to Adam Peiperl for his assistance in the preliminary stages of the work.

4. References

[1] R. A. Robinson, M. M. Davis, M. Paabo, and V. E. Bower, J. Res. NBS **64A,** (Phys. and Chem.) No. 4, 347 (1960).
[2] A. I. Biggs, Trans. Faraday Soc. **52,** 35 (1956).
[3] R. A. Robinson and A. Peiperl, J. Phys. Chem. **67,** 1723 (1963).
[4] R. A. Robinson and A. Peiperl, J. Phys. Chem. **67,** 2860 (1963).
[5] G. F. Allen, R. A. Robinson, and V. E. Bower, J. Phys. Chem., **66,** 171 (1962).
[6] H. von Halban and G. Kortüm, Z. physik. Chem. **A170,** 351 (1934).
[7] G. Kortüm and G. Wilski, Z. physik. Chem. **2,** 256 (1954).
[8] C. M. Judson and M. Kilpatrick, J. Am. Chem. Soc. **71,** 3110 (1949).
[9] D. T. Y. Chen and K. J. Laidler, Trans. Faraday Soc. **58,** 480 (1962).
[10] A. I. Biggs and R. A. Robinson, J. Chem. Soc. (London) 388 (1961).
[11] L. P. Hammett, J. Am. Chem. Soc. **59,** 96 (1937); Physical organic chemistry, ch. VII (McGraw-Hill Book Co., Inc., New York, N.Y., 1940).
[12] R. G. Bates and G. Schwarzenbach, Helv. Chim. Acta **77,** 1069 (1954).
[13] R. A. Robinson and A. I. Biggs, Trans. Faraday Soc. **51,** 901 (1955).
[14] R. G. Bates and R. Gary, J. Res. NBS **65A,** (Phys. and Chem.) No. 6, 495 (1961).
[15] R. A. Robinson and A. K. Kiang, Trans. Faraday Soc. **51,** 1398 (1955).
[16] H. S. Harned and B. B. Owen, The physical chemistry of electrolytic solutions, p. 716, 3d. Ed., (Reinhold Publ. Corp. New York, N.Y., 1958); R. A. Robinson and R. H. Stokes, Electrolyte solutions, p. 491 (Butterworths Scientific Publications, London, 1959).
[17] B. F. Wishaw and R. H. Stokes, Trans. Faraday Soc. **49,** 27 (1953).
[18] H. S. Harned, J. Phys. Chem. **64,** 112 (1958).
[19] F. J. Kelly, R. A. Robinson, and R. H. Stokes, J. Phys. Chem. **65,** 1958 (1961).
[20] V. E. Bower and R. A. Robinson, J. Phys. Chem. **67,** 1524 (1963).
[21] M. Gillois and P. Rumpf, Bull. Soc. Chim. (France) 112 (1954).
[22] M. A. Paul, J. Am. Chem. Soc. **76,** 3236 (1954).
[23] E. Högfeldt and J. Bigeleisen, J. Am. Chem. Soc. **82,** 15 (1960).
[24] J. N. Brønsted, A. Delbanco, and A. Tovborg-Jensen, Z. physik. Chem. **A169,** 361 (1934).
[25] J. W. Murray and N. E. Gordon, J. Am. Chem. Soc. **57,** 110 (1935).
[26] A. Hantzsch, Ber. **32,** 3066 (1899).
[27] M. Paabo, R. G. Bates, and R. A. Robinson, J. Res. NBS **67A** (Phys. and Chem.) No. 6, 573 (1963).
[28] J. F. J. Dippy, S. R. C. Hughes, and J. W. Laxton, J. Chem. Soc. (London) 2995, (1956).
[29] H. H. Jaffé, Chem. Rev. **53,** 191 (1953).
[30] M. M. Davis and H. B. Hetzer, J. Phys. Chem. **61,** 123 (1957).
[31] J. G. Mather and J. Shorter, J. Chem. Soc. (London) 4744 (1961).
[32] L. P. Hammett and M. A. Paul, J. Am. Chem. Soc. **56,** 827 (1934).
[33] V. E. Bower and R. A. Robinson, J. Phys. Chem. **64,** 1078 (1960).
[34] B. M. Wepster, Rec. Trav. Chim. **76,** 357 (1957).
[35] B. M. Wepster, Rec. Trav. Chim. **76,** 335 (1957).

(Paper 68A2–264)

JOURNAL OF RESEARCH of the National Bureau of Standards—A. Physics and Chemistry
Vol. 68A, No. 2, March–April 1964

Stereoregularity in Ionic Polymerization of Acenaphthylene

V. M. Story and G. Canty

(November 15, 1963)

Four distinct polymers were isolated from the polymerizations of acenaphthylene initiated by boron trifluoride and *n*-butyllithium. A syndiotactic or isotactic conformation was assigned to these products on the basis of infrared and NMR evidence. The conformations and reaction details are discussed.

1. Introduction

A survey of the field of stereoregular polymers indicated that little has been done in deliberate control of chain conformation by means of steric hindrance of bulky groups [1].[1,2] In this sense, acenaphthylene as a vinyl monomer was particularly interesting due to the extreme bulk and rigidity of the 1,8-perinaphthylene residue. Additional features were its strained five-membered ring [1a] and well defined conditions for polymerization.

The polymers of acenaphthylene have been extensively investigated. Dziewonski and his coworkers [2] were able to show ionic, thermal, and solid-state polymerization of acenaphthylene before the present-day tools for measuring high molecular weights were available. Their investigations started in 1912 and ended in 1924. Since then, other workers have examined these polymers. Jones [3] and Flowers and Miller [4], for example, have conducted extensive investigations. The only paper on the mechanism of this polymerization was by Imoto and Takemoto [5], using boron trifluoride etherate as an initiator. It should be emphasized that very little was done to measure molecular weights of these polymers [6] and no reference to possible stereoregularity was found.

A study of Fisher-Hirschfelder models of acenaphthylene polymers was made. The *cis*-isotactic polymer I, where A is in the plane of the paper and the B's are in a parallel plane below, was self-terminating. Ring formation was favored. In fact, both a cyclic trimer and tetramer are known [2]. The *cis*-syndiotactic polymer II was impossible to construct beyond the trimer.

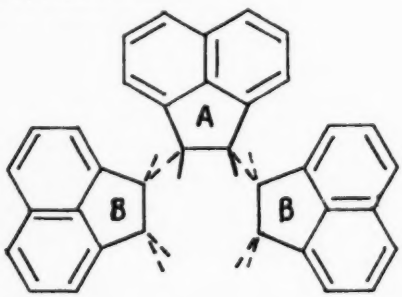

I

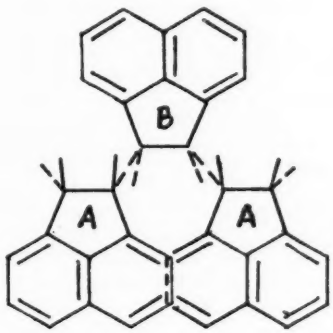

II

The same notation is used here as for I above. The A's were actually twisted out of plane due to steric hindrance. *trans*-Isotactic polyacenaphthylene, III, formed a helix.[3]

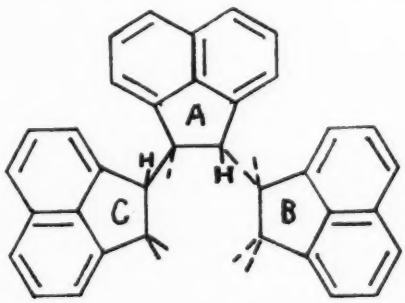

III

[1] Figures in brackets indicate the literature references at the end of this paper.

[2] Note added in proof: The paper by G. Natta, G. Dall'Asta, G. Mazzanti, and G. Metroni (Makromol. Chem. **69**, 124, 1963) describes the polymerization of cyclobutene with Ziegler catalysts. The stereochemistry of the products are apparently identical with the case described here. Instead of *cis* or *trans*, the nomenclature *threo* or *erythro*, respectively, is used.

[3] The limited rotation about the backbone carbon-carbon bonds due to steric hindrance of the 1,8-acenaphthylene residues suggests that change in the sense of the helix of III is not possible if a penultimate effect influences the course of addition. Of course, a mixture of *d* and *l* chains would be produced, unless an assymetric initiator were used.

In this diagram, C is in a parallel plane above the paper, A is in it, and B below it. Similarly, the *trans*-syndiotactic polymer, IV, formed a "stair-stepped" rigid rod. The same

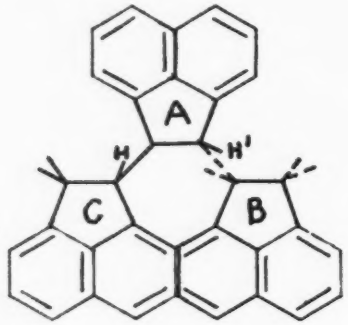

IV

notation is used here as in III. The tertiary aliphatic protons (H) are on the inside of the helix in III and are 1,3-axial. In IV, these protons are isolated (to use the same nomenclature, they are 1,3-equatorial) from each other. H′ is adjacent to the *ortho* aromatic protons of the next residue above (C) and to the π cloud of the residue below (B).

The products of the polymerization of acenaphthylene with boron trifluoride and *n*-butyllithium initiators were investigated for conformations corresponding to III and IV above.

2. Experimental Details

2.1. Materials

Acenaphthylene (Aldrich Chemical Company) was sublimed twice in a vacuum apparatus. The melting point found was 92.5–93 °C. The literature value is 92–93 °C [7]. Boron trifluoride (Matheson Company, Inc.) was transferred to a glass vacuum-line and distilled twice, from a 2,2,4-trimethylpentane slush bath (−107.4 °C), to a trap cooled by liquid nitrogen. The vapor pressure of the redistilled boron trifluoride was found to be 458 mm Hg at −107.4 °C. The literature value is 466 mm Hg [8]. Chlorobenzene and benzene (Fisher Analyzed reagents) were used without further purification. An *n*-butyllithium preparation in *n*-heptane (Foote Mineral Company, Inc.) was used as received.

2.2. Procedures

a. Polymerizations Initiated by Boron Trifluoride

The acenaphthylene was weighed into a round-bottomed flask containing a Teflon-encased magnetic stirring-bar. Chlorobenzene was added and the flask was connected to a vacuum line. The flask contents were degassed by three freeze-pump-thaw cycles. A measured volume of boron trifluoride was transferred to the frozen solution. The flask contents were permitted to warm to the required reaction temperature with stirring. The color of the reaction mixture varied from deep green to black. On completion of the reaction, the flask was vented to the air. This did not cause much color change, and presumably did not destroy all of the complex. On pouring the flask contents into boiling methanol, all color disappeared (except that of residual monomer) and a dense, white precipitate coagulated from the reaction mixture. The precipitate was filtered off, washed with cold methanol, air-dried, and dissolved in benzene, and the solution was filtered through anhydrous sodium sulfate and freeze-dried. The filtrate from the original precipitation was vacuum-evaporated. Any resulting residue was treated in the same way as for the original precipitate.

Co-initiators were added to the acenaphthylene solutions before connection to the vacuum line. In these cases, degassing was confined to one freeze-pump-thaw cycle.

A strong Tyndall effect was observed in all reaction mixtures. However, no solid separated out during or after the reactions. When sufficient water was used as a co-initiator, it was observed as ice droplets in solution or film on the sides of the flask.

b. Polymerization Initiated by *n*-Butyllithium

The reaction was conducted as above, except that the *n*-butyllithium solution was added through a rubber disk with a hypodermic syringe and needle. Again, the complex formed was dark green to black in color. Admission of air immediately destroyed all traces of color. After the solution had been vented to the air, it was extracted twice with 0.1 *N* HCl and washed three times with water. The organic layer was then treated as in (a) above, by precipitation in boiling methanol, etc.

2.3. Physical Properties

Intrinsic viscosities were determined in the standard manner at 35 °C in benzene. Infrared spectra were determined on a Perkin-Elmer 221 with a grating interchange. NMR spectra were obtained, for all polymers isolated, on a Varian A–60 instrument. Carbon tetrachloride was used as the solvent [11] and tetramethylsilane as the external standard. Ultraviolet spectra were made on a Cary Model 14 in benzene at 25 °C. X-ray photographs of powder specimens were taken with a Debye-Scherrer camera, using copper $K\alpha$ radiation.

3. Results and Discussion

The results of the polymerizations of acenaphthylene, initiated by boron trifluoride and *n*-butyllithium with and without cocatalysts, are listed in table 1.

TABLE 1. *Ionic polymerization of acenaphthylene*

Reaction number	$C_{12}H_8$ $[M]$ [2,3]	Initiator,[1] $[I] \times 10^4$	Co-initiator type	Co-initiator conc. $[M] \times 10^4$	Reaction time	Yield
I. Initiation by boron trifluoride						
1	2.35	const.[4]	H_2O [5]	----------	45 min	92.4 [6]
2	2.35	const.[4]	H_2O [5]	----------	4 days	82.4 [6]
3	2.35	const.[4]	H_2O [5]	----------	6 days	89.0 [6]
4	2.35	const.[4]	H_2O [5]	----------	8 days	90.1 [6]
5	0.211	48.1	none [7]	----------	30 min	84.2
6	.211	45.0	none	----------	30 min	87.0
7	.211	35.1	none	----------	30 min	86.8
8	.211	11.3	none	----------	30 min	74.3
9	.211	6.67	none	----------	30 min	82.3
10	.211	32.7	CH_3OH [7]	2.4	30 min	30.2 [8]
11	0.201	8.85	CH_3OH [7]	61.8	30 min	0.0
12	.201	29.1	H_2O [7]	55.6	22 min	69.1
13	0.343	17.4	H_2O [7]	139	30 min	82.4
14	.358	13.9	H_2O [7]	556	30 min	49.6
15	.516	12.2	H_2O [9]	----------	30 min	87.6
II. Initiation by *n*-butyllithium [10]						
16	0.075	6.0	(?)	----------	24 hr	7.0
17	.028	30	----------	----------	24 hr	0.7

[1] $[I]$ indicates the concentration (moles per liter) of ionic initiator if it all dissolved in the monomer solution.
[2] The solvent for these reactions was chlorobenzene. Reactions 1–4 were done at −5 °C and the remainder at −23 °C.
[3] $[M]$ indicates the concentration of acenaphthylene in moles per liter.
[4] A slow flow of BF_3 was supplied to the reaction mixture.
[5] Traces of water were present.
[6] These reaction products were precipitated from cold methanol.
[7] See experimental section for details.
[8] The product soluble in boiling methanol was 30.2%, the insoluble, 2.0%.
[9] Moist air was admitted to the reaction flask during the run.
[10] The solvent was benezene. The reaction temperature was 21 °C. The calculated molarity of *n*-butyllithium in the final solution is reported.

The first four reactions in table 1 duplicate the procedure of Flowers and Miller [4]. It was found that the yields from precipitation of the reaction mixture in cold methanol were not reproducible. The polymeric product was observed to redissolve on standing in the methanol-chlorobenzene mixture. An exhaustive extraction of a portion of polymer precipitated in the above manner showed an 11 percent weight loss. Since the methanol-soluble material showed the same spectra as the parent polymer in the ultraviolet region, it was concluded that oligomers were being extracted. To circumvent the coprecipitation of the oligomers, hot (boiling) methanol was used as the precipitating medium. The precipitated polymer isolated by this method will be designated "insoluble" and the product isolated from the supernatant hot methanol-chlorobenzene solution by cooling and vacuum evaporation will be designated "soluble" in the following discussion.

The residue left after isolating both the "insoluble" and "soluble" polymers was determined to be 90 to 95 percent monomer in all cases. The "insoluble" polymer isolated in the above series was designated type G.

Reactions 5 through 9, table 1, were performed using anhydrous boron trifluoride as initiator. The average total recovery, calculated on the basis of monomer weight, was 97.6 percent. The "soluble" polymer isolated in reaction 7 proved to be similar to the "insoluble" one, but of lower molecular weight.

When water or moist air was used as a cocatalyst (reactions 12 through 15, table 1), the pooled "soluble" polymer for reactions 13, 14, and 15 showed properties different from those of the "insoluble" polymer obtained in the same reactions, as described below in terms of their respective physical properties. It was designated type K.

The most striking change in products was observed when a small amount of methanol was added as co-initiator. In this case (reaction 10, table 1), the "soluble" polymer was the predominant component and proved to be a different macromolecular species, designated type M. The small amount of "insoluble" polymer recovered in this reaction was type G. Increase of the concentration of methanol co-initiator completely inhibited polymer formation, as the data for reaction 11 in table 1 indicate.

The polymerizations of acenaphthylene initiated by *n*-butyllithium gave low yields for the conditions chosen, as shown in table 1, reactions 16 and 17. The separation procedure given above for the polymerizations initiated by boron trifluoride did not give definitive results, because of low yields. The product isolated was different from all others described above and was designated type N.

The physical properties of the polymer types described above are summarized in table 2.

TABLE 2. *Polymeric products of polymerization of acenaphthylene*

Polymer type [1]	Reaction (table 1)	Solubility [2]	[3] $[\eta]^{35°}_{C_6H_6}$	ϵ_A [4]
G	1–4	0	0.039±0.004	6860
	5–9	0	.034±0.001	6870
	7	+	.025 [5]	6570
	10	0	(6)	----------
	12–15	0	.047±0.002	6890
K	12–15	+ [7]	.029	6500
M	10	+	.028	5900
N	16, 17	(8)	.036, 0.100 [9]	6080

[1] The polymer types are as designated in the text.
[2] The solubility refers to the boiling methanol chlorobenzene mixture from which the polymer is precipitated, as described in the experimental section. Reactions 1–4 were precipitated in cold methanol.
[3] Two-point viscometric determinations were made. The $[\eta]$ values were corrected for the presence of 11% oligomer for reactions 1–4 and all "soluble" products (see text). The mean and the average deviation from the mean is reported.
[4] The extinction coefficient was calculated per acenaphthylene residue. The determinations were done in benzene at 2960 Å and at 25 °C. The average error was 2%.
[5] The physical properties were determined on one sample, reaction 7, table 1.
[6] Product was identified by its infrared spectrum. See text for details.
[7] The properties of a pooled sample were determined.
[8] The yield was too low to permit determination of the solubility.
[9] The intrinsic viscosities of the two products were widely different, due to varying experimental conditions (table 1).

3.1. Physical Properties

a. Viscosities and Molecular Weights

Several molecular-weight determinations were made, to index the viscosity determinations given in table 2. An osmotic-pressure determination of one of the polymerization products ($[\eta]^{35°}_{C_6H_6}$=0.036, reaction 1, table 1) initiated by boron trifluoride gave the value 7,070 for a number-average molecular weight. The large effect of molecules of very low molecular weight on this type of measurement led us to make the same determination with a vapor-pressure osmometer. The value 2,670 was obtained

by this means. This is reasonable in view of the low molecular weights and the absence of extensive purification. Taking 3,000 as an approximate number-average molecular weight, the mean degree of polymerization was about 20.

Two groups of workers have reported on the number-average molecular weight of polymers of acenaphthylene initiated by boron trifluoride. Flowers and Miller [4] stated that the moleuclar weight by osmometry was about 150,000. Imoto and Takemoto [6] reported an intrinsic viscosity of 0.040 (30°C, in benzene) and a number-average molecular weight of 125,000 using a collodion membrane. Both the above papers mention "repeated reprecipitation in methanol" from benzene solutions. However, the intrinsic viscosity value reported in the second paper indicated that extensive purification was not obtained, compared to the methods used in this study. We were not able to resolve these large discrepancies.

b. Infrared Spectra

The saturated, tertiary carbon atoms of the backbone of polyacenaphthylene would be expected to show different C—H stretch frequencies for the *trans*-syndiotactic and *trans*-isotactic polymers. Figures 1 and 2 show the C—H stretch spectra corresponding to the four polymer types isolated in this investigation. Polymer type G, table 2, corresponds to spectrum A, figure 1; type K to spectrum B; type M to C; and type N to D and E in figure 2.

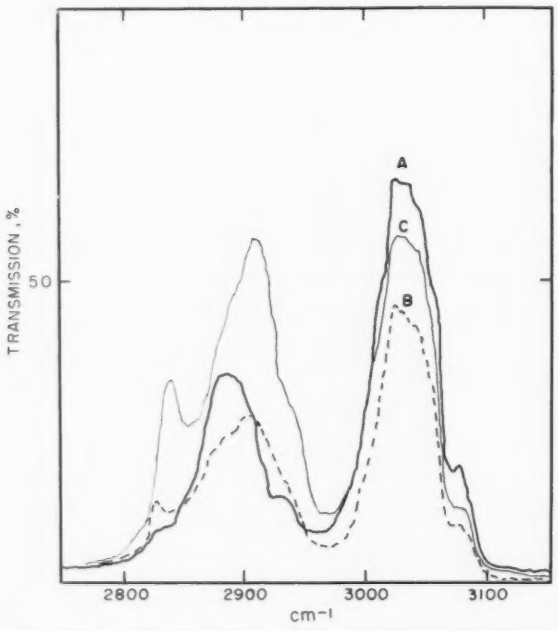

FIGURE 1. *Type G polymer, spectrum* A; *type K, B; and type M, C.*

Ordinates, cm⁻¹; abcissae in arbitrary percent transmission.

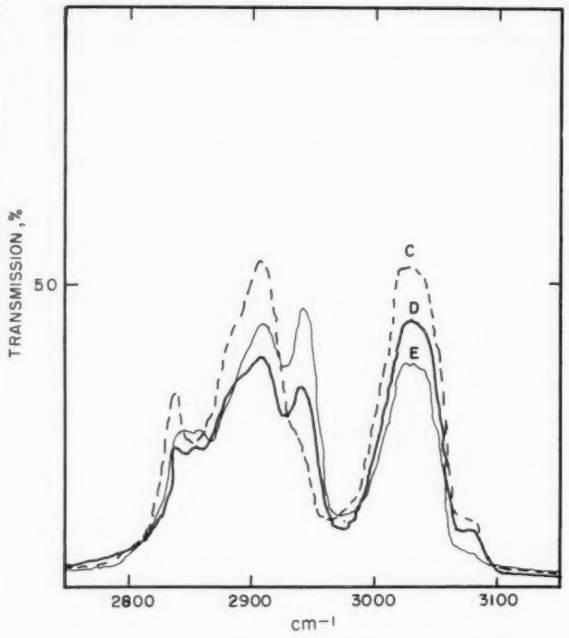

FIGURE 2. *Type M polymer, spectrum* C; *type N, spectra* D *and* E.

D is the spectrum of the product isolated from reaction 16, table 1, and E of that from reaction 17. Ordinates, cm⁻¹; abcissae in arbitrary percent transmission.

The frequencies of the aliphatic C—H stretch bands of these spectra are listed in table 3, together with those of the *cis*- and *trans*-declains and acenaphthene. Although the frequencies are accurate to ± 5 cm^{-1} in this study, comparison with other spectra from the literature are probably accurate to only ± 10 cm^{-1} because of resolution differences and changes of state.

The assignment of the aliphatic C—H stretch frequency of type G polyacenaphthylene is straightforward and unambiguous, since it is almost exactly the 2890 ± 10 cm^{-1} for tertiary C—H established by Fox and Martin [9]. This frequency assignment corresponds to the syndiotactic *trans* polymer (IV), as an isolated tertiary aliphatic C—H bond is unique to this structure.

Spectrum B, figure 1, contains frequencies common to both A and C. We will discuss spectrum C first, to clarify its assignments, before considering B.

A Fisher-Hirschfelder model for the *trans*-isotactic polymer, III, required 1,3-axial proton interactions similar to those of the axial bonds of cyclohexane. The closest analogs found were *cis*- and *trans*-decalin. As shown in table 3, the asymmetric C—H stretch frequency of spectrum C (type M polymer) is at 2908 cm^{-1}, which is 16 cm^{-1} below that of *cis*- and *trans*-decalin at 2924 cm^{-1}. By invoking a limited degree of chain flexibility for polymer configuration III, the decrease in frequency can be attributed to lower "1,3" proton-interaction energy as compared to that of the model compounds.

TABLE 3. *Aliphatic* C—H *infrared frequencies* [1]

Decalin [2]		Acenaphthylene	Polyacenaphthylene [3]			
trans-	cis-		A (type G)	B (type K)	C (type M)	D & E (type N)
2924	2924	2910	2887	2908 2887	2908	2942 2908
2857	2841	2875 2865		2840	2840	2860 2843

[1] The frequencies are given in cm^{-1}; the solvent was carbon tetrachloride, unless otherwise stated.
[2] From American Petroleum Institute, Infrared Spectra 1086 and 1087, respectively. These were spectra taken on pure liquid samples.
[3] The letter designations correspond to the spectra in figures 1 and 2. The type designations are given in the text.

The symmetric C—H stretch frequency at 2840 cm^{-1} for spectrum C corresponds exactly with that of *cis*-decalin. As has been shown by nuclear magnetic resonance spectra [10], *cis*-decalin has one averaged proton-proton interaction, since the ring system is flexible. This fact suggests that the aliphatic protons in polymer M are predominantly 1,3-axial and do not interact with aromatic protons.

With the above assignments in mind, spectrum B can be rationalized as indicating the presence of either a mixture of types G and M, or a block copolymer. Spectra D and E, figure 2, corresponding to type N polymer, are clearly related to spectrum C, but have two more peaks, at 2860 and 2942 cm^{-1}. The first of these can be assigned to the C—H stretch frequency of the CH_2 group, as shown for *trans*-decalin, table 3, and the second to a combination of CH_2 and CH_3 frequencies. This reasoning is based on the assumption that *n*-butyl groups, derived from the *n*-butyllithium initator, were appended to one end of the polymer chain.

c. Nuclear Magnetic Resonance (NMR)

Acenaphthene was investigated as a reference compound under the same conditions as for the polymers. This compound has nine peaks in the aromatic proton range, from 7.07 to 7.54 parts per million of the applied magnetic field (ppm) [12, 13] and a sharp peak at 3.23 ppm corresponding to the secondary aliphatic protons. The latter value is higher than that for aliphatic protons on alkyl groups; for instance, a cyclohexane NMR spectrum gives 1.43 ppm [14]. Acenaphthene is known to have a strained ring [1a], and this fact possibly accounts for a higher screening-constant, because of reduction of the bond angle between the geminal protons.

The aromatic-proton peaks characteristic of acenaphthene were smeared into a broad peak in the same location for all of the polymer spectra. Only type G and type M polymers showed the sharp peaks characteristic of the aliphatic protons. The field shift for type G was 7.25 ppm, and for type M, 1.20 ppm.

The model studies and infrared assignments above required that the III structure have its tertiary aliphatic protons 1,3-axial to each other and on the inside of a helix. Close examination of such structures led to the conclusion that the nearest neighbor interactions were small, due to the flexibility of the backbone. The value found for M, 1.20 ppm, is in complete agreement with this reasoning, and comparison with the NMR spectra of cyclohexane (loc. cit.) supported this argument.

The structure predicted for G, IV above, showed close proximity of the tertiary protons to the π-electron "cloud" and to aromatic protons of adjacent aromatic residues. The chemical shift is expected to be high due to high screening of aromatic rings. The value found for G, 7.25 ppm, is in accord with structure IV.

These NMR spectra complemented the infrared assignments and indicated that the tertiary-proton environments are those predicted from the model studies of polymers G and M. Type K polymer remained indeterminate in structure, since no further information was acquired as to whether it was a mixture or a copolymer. The NMR spectrum for type N was not resolved, due, no doubt, to its higher molecular weight. (High-temperature equipment was not available to increase the resolution.) However, the infrared evidence indicated that N is a derivative of III.

d. Ultraviolet Spectra

It would be expected that *trans*-isotactic polyacenaphthylene would be less accessible to solvent interaction, due to its helical conformation (III), than the *trans*-syndiotactic polymer (IV) and thus show a lower extinction coefficient. The results shown in table 2 support this contention. These data are considered here to be supplementary supporting evidence for the proposed configurations.

e. X-ray spacings

Powder specimens of polyacenaphthylene designated type G, M, and N gave the Bragg spacings shown in table 4. The powder photographs were not sharp. The larger spacings useful for determining the chain conformation were not resolved. There were several spacings which were significantly different among the three polymer types. The 2.81 Å spacing for type G, and the 5.27 Å spacing for type N were clearly different. The 10.8 Å spacing for type M was not significantly different from the

TABLE 4. *Bragg spacings for polyacenaphthylene* [1]

Type G	Type M	Type N	Relative intensity [2]
2.07	2.07	2.06	vw
2.81	2.76	2.75	w
3.95	3.91	3.95	s
5.47	5.47	5.27	m
10.3	10.8	10.4	vs

[1] The spacings are given in angstrom units, and the type designations are given in the text.
[2] vw indicates very weak, w weak, m medium, s strong, and, vs very strong relative intensities.

10.3 and 10.4 Å spacings for types G and N, respectively. Thus, although differences were apparent, no definitive analysis could be made of these data to determine the crystal structures of the polymer types.

3.2. Mechanism

It is useful to consider the chemical nature of initiator and co-initiator complexes before inquiring into the polymerization process. Greenwood and Martin have shown that stable complexes are formed when boron trifluoride reacts with water or methanol [15]. They have also shown that the compounds hydroxyfluoroboric acid ($H^+BF_3OH^-$), dihydroxyfluoroboric acid ($H_3O^+BF_3OH^-$), methoxyfluoroboric acid ($H^+BF_3OCH_3^-$), and dimethoxyfluoroboric acid ($H_2OCH_3^+BF_3OCH_3^-$) have definite and large conductivities in the melt [16]. These data are reported in table 5 in terms of percent ionization in the melt, together with the melting points of the fluoroboric acid compounds measured by the same authors. As solids, these compounds are reported to be partially ionized if crystallized rapidly from solution [17]. Other evidence [18] favors the ionic structures indicated in the empirical formulas. The relative amounts of ionization of the methoxyfluoroboric acids are supported by the calculations of Bender [19] from the equation of Edwards [20]. Bender's calculations indicate that methanol is a stronger nucleophile than water. Thus, the methoxyfluoroboric acid compounds would be expected to show less ionization than the comparable hydroxyfluoroboric acids, in agreement with the results in table 5.

TABLE 5. *Properties of fluoroboric acid complexes* [1]

Acid complex	MP	Ionization [2]
	°C	%
$H^+BF_3OH^-$	5.9–6.0	10
$H_3O^+BF_3OH^-$	6.2	20
$H^+BF_3OCH_3^-$	−18.6	2
$H_2OCH_3^+BF_3OCH_3^-$	−58.1	7

[1] The references are given in the text.
[2] The ionization was measured in the melt at 20 °C.

On the basis of infrared spectra, the greater ionization of the dihydroxyfluoroboric and dimethoxyfluoroboric acids as compared to the corresponding mono-acids (table 5) is attributed by Babushkin et al., to dimer formation, as contrasted to polymer formation for the 1:1 compounds [21]. Diehl [22] reports NMR evidence in accord with this conclusion.

Comparison of the melting points for the fluoroboric acid complexes given in table 5 with the experimental conditions for acenaphthylene polymerization given in table 1 suggest that all but one of the reactions initiated by boron trifluoride were conducted under heterogeneous conditions. As Clark has pointed out [25], traces of water are present even when extreme care is taken to produce 'anhydrous' boron trifluoride for vinyl polymerizations. The observed Tyndall effect must be due to the initiator complex present as a finely divided solid since the polymer is soluble in chlorobenzene. Thus, the fluoroboric acid compounds are solid under the given reaction conditions, as was excess water, but not methanol. In reaction 11, the initiator complex would be dissolved in excess methanol, in contrast to 10 where heterogeneous initiation is expected.

Several attempts were made to determine the rates of polymerization of acenaphthylene under the conditions of experiment 6, table 1. Reaction times as short as 20 sec gave the same yields. It was not feasible to extend these experiments to shorter reaction times.

The deliberate addition of water or methanol had a variable effect on the yield (reactions 10 through 15). With the exception of reaction 13, the excess of co-initiator over the initiator (on a molar basis) depressed the yield as well as changed the nature of the product. These facts suggest that the addition of co-initiator inhibits the formation of both polymers, but that the inhibition is greater for the isotactic product. The exact cause of the increase in yield of reaction 13 compared to 12 and 14 is not known.

Reactions 1 through 4 are comparable to reactions 6 through 9 in yield when corrected for oligomer concentration. These reactions were probably initiated by hydroxyfluoroboric acid while reactions 12 through 15 were initiated predominantly by dihydroxyfluoroboric acid. The degree of polymerization of reactions 12 through 15 was higher (table 2) with respect to the *insoluble* product (type G).

The above discussion is certainly oversimplified, since *both* hydroxyfluoroboric acids are present at all times, but in different proportions [18]. However, we have argued in terms of the predominant species for the sake of clarity.

Before proceeding to the case of acenaphthylene polymerization by initiation with methoxyfluoroboric acid, it is profitable to review the details of acenaphthylene polymerization initiated by hydroxyfluoroboric acid. Consideration of the pertinent data in table 1 show that temperature (footnote 3, table 1), monomer concentration, and reaction time have no discernible effect on the yield under the given reaction-conditions. The degree of polymerization of the products increases when the water concentration increases. The extinction coefficients for the polymers given in table 2 indicate that small amounts of the *trans*-isotactic polymer are present in the "soluble" product. Whether or not the isotactic polymer is or is not present as part of a block copolymer remains undecided. However, a block copolymer is unlikely at these low degrees of polymerization. The primary conclusion from the structure assignments and discussion above is that solid hydroxyfluoroboric acids give, predominantly, *trans*-syndiotactic polyacenaphthylene. It is probable, but not so well established, that the stronger dihydroxyfluoroboric acid decreases the yield, but increases the degree of polymerization.

With the above summary in mind, the heterogeneous initiation of acenaphthene polymerization by methoxyfluoroboric acid (reaction 10, table 1) has only one difference from initiations by the hydroxy-

fluoroboric acids. As shown in table 5, methoxyfluoroboric acid is a distinctly weaker acid or, alternatively, a stronger nucleophile. The predominant polymer found is *trans*-isotactic polyacenaphthylene, with traces of the *trans*-syndiotactic polymer, in contrast to the polymerizations of acenaphthylene by hydroxyfluoroboric acids. It follows that the methoxyfluoroboric acid anion stabilizes the carbonium ion formed after donating its proton to acenaphthylene. Furthermore, the propagating polymer carbonium ion must be stabilized. The increase in nucleophilicity of the methoxyfluoroboric acid over the hydroxyfluoroboric acids is enough to favor formation of the *trans*-isotactic polymer carbonium ion over the corresponding *trans*-syndiotactic carbonium ion. The high steric hindrance of the *trans*-isotactic carbonium ion indicates that a "sufficiently stable" complex must last longer than the comparable syndio carbonium ion, since three of the six Cartesian axes are accessible to monomer attack, compared to four in the *trans*-syndio carbonium ion.

Turning now to acenaphthylene polymerization by *n*-butyllithium, we find a clear precedent set for us. Worsfold and Bywater [23] have shown that previously reported cases of stereoregular polymerization of styrene [24] by *n*-butyllithium in aromatic solvents were dependent on the presence of traces of water. The experiments reported here did not rigorously exclude water in the acenaphthene polymerization with *n*-butyllithium initiation. The product obtained was *trans*-isotactic polyacenaphthylene with *n*-butyl end-groups (loc. cit.).

Although Worsfold and Bywater [23] did not believe that their experiments decided the question of "whether a colloidal surface is necessary," their reactions were run at −30 °C where any added water is certainly frozen to ice. The generation of lithium *n*-butoxide without complete destruction of the initiator probably creates a situation analogous to that discussed above, where mixtures of solid compounds act as stereoregular initiators. The same reasoning applies in detail to reactions 15 and 16 in table 1.

The discussion above leads to the conclusion that all of the effective initiators used were heterogeneous. The nucleophilicity of the fluoroboric acid complex determined the stability of the initiating and propagating carbonium ion and, hence, the predominant stereoregular product. Traces of ice reacting with *n*-butyllithium were probably instrumental in inducing heterogeneous initiation of acenaphthylene polymerization.

4. Summary

The four polymers isolated from acenaphthylene polymerizations initiated by boron trifluoride and *n*-butyllithium were shown to correspond to syndiotactic or isotactic structures on the basis of infrared and NMR spectra. The syndiotactic polymer had a "rod" conformation, and the isotactic, a helix.

We thank J. H. O'Mara for determining the osmotic pressure and W. T. Meyer for determining some of the viscosities. A. Diorio kindly made the powder x-ray photographs. We appreciate helpful discussions with Dr. J. P. Kennedy of Esso Research and Engineering Co., Inc.

5. References

[1] M. Farina and G. Byessan, Makromol. Chem. **61,** 79 (1963).
[1a] H. W. Ehrlich, Acta Cryst. **10,** 699 (1957).
[2] K. Dziewonski and Z. Lylso, Ber. **47,** 1769 (1914); K. Dziewonski and T. Stolyluwo, ibid. **57,** 1531 (1924).
[3] J. I. Jones, J. Appl. Chem. **1,** 568 (1951).
[4] R. G. Flowers and H. F. Miller, J. Am. Chem. Soc. **69,** 1388 (1947).
[5] M. Imoto and K. Takemoto, J. Polymer Sci. **79,** 271 (1955).
[6] Reference 3, 4, and M. Imoto and I. Somatsu, Bull Chem. Soc. Japan **34,** 26 (1961).
[7] A. Behr and W. A. van Dorp, Ber. **6,** 60, 753 (1873); Ann. **172,** 263 (1874); A. Behr and M. Blumenthal, Ber. **7,** 1092 (1874).
[8] O. Ruff. A. Braida, O. Bretschneider, W. Menzel, and H. Plaut, Z. Anorg. Allgem. Chem. **206,** 59 (1932).
[9] J. J. Fox and A. E. Martin, Proc. Roy. Soc. (London), **A175,** 208 (1940).
[10] J. A. Pople, W. G. Schneider, and H. J. Bernstein, High resolution nuclear magnetic resonance spectroscopy, pp. 399 (McGraw-Hill Book Co., New York, N. Y., 1959).
[11] For a discussion of errors due to this type of standardization, see reference 12, pp. 78, 87, and 98.
[12] $\delta(\text{ppm}) = \frac{H_{\text{TMS}} - \text{H}}{H_{\text{TMS}}} = \frac{V - V_{\text{TMS}}}{60} = \frac{\mu}{60}$, the chemical shift, where H refers to the magnetic-field shift, V is the field shift in cycles per second, and the subscript TMS refers to tetramethylsilane.
[13] Benzene gives $\delta = 7.37$.
Spectrum N-53, Catalogue of NMR spectra (Varian Associates, Inc., 1962, Palo Alto, Calif.).
[14] Reference 15, Spectrum N-122.
[15] N. N. Greenwood and R. L. Martin, J. Chem. Soc. **1951,** 1915.
[16] N. N. Greenwood and R. L. Martin, J. Chem. Soc. **1953,** 1427, 757.
[17] P. T. Ford and R. E. Richards, J. Chem. Soc. **1956,** 3870.
[18] J. A. Nieuland, R. R. Vogt, and W. H. Foohey, J. Am. Chem. Soc. **52,** 1018 (1930); L. J. Klinkenberg and J. A. A. Ketelaar, Rec. trav. chim. **54,** 959 (1935); J. L. Hoard, S. Geller, and T. B. Owen, Acta Cryst. **4,** 405 (1951); J. F. McKenna and F. J. Sowa, J. Am. Chem. Soc **59,** 470 (1937); N. F. Toussant and G. F. Heunion, ibid. **62,** 1145 (1940); C. E. Welsh and G. F. Hennion, ibid. **63,** 2603 (1940).
[19] M. L. Bender, Chem. Revs. **60,** 62 (1960).
[20] J. O. Edwards, J. Am. Chem. Soc. **78,** 1819 (1956).
[21] A. A. Babushkin, L. A. Gribov, N. G. Guseva, and V. M. Emel'yanova, Opt. i Spektroskopiya, **5,** 256 (1958).
[22] P. Diehl, Helv. Phys. Acta **31,** 385.43 (1958).
[23] D. J. Worsfold and S. Bywater, Makromol. Chem. **65,** 245 (1963).
[24] D. Braun W. Betz, and W. Kern, Makromol. Chem. **42,** 89 (1960); R. J. Kern, Nature (London) **187,** 410 (1960).
[25] D. Clarke in Cationic polymerization and related complexes. p. 90, P. H. Plesch, Ed. (Heffner, Cambridge, England, 1953).

(Paper 68A2–265)

JOURNAL OF RESEARCH of the National Bureau of Standards—A. Physics and Chemistry
Vol. 68A, No. 2, March–April 1964

Dielectric Behavior of the Film Formed on Mica Cleaved in Moist Air

S. Ruthberg and L. Frenkel

(September 18, 1963)

Water adsorbed on a freshly peeled mica crystal causes the loss tangent, D, to increase by 1 to 2 orders of magnitude. The nature of the film is investigated as a function of relative humidity by the measurement of D for the frequency range 100 to 50,000 c/s with a capacitor comprising concentric, parallel, circular electrodes of different diameter on opposite sides of the dielectric sheet. This geometry is then analyzed as consisting of the two regions of that within the plates where the electric field, E, is normal to the dielectric plane and that at the edge where tangential E exists. The first is considered in terms of an equivalent circuit for a two layered dielectric. The second is considered in terms of transmission line concepts. It is predicted and verified that the adsorbed film causes the first component to vary as $1/t$ and the second as $\sqrt{t}$ where t is the thickness of the crystal. Numerical solutions are used to derive the behavior of D, R, and C of the adsorbed film itself. D for the normal direction is $\sim$0.4 and follows a frequency dependency like fresh snow. Resistivities normal to and parallel to cleavage are considerably different while C is much less than expected for a surface film. It is suggested that the surface film is not continuous but instead is localized in patches.

1. Introduction

The nature of adsorbed water on cleaved mica has long been of interest for its effects on the insulation quality of the material and on the force necessary to split the crystal [1–4].[1] Previous measurements of electrical losses in the presence of moisture have shown the effect to be transient and of a complex behavior [5–13].

The present paper reports results of a study of the a-c properties of the adsorbed film. The effort was to study the conductivity parallel to, as well as normal to, the cleavage plane and to derive a further understanding of the structure of the film itself.

Our examination of the material consisted of the measurement of the loss-tangent for the frequency range 100 to 50,000 c/s, for the relative humidity range of about 6 to 60 percent, and for specimens cleaved to a number of thicknesses. Various capacitor arrangements were used, with one in particular consisting of a sheet of the dielectric with one large circular electrode and one small circular electrode on opposite faces. The procedures used and typical results obtained are discussed in section 2. In section 3, the asymmetrical capacitor is analyzed in terms of two regions. One is that between the electrodes where the E field is always perpendicular to the cleavage plane and the other is that at the edge of the electrodes where there is a parallel component of E. The behavior of the domain within the normal field is analyzed as a two-layered dielectric, mica sheet plus surface film. The region at the edge is considered in terms of transmission line concepts. From these considerations, relationships are derived for dependency of loss tangent on thickness of the dielectric, for a separation of normal and parallel effects, and for deduction of adsorbed film characteristics. The applicability of these expressions was tested by studying the change in loss tangent with thickness and the amount of field fringing as is reported in section 4. Finally, some conclusions on the nature of the film itself are presented in section 5.

2. Experimental Procedures and Nature of Loss Tangent

2.1. Specimens

Specimens used for this work were obtained from the Defense Materials Service of the General Services Administration and were selected for quality (ASTM visual Classification V–1 to V–4 [14]) by the mica experts of that organization. Original samples varied in thickness from about 0.15 to 0.38 mm. All had been well aged since last cleaved.

2.2. Apparatus

A micrometer-driven dielectric sample holder of the Hartshorn type (General Radio Co. Model 1690–A) was modified by placing a cap over the upper movable plate which reduced the 2 in. diam to 1 in. diam. The resultant capacitor was as sketched in figure 1. The upper plate was driven onto the mica sheet so that the specimen was clamped

[1] Figures in brackets indicate the literature references at the end of this paper.

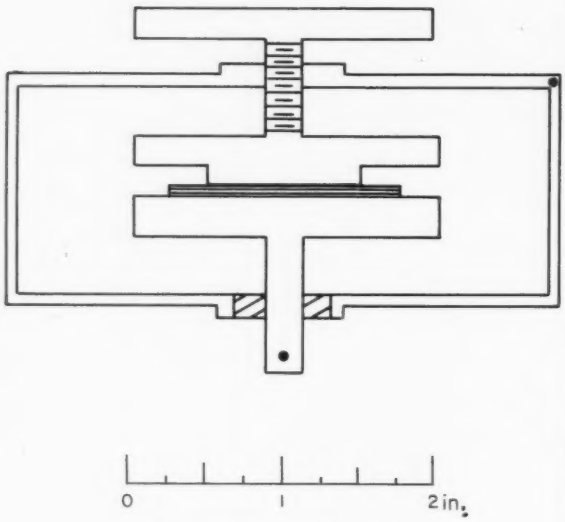

FIGURE 1. *Capacitor geometry.*

Plates are to scale; mica thickness is not.

between the smaller upper and larger lower plates. Loss tangent and capacity were determined by substitution with a Schering bridge and associated circuitry (General Radio Type 1610–A Capacitance Measuring Assembly) for frequencies of 100 to 50,000 c/s. Capacitance readings with this bridge are accurate to about ± 1 pf in substitution measurements, and loss tangent readings are accurate to about $\pm 5\times 10^{-5}$ or to ± 2 percent, whichever is larger.

The capacitor head was placed in a humidity chamber. Relative humidity was varied from about 6 to 60 percent as measured with a surface film hygrometer (Aminco). Mica sheets were cleaved while within the chamber and were then moved at constant humidity directly into the capacitor head.

2.3. Correction for Residual Airgap

Because of the existence of residual airgaps between the sample holder and the specimen, it was necessary to correct the measured values of capacitance and D. The assumed equivalent circuit for the sample holder is shown in figure 2. C_m and D_m are the measured values of capacitance and loss tangent of the holder with specimen, C_s represents the stray capacitance, and C_a represents the residual airgap. The mica specimen is represented as the general series combination of R_x and C_x. With the assumption that the effective D for the mica with surface film is very much less than one (as shown later to be true),

$$\frac{1}{C_x}=\frac{1}{C_m-C_s}-\frac{1}{C_a}. \tag{1}$$

But $C_x \propto \epsilon/t$, where t is thickness and ϵ is the dielectric constant of the specimen. If micas of various thicknesses are inserted into the holder, C_a and ϵ can be determined from eq (1) provided C_a and ϵ are constant. With C_s determined by substitution as 68 pf, figure 3 shows a plot of $1/(C_m-C_s)$ versus thickness as measured for specimens of V–4 Brazil Ruby mica and for V–2 India Ruby mica. A fit of the data gives 425 pf for C_a. Both C_s and C_m showed less than 1 percent change with frequency over the range considered.

The loss tangent, $D_x=\omega R_x C_x$, for the mica crystal can be derived straightforwardly from the equivalent circuit. With the assumption that $D_x<<1$ and with eq (1),

$$D_x=\frac{D_m C_m C_a}{\{C_a-C_m+C_s\}\{C_m-C_s\}}. \tag{2}$$

The functional dependence of the ratio D_x/D_m on C_m is shown in figure 4. Experimental effort was limited to the central region of the dependency where a reasonable approximate value of the ratio has been taken as 2.3.

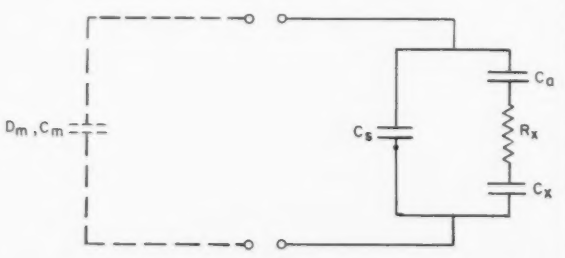

FIGURE 2. *Equivalent circuit for capacitor assembly.*

The cleaved mica lamina is represented here by the series combination of R_x and C_x.

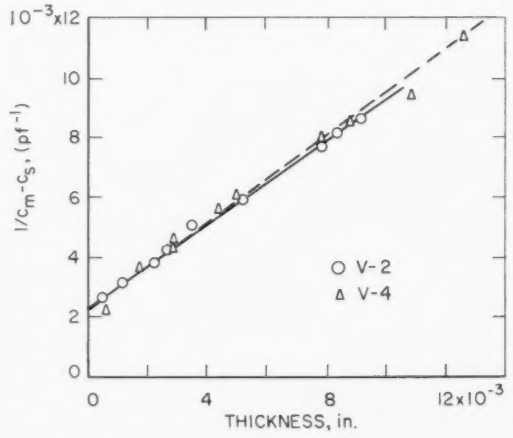

FIGURE 3. $1/(C_m-C_s)$ *versus thickness for cleaved specimens of V–2 India Ruby and V–4 Brazil Ruby.*

For Rh~40% and frequency of 1000 c/s.

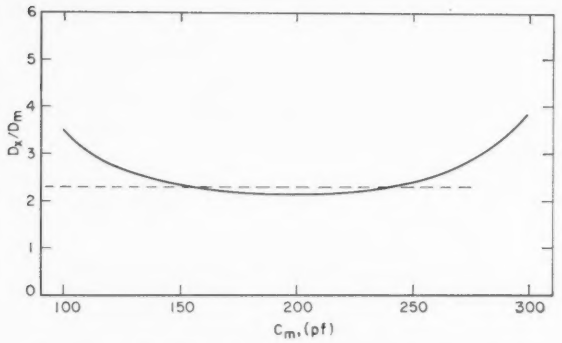

FIGURE 4. *Correction factor* D_x/D_m *as a function of* C_m.

D_m is measured loss tangent; D_x is that for mica proper. C_m is total measured capacitance.

2.4. Behavior of Loss Tangent

Typical loss tangent data are given in table 1 for measurements made on a sample of V–2 India Ruby mica at 1000 c/s and at rh∼40 percent. The sample was first measured as received. It was then removed, and a thin lamina was cleaved from one side. Each resultant piece, thick and thin, was then examined with the apparatus. The freshly peeled surface was placed first against the small plate and then against the large plate. As can be seen peeling has caused a very large increase in the measured value of loss tangent and a strong orientation effect.

TABLE 1. *Measured loss tangent for cleaved sections with fresh face oriented first to large and then to small electrode for a V–2 India Ruby at 1000 c/s*

Rh of ∼40%

	Loss tangent
1. Original sample, 0.267 mm thick	<0.0001
2. Losses of thick layer 0.224 mm thick	
a. Fresh surface against large electrode	.0010
b. Fresh surface against small electrode	.0072
3. Losses of thin layer 0.043 mm thick	
a. Fresh surface against large electrode	.0060
b. Fresh surface against small electrode	.0080

Measurements were made to determine the change in loss tangent with time. Results of aging at two temperatures for room ambient rh∼50 percent and for 1000 c/s are shown in figure 5. For these data the original sample was cleaved into two approximately equal thicknesses. For the higher temperature, the sample was then aged in an oven and removed only long enough for each measurement. Two to three minutes were needed for each of these measurements, during which time the sample had cooled to room temperature (as determined with a similar specimen and a fine thermocouple placed between laminae).

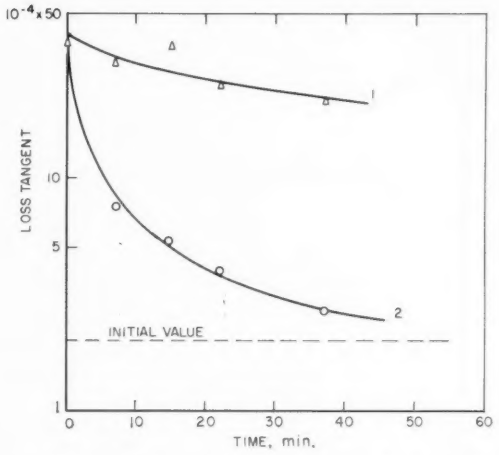

FIGURE 5. *Decay in loss tangent after cleavage at room temperature.*

The original specimen was cleaved into two laminae of equal thicknesses. One was then held at room temperature (curve 1). The second was ovened at 125 °C (curve 2). Ambient Rh of 50%. Frequency of 1000 c/s.

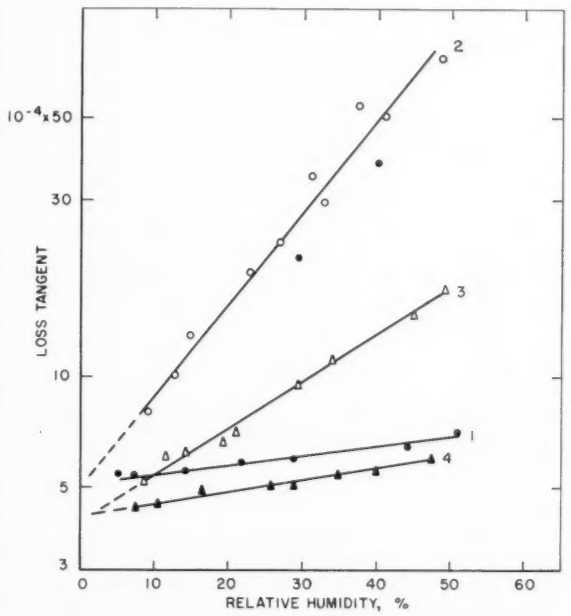

FIGURE 6. *Measured loss tangent as a function of* Rh.

1. Initial values before splitting. (thickness of 12×10^{-3} in.). 2. Cleaved face to small plate (thickness of 10×10^{-3} in.). Solid points represent values obtained with decreasing humidity. 3. Cleaved face to large plate. 4. Layer of petrolatum over cleaved face and cleaved face to small plate (thickness of 9.4×10^{-3} in.). Frequency of 1000 c/s.

The dependence of the loss tangent on the relative humidity is displayed in figure 6. The procedure used to obtain these data was as follows. A thin lamina was cleaved from the original specimen at an rh of <10 percent at room temperature. The remaining thick section was oriented with the freshly

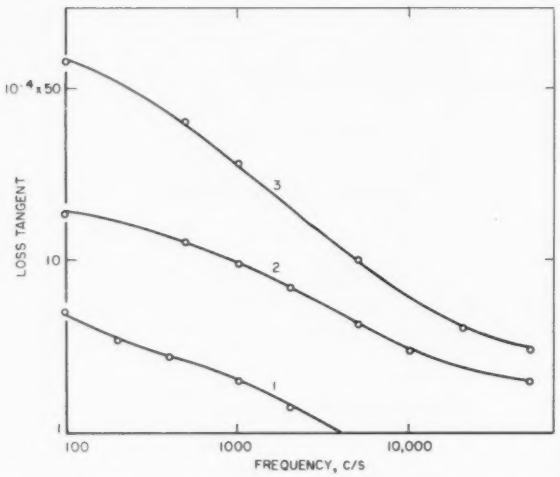

FIGURE 7. *Measured frequency dependence of loss tangent for both orientations of peeled surface.*

1. Before splitting. 2. After splitting, cleaved side to large plate. 3. Cleaved side to small plate. Rh, 40%. Thickness after peeling, 0.010 in.

peeled face to the small electrode. Relative humidity was increased in stages to about 50 percent and D was measured after each increment. D responded quickly to change in rh. Steady state occurred within 2 min after each change. The rh was quickly returned to <10 percent, the section was turned over to orient the freshly peeled face to the larger plate, and the cycle was repeated. Then a layer of petrolatum was spread over the fresh surface, the sample was reinserted with freshly peeled face to small electrode, and the data of curve 4 resulted. Each cycle was of ½ hr duration. The data indicate that D increases exponentially with rh as

$$\log D - \log D_0 = a \cdot \text{rh}. \tag{3}$$

The value of the slope, a, depends upon the orientation of the freshly peeled surface.

3. Theory

Let us assume the capacitor is composed of two regions, the first region being that under the small electrode where the E field is always normal to the dielectric plane, and the second region being the edge where fringing occurs in the E field. The loss tangent for the holder and specimen is by definition the ratio of the resistive and reactive components of the total current, I, passing between the electrodes. The total current is the sum of that under the small plate, I_{plate}, and that at the edge, I_{edge}, and the corresponding loss tangent, D_t, is

$$D_t = \frac{\text{Re}\,[I_{\text{plate}}]}{\text{Im}\,[I_{\text{plate}}+I_{\text{edge}}]} + \frac{\text{Re}\,[I_{\text{edge}}]}{\text{Im}\,[I_{\text{plate}}+I_{\text{edge}}]}.$$

Assuming $I_{\text{edge}} << I_{\text{plate}}$, we have

$$D_t = D_s + D_e, \tag{4}$$

where

$$D_s = \frac{\text{Re}\,[I_{\text{plate}}]}{\text{Im}\,[I_{\text{plate}}]}$$

and

$$D_e = \frac{\text{Re}\,[I_{\text{edge}}]}{\text{Im}\,[I_{\text{plate}}]}. \tag{5}$$

3.1. Region Within the Normal Field

Although the surface film may itself be multilayered or otherwise complicated, it is here considered as a single layer for simplification. The material is thus treated as a two layered dielectric, mica and surface film, as shown in figure 8, where each is considered as a parallel combination of a resistance and capacitance. The loss tangents for the film and the mica are respectively

$$D_1 = \frac{1}{R_1 \omega C_1},$$

$$D_2 = \frac{1}{R_2 \omega C_2}. \tag{6}$$

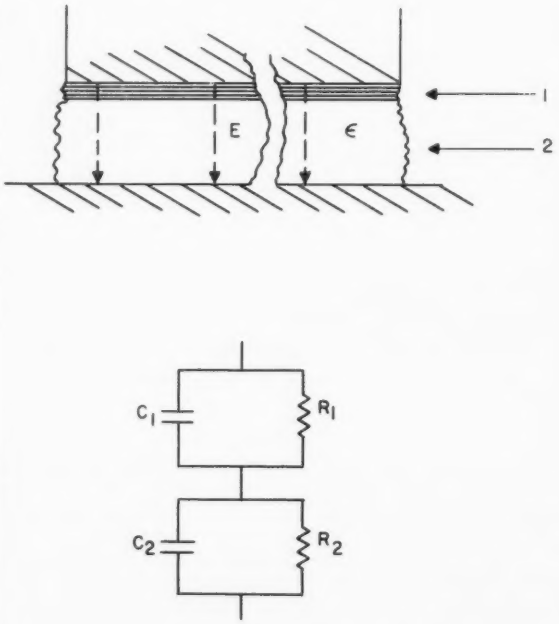

FIGURE 8. *Representation of the area under the plates of the capacitor where the field is normal to the dielectric plane.*

C_1 and R_1 represent the adsorbed layer, while C_2 and R_2 represent the mica crystal.

The loss tangent for the combination, obtained from the ratio of the real to the imaginary components of the total impedance, is

$$D_s=\frac{R_1[(R_2\omega C_2)^2+1]+R_2[(R_1\omega C_1)^2+1]}{R_1^2\omega C_1[(R_2\omega C_2)^2+1]+R_2^2\omega C_2[(R_1\omega C_1)^2+1]}. \quad (7)$$

Assuming $R_2\omega C_2>>1$ (i.e., $D_2<<1$) and $C_1>>C_2$, eq (7) becomes

$$D_s\cong\frac{R_1\omega C_2}{1+(R_1\omega C_1)^2}+D_2. \quad (8)$$

This last expression has the frequency dependence of a relaxation process. It further indicates that the increase in loss tangent due to the surface film is a direct function of the capacitance of the bulk mica and, hence, is a function of the thickness of the mica specimen. If a specimen is cleaved into two samples of thicknesses t' and t'' having identical surface films, then by eq (8)

$$D_s'-D_2=D'\propto\frac{\epsilon_2}{t'}, \quad (9)$$

and

$$D_s''-D_2=D''=\frac{t'}{t''}D'. \quad (10)$$

Thus, if after cleavage the two resultant samples are measured with the cleaved faces toward the larger electrode, the loss tangent of the thin section should be greater than the thick by the ratio of the thicknesses.

3.2. Region of the Fringe Field

Consider the region at the edge to be a distributed constant radial transmission line. Let it be composed of a number of parallel sections of unit width—a good approximation because of the small extent of the fringe pattern. For the present case, with the assumption of a sufficiently large surface conductivity, most of the fringe field will be confined to the resistive film and the dielectric slab. The potential applied to the terminals of the transmission lines is just that between the capacitor plates. The situation is pictured in figure 9. The fringe field is of short extent and the attenuation is therefore great enough so that only the outgoing wave need be considered, i.e., no termination and consequent reflection. The resultant current determines the edge loss tangent, D_e. The current, J, down the unit width line is V/Z_0, where $Z_0=\sqrt{Z_sZ_p}$ is the characteristic impedance, Z_s is the series impedance/unit length, and Z_p is the parallel or shunt value/unit length [15]. With R' as the surface resistance/unit square and C' as the capacitance/unit square, which is taken identical to that between the plates (i.e., C_2/A with A being the area of the small electrode)

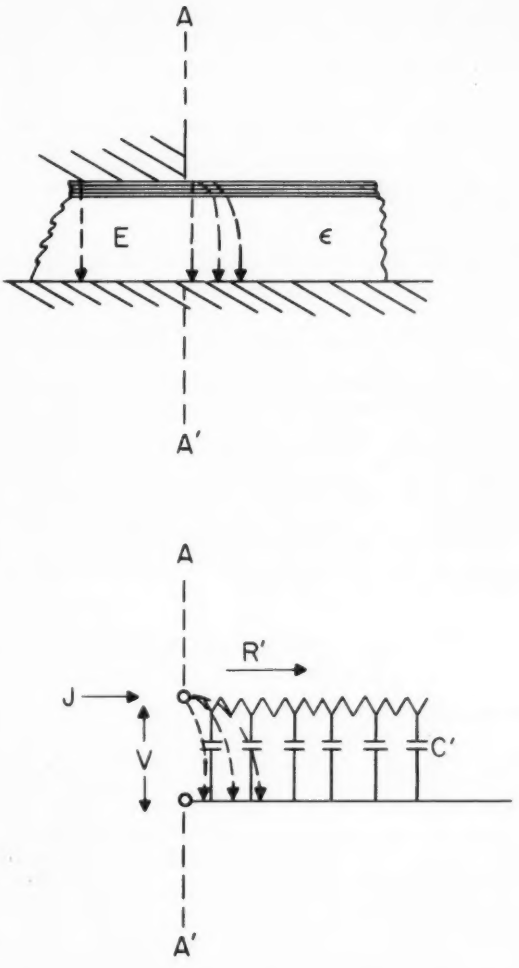

FIGURE 9. *Representation of the fringe field at the edge of the capacitor by a transmission line.*

The parallel resistance per square of the surface film is R'. The capacitance per cm² of the mica is C'.

$$Z_0\equiv\sqrt{Z_sZ_p}=\sqrt{-\frac{iR'}{\omega C'}}, \quad (11)$$

and

$$J=V/Z_0=V\frac{1+i}{\sqrt{2}}\sqrt{\frac{\omega C'}{R'}}. \quad (12)$$

By eq (5), D_e is the ratio of the real component of the edge current to the total capacitative current. Therefore,

$$D_e=\frac{2\pi r\,\mathrm{Re}\,(J)}{I_e}=\frac{2}{r}\frac{1}{\sqrt{2R'\omega C'}}\propto\frac{2}{r}\sqrt{\frac{t}{2R'\omega\epsilon'}}, \quad (13)$$

716-919—64——3

where $I_e \cong \omega C' A V$ and r is the radius of the small electrode. For two thicknesses t' and t'' cleaved from the specimen,

$$D'_e = \sqrt{\frac{t'}{t''}}\, D''_e, \tag{14}$$

where D'_e and D''_e are the edge dissipation factors for the two thicknesses.

4. Experimental Verification of Expressions for Loss Tangent

4.1. Loss Tangent and Thickness

The experimentally determined values are (1) the initial uncleaved value or $\sim D_2$, (2) the value for the cleaved face against the large electrode or D_s, and (3) the value for the cleaved face against the small electrode or D_t, the total loss tangent. Each of these is obtained from the actually measured values after correction for airgap effect. Thus, the expected value of loss tangent for a thin section, D''_t, as compared to its complementary thick section D'_t, is by eqs (4), (9), (10), and (14)

$$D''_t = n(D'_s - D_2) + D_2 + \frac{D'_t - D'_s}{\sqrt{n}}, \tag{15}$$

where n is the ratio t'/t''.

A number of crystals were split in such a way that a variety of values of n were achieved. Table 2 lists results comparing the experimental value of loss tangent for the thin section to the value predicted from the data of the complementary thick section. Since the correction factor for airgap effect should be applied to each of the terms of eq (15) and hence is common, data are given as the actually measured values.

The ratios of measured to predicted values show an average difference from unity of about 17 percent and 15 percent for D_s and D_t respectively. These are reasonable values. In addition to the assumptions made for analytical purposes, it was also assumed that the surface states were the same in each complement after cleavage. This may not be strictly true. On the other hand, it is to be remembered that the surface is very sensitive to handling and contact [5]. Each complement had to be handled separately so that the chance always existed of introducing a discrepancy. Further, elapsed time between measurements for each section allowed D to undergo a relative decay (see fig. 5).

4.2. Extent of Fringe Field

The current falls to $1/e$ of its initial value at a distance down the transmission line equal to the reciprocal of the attenuation constant, α. This then is a measure of the extent of the fringing field. Since [15]

$$\alpha = \mathrm{Re}\,[\sqrt{Z_s/Z_p}] = \sqrt{\frac{\omega R' C'}{2}},$$

by eq (13)

$$\alpha = \frac{1}{rD_e}. \tag{16}$$

From the data of figure 6 and with eq (4), the corrected values of D_e range from about 16×10^{-3} at 50 percent rh down to about zero at 0 percent rh. Thus, for the dielectric slab of 0.254 mm thickness the computed attenuation distance ranged from about 0.2 mm down to about zero, with a value of 0.01 mm at 10 percent rh. The significance of zero attenuation distance for this model (see fig. 9) is that the surface resistance per square (R') is infinite and the fringe field is reduced to the normal capacitive situation.

Upon the assumption that the field is essentially contained between the surface conducting film and the opposite electrode, a guard ring structure would show little effect until the guard-electrode gap became comparable to the attenuation distance. As a check on this, a capacitor was made with tin foil electrodes. A 1 in. diam electrode and a guard ring with a 0.010 in. guard gap were formed, rolled out on a sheet of plate glass, greased with petrolatum, heated at 100 °C, lifted from the glass, and rolled carefully onto the cleaved face of a 0.010 in. thick mica crystal, first without the guard and then with the guard. Care was taken that only a thin film of

TABLE 2. *Testing of derived expressions of loss tangents by comparing predicted to experimental values for thick and thin complements*

1. n	2. $D'_s - D_2$	3. $D''_s - D_2$	4. $D'_t - D_2$	5. $D''_t - D_2$	6. $\frac{D''_s}{D''_s \text{ (predicted)}}$	7. $\frac{D''_t}{D''_t \text{ (predicted)}}$
1.20	8.1×10^{-4}	10.4×10^{-4}	69×10^{-4}	64×10^{-4}	1.06	1.00
1.8	3.6	8.4	76	67	1.29	1.06
3.3	9.1	35	57	75	1.18	1.33
4.5	9.9	59	74	87	1.32	1.17
4.7	7.3	42	54	69	1.21	1.23
8.2	7.1	50	64	100	0.85	1.28
9.0	16.0	150	86	164	1.04	0.98
15.6	9.2	121	82	145	0.84	.90

Notes:
Rh ~ 40 percent. Frequency is 1000 c/s.
Thickness measured by direct reading micrometer for specimens of thickness >0.002 in. and by dial comparator (least reading of 0.00002 in.) for specimens of thickness ≤0.002 in. Cleaved sections often have faults causing thickness changes of ≤0.0001 in. magnitude as well as wedge shaped cross sections. Larger n values are subject to consequent errors of several percent.

petrolatum remained on the foil and did not spread into the guard-electrode gap. The rh was varied and loss tangent measurements were made. The measured loss tangent ranged from 8×10^{-4} at 8 percent rh to 30×10^{-4} at 50 percent rh and was not diminished when the guard ring was added. Then, a second capacitor plate system was constructed. This comprised a thick center electrode of 1.650 in. diam and $\frac{3}{8}$ in. thickness, a guard ring of the same thickness but of 0.300 in. width, and a guard-to-plate gap of 0.0025 in. The cleaved specimen was 16.3 $\times10^{-3}$ in. in thickness. The effect of rh on D is displayed in figure 10. The difference in value with and without the guard is considerable, but the slopes of the loss tangent-rh dependencies are the same down to a low rh of ~15 percent. The extent of the fringe field was apparently affected, as D was diminished by the guard, but the tangential surface interaction persisted. For if the tangential surface interaction were voided, one would expect a slope indicative of normal field only.

5. Nature of the Surface Film

D_1, R_1, and C_1 (sec. 3.1) can be computed from eq (8) and frequency characteristics such as those of figure 7. Equation (8) has the form

$$D_s - D_2 \cong \frac{\xi f}{1+(\beta f)^2}, \qquad (8')$$

where $\xi=2\pi R_1 C_2$, $\beta=2\pi R_1 C_1$, and f is the frequency. We make the approximation that within a small frequency interval β and ξ remain constant; e.g., 100 to 200 c/s at one end of the spectrum and 5000 to 10,000 c/s at the other. This allows solution for β and ξ with the values for D_s and D_2 at the two endpoints of the frequency interval, i.e., two simultaneous equations. D_1 is then $1/\beta\bar{f}$, where $\bar{f}$ is the mean frequency, and C_1 is related to C_2 by the ratio β/ξ. For this D_2, D_s, and C_2 are first corrected for airgap effect. Results obtained for D_1 for successive frequency intervals from the data of figure 7 are given in figure 11 at the mean frequency along with the loss tangents of conductivity water, ice, and fresh snow [16]. Results for R_1 and C_1 are given in figure 12. Quantities are all reduced to values per cm², e.g., pf/cm² and Ω/cm² in the direction normal to the surface.

D_e is obtained from figure 7 by eq (4). R' is then found by eq (13). Results for D_e and R' are given in figure 13.

These results indicate that the frequency characteristic of D_1 is not that of pure bulk water or ice. It appears to be more like that of fresh snow, a dispersed structure. The characteristics of R_1 and D_e also seem reasonable.

The derived natures of C_1 and R' raise the question as to whether such behavior is intrinsic or only due to oversimplification of equivalent circuits. Therefore, the equivalent circuit for the surface film in the normal direction (fig. 8) was modified by the addition of a series resistance to C_1 (see fig. 14). For example, such an equivalent circuit has been suggested as an empirical fit for pure water [17]. The resultant equations for the complete circuit are given in appendix A. Some numerical results have been included in figures 11 and 12, where they are labeled as 3-point data (computation now requires three data

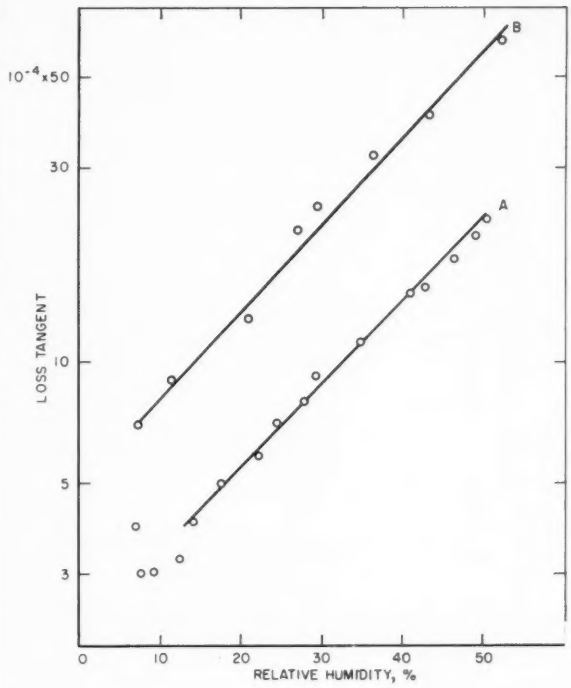

FIGURE 10. *Effect on loss tangent of a closely spaced guard ring for a cleaved sample as a function of* Rh.

Thickness is 16.3×10^{-3} in. Guard-to-plate gap is 2.5×10^{-3} in. Center plate diameter is 1.6 in. A. with guard. B. without guard. Frequency of 1000 c/s.

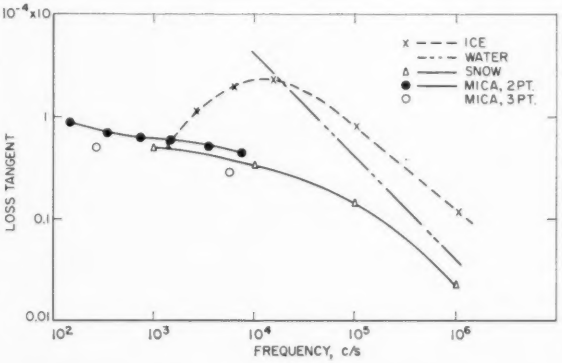

FIGURE 11. *Loss tangent versus frequency for the surface film on mica as derived by 2 and 3 point analyses (from the data of figure 7) and for the several forms of water: conductivity liquid at 25 °C, ice, and snow (see ref. 16).*

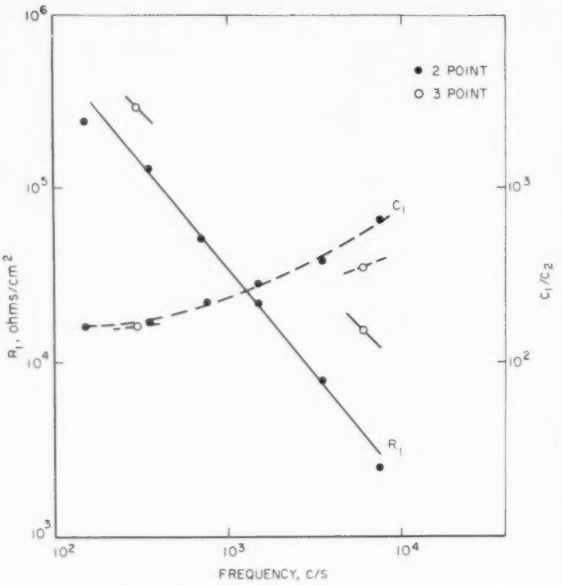

FIGURE 12. R_1 *and* C_1/C_2 *versus frequency as derived from 2 and 3 point analyses for a Tanganyika Ruby mica from the data of figure 7.*

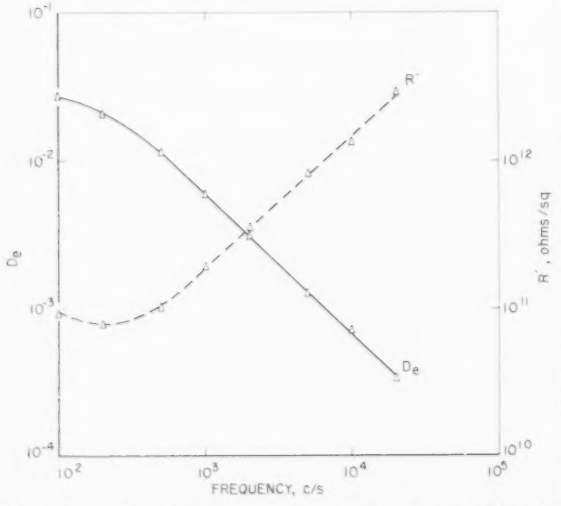

FIGURE 13. *Loss tangent at the edge and resistance along the surface as a function of frequency for a Tanganyika Ruby mica as derived from the data of figure 7.*

points within any chosen frequency interval). As indicated the behaviors of the quantities are essentially as before, although C_1 now shows a smaller frequency dependence. It is assumed from this that further circuit modification would lead to constant C_1 in this frequency range but that the magnitudes of the quantities are essentially as given. Presumably then, D_1 has a characteristic different from that of a sheet of liquid water or of ice and more like that of a dispersed structure.

The assumption of a uniform surface film is inconsistent with the magnitudes of the derived quantities. For example, from figure 12 at 1000 c/s C_1 has the value of 6×10^{-9} f/cm^2 (C_2=30 pf/cm^2), which, if ϵ_1 were 1, would lead to a film thickness of about 1300 A. If ϵ_1 were greater than unity, the thickness would have to be correspondingly greater. But, a film of this thickness is unreasonable [5, 18]. Similar inconsistencies arise in the values of R_1 and R'. As R' is the resistance along the plane of a cm^2 of thickness, t, and R_1 is the resistance normal to the plane for the same section, i.e., $R'=\rho_p/t$ while $R_1=\rho_n t$, where ρ_n and ρ_p are the resistivities normal to and parallel to the plane respectively,

$$R_1R'=\rho_n\rho_p.$$

If ρ_n and ρ_p are taken as equal, then ρ is found to be $\sim10^8$ Ω cm at 1000 c/s where $R'=2\times10^{11}$ Ω and $R_1=3\times10^4$ Ω. But, from this value for ρ, t would have to have been >30,000 Å as computed from either of the expressions for R_1 and R'. To bring t to within a reasonable limit as computed from R_1 and from R', ρ_n should be orders of magnitude greater than 10^8 Ω cm and ρ_p should be correspondingly less than 10^8 Ω cm. Thus, the resistivity in the normal direction must be considerably greater than that along the surface. In fact, a factor of ρ_n to ρ_p of more than 100 would be required to bring t to within reasonable limits [18]. This, however, conflicts with the derived values of D_1. Since

$$D_1\cong\frac{1}{R_1\omega C_1}=\frac{2}{\rho_n\epsilon f}\cdot9\times10^{11}, \qquad (17)$$

a value for D_1 of 0.5 at 1000 c/s with ϵ of 1 leads to a ρ_n of $\sim4\times10^9$ Ω cm. This is only a factor of 40 over 10^8. Any larger increase in ρ_n as, say, a factor >100, would cause D_1 to be less than the derived values.

A conclusion from these results is that the surface film has a more complex structure than has been suggested [5]. One possibility is that the adsorbed layer is composed of small islands or patches. Such a formation would also be compatible with the observation of alternately electrically charged areas on the surface of cleaved mica [3, 4]. Then with the smaller area, C_1 would be smaller than for a continuous film, R_1 would be larger, and yet D_1 would remain the same as this is only dependent on the material according to eq (17). The compatibility of the patch formation and the limitations imposed are discussed in appendix B as based upon suitable equivalent circuit analysis.

Lastly, from eq (8) and the derived magnitude of D_1 (see fig. 11), the change in D_s-D_2 is essentially that due to the change in R_1. Since D_s-D_2 increased with rh, according to the patch concept the islands of loosely bound film must increase in depth with rh rather than expand in diameter in order to cause R_1 and hence D_s-D_2 to increase. Such formation would be sensitive to rh as is the case.

6. Appendix A. Modified Equivalent Circuit and 3-Point Analysis

The equivalent circuit for the surface film is now taken as one which has been suggested for liquid water [17]. The resultant equivalent circuit for film and mica is shown in figure 14. The admittance for the film itself is

$$Y_1=\frac{1}{R_1}+\frac{R(\omega C_1)^2}{1+(R\omega C_1)^2}+i\,\frac{\omega C_1}{1+(R\omega C_1)^2}. \tag{18}$$

In terms of the complex dielectric constant, $\epsilon^*=\epsilon'-i\epsilon''$, and with $Y_1\equiv i\omega C$,

$$Y_1=\omega\epsilon''\,\frac{C_0}{\epsilon_0}+i\epsilon'\,\frac{\omega C_0}{\epsilon_0}, \tag{19}$$

where $C=(\epsilon^*/\epsilon_0)C_0$ and C_0 is the equivalent free space capacitance of the film. Thus

$$\epsilon_1'=\epsilon_0\cdot\frac{C_1}{C_0}\cdot\frac{1}{1+(R\omega C_1)^2}. \tag{20}$$

The loss tangent for the film is

$$D_1=\frac{1+R(\omega C_1)^2(R+R_1)}{R_1\omega C_1}. \tag{21}$$

On the expectation that R is sufficiently smaller than R_1, i.e., $R<R_1$,

$$D_1\cong\frac{1}{R_1\omega C_1}+R\omega C_1. \tag{22}$$

With the same assumption that $R<R_1$, the loss tangent for the double layer is

$$D_s=\frac{[R_1^2R\omega^2C_1^2+R_1][(R_2\omega C_2)^2+1]+R_2[(R_1\omega C_1)^2+1]}{R_1^2\omega C_1[(R_2\omega C_2)^2+1]+R_2^2\omega C_2[(R_1\omega C_1)^2+1]}. \tag{23}$$

Then, under the assumption that $R_2\omega C_2>>1$ and $C_1>>C_2$,

$$D_s\cong\frac{R_1\omega C_2}{1+(R_1\omega C_1)^2}+D_2+\frac{R(R_1\omega C_1)^2\omega C_2}{1+(R_1\omega C_1)^2}. \tag{24}$$

This has the form

$$\frac{D_s-D_2}{2}[1+(\beta f)^2]=\xi+2\pi R(\beta f)^2C_2, \tag{25}$$

where again $\xi=2\pi R_1C_2$ and $\beta=2\pi R_1C_1$. Similarly as before β, ξ, and R are considered constant over a given frequency interval. D_s, D_2, and f are now obtained from three data points in the given frequency interval which allow three simultaneous equations to be solved for β, ξ, and R. Data for two such frequency intervals as taken from figure 7 are listed in table 3 and included in figures 11 and 12.

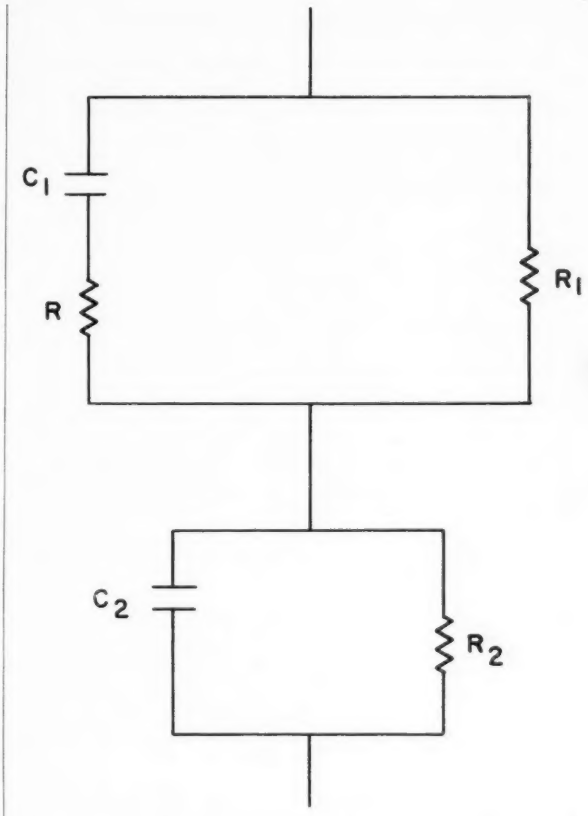

FIGURE 14. *Modified equivalent circuit with the adsorbed film represented by an empirically suggested circuit for pure water (see Von Hippel, ref. 16).*

It is seen that D_1 is slightly smaller than for the 2-point treatment, and R is 1 to 3 percent of R_1. The term $R\omega C_1$ has the value of $\sim$0.03 to $\sim$0.08. Therefore, the second term of eq (22) is some 15 to 20 percent of the first term. In eq (20) $(R\omega C_1)^2$ may be neglected so that C_1 is again a measure of ϵ_1'. The second term on the right of eq (25) is 10 to 15 percent of ξ.

TABLE 3.—*Derived values for loss tangent and equivalen circuit elements through 3-point analysis**

f[a]	$\bar{f}$[b]	ξ	β	R Ω	C_1/C_2	R_1 Ω	D_1
c/s	c/s						
1. 10,000							
2. 5,000	5700	2×10^{-6}	6.9×10^{-4}	67	350	10^4	0.28
3. 2,000							
1. 500							
2. 200	270	5.5×10^{-5}	8.8×10^{-3}	9900	160	2.9×10^5	0.5
3. 100							

*Values listed are per cm².

[a] f represents the frequency of the 3 data points chosen in the frequency interval considered.

[b] $\bar{f}$ represents the approximate average frequency of the 3 points, f.

7. Appendix B. Patch Formation

The previous analyses considered the normal E field region of the test capacitor as an airgap in series with the adsorbed film and mica substrate, i.e., the equivalent circuit of figure 8 in series with the airgap capacitance, C_a. However, in the case of small and numerous patches adsorbed on the mica surface we must consider two regions of the E field. In one region E lines pass through an airgap directly into the mica substrate. In the second, E lines pass through an airgap into the patches, in which case there may be some refraction. Such a situation becomes that of figure 15, where C_a now represents an airgap of thickness equal to the distance from the capacitor plate to the top of a patch, R_1 and C_1 represent the patches, R_2' and C_2' represent the mica for the area under the patches, C_3 is the air film of thickness equal to the height of the patches, R_2'' and C_2'' represent the mica under the air film. Similarly to before, eq (4), for the region below the airgap, C_a,

$$D=\frac{\mathrm{Re}\,[I_a+I_b]}{\mathrm{Im}\,[I]}=\frac{\mathrm{Re}\,[Y_a]}{\mathrm{Im}\,[Y]}+\frac{\mathrm{Re}\,[Y_b]}{\mathrm{Im}\,[Y]}, \tag{26}$$

where Im $[Y]$ is essentially ωC_2. Then for branch (a) of figure 15 with $C_1>>C_2''$, $\omega R_2'C_2''>>1$, and $R_2'>R_1$ the expression for D_a becomes identical in form to that of eq (8), or

$$D_a\cong\frac{1}{\omega R_2'C_2'}+\frac{R_1\omega C_2''^2}{1+(\omega R_1C_1)^2}\cdot\frac{1}{C_2'}. \tag{27}$$

For the second term of eq (26) we have, with $C_3>>C_2''$,

$$D_b\cong\frac{1}{\omega C_2'}\cdot\frac{\omega^2R_2''C_3^2}{1+(\omega R_2''C_3)^2}.$$

With multiplication of $\omega R_2''C_3$ by C_2''/C_2'' and as $\omega R_2''C_2''=\frac{1}{D_2}>>1$,

$$D_b\cong\frac{1}{\omega R_2''C_2'}. \tag{28}$$

The limiting behavior of the patches can now be seen from eq (27) and (28). The first limit is that for which the E field does not deviate, i.e., there is no refraction at the patches and all field lines are parallel to each other. Then C_2' is the capacitance of the mica area directly under the patches, or if A is the patch area/cm^2,

$$C_2'=C_2\cdot A$$

and

$$C_2''=C_2(1-A).$$

Since $$\frac{1}{\omega R_2'C_2'}=D_2=\frac{1}{\omega R_2''C_2''},$$

the loss tangent is

$$D=D_2+A\,\frac{R_1\omega C_2'}{1+(R_1\omega C_1)^2}. \tag{29}$$

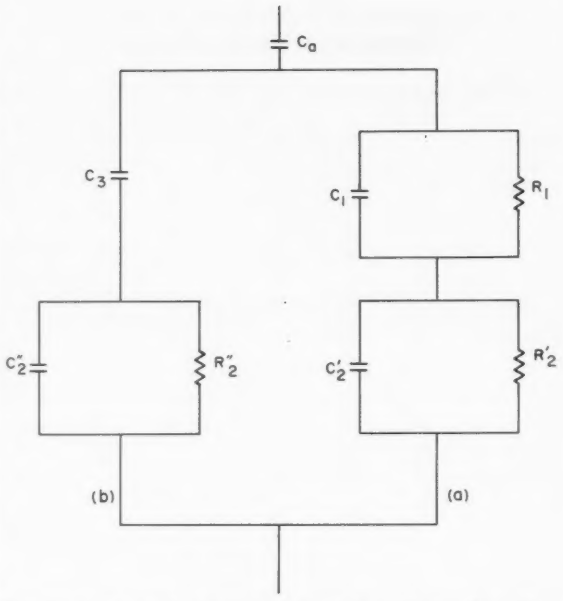

FIGURE 15. *Equivalent circuit for patch formation on the surface of peeled mica.*

In this case as A becomes small, $D\rightarrow D_2$. But this also means that when D is equated to the derived values of D_s, $R_1\omega C_2'/[1+(R_1\omega C_1)^2]$ must be correspondingly greater by $1/A$ than the value determined by eq (8) so that R_1 would be found to be even greater than before and C_1' even less. This compounds the difficulties already established.

The other limiting case is that for which refraction does occur in the E field to the extent that all E field passes through the patches before entering the mica. For this case $C_2'=C_2$, $C_2''=0$, $R_2''\rightarrow\infty$ and we again have eq (8) from eqs (27) and (28). To realize this limit physically, the patches would have to be small in area, be very numerous, be of sufficient height to cause distortion of E, and have sufficient dielectric constant.

It is thus possible for the patch concept to give the derived values. The values of R_1 can be larger and those of C_1 can be smaller than for a continuous film; yet, the adsorbed layer character of resistivity, dielectric constant and thickness need not be abnormal. We cannot now equate R_1 to $\rho_a t/A$, however, for there are for this case tangential components of the field within the patch, although obviously not of the order of those of the fringing field at the plate edge. One would expect a situation somewhere between these two extremes but closer to the second, since $D_s\sim 1/t$ rather than $\sqrt{t}$.

8. References

[1] Lord Rayleigh, Collected papers vol. III, 523.
[2] J. W. Obreimoff, Proc. Roy. Soc. **127,** 290 (1930).
[3] M. S. Metsik, Sov. Phys. Sol. State **1,** 991 (1960).
[4] B. V. Deryagin and M. S. Metsik, Sov. Phys. Sol. State **1,** 1393 (1960).

[5] J. M. Macauley and D. Carson, J. of Roy. Tech. Cl. Glasgow **2,** 161 (1930).
[6] R. H. Jahns and F. W. Lancaster, Geol. Survey Prof. Paper 225 (1950).
[7] J. R. Weeks, Phys. Rev. **19,** 319 (1922).
[8] D. W. Dye and L. Hartshorn, Proc. Phys. Soc. Lond. **37,** 42 (1924).
[9] A. B. Lewis, E. L. Hall, and F. R. Caldwell, BS J. Research **7,** 403 (1931).
[10] S. Datta, J. Sen Gupta, and P. C. Mahanti, Ind. J. Phys. **17,** 79 (1943).
[11] P. C. Mahanti, M. K. Mukhergie, and P. B. Roy, Ind. J. Phys. **19,** 83 (1945).
[12] P. C. Mahanti and S. S. Mandel, Ind. J. Phys. **22,** 7 (1948).
[13] E. L. Hall, Proc. IRE **32,** 393 (1944).
[14] American Society for Testing Materials Spec. D 351–53T.
[15] J. C. Slater, Microwave transmission, ch. 1 (McGraw-Hill Book Co., Inc., New York, N.Y., 1942).
[16] A. R. Von Hippel, Dielectric Materials and Applications (Technology Press of M.I.T. and John Wiley & Sons, Inc., New York, N.Y., 1954) pp. 301 and 361; R. P. Auty and R. H. Cole, J. Chem. Phys. **20,** 1309 (1952).
[17] A. R. Von Hippel, Dielectrics and waves, p. 87 (John Wiley & Sons, Inc., New York, N.Y., 1954).
[18] W. A. Yager and S. O. Morgan, J. Phys. Chem. **35,** 2026 (1932).

(Paper 68A2–266)

JOURNAL OF RESEARCH of the National Bureau of Standards—A. Physics and Chemistry
Vol. 68A, No. 2, March–April 1964

On the Measurement of Dielectric Losses and Surface Conductivity of Dielectrics in Parallel Plane Test Capacitors

Lothar Frenkel

(September 18, 1963)

Thin slabs of dielectric materials are often tested for their dielectric properties in plane parallel plate capacitors. When surface conductivity is present, as for instance in freshly split mica, losses not connected with the bulk of the material arise. The present paper deals with the general theory of such measurements. The system is reduced to an assembly of lumped elements superimposed on distributed transmission lines. The treatment includes the presence of possible airgaps underneath the plates of the test condenser. It is shown that such losses depend on the reciprocal square root of the frequency. Losses due to this effect cannot be eliminated by guard ring measurement and much of the published data on the losses in mica must be reexamined in the light of the present work. Similar considerations may apply in the case of other materials.

1. Introduction

The present paper had its origin in an attempt to interpret the results of some recent work on mica described in a paper by S. Ruthberg and L. Frenkel [1] which will henceforth be referred to as (I). In (I) we describe some results obtained during measurements of the dielectric losses of freshly split mica and attempt to account for these in terms of the physical properties of an assumed surface layer on the mica. The present paper extends and generalizes the theory of loss measurements in the presence of surface conductivity. It is shown that all the features described in (I) may alternatively be accounted for in a simple manner by the surface conductivity of the specimen alone.

The present paper is however a general contribution to the theory of dielectric measurement and the applicability of this theory is not limited to any particular dielectric. Furthermore some loss measurements in mica and other dielectrics should be reexamined in the light of the theory given here to sort out what part of the losses reported may be ascribed to the bulk of the dielectric and what part is in fact due to surface conduction.

Before introducing a specific model for theoretical analysis we shall examine briefly the salient features of the results reported in (I).

The experimental arrangement used is shown in figure 1 and consists of a parallel plate capacitor made up of a large grounded plate (A), a sheet of the dielectric under test (B) and a disk electrode (C) which is connected to a suitable bridge.

Suppose now that a dielectric having one slightly conducting surface is placed in the capacitor with the conducting face resting on the smaller disk (arrangement 1).

It is clear that current will flow away from the edge of the small disk via surface conduction thus

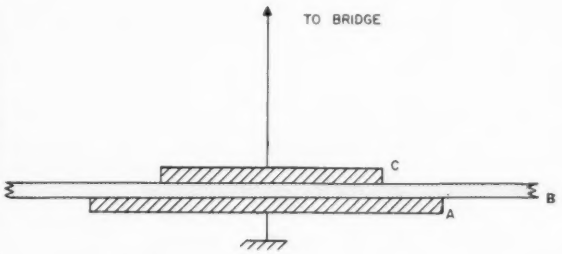

FIGURE 1. *Experimental arrangement for the measurement of dissipation in mica.*

giving rise to losses which are added to the losses incurred in the bulk of the material, and it is shown in (I) that these losses are inversely proportional to the square root of the capacitance of the capacitor formed in the manner described above.

The depth of penetration of this edge effect is quite small. This may be seen as follows: A typical value of the surface resistance on freshly split mica [2] is 10^{11} Ω while the capacitance across a typical sample is 10 μf per cm^2 thus the resistive component of the impedance along a square of 1 cm edge is in the order of 10^{11} Ω while the shunting impedance across the sample to ground at 1000 c/s is of order 10^7 Ω. The edge current is therefore quickly attenuated. This fact, as is pointed out in (I) makes it impossible to exclude such losses by means of guardring methods.

Suppose now that the sample is reversed so that the conducting surface is resting on the large, grounded plate (arrangement 2). In this arrangement the field lines all cross the conducting surface at right angles and there are no losses due to surface currents. Since, however, the conductive layer on the surface will also have transverse conductivity one might

[1] S. Ruthberg and L. Frenkel, Dielectric behavior of the film formed on mica cleaved in moist air, J. Res. NBS **68A** (Phys. and Chem.) No. 2, 173 (1964).

[2] J. M. MaCaulay and D. Carson, J. Roy. Tech. Coll., Glasgow **2**, 161 (1930).

expect some losses to occur in this case also. The value of the losses in the two arrangements as well as their dependence on the thickness of the dielectric and on the frequency used are subject to physical and instrumental interpretation.

In attempting to explain the losses in the transverse field (arrangement 2) in terms of the physical properties of the surface layer one runs into difficulties. In particular the magnitude of the losses is such that one must assume either a dielectric constant smaller than 1 or a thickness of the layer of the order of millimeters. Neither of these conditions is reasonable.

The salient experimental features which any theory of this effect must explain are listed below.

I. The loss induced by splitting is *proportional* to the capacitance of the piece when measured with the fresh side in contact with the large plate (arrangement 2).

II. If the fresh side is placed in contact with the smaller plate the losses increase due to the edge effect. This difference in loss is found to be *inversely proportional* to the square root of the capacitance of the piece.

III. All induced losses vary as the inverse square root of the frequency.

The order of magnitude of the losses with the two arrangements is the same.

One further feature of the experiments must now be described since it provided the clue for the present solution of the problem. If one examines the capacitance of the test capacitor with progressively thinner pieces of the mica between the plates one finds upon plotting the inverse of the capacitance versus the thickness of the dielectric that the resulting straight line does not go through the origin but has, at zero thickness, a positive intercept. This indicates that in practice there is a fixed effective airgap between the plates of the test capacitor and the dielectric. Causes for the airgap may either be inherent in the mica surface or of an instrumental nature. Whatever its origin however the existence of the airgap suggests that surface currents will occur also when the lossy surface is exposed to the large plate since there will be currents along the surface wherever the surface contact with the plate is interrupted. In (I) the existence of the gap was taken into account by a correction applicable for measurements in uniform airgaps but no actual losses at the contact edges underneath the plates were assumed to occur.

The magnitude of the correction is quite large and corresponds, for thin samples, to airgap thicknesses amounting to several percent of the thickness of the specimen under test. Consequently the losses associated with this type of contact current cannot be neglected.

2. Description of the Model

We are now ready to set up a model representative of the arrangement described above. In practice there may be many areas of contact under the plates and their shape and thickness may be quite varied. Remembering however that the attenuation is quite rapid and that the losses in the various gaps may be summed we need to treat only one typical case, i.e., the loss in a cavity under the plates. It will be easily seen that the edge loss is only a special case of the general model, namely the special case where the airgap capacitance has gone to zero.

The equivalent circuit with the airgap under the plates is indicated in figure 2. A represents the region beyond the edge of the smaller plate where the capacitance of the sample is in series with the resistance of the surface. The region B represents the area under the small plate where the resistive path is shunted by the effective airgap. C_1 is the capacitance across unit area of the sample, R is the surface resistivity of a unit square of the surface and C_2 is the capacitance across unit area of the airgap.

Since the edge effects are confined to a small area near each contact edge one may regard the surface near the edge as forming a part of an infinite parallel plane transmission line, of width equal to the length of the respective edge. In the case of the edge of the upper plate this length is the circumference of the plate but under the airgap one cannot determine the length of the contact edges directly. The qualitative features of the model do not depend on the length of these edges however, and the actual lengths required to account for the phenomena described in (I) are of the order of the plate circumference which is entirely reasonable.

Because the attenuation is very high we may assume that the characteristic inductance of the line is negligible and that the progress of the wave into the line is slow. The progress of the signal along the metal plates by contrast is infinitely fast. These assumptions may be made plausible as follows: Assume that a potential V is suddenly applied to the upper plate. The potential V will be established across the entire upper plate with a speed close to the speed of light and the surface of the mica will assume

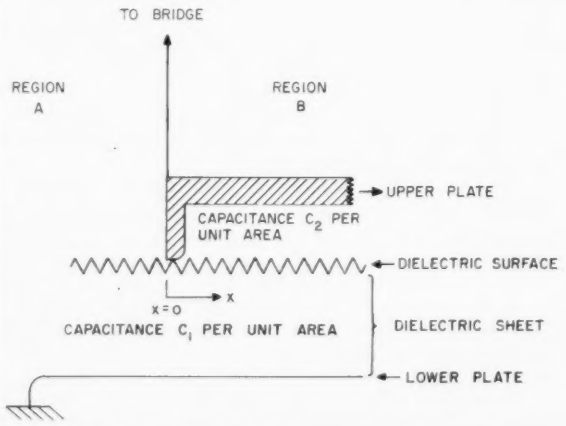

FIGURE 2. *Equivalent circuit representing the mica capacitor near the edge of the upper plate.*
Only the edge of the upper plate touches the mica surface

a potential determined by the capacitance divider consisting of C_1 and C_2. After a time determined by the time constant (C_1R) the surface of the dielectric will however reach the potential V by conduction along the surface. Our assumption now implies that this time is long compared to the time required to establish initial equilibrium in the upper plate.

3. Theory

In practice a sinewave in a frequency range from 10 to 1000 c/s is used for this experiment and the upper plate is therefore at potential:

$$V(t)=V_0e^{i\omega t}. \tag{1}$$

Our task is to calculate the in-phase component of the current in section B.

Our plan of attack is the following. We shall establish transmission line equations for the surface potential $V_s(x,t)$ and the surface current $I_s(x,t)$ in order to find the current into the line, $I_s(o,t)$. To this we will add the current flowing at any time into the airgap. This current is determined for each point x on the surface by the potential difference $(V(t)-V_s(x,t).)$. The airgap current must therefore be obtained as an integral over the entire line. This transmission line is described by:

$$\frac{\partial I_s}{\partial x}=-C_1\frac{\partial Vt}{\partial t}+C_2\left(\frac{\partial Vt}{\partial t}-\frac{\partial V_s}{\partial t}\right) \tag{2}$$

and

$$\frac{\partial V_s}{\partial x}=-I_sR. \tag{3}$$

The solution can easily be guessed. We note that for large values of x, V_s must approach a fixed value.

$$\lim_{x\to\infty}V_s(x,t)=V_0e^{i\omega t}\frac{C_2}{C_1+C_2} \tag{4}$$

while at $x=0$

$$V_s(0,t)=V_0e^{i\omega t}; \tag{5}$$

accordingly we try:

$$V_s=V_0e^{i\omega t}\left[e^{-x(\alpha+ik)}\left\{1-\frac{C_2}{C_1+C_2}\right\}+\frac{C_2}{C_1+C_2}\right] \tag{6}$$

since this function has the correct limiting dependence.

Further we assume

$$I_s=I_{s,0}e^{i\omega t-x(\alpha+ik)}; \tag{7}$$

substitution of the trial solutions (6) and (7) into eqs (2) and (3) gives

$$I_{s,0}R=V_0(\alpha+ik)\left[\frac{C_1}{C_1+C_2}\right] \tag{8}$$

and

$$I_{s,0}(\alpha+ik)=V_0i\omega C_1; \tag{9}$$

from (8) and (9) we obtain by elimination of $(\alpha+ik)$

$$I_{s,0}=V_0\sqrt{\frac{i\omega C_1}{R}}\sqrt{\frac{C_1}{C_1+C_2}}. \tag{10}$$

The loss factor depends on the real part of this expression.

We must next calculate the real part of the current entering the capacitance C_2 via the metal surface above the airgap. This current is given by:

$$I_{C_2}=C_2\int_0^z\frac{\partial}{\partial t}(V(t)-V_s)dx \tag{11}$$

where z is the extent of the line.

Using our solution (6) for V_s this becomes:

$$I_{C_2}=i\omega\frac{C_1C_2}{C_1+C_2}V(t)\int^z(1-e^{-x(\alpha+ik)})dx \tag{12}$$

we note that for very high resistivity the integral is

$$I_{C_2}=i\omega V(t)\frac{C_1C_2}{C_1+C_2}z \tag{13}$$

as expected.

We are however interested in the general case and particularly in the real amplitude

$$I_{C_{2,0}}\text{ real}=-\frac{C_1C_2}{C_1+C_2}V_0\omega\int_0^z\sin kxe^{-\alpha x}dx. \tag{14}$$

Now α may be found from (8) and (9) to be

$$\alpha=k=\frac{1}{\sqrt{2}}\sqrt{\omega R(C_1+C_2)} \tag{15}$$

and the integral (14) evaluated for a sufficiently large upper limit gives

$$I_{C_{2,0}}\text{ real}=-\frac{\omega V_0}{2\alpha}\frac{C_1C_2}{C_1+C_2} \tag{16}$$

combining (15) and (16) gives

$$I_{C_{2,0}}\text{ real}=-\sqrt{\frac{\omega C_1}{2R}}\sqrt{\frac{C_1}{C_1+C_2}}\left(\frac{C_2}{C_1+C_2}\right). \tag{17}$$

The total "in phase current" per unit edge of section B consists of the real parts of eqs (17) and (10), i.e.,

$$I\text{ real}_B=\sqrt{\frac{\omega C_1}{2R}}\left(\frac{C_1}{C_1+C_2}\right)^{3/2}. \tag{18}$$

In section A, C_1 is unchanged and $C_2=0$ so that from (18)

$$I\text{ real}_A=\sqrt{\frac{\omega C_1}{2R}}. \tag{19}$$

This formula was reported in (1) but may now be regarded as a special case of (18).

We must next determine the total current in the capacitor so as to form the loss factor. This current will arise from contributions of many sections of the capacitor having various values of C_2 but since we can only measure an average value of C_2 we proceed as if C_2 were the same at all points, then

$$I \text{ imag} = \omega V_0 \left(\frac{a C_1 C_2}{C_1 + C_2} \right) \tag{20}$$

where a is the area of the capacitor, i.e., the area of the small plate.

We are now in a position to calculate separately the loss tangents due to sections A and B of figure 2. Dividing (18) and (19) by (20) and multiplying each of the resulting expressions by an effective edge length gives:

$$\phi_B = \frac{l_B}{a} \frac{C_1}{C_2} \sqrt{\frac{1}{2R\omega}} \sqrt{\frac{1}{C_1 + C_2}} \tag{21}$$

and

$$\phi_A = \frac{l_A}{a} \frac{1}{\sqrt{C_1}} \sqrt{\frac{1}{2R\omega}} \left(\frac{C_1 + C_2}{C_2} \right). \tag{22}$$

4. Discussion

For large values of C_2 eqs (21) and (22) reduce to

$$\phi_B \propto C_1 1/\sqrt{\omega} \tag{23}$$

and

$$\phi_A \propto (1/\sqrt{C_1})(1/\sqrt{\omega}) \tag{24}$$

respectively. If now the sample has its conductive face on the larger plate, there are no edge effects and (23) is applicable thus confirming that much of the experimental observations. If on the other hand, the sample is reversed, then both effects operate and the difference will be due to ϕ_A thus confirming the remainder of the observed dependence on capacitance.

In practice the approximations (23) and (24) are not justified since C_1 and C_2 are generally of the same order, but it must be remembered that the correction as used in (I) is now included in (21) and (22). A check on the results in (I) showed that agreement with experiment is just as good using (21) and (22) on the experimental values that were quoted in (I) provided that the corrections used there are discarded.

It also follows from eqs (21) and (22) that the losses due to tangential current in the surface all depend on the inverse of the square root of the frequency. We reproduce in figure 3 the frequency dependence of the losses of split and unsplit mica together with arbitrarily drawn lines of slope $(-1/2)$.

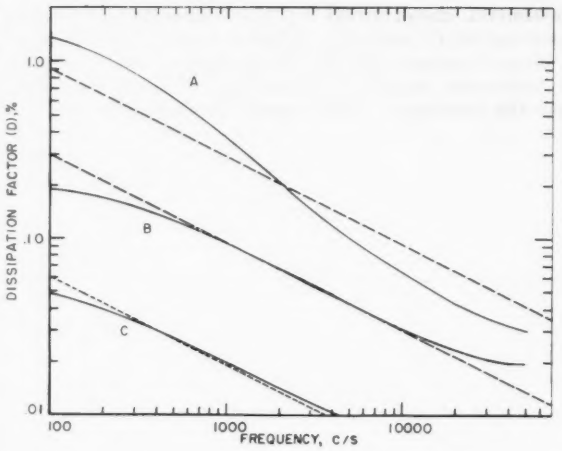

FIGURE 3. *Relationship between the dissipation in a mica capacitor and frequency for various experimental arrangements.*

The agreement of the two curves representing split samples is very gratifying. Of considerable interest is the fact that the curve for the old surface also follows the $-1/1$ power law. This indicates that all losses measured in mica are possibly due to surface currents and the intrinsic losses in this material may be much smaller than values usually quoted in the literature.

The final question arises whether the effective airgap is physical or instrumental. If it were physical we would have to suppose that the mica surface is uneven to a sufficient degree to cause the effective airgap. If the explanation were instrumental one would have to suppose that the mica sample, though smooth, did not make good contact with the plates perhaps because of a warping in the plates. In any case it is hoped that the theory presented here will be generally useful in the measurement of dielectric properties of thin samples.

5. Conclusions

The present work indicates that whenever thin slabs of material are examined for loss characteristics, one must expect disturbing influences due to surface losses. These generally depend on the inverse square root of the frequency. Though the theory is developed specifically to account for a rather esoteric experiment with mica, its general significance for dielectric measurements is obvious.

(Paper 68A–267

JOURNAL OF RESEARCH of the National Bureau of Standards—A. Physics and Chemistry
Vol. 68A, No. 2, March-April 1964

Polymorphism of Bismuth Sesquioxide. I. Pure Bi_2O_3

Ernest M. Levin and Robert S. Roth

(December 3, 1963)

Stability relationships of the four polymorphs of bismuth oxide have been determined by means of DTA and high-temperature x-ray studies. The stable low-temperature monoclinic form transforms to the stable cubic form at 730 ±5 °C, which then melts at 825 ±5 °C. By controlled cooling, the metastable tetragonal phase and/or the metastable body-centered cubic (b.c.c.) phase appear at about 645 °C. Whereas b.c.c. can be preserved to room temperature, tetragonal will transform to monoclinic between 550 and 500 °C. Tetragonal Bi_2O_3, however, is easily prepared by decomposing bismutite (Bi_2O_3·CO_2) at 400 °C for several hours. The greatest transition expansion occurs at the monoclinic to cubic inversion, and cubic Bi_2O_3 shows the greatest coefficient of volume expansion. With exposure to air, Bi_2O_3 carbonates and partially transforms to bismutite and an unknown phase.

1. Introduction

Bismuth oxide is assuming an increasing importance in the ceramic field, particularly in the glass and electronics industries. A literature survey of the polymorphism of Bi_2O_3, in connection with phase studies of the systems Bi_2O_3—B_2O_3[1][1] and Bi_2O_3—Nb_2O_5[2], revealed unexplained inconsistencies in the data and no unequivocal interpretation. Furthermore, it was realized that a conclusive study of the polymorphic relationships would involve an identification of phases at temperature.

A number of investigators [3–10] have reported on temperatures of transitions and phase changes in Bi_2O_3. Schumb and Rittner [6] have reviewed the work prior to 1943. Table 1 summarizes the literature data through the work of the present authors, and includes, when given, methods of preparation and study, stable and unstable polymorphs, and temperatures of transitions.

It can be seen from the table that both pure and impure forms of Bi_2O_3 have been reported, with disagreement among investigators both as regards the identity and the stability of the pure phases. The essential conclusions which may be drawn from the previously reported data, as given in table 1, are as follows:

(1) All investigators agree that monoclinic (Mon), pseudo-orthorhombic, (α-Bi_2O_3) is the stable low temperature form.

(2) Schumb and Rittner believe that the tetragonal (Tet), or pseudocubic form (β-Bi_2O_3) is stable above 710 °C. Sillén suggested that this form might be simple cubic at higher temperatures. He based his hypothesis, in part, on analogy with cubic (C) As_2O_3 and Sb_2O_3.

(3) Schumb and Rittner discovered a b.c.c. phase (γ-Bi_2O_3) representing a metastable form of Bi_2O_3. The finding was confirmed later by Aurivillius and Sillén, who agreed that the unit cell probably contained $Bi_{26}O_{39}$.

(4) Gattow and Schröder, from the results of high-temperature x-ray, differential thermal analysis, and linear thermal expansion studies have found only two polymorphs of Bi_2O_3, namely the low temperature Mon form which transforms reversibly to a high temperature, face-centered cubic form, designated δ-Bi_2O_3.

(5) A number of investigators have reported an impure b.c.c. phase, formed by contamination with porcelain, Si, Fe, Al, and other impurities. Sillén suggested the ideal formula type $Me_2Bi_{24}O_{40}$.

(6) Gattow and Schröder[2] propose the designation δ^*, β^*, γ^* for the impurity forms of C-, Tet-, and b.c.c.Bi_2O_3, respectively.

(7) Previous investigators, usually using a cooling curve method, have reported transition temperatures between 700 and 717 °C. Liquidus temperatures vary from 817 to 825 °C.

The objective of this work (part I) was to clarify the polymorphic relationships of pure Bi_2O_3. This could best be accomplished by the method of high-temperature x-ray diffractometry, which avoids the problem of nonquenchable phases. The study was enlarged (part II) to include the effect of oxide additions on the polymorphism of Bi_2O_3, when a modification of the x-ray furnace permitted the determination of solidus temperatures and even, under favorable conditions, of liquidus temperatures. It was expected that the latter study would provide information on the impure forms.

[1] Figures in brackets indicate the literature references at the end of this paper.

[2] Gattow and Schröder [10] report a metastable bismuth oxide phase, Bi_2O_5, formed under oxidizing conditions and very similar in structure to Tet, β-Bi_2O_3; however, no identifying characteristics other than chemical analysis are given. Moreover, it transforms to β-Bi_2O_3 in about 3 months at 20 °C, or more rapidly at 470 ±50 °C, or in a partial vacuum.

TABLE 1. *Literature summary on polymorphism of Bi_2O_3*

Investigator	Form	Method of preparation	Notes	Method of study	Transition temp.	Melting temp.
Guertler (1903) [3]		From basic nitrate in porcelain crucible.	(Contains 1.3% silic acid)	Cooling curve. Heating curve. Cooling curve.	704±1 °C 705±1 °C	820±2°C 825±5° 860°
Belladen (1922) [4]		Calcination of basic nitrate.		Cooling curve.		817°
Sillén (1937) [5]	α-Bi_2O_3 (Mon) β-Bi_2O_3 (Tet)	$Bi(NO_3)_3$ (aq)+KOH (aq). Condensation of bismuth vaper from graphite furnace, in O_2 stream.	Stable low-temp. form. May be cubic at higher temperatures. a=10.93 c=5.62 kx.			
	b. c. c.	Fused in porcelain at 900°C for 5 min a or with Al_2O_3 or Fe_2O_3.	Suggested formula type: $Me_2Bi_{24}O_{36}$. a=10.08 kx'			
	Cubic Bi_2O_3	Fused in porcelain at 900 °C for 20 min.	Contaminated with silicon, a=5.525 kx.			
Schumb and Rittner (1943) [6]	α-Bi_2O_3 (Mon)	Purification of C. P. Bi_2O_3 by heating at 750°C and leaching.	99.99±0.06% Bi_2O_3. Stable below 709 °C.	X ray examination of rapidly cooled Sample	710°	
	β-Bi_2O_3 (Tet)	Arc between graphite electrode and molten bismuth in O_2 stream.	99.8±0.2% Bi_2O_3. Stable above 710°. a=10.93 c=5.63 kx.			
	γ-Bi_2O_3 (b. c. c.)	Controlled cooling of β-Bi_2O_3 from 750-800 °C in Pt crucible.	Metastable: probably $Bi_{38}O_{39}$. a=10.245 kx.			
	b. c. c.	Fusion (875 °C) of Bi_2O_3 in porcelain and with SiO_2.	Impure phase: a=10.090 kx.			
	Cubic Bi_2O_3	Fusion (875 °C) of Bi_2O_3 in porcelain or silica crucible at 875° and water quenching.	Impure phase: a=5.525 kx.			
Aurivillius and Sillén (1945) [7].		Not given.	Stated to be pure Bi_2O_3.	Cooling curve of a large quantity in Pt crucible.	≈700°	
	γ-Bi_2O_3 (b. c. c.)	Same as Schumb and Rittner (1943).	Probably $Bi_{38}O_{39}$. a=10.243 kx.			
Royen and Swars (1957) [8].	β-Bi_2O_3 (Tet)	Quenched molten Bi_2O_3 from "850° or perhaps 920° C".	α-Bi_2O_3 may also be present in minor amt.			
Belayev and Smolaynenov (1962) [9].		Bi_2O_3 calcined at 500 °C/1-1.5 hr.		Visual polythermal.	704°	819°
Gattow and Schröder (1962) [10].	α-Bi_2O_3 (Mon)	Not given.	100.0±0.1% Bi_2O_3. Stable low-temp. form.	DTA and high-temp. x ray.	717±7 °C	
	δ-Bi_2O_3 (Cubic)		Stable high-temp. form. a=5.65±0.008 Å (at 750 °C).	High-temp. x ray.		824±2 °C
	δ*-Bi_2O_3		Cubic impurity form.[a]	X ray.		
	β*-Bi_2O_3		Tetragonal impurity form.[b]	X ray.		
	γ*-Bi_2O_3		Body-centered cubic impurity form.[c]	X ray.		
Levin and Roth (present work)[d]	Mon Bi_2O_3	Commercial "Spec. pure" and ACS Grades.	Stable low-temp. form.	DTA and high-temp. x ray.	730±5 °C	
	Cubic Bi_2O_3	....do....	Stable high-temp. form. a=5.66 Å (at 750°C).	High-temp. x ray.		825±5 °C
	Tet Bi_2O_3[e]	....do....	Metastable: formed from super-cooling Cubic Bi_2O_3. a=10.93 Å c=5.63 Å	DTA and high-temp. x ray.		
	b. c. c.[f]	....do....	Metastable: formed from supercooling cubic Bi_2O_3. Anion impurities may be important. a=10.268 Å.	High-temp. x ray.		

[a] Obtained by fast quenching of molten bismuth oxide mixtures heated at 800 to 1000 °C for 15 to 60 min. Bi_2O_3 mixed with: As_2O_3, Sb_2O_3, La_2O_3, Nd_2O_3, Cr_2O_3, SiO_2, SnO_2, TiO_2, V_2O_5, Nb_2O_5, Ta_2O_5, WO_3. The same phase was obtained from aqueous solution in the system Bi_2O_3-MoO_3.

[b] Obtained under certain conditions with mixtures of Bi_2O_3 and: Al_2O_3, Ga_2O_3, In_2O_3, Y_2O_3, Ti_2O_3, Fe_2O_3, Cr_2O_3, PbO_2, MnO_2, CeO_2, ZrO_2, ThO_2.

[c] Sillén's body-centered cubic (b. c. c.) type. Impurity oxides not listed.

[d] See also [1, 2].

[e] Pure tetragonal Bi_2O_3 at room temperature can be obtained easily by heating $Bi_2O_3 \cdot CO_2$ (bismutite) at about 400 °C for 2 to 16 hr.

[f] A related b. c. c. form is either stable or metastable depending on the cation impurity (discussed in part II).

2. Starting Materials

Two commercially available grades of bismuth oxide were used. One sample was of reported spectrographic purity; the other sample was certified reagent grade (ACS). The results of a qualitative spectrochemical analysis by the Analytical and Inorganic Chemistry Division of the National Bureau of Standards showed that the reagent grade sample contained iron and silicon (0.01 to 0.001%) in significantly higher concentrations than the spectrographic grade (less than 0.001%). Minor differences between the two samples were observed for a number of other elements (Ag, Al, Ca, Cr, Cu, Mg, Mn, Na, Ni, and Pb), which were each estimated to be present at less than 10 ppm metal in Bi_2O_3.

The following commercially available compounds were used for studying decomposition effects on the polymorphism of Bi_2O_3: bismutite ($Bi_2O_3 \cdot CO_2$), bismuth hydroxide, bismuth nitrate ($Bi(NO_3)_3 \cdot 5H_2O$), bismuth subnitrate, bismuth subgallate, and bismuth subsalicylate.

3. Apparatus and Method

Polymorphic relationships in Bi_2O_3 were first deduced from differential thermal analyses of approximately 0.3 g samples. A few experiments on larger samples (approximately 3 g) gave no significant differences. The deduced relationships were then confirmed with the aid of the high-temperature x-ray diffractometer furnace. The diffraction data were obtained with a modification of the diffractometer furnace described by Mauer and Bolz [11]. The essential feature of the modification [12] involved a platinum sample holder to which the powdered samples could be made to adhere by using a thin smear of petroleum jelly. The petroleum jelly volatilizes at a low temperature, leaving the sample adhered to the surface.

It may be noted that the standard quenching technique was of limited value in this study, because the high-temperature form of Bi_2O_3 could not be quenched. However, in experiments dealing with the preservation at room temperature of the Tet and b.c.c. metastable phases a small quench furnace of low heat capacity was used. The furnace enabled one to control the cooling rate between two temperatures prior to quenching.

4. Results and Discussion

4.1. DTA and High-Temperature X-Ray Results

The results of differential thermal analyses of small samples (0.3 g) are summarized in figure 1. Phase identification was verified by comparison with the results obtained from the high-temperature x-ray diffraction experiments, also shown in figure 1.

The basic phase equilibrium relationships are revealed. At 730 ±5 °C, the low temperature Mon form transforms to cubic Bi_2O_3 (C),[3] which remains stable up to the melting point, 825 ±5 °C. If the sample is not heated above about 745 °C (see high-temperature x-ray results), or is heated very rapidly to higher temperatures, then, on cooling, inversion to the Mon form takes place at 700 °C. If some of the Mon form persists above the transition, it will nucleate the inversion, on cooling.

If the C form is heated above about 775 °C, considerable supercooling of the C phase occurs, and tetragonal Bi_2O_3 forms at 650 to 645 °C. The Tet phase formed in this manner cannot be preserved to room temperature but transforms to the Mon phase at temperatures varying between 550 and 450 °C. If, however, the Tet phase is heated, conversion to the cubic form occurs between 660 and 670 °C.

Data from the high-temperature x-ray experiments revealed the b.c.c. phase in addition to the Tet phase. The b.c.c. phase appeared at a temperature slightly below that at which the Tet phase formed, and on reheating, the b.c.c. to C transition occurred slightly below that of the Tet to C transition. Once formed the b.c.c. phase could be preserved to room temperature by "furnace cooling." Slow heating of the b.c.c. phase from room temperature yielded the stable Mon phase at about 625 °C.

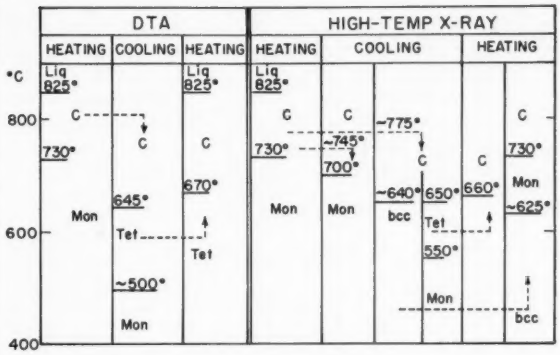

FIGURE 1. *Schematic representation of results of differential thermal analysis (DTA) and high-temperature x-ray experiments on* Bi_2O_3.
Dashed arrows indicate changes in direction of the heating and cooling schedule. Polymorphs: Mon—monoclinic, C—cubic, Tet—tetragonal, b.c.c.—body-centered cubic.

A weight-loss determination on 0.3 g of the ACS grade Bi_2O_3 was made simultaneously with a DTA experiment (DTGA) on an independent sample. No detectable change in weight (within 0.001 g) was observed during heating and cooling through the various inversion temperatures.

Figure 2 is a postulated stability diagram for the polymorphs of Bi_2O_3, based on the data in figure 1 and supported by additional experiments with the low-heat capacity quench furnace, to be discussed later. The ordinate in figure 2 is an undefined measure of stability, for example, free energy of formation or vapor pressure. The metastable melting point of Mon Bi_2O_3 is shown at approximately 800 °C, the temperature at which liquid was detected in the high-temperature x-ray furnace during rapid heating of the Mon form.

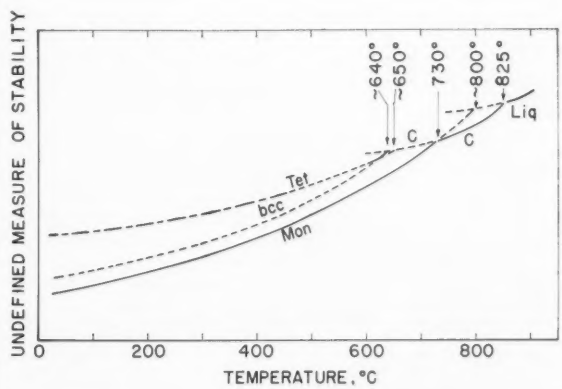

FIGURE 2. *Postulated stability diagram of* Bi_2O_3.
Polymorphs: Mon—monoclinic, C—cubic, Tet—tetragonal, b.c.c.—body centered cubic, Liq—liquid.

[3] The x-ray diffraction powder data fit a face-centered cubic cell. Sillén has interpreted the cubic phase as being simple cubic, whereas Gattow and Schröder [10] consider the symmetry to be face-centered cubic.

In the high-temperature x-ray experiments, the Tet phase appeared first on cooling of the C phase and disappeared last when transformation to the C form occurred. Therefore, in figure 2, the metastable C to Tet inversion is shown at a slightly higher temperature than the metastable C to b.c.c. inversion. However, considerable overlapping of the two forms occurred, indicating that the two inversion temperatures are near to each other. Below about 640 °C the b.c.c. phase is shown as more stable than the tetragonal phase, because only the former could be preserved to room temperature by supercooling from high temperatures.

Figure 3 shows a plot of pseudocell dimensions of the various polymorphs of Bi_2O_3 versus temperature. The data were obtained by use of the high-temperature x-ray furnace. For comparison purposes, the cell dimensions were reduced to correspond to a pseudounit cell volume for two molecules of Bi_2O_3, according to the arbitrary manner given in the caption of figure 3. The coefficient α of linear thermal expansion for each cell direction was calculated on the original unit cell data by applying least squares to the several sets of data. The cell dimension data were obtained for relatively low 2θ values (below 50°); and, consequently, the accuracy of the thermal expansion values is estimated to be in the order of $\pm 0.2 \times 10^{-5}$.

The pseudo-orthorhombic (Mon) form showed low linear thermal expansion coefficients, namely, 0.5 $\times 10^{-5}$, 1.3 $\times 10^{-5}$, and 1.5 $\times 10^{-5}$ Å/Å/deg for the a, b, and c directions, respectively. The average of these three x-ray determined values is 1.1 $\times 10^{-5}$/deg, in fair agreement with the values reported by Gattow and Schröder [10], using a dilatometric method. Their values ranged from 1.22 $\times 10^{-5}$/deg at 100 to 200 °C to 1.48 $\times 10^{-5}$/deg at 575 to 675 °C. The coefficient of linear thermal expansion found in the present work for the C form, 2.4 $\times 10^{-5}$/deg, is almost half that reported by Gattow and Schröder, 4.36 $\times 10^{-5}$/deg. The c axis for Tet Bi_2O_3 showed the largest coefficient of linear thermal expansion, 3.5 $\times 10^{-5}$/deg. Based on volume expansion, however, the C form would show the greatest coefficient of expansion (7.2 $\times 10^{-5}$/deg), and the Mon form, the lowest expansion (3.3 $\times 10^{-5}$/deg).

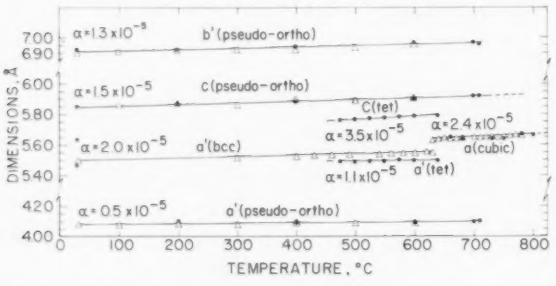

FIGURE 3. *Pseudocell dimensions (based on Z=2) of the polymorphs of Bi_2O_3 versus temperature.*

Cell dimensions have been reduced to correspond to $Z=2Bi_2O_3$, in the following arbitrary manner:
pseudo-orthorhombic—monoclinic polymorph
$a'(Z=2)=(1/2)a(Z=8)$, $b'(Z=2)=(1/2)b(Z=8)$, $c(Z=2)=c(Z=8)$.
Cubic—cubic polymorph
$a(Z=2)=a(Z=2)$.
Tet—tetragonal polymorph
$a'(Z=2)=(1/2)a(Z=8)$, $c(Z=2)=c(Z=8)$.
b.c.c.—body-centered cubic polymorph
$a'(Z=2)=\sqrt{2}/13$ $(Z=13)$.
α=coefficient of linear thermal expansion, calculated by method of least squares on original data.
●—from certified reagent grade (ACS) Bi_2O_3.
Δ—from "Spec. pure" grade Bi_2O_3.

It may be seen that the Mon phase shows a large expansion, 6.9 percent, when transforming to the C phase at 730 °C. Gattow and Schröder reported a volume expansion at the transition temperature of 4.11±0.06 percent. Thus the present authors obtained a higher percentage of volume expansion at the Mon to C transition temperature and a lower coefficient of linear thermal expansion for the cubic form, than did Gattow and Schröder. Gattow and Schröder used a relatively fast heating rate of 7°/min, but the Mon to C transition is not instantaneous

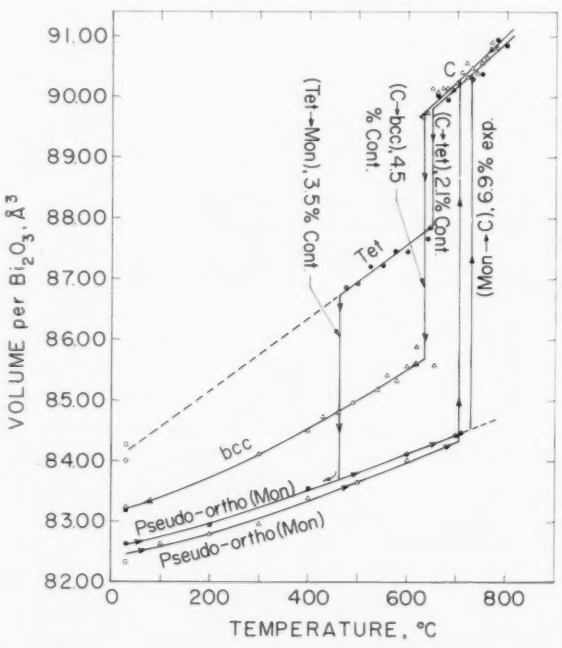

FIGURE 4. *Volume per molecule versus temperature for the polymorphs of Bi_2O_3.*

(Calculated from the unit cell dimensions obtained with the high-temperature x-ray diffractometer furnace).
Polymorphs: Pseudo-orthorhombic (Mon)—monoclinic, C—cubic, Tet—tetragonal, b.c.c.—body-centered cubic.
% exp.—percentage expansion at transition.
% cont.—percentage contraction at transition.
●—from certified reagent grade (ACS) Bi_2O_3.
Δ—from "spec pure" grade Bi_2O_3.
◇—from decomposition of bismutite.
□—data taken from Sillén [5].
■—data taken from Schumb and Rittner [6].

and occurs over a temperature range. Gattow and Schröder's results may be explained on the basis that in their experiments all of the Mon form did not transform at the inversion temperature but continued to transform during heating of the C phase. Such a situation would lead to an apparently low Mon to C expansion and an apparently high thermal expansion of the C phase.

The C to Tet transition involves a relatively small contraction, 2.1 percent, indicating the similarity in unit cell volumes of the two forms. The contraction in the transition from the C to b.c.c. is 4.5 percent. It is seen that the temperature dependence of the volume per Bi_2O_3 varies for the polymorphs and that the room temperature volume differences are considerably less than at higher temperatures.

4.2. Low-Heat Capacity Furnace Results

The C form of Bi_2O_3 cannot be "quenched" at room temperature. In previous phase equilibrium studies by the present investigators [1, 2] only the Mon phase was obtained in pure Bi_2O_3 by quenching samples in sealed platinum tubes from all temperatures up to 100 °C above the melting point of Bi_2O_3. The stability diagram (fig. 2), however, indicated a method whereby the metastable phases might be obtained at room temperature, as follows: (a) Heating a sample in a sealed platinum tube to a temperature at which it would be definitely all cubic (above about 775 °C) or liquid. (b) Slow cooling of the sample to about 625 °C, with the possibility that the C phase would be supercooled below 730 °C and would transform to one of the metastable phases. (c) Quenching the metastable phase existing at temperature.

Accordingly, a number of experiments were performed with the low heat capacity furnace in which temperatures and rates of cooling were varied. Identification was by means of the x-ray powder diffraction method applied to the quenched samples. The essential results are summarized as follows:

(a) Pure b.c.c. Bi_2O_3 was formed by heating a sample above the liquidus, at 850 °C for 10 min, cooling to 625° C in about 45 min, and continued heating at this temperature for 5 min, before quenching.

(b) Body-centered cubic Bi_2O_3 with a trace of Tet Bi_2O_3 could be formed by heating a sample below the liquidus, to 775 °C. The cooling schedule was similar to that in (a).

(c) Pure b.c.c. Bi_2O_3 could be formed readily below the liquidus temperature by a recycling heat treatment, namely, by heating twice to 780 to 785 °C and cooling twice to about 625 °C, before quenching.

(d) These experiments never yielded a large amount of Tet Bi_2O_3. In several cases, however, the Mon phase was found with a trace of the Tet; it seems probable that at temperature the specimens were Tet.

The work of Royen and Swars [8] is related to the problem of forming Tet Bi_2O_3 from pure bismuth oxide. They formed some Tet Bi_2O_3 by fast quenching of molten Bi_2O_3 from temperatures above about 850 °C. Their work was essentially substantiated in the present investigation, by quenching specimens enclosed in platinum foil envelopes from temperatures of 930 °C (5 min heating period) and 980 °C (1 min heating period). It may be noted that although the Tet phase was present in appreciable amounts, the major phase consisted of Mon Bi_2O_3. Quenching from the higher temperature did not yield an appreciable higher percentage of the Tet phase. However, samples contained in sealed platinum tubes and quenched from the same temperatures showed only Mon Bi_2O_3.

4.3. Aging Experiments on Bi_2O_3

During the course of the work, an aging effect on Bi_2O_3 was discovered. Material from a freshly opened bottle of Bi_2O_3 gave an x-ray powder pattern

TABLE 2. *Aging experiments on* Bi_2O_3

Sample grade	Environment		Time	X ray results[a]
	Atmosphere	Temp.		
		°C	*Days*	
ACS	Air	≈25	76	Mon (m)+Bi_2O_3·CO_2 (m)+X[b] (l)
"Spec pure"	Air	≈25	76	Mon (m)+Bi_2O_3·CO_2 (s)+X[b] (l)
ACS	Air	≈25	147	Mon (m)+Bi_2O_3·CO_2 (tr)+X[b] (l)
"Spec pure"	Air	≈25	147	Mon (m)+Bi_2O_3·CO_2 (s−)+X[b] (l)
ACS	H_2O sat. air+CO_2[c]	≈25	17	Mon (l)+Bi_2O_3·CO_2 (s+)
"Spec pure"	H_2O sat. air+CO_2[c]	≈25	17	Mon (l)+Bi_2O_3·CO_2 (m)
ACS	H_2O sat. air+CO_2[c]	≈25	55	Mon (l)+Bi_2O_3·CO_2 (s)
"Spec pure"	H_2O sat. air+CO_2[c]	≈25	55	Mon (l)+Bi_2O_3·CO_2 (m)
ACS	H_2O sat. air+CO_2[c]	≈25	76	Mon (l)+Bi_2O_3·CO_2 (s−)+X[b] (l)
"Spec pure"	H_2O sat. air+CO_2[c]	≈25	76	Mon (l)+Bi_2O_3·CO_2 (m)+X[b] (m)
ACS	H_2O sat. air	≈25	167	Mon (m)+Bi_2O_3·CO_2 (tr)+X[b] (l)
"Spec pure"	H_2O sat. air	≈25	167	Mon (m)+Bi_2O_3·CO_2 (s−)+X[b] (m)
ACS	H_2O sat. air[d]	140	1	Mon (l)
ACS	CO_2[d]	157	1	Mon (l)
ACS	H_2O sat. CO_2[d]	145	2¾	Mon (l)

[a] Mon-monoclinic phase: l—large percentage, m—moderate percentage, s—small percentage, tr—trace.

[b] Unknown phase: *d* values of 3.71 Å, 3.68 Å, 3.02 Å (l), 2.74 Å, 2.45 Å.

[c] Specimen in stoppered flask, suspended over water, with periodic additions of dry ice.

[d] Gas or vapor stream directed through heated chamber containing specimen.

for pure Mon Bi_2O_3. About six months later, however, material from the same bottle, which had not been desiccated, showed the prominent diffraction peaks corresponding to bismutite ($Bi_2O_3 \cdot CO_2$). The effect of the bismutite formation seemed to be a tendency toward lowering of the temperature of the Mon to C inversion to about 715 °C and also toward increasing the probability of forming the b.c.c. phase during supercooling of cubic Bi_2O_3. This effect may be seen in figure 4, for a sample of spectrographic purity and offers a possible explanation for the lower inversion temperature reported by previous investigators (see table 1). It should be emphasized, however, that the b.c.c. phase could be formed from pure material, as discussed previously under 4.1 and 4.2, above.

This chance discovery of an aging effect led to a number of experiments (summarized in table 2) in an attempt to accelerate the process. Experiments in which pure Bi_2O_3 was suspended over water in a stoppered flask and to which additions of dry ice were made periodically produced bismutite in small to moderate amounts, after 17 days. At the end of 55 days there was no increase in amount of bis-

TABLE 3. *Thermal decomposition experiments on bismuth compounds*

Chemical		Heat schedule		Total ignition Loss	X ray results [a]
Name	Approximate formula (theoretical ignition loss)	Temp.	Time		
		°C	hr		
Bismutite (U.S.P.)	$Bi_2O_3 \cdot CO_2$ (8.63%)	300	1.5	8.08	Tet Bi_2O_3
		390	66	8.65	Tet Bi_2O_3 a-10.9 Å, c-5.62 Å
		490	1.5	8.75	Mon Bi_2O_3
		800	1[b]	8.90	b.c.c. Bi_2O_3+? (tr)
Bismutite (U.S.P.)	$Bi_2O_3 \cdot CO_2$ (8.63%)	200	16	0.29	$Bi_2O_3 \cdot CO_2$
		300	18	1.05	$Bi_2O_3 \cdot CO_2$
		350	4	5.47	Tet Bi_2O_3 (l)+$Bi_2O_3 \cdot CO_2$
		400	18	9.08	Tet Bi_2O_3
		800	¼[b]		b.c.c. Bi_2O_3
		775	2		Mon Bi_2O_3
Bismuth subsalicylate (powder, U.S.P.)	$Bi(C_7H_5O_3)_3Bi_2O_3$ (35.6%)	137	16	0.06	Bismuth subsalicylate (?)
		200	16	.42	Subsalicylate (?)+unknown
		300	16	35.0	Tet Bi_2O_3
		400	16	35.54	Mon Bi_2O_3
		450	16	35.57	Mon Bi_2O_3
		500	16	35.57	
Bismuth subgallate (powder)	$Bi(OH)_2C_7H_3OH$ (43.4%)	137	16	10.10	Bismuth subgallate (?)[c]
		200	16	14.02	Unknown
		300	16	45.71	Tet Bi_2O_3
		400	16	45.91	Mon Bi_2O_3
		450	16	45.92	Mon Bi_2O_3
		500	16	45.92	
Bismuth hydroxide[d]	$Bi(OH)_3$ (10.4%)	137	16	0.13	$Bi_2O_3 \cdot CO_2$ (l)+? (s)
		200	16	.28	$Bi_2O_3 \cdot CO_2$ (l)+? (s)
		300	16	1.13	$Bi_2O_3 \cdot CO_2$
		400	16	8.18	Tet Bi_2O_3 (l)+b.c.c. (s)
		450	16	8.42	b.c.c. Bi_2O_3 (l)+Mon Bi_2O_3 (s)
		500	16	8.46	b.c.c. Bi_2O_3 (l)+Mon Bi_2O_3 (s)
		600	2	8.50	Mon Bi_2O_3 (m)+b.c.c. Bi_2O_3 (m)[c]
		700	18	8.50	Mon Bi_2O_3 (l)+b.c.c. Bi_2O_3 (s)[c]
Bismuth nitrate (crystals, ACS)	$Bi(NO_3)_3 \cdot 5H_2O$ (52.0%)	137	16	37.50	Unknown
		200	16	39.58	Unknown
		300	16	45.38	Amorphous (l)+Unknown (m)
		400	16	49.60	Unknown (l)+Tet Bi_2O_3 (m)
		450	16	51.44	Mon Bi_2O_3
		500	16	51.44	Mon Bi_2O_3
		800[f]			b.c.c. Bi_2O_3+? (tr)[f]
Bismuth subnitrate (powder)	$Bi(OH)_2NO_3$ (23.6%)	137	16	2.95	Amorphous+Unknown
		200	16	4.44	Amorphous+Unknown
		300	16	10.81	Amorphous+Unknown
		400	16	16.52	Intermediate Unknown
		450	16	19.36	Mon Bi_2O_3+Tet Bi_2O_3 (s)+Intermediate Unknown
		500	16	20.25	Mon Bi_2O_3
Bismuth oxyhydroxide[g]	BiO(OH) (3.72%)	135	16	.35	Amorphous+Unknown
		200	16	.95	Amorphous+Unknown
		250	16	1.57	Amorphous+Unknown
		300	17	1.71	Unknown+Mon Bi_2O_3 (s)
		350	7	1.74	Unknown+Mon Bi_2O_3 (m)
		400	16	2.77	Unknown+Mon Bi_2O_3 (m+)
		450	7	5.48	Mon Bi_2O_3
		500	16	5.62	Mon Bi_2O_3
		550	16	5.62	

[a] Polymorphs: Mon-monoclinic, Tet-tetragonal, b.c.c.-body-centered cubic. Percentages: l-large, m-moderate, s-small, tr-trace.

[b] Platinum crucible containing specimen removed from furnace at temperature and immediately chilled by dipping into ice water. (Water did not touch specimen.)

[c] Poorly crystalline.

[d] Commercially obtained preparation, essentially bismutite by x-ray analysis.

[e] d values show shift, indicating smaller unit cell.

[f] X ray analysis after a DTA experiment.

[g] Prepared in National Bureau of Standards Laboratory by Johan H. deGroot by adding bismuth nitrate to boiling 20 percent NaOH soln., in Pt dish. Material dried at 60 °C for 17 hr, then at 85 °C for 65 hr.

mutite formed. After 76 days, samples exposed to water vapor and CO_2 or to air at room temperature showed a large amount of an unidentified phase (X in table 2). With continued exposure the unidentified phase, in both experiments, increased at the expense of the bismutite and Mon phases. Attempts to rapidly accelerate the formation of bismutite or the unknown phase by passing over the heated sample a stream of (1) CO_2 gas, (2) CO_2 saturated water vapor, or (3) water saturated air, were unsuccessful (see last 3 experiments of table 2). The aging experiments demonstrate the fact that Bi_2O_3 is reactive under atmospheric conditions and must be tightly sealed and desiccated to avoid compositional changes.

4.4. Thermal Decomposition Experiments

The discovery of bismutite ($Bi_2O_3 \cdot CO_2$) in aged bismuth oxide samples led directly to thermal decomposition studies of bismutite and other bismuth containing organic compounds (see table 3). Approximately 1 g samples were accurately weighed into 30 ml platinum crucibles, heated in an electric resistance furnace at successively higher temperatures, and cooled in air. Ignition losses and x-ray powder diffraction patterns of the samples were obtained for the successive heat treatments.

It is seen from table 3 that bismutite heated at 390 °C for 66 hr or at 400 °C for 18 hr produced pure Tet Bi_2O_3. Within the limit of accuracy of the weight loss measurements, it appears that all of the CO_2 was driven off. At 490 °C, the Tet Bi_2O_3 was transformed to the stable Mon phase. Rapid cooling of a sample from 800 °C, by immersion of the bottom of the crucible in cold water, produced the b.c.c. phase.

Bismuth subsalicylate and bismuth subgallate when heated at 300 °C for 16 hr also yielded pure Tet Bi_2O_3. At the 400 °C heat treatment, the Tet phase was converted to the Mon phase.

The bismuth hydroxide sample, which was shown by x-ray analysis to be mainly bismutite, yielded three forms of Bi_2O_3 during decomposition. A large amount of the tetragonal phase was formed at 400 °C. At 450 and 500 °C, the Tet phase had disappeared, and the sample contained a large amount of the b.c.c. phase plus a small amount of the Mon phase. This transition supports the previously drawn conclusion that, at lower temperatures, the b.c.c. phase is more stable than the Tet phase. The 600 °C heat treatment produced an increasing amount of the Mon phase, at the expense of the b.c.c. phase. The remaining b.c.c. phase showed a shift in diffraction peaks corresponding to smaller d values. This shift would be consistent with a decrease in unit cell size, when certain foreign ions are added to pure Bi_2O_3, as will be discussed in part II.

Bismuth nitrate and bismuth subnitrate yielded some Tet Bi_2O_3 during decomposition, but never in major amount. By the end of the 500 °C heat treatment the samples were all Mon Bi_2O_3. Bismuth oxyhydroxide transforn.ed directly from the amorphous state to the Mon form of Bi_2O_3.

These experiments indicate that the decomposition of organic bismuth compounds at temperatures below 400 °C tend to produce the tetragonal form of Bi_2O_3. If, however, higher temperatures are required for complete decomposition, then the stable Mon Bi_2O_3 phase is formed.

5. Summary

By means of DTA and high-temperature x-ray studies it has been shown that pure bismuth oxide possesses two stable and two metastable polymorphs. A stable reversible transition between the low temperature Mon and the high temperature cubic form occurs at 730 ± 5 °C. The Mon to cubic transition is accompanied by a volume expansion of 6.9 percent. The cubic form shows the greatest coefficient of volume expansion (7.2×10^{-5}/deg). The melting point of the cubic phase is 825 ± 5 °C. Supercooling of the cubic form below the 730 °C Mon transition produces either the metastable tet form at 650 °C or the metastable b.c.c. form at about 640 °C. The results are given in table 1. Whereas by fast cooling, the b.c.c. phase can be preserved to room temperature, the tetragonal phase transforms to the stable Mon phase between 550 and 450 °C. Tetragonal bismuth oxide, however, can be formed readily by the decomposition of bismutite at 400 °C for 18 hr or by the decomposition of bismuth subgallate and bismuth subsalicylate at 300 °C for 16 hr. The Tet bismuth oxide so formed is preserved at room temperature. Bismuth oxide is subject to an aging effect in air and transforms partially to bismutite. With continued exposure an unidentified phase forms.

6. References

[1] E. M. Levin and C. L. McDaniel, J. Am. Ceram. Soc. **45** [8] 355–360 (1962).
[2] R. S. Roth and J. L. Waring, J. Res. NBS **66A** (Phys. and Chem.) No. 6, 451–463 (1962).
[3] W. Guertler, Z. Anorg. Chem. **37,** 222–224 (1903).
[4] L. Belladen, Gazz. Chim. Ital. **52II,** 160–164 (1922).
[5] L. G. Sillén, Arkiv Kemi, Mineralogi och Geologi **12A** [18] 1–13 (1937).
[6] W. C. Schumb and E. S. Rittner, J. Am. Chem. Soc. **65,** 1055–1060 (1943).
[7] B. Aurivillius and L. G. Sillén, Nature **155,** No. 3932, 305–306 (1945).
[8] P. Royen and K. Swars, Angew. Chem. **69** [24] 779 (1957).
[9] I. N. Belyaev and N. P. Smolyaninov, Zhur. Neorg. Khimi. **VII** [5] 1126–1131 (1962).
[10] G. Gattow and H. Schröder, Zeit. Anorg. Allgem. Chem. **318** [3–4] 176–189 (1962).
[11] F. A. Mauer and L. H. Bolz, WADC (Wright Air Develop. Center) Tech. Rept., No. 55–473 (December 1955).
[12] E. M. Levin and F. A. Mauer, J. Am. Ceram. Soc. **46** [1] 59–60 (1963).

(Paper 68A2–268)

Journal of Research of the National Bureau of Standards—A. Physics and Chemistry
Vol. 68A, No. 2, March–April 1964

Polymorphism of Bismuth Sesquioxide. II. Effect of Oxide Additions on the Polymorphism of Bi_2O_3

Ernest M. Levin and Robert S. Roth

The effect of small oxide additions on the polymorphism of Bi_2O_3 was studied by means of high-temperature x-ray diffractometry. Solidus and occasional liquidus temperatures were approximated, so that tentative partial phase diagrams for 33 oxide additions were constructed. Only the monoclinic and the cubic forms of Bi_2O_3 were found to be stable. Other phases, frequently reported by previous investigators, such as tetragonal and body-centered cubic (b.c.c.), were shown to form metastably from cooled liquid or cubic. An impure b.c.c. phase of distinct but variable composition appeared in systems of ZnO, PbO, B_2O_3, Al_2O_3, Ga_2O_3, Fe_2O_3, SiO_2, GeO_2, TiO_2, and P_2O_5. The impure b.c.c. phase in the systems with SiO_2, GeO_2, and TiO_2 melted congruently about 100 °C above the m.p. of Bi_2O_3. The impure b.c.c. phase was formed metastably in systems with Rb_2O, NiO, MnO, CdO, V_2O_5, and Nb_2O_5; the conditions of formation were dependent on composition, preparation, and heating schedules. The impure b.c.c. phases, both stable and metastable, had smaller unit cell dimensions than that of pure Bi_2O_3.

1. Introduction

Part I of this paper was an attempt to clarify the stable and metastable relationships of pure Bi_2O_3. It can be seen in table 1 of that part, however, that several investigators [1,2,3] [1] have reported phases of Bi_2O_3 which contained, or were contaminated by, other oxides. Sillén [1] obtained a body centered cubic (b.c.c.) form by fusing Bi_2O_3 in porcelain, or with Al_2O_3 or Fe_2O_3, for 5 min at 900 °C. He suggested the unit cell formula $Me_2Bi_{24}O_{40}$. Fusion of Bi_2O_3 in a porcelain crucible for 20 min yielded cubic Bi_2O_3. Schumb and Rittner [2] also obtained the impure b.c.c. phase by fusing Bi_2O_3 at 875 °C in porcelain or with SiO_2. By quenching the fused mixture in water, they produced an impure cubic (C) phase. Gattow and Schröder [3] reported impurity forms of b.c.c., C, and tetragonal-symmetry, designated respectively, as γ^*, δ^*, β^*.

The previous work can be questioned on two grounds: Firstly, in most cases the exact compositions were not controlled and were not known; secondly, in no instances were the phases studied at temperature and, consequently, might not represent stable equilibrium phases. Quenched liquids, for example, could hardly be expected to give equilibrium phases for any temperature. Furthermore, as the stable phases of Bi_2O_3 have been shown to be monoclinic and cubic-bismuth oxide, any other phase, e.g., impure tetragonal (Tet) or b.c.c. must represent either a metastable form of Bi_2O_3 or a discrete phase, whose composition limits does not include Bi_2O_3.

The major objective of this portion of the study, therefore, was to obtain information on the impure forms of bismuth oxide, in particular, on the b.c.c. phase. To eliminate objections applicable to previous work, mixtures were formulated from pure materials and of known compositions and were studied in a high-temperature x-ray diffractometer furnace.

[1] Figures in brackets indicate the literature references at the end of this paper.

2. Materials and Methods

2.1. Materials

For the admixture study, reagent grade chemicals (ACS) or those of higher purity were used. Starting materials for formulating oxide mixtures with Bi_2O_3 were as follows: Li_2CO_3, Rb_2CO_3, NiO, ZnO, CdO, MgO, $CaCO_3$, $SrCO_3$, $BaCO_3$, PbO, B_2O_3, Al_2O_3, Ga_2O_3, Fe_2O_3, $MnCO_3$, Sb_2O_3, Lu_2O_3, Sm_2O_3, La_2O_3, SiO_2, GeO_2, TiO_2, TeO_2, SnO_2, ZrO_2, CeO_2, P_2O_5, V_2O_5, Sb_2O_5, Ta_2O_5, Nb_2O_5, Cr_2O_3, WO_3, and MoO_3. These materials were chosen from crystal chemistry considerations, such as charge, ionic radius, coordination number, and polarizability of the cations.

2.2. Preparation of Mixtures

Binary mixtures were formulated from Bi_2O_3 and a second substance, to give an atomic ratio in most cases of 12Bi to 1Me, where Me represents the second cation. The intent was to determine which oxides formed Sillén's [1] impure b.c.c. phase at the above ratio. Thus for monovalent, trivalent, and pentavalent cations, oxide compositions would correspond to $12Bi_2O_3$:Me_2O, $12Bi_2O_3$:Me_2O_3, and $12Bi_2O_3$:Me_2O_5. For divalent, tetravalent, and hexavalent cations, oxide compositions would correspond to $6Bi_2O_3$:MeO, $6Bi_2O_3$:MeO_2, and $6Bi_2O_3$:MeO_3. Additional compositions were prepared in many of the systems, as designated on the individual phase diagrams.

Preliminary treatment of the mixtures consisted of three cycles of grinding together calculated amounts of the starting materials, pressing the material in a mold, and then heating the disk at a temperature below the solidus, as described in previous publications [4,5].

2.3. Apparatus

The high-temperature, x-ray diffractometer furnace noted in Part I was used also for the admixture study. The modification of the sample holder [6] which permitted the use of a thin layer of powered specimen was of especial importance for this part of the study. X-ray diffraction patterns of crystalline phases could be obtained in the presence of liquid, which did not flow off the platinum holder. Thus, it was possible to approximate solidus temperatures (± 10 °) and under favorable conditions even the liquidus temperatures.

3. Results and Discussion

3.1. Phase Diagrams

a. General Remarks

The data obtained by use of the high-temperature x-ray furnace can be presented in the form of phase diagrams, as shown in figures 1 through 6. Arrangement of the figures is according to the Periodic Table. Within each figure, diagrams are arranged, in general, according to a combination of the Periodic Table subgroups and ionic radii of the atoms. As no table of data is given, figure captions include selected notes. In most instances, the rate of disappearance of old phases and of the appearance of new ones on the indicated boundary curves was not rapid but took place over a temperature interval. Phases which have been interpreted as nonequilibrium ones are not shown in the diagrams.

It is emphasized that these phase diagrams represent the best interpretation of the data within the limitations of the experimental method. The major limitation is due to volatility of the samples or of the constituents. The high surface-to-volume ratio inherent with a thin film method, increases the effect of volatilization on composition. Thus, verification of equilibrium by long soaking periods, especially at high temperatures, was precluded.

b. General Conclusions

From inspection of all of the diagrams, several general conclusions become evident:

(1) The only stable phases of pure bismuth oxide are Mon and C. The b.c.c. or Tet phases of pure Bi_2O_3 do not appear. The conclusion is consistent with the stability relationships for Bi_2O_3 as deduced in Part I.

(2) Monoclinic Bi_2O_3 shows little or no solid solution.

(3) The C phase of Bi_2O_3, however, may show extensive solid solution; and in such cases, the Mon to C transition temperature is lowered.

(4) Except for the CdO and PbO systems (fig. 2 G& H), the effect of solid solution in the C phase is to raise solidus and liquidus temperatures.

(5) A b.c.c. phase distinct from that of pure Bi_2O_3 appears in a number of systems. This b.c.c. phase may vary in composition for different systems (see figs. 2F, 3B & C, 4A, 5A), may melt congruently (fig. 4A, B & C), or melt incongruently (figs. 2H, 3A & B), and when stable is separated from Bi_2O_3 by a two-phase region.

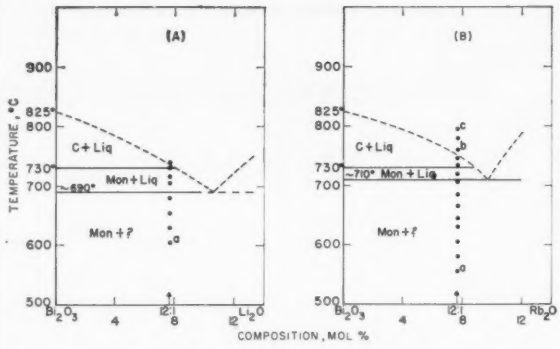

FIGURE 1. Bi_2O_3 *rich regions of* $Bi_2O_3-R_2O$ *systems, as determined from high-temperature x-ray diffraction data.*

Phases: Mon—monoclinic, C—cubic, ?—unknown, Liq—liquid
(A) $Bi_2O_3-Li_2O$
a—Trace of unknown phase observed.
(B) $Bi_2O_3-Rb_2O$
a—No second phase seen.
b—Rb_2O apparently volatilizes from liquid.
c—Liquid cools to b.c.c. phase: a=10.22A.

c. Individual Phase Diagrams

In the following section, individual figures and selected diagrams will be discussed. Only two alkali oxide systems, representing extremes in cation radii, were studied (fig. 1). Both Li_2O and Rb_2O, in the region studied, were simple eutectic types with no solid solutions. It should not be inferred, however, that oxides of the intermediate cations necessarily would behave similarly.

For oxides of the divalent cations (fig. 2) the phase diagrams showed a number of variations, e.g., simple eutectic system (A), congruently melting b.c.c. phase (F), incongruently melting b.c.c. phase (H), C solid solution with liquidus and solidus raised (B), and C solid solution with liquidus and solidus lowered (H).

In the systems with CaO, SrO, and BaO, the rhombohedral solid solution phase described previously [7, 8] was found to be an equilibrium phase. Sillén and Aurivillius had found the phase in samples cooled rapidly from the liquid. The unit cell dimensions at 700 °C for the bismuth oxide-rich compositions of the solid solution phase are given in table 1.

Sillén and Sillén [9] report finding several phases in the Bi_2O_3-CdO system, one of which might be the

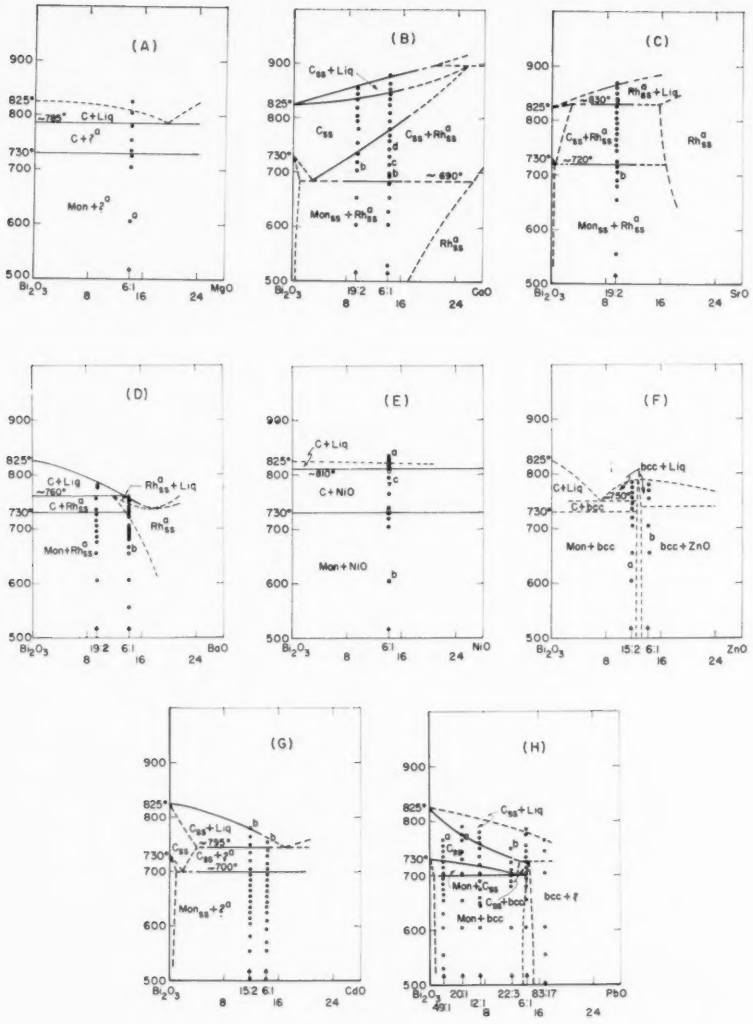

FIGURE 2. Bi_2O_3 *rich regions of* Bi_2O_3-RO *systems, as determined from high-temperature x-ray diffraction data.*

Phases: Mon—monoclinic, C—cubic, b.c.c.—body-centered cubic, ?—unknown, Rh—rhombohedral, ss—solid solution, Liq—liquid

(A) Bi_2O_3-MgO
a—Second phase, possibly MgO.

(B) Bi_2O_3-CaO
a—Described by Aurivillius (1943) [7].
b—Cubic Bi_2O_3 ss starting to form.
c—Cubic Bi_2O_3 ss increasing; Mon Bi_2O_3 decreasing.
d—Mon Bi_2O_3 gone.
The 6:1 composition slow-cooled from 700 °C (after 107 hr soaking period) shows single phase Rh_{ss}. See table 1 for unit cell dimensions.

(C) Bi_2O_3-SrO
a—Described by Sillén and Aurivillius (1939) [8].
b—Rh_{ss} increasing; Mon decreasing. See table 1 for unit cell dimensions.

(D) Bi_2O_3-BaO
a—Described by Aurivillius (1943) [7].
b—Rh_{ss} increasing; Mon decreasing. See table 1 for unit cell dimensions.

(E) Bi_2O_3-NiO
a—Liq cools to b.c.c.
●—First heat
□—b.c.c. reheated
■—Superposition of ● and □.
▼—Reheated sample cooled from liq to 780 °C
b—b.c.c. decomposing to Mon.
c—Cubic phase when cooled to room temperature shows b.c.c.

(F) Bi_2O_3-ZnO
a—No Mon detected.
b—ZnO detected only in specimen soaked 107 hr at 700 °C and then slow-cooled.
The two compositions studied indicate that the b.c.c. phase is stable and melts congruently. Beyond this the diagram is conjectural.

(G) Bi_2O_3-CdO
a—Possibly one of Sillén's reported $CdO-Bi_2O_3$ phases [9].
b—Liq cools to b.c.c.

(H) Bi_2O_3-PbO
a—C_{ss} cools to b.c.c.
b—C_{ss}+ Liq cools to b.c.c.

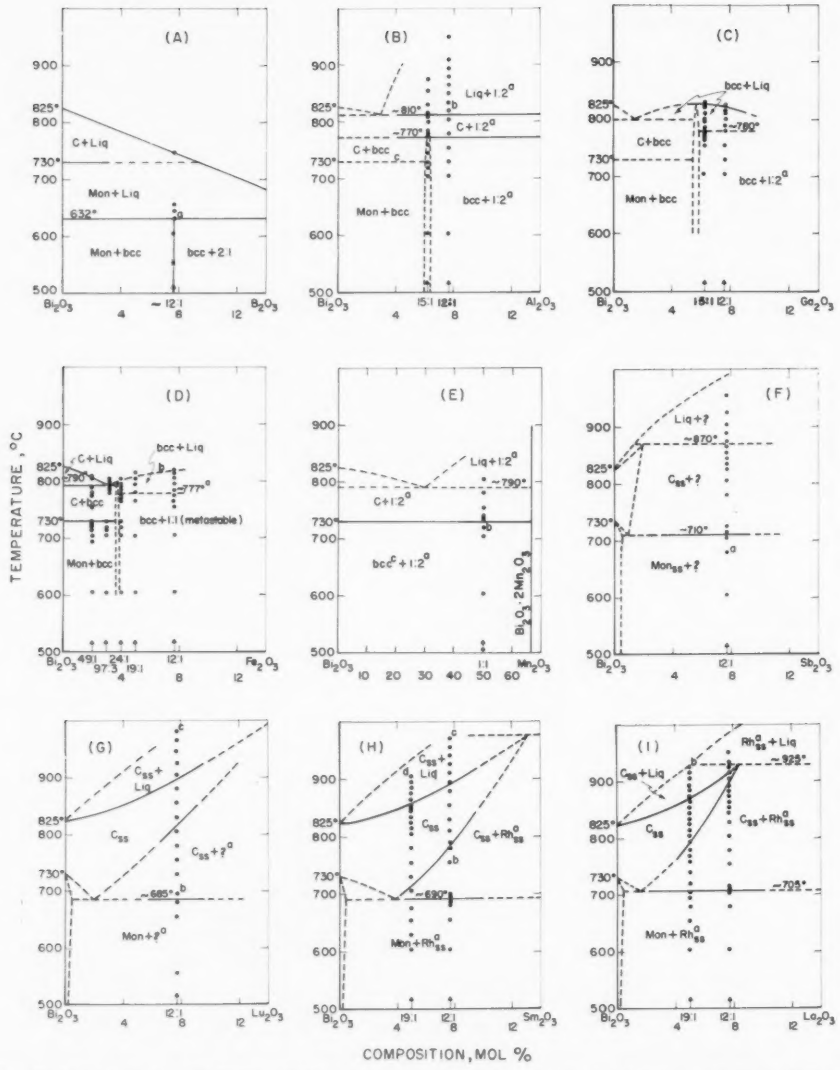

FIGURE 3. Bi_2O_3 *rich regions of* $Bi_2O_3-R_2O_3$ *systems, as determined from high-temperature x-ray diffraction data.*

Phases: Mon—monoclinic, C—cubic, b.c.c.—body-centered cubic, ?—unknown, Rh—rhombohedral, ss—solid solution, Liq—liquid.

(A) $Bi_2O_3-B_2O_3$
Diagram taken from Levin et al. [4].
a—Unreacted $2Bi_2O_3{\cdot}B_2O_3$(2:1) and Mon Bi_2O_3 at lower temperatures form single phase b.c.c.

B) $Bi_2O_3-Al_2O_3$
a—Isostructural with 1:2 compounds in systems of Bi_2O_3 with Fe_2O_3, Ga_2O_3, and Mn_2O_3, according to unpublished work of R. S. Roth.
b—Very strong peak at *d* value about 2.9A; probably orientation of $Bi_2O_3{\cdot}2Al_2O_3$.
c—Effect of Al_2O_3 on Mon to C transition temperature not determined.

(C) $Bi_2O_3-Ga_2O_3$
a—Isostructural with 1:2 compounds in systems of Bi_2O_3 with Fe_2O_3, Al_2O_3, Mn_2O_3, according to unpublished work of R. S. Roth.
The two compositions studied indicate that the b.c.c. phase is stable and melts congruently. Beyond this the diagram is conjectural.

(D) $Bi_2O_3-Fe_2O_3$ (Does not obey phase rule.)
a—May represent metastable eutectic between b.c.c. and metastable $BiFeO_3$.
b—Liquidus curve does not show maximum temperature at melting of b.c.c. phase.
The $BiFeO_3$ phase is believed to be metastable because the compound composition can never be made single phase, according to the unpublished work of R. S. Roth.

(E) $Bi_2O_3-Mn_2O_3$ (Note different composition scale.) $MnCO_3$ used as starting material, and mixture ground in alcohol, which tends to give b.c.c.[17].
a—Isostructural with 1:2 compounds in systems of Bi_2O_3 with Fe_2O_3, Al_2O_3, Ga_2O_3, according to unpublished work of R. S. Roth.
b—Samples at this temperature and below show b.c.c., believed to be metastable, as it disappears at Mon to C inversion (730 °C).
c—Mon Bi_2O_3 probably stable phase (see b).

(F) $Bi_2O_3-Sb_2O_3$
a—Above about 650 °C oxidation state of the antimony is unknown. Starting with Sb_2O_3, same phases occur, but solidus appears to be lower (~855 °C).

(G) $Bi_2O_3-Lu_2O_3$
a—Second phase observed, with major *d* value at 2.95A.
b—As Mon transforms to C, unreacted Lu_2O_3 transforms to ? phase.
c—Liq+C_{ss} cools to metastable tetragonal$_{ss}$.

(H) $Bi_2O_3-Sm_2O_3$
a—Essentially isostructural with Rh_{ss} phase in CaO—, SrO—, and BaO—Bi_2O_3 systems. See table 1 for unit cell dimensions.
b—When cooled to 450 °C shows Rh_{ss}+ tetragonal (Tet)$_{ss}$ (metastable).
c—Liq+C_{ss} cools to Tet$_{ss}$+C_{ss} (both metastable).
d—Liq+C_{ss} cools to Tet$_{ss}$ (metastable). Single phase Tet$_{ss}$ (19:1) reheated to 625 °C transforms first to C_{ss}+Rh_{ss}, then the C_{ss} transforms to the equilibrium Mon phase.

(I) $Bi_2O_3-La_2O_3$
a—Essentially isostructural with Rh_{ss} phase in CaO—, SrO—, and BaO—Bi_2O_3 systems. See table 1 for unit cell dimensions.
b—Cools to C_{ss} (metastable)

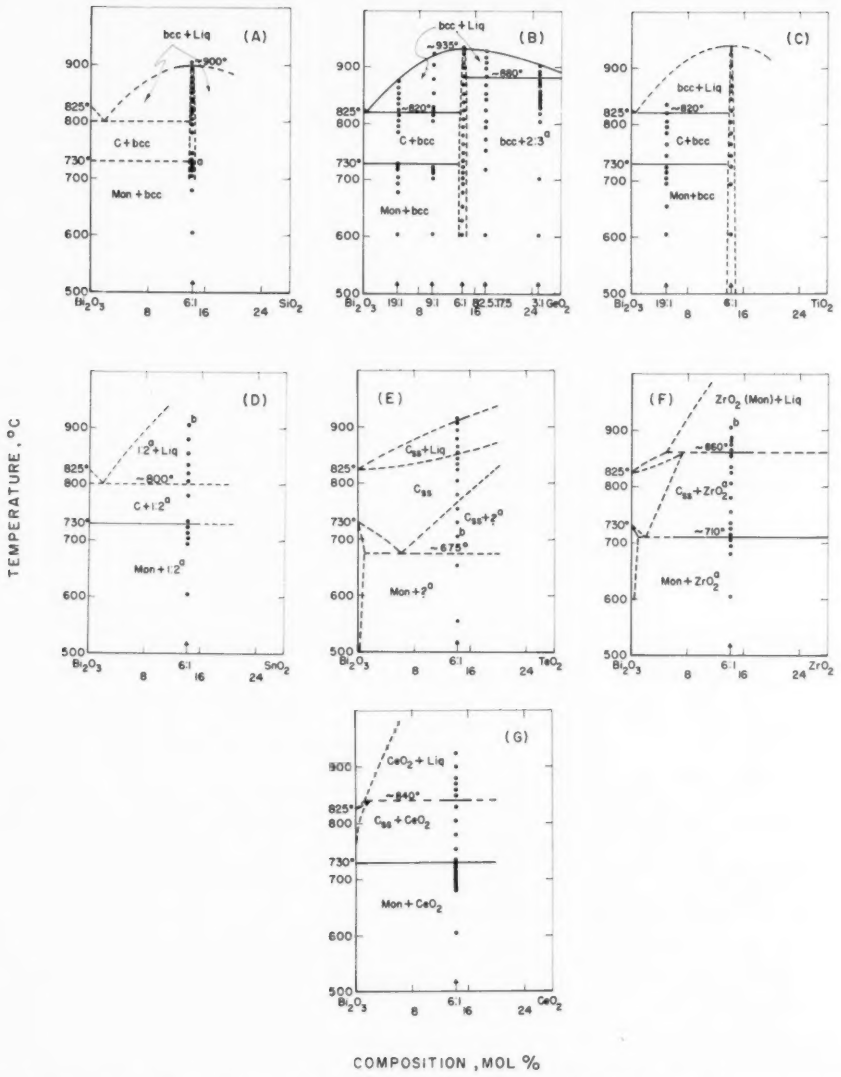

FIGURE 4. Bi_2O_3 *rich regions of* $Bi_2O_3-RO_2$ *systems, as determined from high-temperature x-ray diffraction data.*

Phases: Mon—monoclinic, C—cubic, b.c.c.—body-centered cubic, ?—unknown, ss—solid solution, Liq—liquid

(A) $Bi_2O_3-SiO_2$
a—Unreacted Mon transforms to C, on heating.
Composition studied shows that the b.c.c. phase (6:1) melts congruently. Beyond this the diagram is conjectural.

(B) $Bi_2O_3-GeO_2$
a—Unpublished work of C. R. Robbins, NBS.
Compositions studied show that the b.c.c. phase melts congruently, near to but not necessarily at the 6:1 composition.

(C) $Bi_2O_3-TiO_2$
Compositions studied show that the b.c.c. phase melts congruently, near to but not necessarily at the 6:1 composition.

(D) $Bi_2O_3-SnO_2$
a—Compound described by R. S. Roth [14].
b—1:2 + Liq cools to 1:2 + Mon + b.c.c. (trace).

(E) $Bi_2O_3-TeO_2$
Oxidation state of tellurium at high temperature is unknown.
a—Unknown composition, apparently of cubic symmetry.
b—Unit cell dimensions at 700 °C: C_{ss}, a=5.63A; ?, a=5.57A

(F) $Bi_2O_3-ZrO_2$
a—ZrO_2 does not show in x-ray pattern below solidus.
b—Liq + ZrO_2 (Mon) cools to Tet Bi_2O_{3ss}.
No b.c.c. found in this system although reported by Aurivillius and Sillén [15].

(G) $Bi_2O_3-CeO_2$
No b.c.c. found in this system although reported by Aurivillius and Sillén [15].

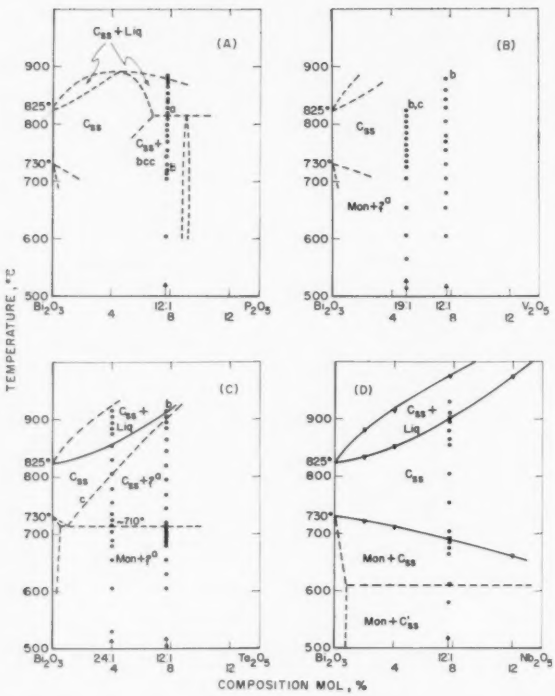

FIGURE 5. Bi_2O_3 *rich regions of* $Bi_2O_3-R_2O_5$ *systems, as determined from high-temperature x-ray diffraction data.*

Phases: Mon—monoclinic, C—cubic, C′—pseudocubic, b.c.c.—body-centered cubic, ?—unknown, ss—solid solution, Liq—liquid

(A) $Bi_2O_3-P_2O_5$
- a—The b.c.c. phase decreases markedly in amount at about 815 °C, but persists in diminishing amounts to about 850 °C. It is possible, therefore, that the true solidus is at 850 °C and (1) a 2-phase region of C_{ss} + ? exists between 815 ° and 850 °C or (2) the decomposition temp. of b.c.c. should be raised to 850 °C.
- b—The Mon to C transition with the high-temp. x ray occurs at about 720 °C. However, a sample held at 700 °C for 107 hr and slow-cooled does not show Mon. Therefore, the temperature of the Mon to C inversion is in doubt.

(B) $Bi_2O_3-V_2O_5$
A more complete phase diagram could not be postulated because of inconsistencies in the temperatures of transitions and the relative amounts of phases present.
- a—b.c.c., if a stable phase; otherwise, unknown phase.
- b—Above 815 °, only C_{ss}; between 715 ° and 815 °C, C_{ss} + b.c.c.; below 715 °C, phases present depend on previous heat treatment. Stability and approximate composition of b.c.c. could not be ascertained.
- c—C_{ss} cools to b.c.c.

(C) $Bi_2O_3-Ta_2O_5$
- a—Apparently cubic symmetry; composition may correspond to C′ phase in $Bi_2O_3-Nb_2O_5$ system [17] (about 4:1).
- b—Liq + C_{ss} cooled slowly shows only C_{ss} at all temps.
- c—Because of nonreversibility (see b), this boundary may actually be much lower, as in the $Bi_2O_3-Nb_2O_5$ system (D).

(D) $Bi_2O_3-Nb_2O_5$
- ▼—Values taken from phase diagram of Roth and Waring [17].

unknown phase in the present study of the cadmium oxide system (fig. 2G).

The PbO-Bi_2O_3 system (fig. 2H) is interesting for several reasons. It varies significantly from the reported phase diagram of Belladen [10, 11]. The latter shows neither the Mon to C transition, nor the solid solution of PbO in Bi_2O_3, nor the b.c.c. phase at the $6Bi_2O_3$·PbO composition. It is evident from the present diagram that the molal heat of fusion of Bi_2O_3 calculated by Kelley [12] from the liquidus curve of Belladen's diagram (6800 cal/mole) is in error. The molal heat of fusion of Bi_2O_3 was discussed by Levin and McDaniel [4].

With regard to the systems of bismuth oxide with oxides of the trivalent cations, the Bi_2O_3-B_2O_3 system (fig. 3A) was reported previously [4], as determined by the quenching technique. However, one composition, $12Bi_2O_3:B_2O_3$, was used to compare both methods and to show that agreement was satisfactory.

Apparently isostructural 1:2 compounds were found in systems of Bi_2O_3 with Al_2O_3 (fig. 3B), Ga_2O_3 (fig. 3C), and Mn_2O_3 (fig. 3E). An isostructural 1:2 compound also exists in the Bi_2O_3–Fe_2O_3 system; however, the high-temperature x-ray study revealed only a 1:1 compound (fig. 3D). The

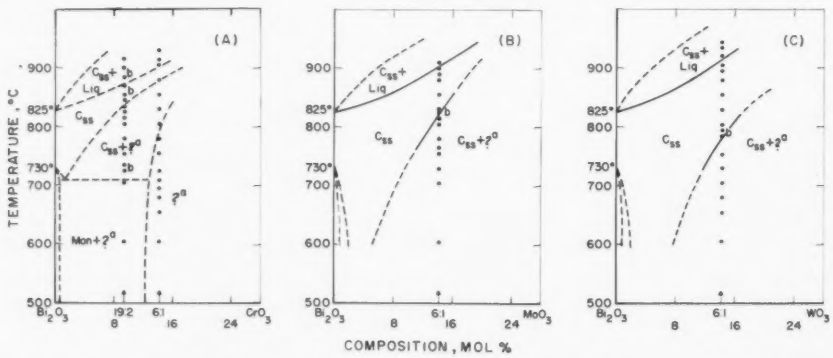

FIGURE 6. Bi_2O_3 *rich regions of* $Bi_2O_3-RO_3$ *systems, as determined from high-temperature x-ray diffraction data.*

Phases: Mon—monoclinic, C—cubic, ss—solid solution, ?—unknown, Liq—liquid

(A) $Bi_2O_3-CrO_3$
Compositions formulated from Cr_2O_3. Diagram shown on CrO_3 basis because on calcining, specimens changed in color from green to red, and ? phase is similar to that formed with the hexavalent ions.
- a—Unknown composition, apparently pseudotetragonal (similar to the phase in the $Bi_2O_3-MoO_3$ and $Bi_2O_3-WO_3$ systems).
- b—Phases found at these temps. do not agree entirely with postulated phase boundaries, because system may be pseudobinary.

(B) $Bi_2O_3-MoO_3$
- a—Unknown composition, apparently pseudotetragonal (similar to the phase in the $Bi_2O_3-CrO_3$ and $Bi_2O_3-WO_3$ systems).
- b—Reversibility demonstrated with high-temp. x ray.

(C) $Bi_2O_3-WO_3$
- a—Unknown composition, apparently pseudotetragonal (similar to the phase in the $Bi_2O_3-CrO_3$ and $Bi_2O_3-MoO_3$ systems).
- b—Reversibility demonstrated with high-temp. x ray.

TABLE 1. *Unit cell demensions of rhombohedral phases formed in* Bi_2O_3 *systems*

Oxide addition	Starting composition	Final heat treatment	Additional phases present	Ionic radius of cation (Ahrens)	Unit cell dimensions				
					Hexagonal			Rhombohedral	
		°C/hr			a A	c A	c/a	a A	α
CaO [a]	$6Bi_2O_3$:CaO	700°/107	None	0.99	3.94_1	27.9_5	7.09	9.59_0	23°44′
SrO [a,b]	$19Bi_2O_3$:2SrO	699°/144	Mon Bi_2O_3 (moderate)	1.12	3.95_2	28.0_9	7.11	9.63_7	23°40′
BaO [a]	$6Bi_2O_3$:BaO	700°/107	b.c.c. Bi_2O_3 (small)	1.34	3.97_2	28.5_4	7.18_5	9.78_6	23°26′
Sm_2O_3	$12Bi_2O_3$:Sm_2O_3	700°/107	tr?	1.00	3.95_6	27.9_3	7.07	9.58_5	23°46′
La_2O_3	$12Bi_2O_3$:La_2O_3	700°/107	b.c.c. Bi_2O_3 (moderate)	1.14	3.97_5	28.1_0	7.07	9.64_4	23°48′

[a] Rhombohedral phase described by Aurivillius [7].
[b] Rhombohedral phase described by Sillén and Aurivillius [8].

$BiFeO_3$ phase is believed to be metastable, because according to the unpublished work of R. S. Roth, the compound composition can never be made single phase. It should also be noted that the portion of the diagram to the right of the b.c.c. phase does not obey the phase rule. Royen and Swars [13] who also have studied this system reported two Tet phases of approximately 30:1 and (12–13):1 compositions, a b.c.c. phase of composition 15:1, as well as 2:1 and 1:1 compounds. The present work does not substantiate the 30:1, (12–13):1, and 2:1 compounds; and the composition of the b.c.c. phase appeared slightly greater than $24Bi_2O_3$:Fe_2O_3. As Royen and Swars obtained their compounds from fused mixtures, it is believed that some of them represented metastable states.

The system with the rare earth oxides Sm_2O_3 (fig. 3H) and La_2O_3 (fig. 3I), showed the same rhombohedral solid solution phase as was found in the CaO, SrO, and BaO systems (fig. 2B–D). The unit cell dimensions are given in table 1. The phase did not form in the Lu_2O_3 system (fig. 3G) nor in the MgO system (fig. 2A); consequently, the minimum cationic radius required for formation of this phase lies between that of Lu^{3+} and Ca^{2+} or between 0.85 and 0.99A (Ahrens).

In the systems studied with the group IV cations (fig. 4), SiO_2 (A), GeO_2 (B), and TiO_2 (C) showed a congruently melting b.c.c. phase at or near the 6:1 composition. The phase diagrams provide positive proof, for the first time, that the impure b.c.c. phase is a discrete composition and not a solid solution phase of Bi_2O_3.

The Bi_2O_3-SnO_2 system (fig. 4D) contains a 1:2 compound described by R. S. Roth [14] as having a distorted pyrochlore-type structure.

No b.c.c. phase was found in the ZrO_2 and CeO_2 systems, although this phase was obtained from fused mixtures by Aurivillius and Sillén [15]. As will be discussed later under the b.c.c. phase, cooling of the liquid or C phases tends to form metastable phases.

In the group V cations (fig. 5), systems with P_2O_5 (A) and V_2O_5 (B) showed inconsistencies which could not be reconciled, and these diagrams are most questionable. The systems with Ta_2O_5 (C) and Nb_2O_5 (D) are similar, and it is possible that the boundary curve in the Ta_2O_5 system between (Css+?) and Css should descend continuously as in the Nb_2O_5 system (see b and c in legend to fig. 5C).

Finally, in the Bi_2O_3–RO_3 systems (fig. 6), the three systems studied are similar, including the occurrence of a phase of apparently pseudotetragonal symmetry but of unknown composition. Gattow [16] prepared a mixed oxide $2Bi_2O_3$·MoO_3, by precipitation from solution, and studied it by means of x-ray and thermal analysis. Because of insufficient data, however, it was not possible to compare the unknown phase in the present study with Gattow's.

3.2. Metastable Phases

The results of the high-temperature x-ray experiments were especially informative regarding the occurrence of metastable phases observed at room temperature in samples cooled from higher temperatures. Such information is included in the figure captions. Illustrative examples are as follows:

(1) Liquid cooled to a metastable b.c.c. phase in Bi_2O_3 systems with Rb_2O (see c to caption of fig. 1B), NiO (a of fig. 2E), and CdO (b of fig. 2G).
(2) Cubic or cubic solid solution cooled to a metastable b.c.c. phase in systems with NiO (c of fig. 2E) and V_2O_5 (c of fig. 5B).
(3) Liquid+cubic solid solution cooled to metastable cubic solid solution in systems with La_2O_3 (b of fig. 3I), Ta_2O_5 (b of fig. 5C), and Nb_2O_5 [17].
(4) Liquid+cubic solid solution also cooled to metastable Tet in systems with Lu_2O_3 (c of fig. 3G), Sm_2O_3 (b and d of fig. 3H), and Nb_2O_5 [17].
(5) In the zirconia system, liquid+ZrO_2 cooled to metastable tetragonal.

It is emphasized that an exhaustive study of the formation of metastable phases was not attempted. In general, only one cooling cycle for a limited number of compositions was studied in each system. It is apparent, however, from the frequency and diversity of the matastable phases found, that phases obtained by the cooling of fused mixtures or of high-temperature forms may well represent nonequilibrium states at all temperatures. It is not surprising, therefore, that previous investigators [1, 2, 13, 15] studying fused samples of unknown compositions obtained various impurity phases. Many of these are metastable phases and have no place in the equilibrium diagrams.

3.3. Body-Centered Cubic Phase

Table 2 gives the unit cell dimensions for the stable and metastable b.c.c. phases of bismuth oxide found in this study. The unit cell dimensions were obtained at room temperature; and except for Rb_2O and Bi_2O_3 (see footnotes d and e, respectively) the samples were heated in sealed platinum tubes according to the schedule given in the column under "Final Heat Treatment". As observed from the x-ray diffraction patterns, most of the compositions studied were not single phase but showed a second phase.

Concerning the systems with a stable b.c.c. phase, it is seen that an exact 12Bi to 1Me atom ratio was not substantiated in most cases. Except for PbO and B_2O_3, systems with divalent and trivalent cations would show single phase b.c.c. at ratios of Bi to Me greater than 12:1. Systems with the tetravalent ions Si^{4+}, Ge^{4+}, and Ti^{4+} approached most closely the ideal ratio of 12Bi:1Me, proposed by Sillén [1]. This conclusion is more apparent from figure 4A,B,C, where the b.c.c. phase in these systems is seen to melt congruently at a temperature about 100 °C above the melting point of Bi_2O_3. With the oxide of the pentavalent cation, P^{5+}, the single phase b.c.c. composition appears to be less than 12Bi:1Me (fig. 5A). It can be seen from table 2 that within each valence group increased ionic radius of the cation is associated with increased unit cell dimensions of the b.c.c. phase. Unit cell dimensions versus ionic radius for all of the cations are plotted in figure 7. The general correlation between the two for the stable phases (solid points) is seen to be good, although not linear.

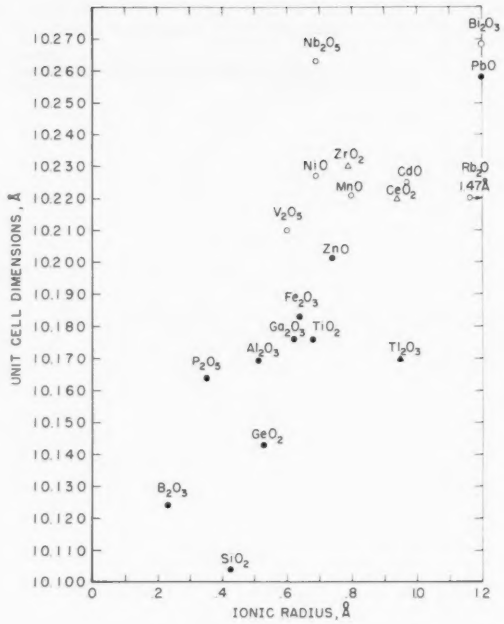

FIGURE 7. *Unit cell dimensions versus ionic radius for impure body-centered cubic phases of* Bi_2O_3.

Oxides shown in the figure refer to the impurity additions. See figures 2 through 5 for approximate compositions of the phases.
●—equilibrium phases
○—metastable phases
▲, △—unit cell dimensions after Aurivillius and Sillén [15].

TABLE 2. *Unit cell dimensions of body-centered cubic phases formed by small additions of oxides to* Bi_2O_3

Oxide addition	Starting composition	Final heat treatment	Additional phases present	Ionic radius of cation (Ahrens)	Levin and Roth	Aurivillius' and Sillen [15]
		°C/hr		Å	Å	Å [a]
Stable phases						
ZnO	$6Bi_2O_3$:ZnO	700°/107	Trace ZnO	0.74	10.20$_1$	
PbO	$6Bi_2O_3$:PbO	725°/1	None	1.20	10.25$_8$	10.25 [b]
B_2O_3	$12Bi_2O_3$:B_2O_3	600°/65	Trace Bi_2O_3+ trace 2:1	0.23	10.12$_4$	
Al_2O_3	$12Bi_2O_3$:Al_2O_3	700°/107	Trace Bi_2O_3·$2Al_2O_3$	.51	10.16$_9$	10.16
Ga_2O_3	$12Bi_2O_3$:Ga_2O_3	700°/107	Trace Bi_2O_3·$2Ga_2O_3$	.62	10.17$_6$	
Fe_2O_3	$19Bi_2O_3$:Fe_2O_3 [c]	700°/3	Trace $BiFeO_3$	.64	10.18$_3$	10.18
Tl_2O_3				.95		10.17
SiO_2	$6Bi_2O_3$:SiO_2	700°/107	Small amt. Bi_2O_3	.42	10.10$_1$	10.10
GeO_2	$6Bi_2O_3$:GeO_2	700°/107	Trace GeO_2	.53	10.14$_3$	
TiO_2	$6Bi_2O_3$:TiO_2	700°/107	None	.68	10.17$_6$	
P_2O_5	$12Bi_2O_3$:P_2O_5	700°/107	Trace?	.35	10.16$_4$	
Metastable phases						
Rb_2O	$12Bi_2O_3$:Rb_2O	795°/0.1 [d]	Trace Bi_2O_3	1.47	10.22	
NiO	Bi_2O_3:NiO [c]	785°/1	NiO	0.69	10.22$_7$	
MnO	Bi_2O_3:MnO [c]	735°/1	Moderate amt. Bi_2O_3·$2Mn_2O_3$	.80	10.22$_1$	
CdO	$6Bi_2O_3$:CdO	700°/107	Trace CdO	.97	10.22$_5$	
Bi_2O_3	Bi_2O_3	780°/0.1 [e]	Small amt. Mon Bi_2O_3	1.20 [f]	10.26$_8$	10.264 [g]
ZrO_2				0.79		10.23
CeO_2				.94		10.22
V_2O_5	$12Bi_2O_3$:V_2O_5	700°/107	Small amt. Tet. Bi_2O_3 ss	.59	10.21$_9$	
Nb_2O_5	$6Bi_2O_3$:Nb_2O_5 [c]	700°/3	Moderate amt. cubic (C′ [17])	.69	10.19	
Nb_2O_5	$24Bi_2O_3$:Nb_2O_5 [c]	700°/3	Trace cubic (C′ [17])	.69	10.26$_3$	

[a] Converted from kx units.
[b] Cation is tetravalent according to Aurivillius and Sillen [15].
[c] Starting materials ground together in alcohol.
[d] Sample cooled from liq. in high-temp., x-ray furnace.
[e] Slow-cooled in high-temp., x-ray furnace.
[f] Ahrens gives 0.96Å, which is low. See [4].
[g] Agrees with value obtained by Schumb & Rittner [2].

An interesting and surprising finding is that oxides of cations so diverse in ionic radius, oxygen coordination number, and polarizability as Zn^{2+}, B^{3+}, Ti^{4+}, and Pb^{2+} can form with bismuth oxide a discrete phase of the same symmetry. An appealing explanation is the concept of a clathrate- or cage-type structure, in which as postulated by Sillén [1] for $Si_2Bi_{24}O_{40}$, central Si atoms are surrounded by spheres of $Bi_{12}O_{20}$ atoms. For the case of a central ion with valence different from 4, charge balance would be achieved through cation or oxygen adjustments.

Regarding the metastable b.c.c. phase, the monovalent ion Rb^+ formed the phase on cooling in the high temperature x-ray experiments. The compositions containing NiO, MnO, and Nb_2O_5, which in the process of preparation were ground in alcohol, also formed the b.c.c. phase, metastably. These results would seem to support the conclusion that an impure b.c.c. phase of Bi_2O_3 might be formed (metastably) with most cations, under the proper conditions of composition, grinding, and heating schedules.

It is seen from figure 7 that with the exception of PbO the unit cell dimensions of the metastable phases are larger than those of the stable phases. The cell dimensions of the metastable impure phases, also, are less than those for the b.c.c. metastable phase of pure Bi_2O_3. Therefore, the compositions of the impure metastable phases cannot be that of pure Bi_2O_3. However, contrary to the case of the stable b.c.c. phases, no correlation exists between unit cell dimensions and ionic radius for the metastable b.c.c. phases. The x-ray diffraction patterns of the b.c.c. phases of the stable and metastable impurity forms are similar in *d* spacings and intensities to the pattern for pure Bi_2O_3. It is a reasonable assumption that the structures are similar.

To summarize (see fig. 7), the b.c.c. phase of pure Bi_2O_3 has the largest unit cell dimensions, and the addition of a foreign ion to Bi_2O_3 tends to decrease the dimensions. This decrease is least for the larger ions, which tend to form the metastable b.c.c. phase. The decrease in cell dimensions is greatest for the smaller ions, which tend to form the stable b.c.c. phase. Whereas the stable b.c.c. phases show correlation with ionic radius, the metastable phases do not. These findings are compatible with a cage-type structure in which a central cation, including Bi, is surrounded by a sphere of atoms of approximately $Bi_{12}O_{20}$ composition.

4. Summary

The important phase equilibria relationships for the bismuth-rich portions of the phase diagrams are shown schematically in figure 8. Elements in boldfaced type refer to the respective oxide mixtures studied. Elements enclosed in heavy outlines represent oxides which formed the stable b.c.c. phase with bismuth oxide. Composition of the b.c.c. phase was found to be variable for different systems, but most nearly approached the ideal 12Bi:1Me ratio for oxides of the tetravalent ions Si^{4+}, Ti^{4+}, and Ge^{4+}. Designations in the upper right-hand corners of the boxes for the stable b.c.c. phases refer to the nature of melting, e.g., congruent, incongruent, or decomposition. Oxides of elements which formed the metastable b.c.c. phase are indicated by an *M* in the upper right-hand corner of the box, and those that formed the rhombohedral solid solution phase, by *Rh*. The nature of the liquidus curves is indicated by a designation in the lower right-hand corner of each box, as follows: *E*, simple eutectic; ss_r, solid solution type with liquidus and solidus raised; ss_L, solid solution type with liquidus and solidus lowered.

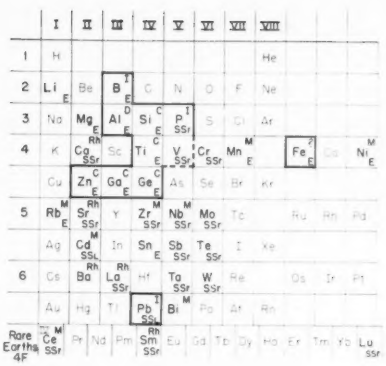

FIGURE 8. *Summary of some phase equilibria data on the effect of oxide additions to* Bi_2O_3. *Elements shown in boldfaced type on the Periodic Table refer to oxide additions.*

Elements enclosed in heavy outlines represent oxides which form stable body-centered cubic phases with bismuth oxide:
C—congruently melting
I—incongruently melting
D—decomposes
M—metastable body-centered cubic phase
E—eutectic-type system
SS_r—solid solution of oxide in Bi_2O_3, with solidus and liquidus raised
SS_L—solid solution, with solidus and liquidus lowered
Rh—rhombohedral solid solution phase [7, 8].

The authors acknowledge their sincere appreciation to Robert Friedman, who as a guest worker, summer 1961, from the University of Chicago, prepared the compositions and obtained some of the unit cell dimensions.

5. References

[1] L. G. Sillén, Arkiv fr Kemi, Mineral. Geol. **12A** [18] 1–13 (1937).
[2] W. C. Schumb and E. S. Rittner, J. Am. Chem. Soc. **65,** 1055–1060 (1943).
[3] G. Gattow and H. Schröder, Z. anorg. u allgem. Chem. **318** [3–4] 176–189 (1962).
[4] E. M. Levin and C. L. McDaniel, J. Am. Ceram. Soc. **45** [8] 355–360 (1962)
[5] E. M. Levin, C. R. Robbins, and J. L. Waring, J. Am. Ceram. Soc. **44** [2] 87–91 (1961).

[6] E. M. Levin and F. A. Mauer, J. Am. Ceram. Soc. **46** [1] 59–60 (1963).
[7] B. Aurivillius, Arkiv. Kemi, Mineral. Geol. **16A,** No. 17, 1–13 (1943).
[8] L. G. Sillén and B. Aurivillius, Z. Krist. **101,** 483–495 (1939).
[9] L. G. Sillén and B. Sillén, Z. Phys. Chem. **B49,** 27–33 (1944).
[10] L. Belladen, Gazz. chim. ital. **52II,** 160–164 (1922).
[11] See also, E. M. Levin, H. F. McMurdie, and F. P. Hall "Phase Diagrams for Ceramists", The American Ceramic Soc., Inc., fig. 97, p 58 (1956).
[12] K. K. Kelley, U.S. Bur. Mines Bull., No. 393, 166 pp (1936); p 26; Ceram. Absts., **16** [5] 162 (1937).
[13] P. Royen and K. Swars, Angew. Chem. **69** [24] 779 (1957).
[14] R. S. Roth, J. Research NBS **56** [1] 17–25 (1956); RP 2643.
[15] B. Aurivillius and L. G. Sillén, Nature **155,** No. 3932, 305–306 (1945).
[16] G. Gattow, Z. anorg. Chem. **298,** 65–71 (1959)
[17] R. S. Roth and J. L. Waring, J. Research NBS **66A** [6] 451–463 (1962).

(Paper 68A 2–269)

JOURNAL OF RESEARCH of the National Bureau of Standards—A. Physics and Chemistry
Vol. 68A, No. 2, March–April 1964

Second Spectrum of Tungsten (W II)

Donald D. Laun[1]

(October 30, 1963)

A preliminary report on the second spectrum of tungsten, published in 1938, presented 27 even energy levels and 50 odd energy levels that were derived from 500 W II lines ranging in wavelength from 1961.43 Å to 4348.13 Å. The present paper submits data on 62 even levels, 132 odd levels, and 2,173 classified lines of W II, ranging in wavelength from 1756.6 Å to 6219.77 Å. The ground state of the W^+ ion is represented by the $^6D_{0\frac{1}{2}}$ level of a sextet D term arising from the $5d^46s^1$ electron configuration, but the level intervals and magnetic splitting factors indicate considerable departure from *LS*-coupling, suggesting that coupling intermediate between *LS* and *Jj* may be more appropriate for the spectrum W II.

1. Introduction

The search for regularities among spectral lines emitted by tungsten arcs and sparks was initiated at the National Bureau of Standards in 1925 when O. Laporte and I were both new (temporary) members of the Spectroscopy Section. By exploiting existing data on wavelengths, intensities, and Zeeman patterns, Laporte [1][2] identified the first spectral terms and classified lines of W I. Zeeman data confirmed the designation of the six lowest energy levels as ^5D from $5d^46s^2$ and ^7S from $5d^56s^1$. This term analysis and quantum interpretation of W I was later greatly extended by Laporte and Mack [2] until it included 300 energy levels and 2,378 classified lines ranging in wavelength from 2008.64 Å to 11477.97 Å.

Shortly after Laporte found the low-energy terms in W I, I began a search for the theoretical low ^6D (from $5d^46s^1$) and ^6S (from $5d^5$) terms in W II, assuming that ionization removed one *s* electron. This initial search failed because of insufficient information about the spectrum W II. Then I undertook to reobserve the ultraviolet arc and spark spectra of tungsten, to distinguish W II from W I, to refine the wavelengths, and to observe Zeeman patterns of W II lines. From these observations, 27 even levels (including ^6D and ^6S) and 50 odd levels were derived from 500 W II lines ranging in wavelength from 1961.43 Å to 4348.13 Å; these results were published [3] in 1938 as a preliminary report on lines and levels of the spectrum W II. From time to time during the following quarter century, further improvements in observations and extensions of analyses have been made; the purpose of the present paper is to present the final data on 62 even levels, 132 odd levels, and 2,173 classified lines of W II, ranging in wavelength from 1756.6 Å to 6219.77 Å.

[1] Former member of Spectroscopy Section, NBS; present address: Kiel, Wis.
[2] Figures in brackets indicate the literature references at the end of this paper.

2. Experimental Procedure

Small rods of very pure tungsten were used as electrodes in the arcs and sparks that served as light sources. The arcs were operated with applied potential of 220 v and 6 amp dc, the sparks with 30,000 v, about 30 ma, ac, and 0.006 μf capacitance.

The first spectrograms were made in 1925 with a Hilger E 1 (Littrow) quartz spectrograph which could be effectively employed in the ultraviolet down to wavelength 1900 A. Later, these spectrograms were supplemented by a new series obtained by C. C. Kiess with the first Hilger E 185 (Littrow) quartz spectrograph that was delivered to the Bureau of Standards in 1932. This larger spectrograph has a focal length of 3 m, and reciprocal dispersion, or plate factor, of 0.3 Å/mm at 2100 Å and 1 Å/mm at 3000 A. These observations of tungsten lines on photographic plates exposed in quartz spectrographs were presented by me as a Master's Thesis at the University of Chicago [4]. Additional spectrograms were made in 1933 by Kiess with a concave grating of 22-ft radius, and 30,000 lines per inch. In a Wadsworth mounting, this grating produced spectra down to 1900 Å with a plate factor of 2.44 Å/mm in the first order, and with a plate factor of 0.88 Å/mm in the second order from 3200 to 4400 Å. This grating spectrograph was employed also to photograph tungsten spectra throughout the visible range.

Since all the above-mentioned spectrographs were stigmatic, movable diaphragms before the slits permitted placing strips of juxtaposed spectra on photographic plates. The usual procedure was to photograph the iron-arc spectrum containing standard wavelengths, then the tungsten arcs and sparks in adjacent strips and another iron spectrum beside the tungsten spark. The positions of tungsten spectral lines relative to iron lines were measured on Gaertner comparators, in 1925–26 at the Bureau of Standards; and in 1933–34 at Marquette University by courtesy of the late Fr. Joseph Carroll, S. J. Linear scale readings allowed the wavelengths of tungsten lines to be interpolated between iron

standards in the case of prismatic spectra with the aid of Hartmann's dispersion formula, and from grating spectrograms by assuming linear dispersion. In both cases, small corrections were made when the interpolated values of iron wavelengths departed from their standard values. For purposes of analysis, the final wavelengths of tungsten lines were converted to vacuum wavenumbers with the aid of the Table of Wavenumbers published by Coleman, Bozman, and Meggers [5].

At the same time that the positions or wavelengths of tungsten lines were being measured, their relative intensities were estimated in both sources. Although this intensity scale, ranging from 1 for a barely discernible line to 1000 for the strongest, is more or less arbitrary, it is primarily useful in separating W II from W I, and also qualitatively supports the subsequent analysis in which intensities are related to quantum numbers. In some cases W II lines appear to coincide with W I, and if a W II line sometimes appears stronger in the arc than in the spark, it may be an example of pole effect. Unfortunately, no deliberate attempt to exclude or exploit pole effect in the tungsten arc was made.

Finally, some information about tungsten spectra in the vacuum ultraviolet was obtained by measuring two spectrograms made by J. C. Boyce at the Massachusetts Institute of Technology in 1940 and kindly presented to the Bureau of Standards. These spectrograms were obtained with an evacuated grating spectrograph having a plate factor of 4.26 Å/mm. The spectra were measured down to 1200 Å. Although the excitation conditions were altered, the differences between spectra were so slight that only above 1756 Å was it possible positively to identify W II lines. The wavelengths from this point to 1950 Å were finally corrected to the scale of values calculated from atomic energy levels.

My preliminary paper [3] of 1938 reported Zeeman-effect measurements of spectrograms made with a Weiss magnet and quartz spectrographs at the Bureau of Standards. These data have been superseded by those obtained with the more powerful Bitter magnet and grating spectrographs at the Massachusetts Institute of Technology. These results will be mentioned in the next section.

3. Results

The main result of the experiments mentioned above is that the wavelengths of about 13,000 spectral lines characteristic of arcs and sparks between tungsten electrodes have been measured. Among these, about 4,000 have been attributed to W II and 2,173 of these lines, including 90 percent of the total intensity, have been shown to arise from transitions between 194 derived energy levels, 62 even and 132 odd. The even levels are displayed in table 1 and the odd levels in table 2. In these tables, the electron configuration is given in column 1, the spectral term designation in column 2, total angular momentum, J, in column 3, relative values of energy levels in column 4, intervals between levels of complex terms in column 5, and observed magnetic splitting factor, g, in column 6. Most of these data were supplied in 1956 for the third volume of Atomic Energy Levels [6] which contains J and level values for 45 even and 90 odd levels. In that volume, g-factors were reported for 38 even levels and for 58 odd. These were derived from MIT Zeeman spectrograms measured by J. E. Mack and Mrs. Taschek at the University of Wisconsin. Since 1956, the number of even levels has increased from 45 to 62 and odd levels from 90 to 132. Likewise, g-factors are now available for 46 even and 71 odd levels as compared with 38 and 58 respectively, in 1956.

In Atomic Energy Levels [6], it is stated that because of departure from LS-coupling it is difficult to assign term designations except for the lowest terms. Consequently, only six even terms, comprising 21 levels between 0 and 17437 K, were completely grouped and designated, and 24 higher even levels, between 18000 and 26929 K, were tentatively designated, guided by analogy with Mo II, g-factors, and theoretical calculations of the late R. E. Trees. Likewise, two odd terms, comprising six levels, were tentatively designated ^{6}F and ^{2}S, but the remaining 84 levels were given as miscellaneous. In the present paper, additional levels and g-factors are reported but no revision or extension of designations has been made.

The spectral lines of tungsten from which all the information in tables 1 and 2 was derived, are listed in table 3 in order of increasing wavelength. Each line is described by its measured wavelength in angstroms, by its estimated intensity in a tungsten arc and/or spark, by its appropriate vacuum wavenumber in kaysers (1 K=1 cm^{-1}), by the difference $(O-C)$ between the observed wavenumber and that calculated from the combination of energy levels shown in the next-to-last column. Abbreviated notes about the observed Zeeman patterns for 307 lines appear in the final column.

Table 3 contains 2,173 classified lines of W II, including 42 doubly classified. The only other table of classified W II lines was published [3] in 1938; it contained 500 lines, including 6 doubly classified. In addition to 2,173 classified lines, table 3 also contains wavelengths, intensities, and wavenumbers of 25 of the strongest W II lines still unclassified; these are included with the hope that the blank spaces under "combinations" may eventually be filled in.

The "Intensity" column of table 3 shows that the great majority of these W II lines were observed in arc as well as spark sources but with generally higher intensity in the latter when spectrogram exposures were chosen to make W I lines appear in both sources with nearly equal intensities. In a few cases, W II lines appear only, or stronger, in arc spectra; most if not all such deviations may be explained by coincident W I lines, pole effects, or air lines that occa-

sionally mask metal lines in sparks operated at atmospheric pressure. Where the letter *A* follows an arc intensity, a line with nearly identical wavelength has actually been classified as a combination of W I energy levels. The letter *d* in table 3 indicates a double line.

The observed minus calculated wavenumbers (*O*−*C*) have an average value of 0.1 K for wavelengths measured in air, that is, above 2000 Å. This means that the average error in these wavelength measurements is of the order of 0.01 Å, and there is high confidence that the great majority of the combinations are real, rather than accidental. However, in the vacuum ultraviolet, below 2000 Å, the average *O*−*C* is considerably greater, in a few cases as large as 5 K, which entails an error in wavelength of the order of 0.2 Å. In such cases, confidence that the combinations are genuine is greatly reduced but they have been tentatively retained for the following reasons. Since the scale of wavenumbers is greatly compressed in the vacuum region, and the tungsten spectra below 2000 Å were photographed with relatively small dispersion and measured without adequate standard wavelengths, it was inevitable that these measured wavelengths of W II lines would be more or less uncertain. Furthermore, it appears that most of these W II short waves involve the lowest and adjacent metastable energy levels, which is precisely what should be expected of strong lines with high energy. Therefore, these combinations with relatively large *O*−*C* may be regarded as real pending wavelength measurements of higher accuracy.

In the introduction, I mentioned that the first spectral terms, both in W I and in W II, were found from Zeeman-effect observations. In both spectra, such observations have greatly facilitated their analyses, and constitute the supreme test of validity. In the last column of table 3, are found some notes about the observed Zeeman patterns of 307 W II lines extending from 2216 Å to 4358 Å. The Zeeman patterns of W I and W II on MIT spectrograms were measured at the University of Wisconsin by J. E. Mack and Mrs. Taschek who supplied most of the magnetic splitting factors (*g*-factors) for tungsten levels that appear in Atomic Energy Levels [6]. Recently, those spectrograms were kindly loaned to me for examination. Without giving any details, I have merely written "res" to indicate resolved Zeeman patterns that agree with the combinations of W II lines in table 3. Unresolved Zeeman patterns are numbered 4, 5, 6, and 7, according to the notation of Back and Landé [7]. Incidentally, Zeeman types 4, 5, and 6 uniquely characterize, and fix *J*-values of, energy levels belonging to even multiplicities such as those responsible for W II lines. All the Zeeman-effect spectrograms are thickly covered by patterns of W I lines, and the W II patterns are often obscured, or vice versa, but despite these difficulties, the combinations are generally verified.

Finally, reference is made to the Tables of Spectral-Line Intensities by Meggers, Corliss, and Scribner [8] which list 1,300 tungsten lines, 1168 W I and 132 W II, observed in an arc between copper electrodes containing 0.1 atomic percent of tungsten. It is noteworthy that no W II lines appear among the first 28 lines of highest intensity; they are all W I. Tungsten is similar to rhenium in this respect, but unlike thorium or uranium in which spark lines predominate in this type of arc source. Ionization potentials may be responsible for this difference, since the I.P. of copper is less than that of tungsten or rhenium but greater than that of thorium or uranium. In the list of all observed lines of tungsten [8], all of the W II lines are now classified, and will be given in this paper.

In conclusion, let me say that since my association with the Bureau of Standards in 1925–26, when this investigation began, and again in 1943–44, when I collaborated on the uranium project [9], this work on W II has been pursued as a part-time occasional avocation with the goal of finding order in a complex spectrum.

TABLE 1. *Even levels of W II*

Configuration	Designation	*J*	Level	Interval	Obs. *g*
$5d^4(^5D)6s$	$a\ ^6D$	$0\frac{1}{2}$	0. 00		3. 186
				1518. 78	
		$1\frac{1}{2}$	1518. 78		1. 839
				1653. 74	
		$2\frac{1}{2}$	3172. 52		1. 639
				1543. 80	
		$3\frac{1}{2}$	4716. 32		1. 563
				1430. 84	
		$4\frac{1}{2}$	6147. 16		1. 522
$5d^5$	$a\ ^6S$	$2\frac{1}{2}$	7420. 43		1. 913
$5d^4(^3F)6s$	$a\ ^4F$	$1\frac{1}{2}$	8711. 26		0. 624
				2589. 82	
		$2\frac{1}{2}$	11301. 08		1. 084
				2110. 88	
		$3\frac{1}{2}$	13411. 96		1. 186
				1445. 26	
		$4\frac{1}{2}$	14857. 22		1. 234

716-919—64——5

TABLE 1. *Even levels of W* II—Continued

Configuration	Designation	J	Level	Interval	Obs. g
$5d^4(^3P)6s$	$a\ ^4P$	$0\frac{1}{2}$	8832. 66		2. 383
				1759. 86	
		$1\frac{1}{2}$	10592. 52		1. 471
				2841. 58	
		$2\frac{1}{2}$	13434. 10		1. 526
$5d^4(^5D)6s$	$a\ ^4D$	$0\frac{1}{2}$	13173. 38		0. 455
				1460. 98	
		$1\frac{1}{2}$	14634. 36		1. 183
				333. 46	
		$2\frac{1}{2}$	14967. 82		1. 013
				179. 20	
		$3\frac{1}{2}$	15147. 02		0. 872
$5d^4(^3G)6s$	$a\ ^4G$	$2\frac{1}{2}$	16234. 84		0. 995
				354. 83	
		$3\frac{1}{2}$	16589. 67		1. 153
				−36. 53	
		$4\frac{1}{2}$	16553. 14		1. 137
				883. 88	
		$5\frac{1}{2}$	17437. 02		1. 181
$5d^4(^3H)6s$	^4H	$3\frac{1}{2}$	18000. 70		1. 098
$5d^5$	^2D	$1\frac{1}{2}$	18990. 96		0. 90
$5d^5$	^4G	$4\frac{1}{2}$	19070. 68		1. 102
$5d^5$	^4G	$2\frac{1}{2}$	19276. 52		0. 997
$5d^4(^3P)6s$	^2P	$0\frac{1}{2}$	19404. 08		0. 64
$5d^4(^3H)6s$	^4H	$6\frac{1}{2}$	19442. 54		
$5d^5$	^2D	$2\frac{1}{2}$	19637. 38		1. 102
$5d^5$	^4G	$3\frac{1}{2}$	20039. 74		1. 107
$5d^5$	^4D	$1\frac{1}{2}$	20455. 93		0. 51
$5d^5$	^4G	$5\frac{1}{2}$	20534. 35		1. 197
$5d^4(^3H)6s$	^4H	$4\frac{1}{2}$	20780. 38		1. 065
$5d^5$	^4F	$2\frac{1}{2}$	22139. 97		1. 06
$5d^5$	^4F	$3\frac{1}{2}$	22194. 08		1. 119
$5d^4(^3P)6s$	^2P	$1\frac{1}{2}$	22503. 06		1. 22
		$0\frac{1}{2}$	22535. 80		2. 2
$5d^4(^3D)6s$	^4D	$3\frac{1}{2}$	23046. 80		0. 86
$5d^5$	^4F	$4\frac{1}{2}$	23234. 87		1. 249
$5d^5$	^4D	$2\frac{1}{2}$	23450. 50		1. 297
$5d^5$	^4D	$3\frac{1}{2}$	23803. 84		
$5d^5$	^2I	$5\frac{1}{2}$	23955. 40		1. 10
		$3\frac{1}{2}$	24804. 67		1. 10
		$1\frac{1}{2}$	24918. 10		
$5d^5$	^4F	$1\frac{1}{2}$	24991. 56		0. 9
		$0\frac{1}{2}$	25045. 20		0. 32
$5d^5$	^4P	$1\frac{1}{2}$	25169. 87		1. 64
		$4\frac{1}{2}$	25209. 28		
		$2\frac{1}{2}$	25672. 16		0. 9
$5d^4(^3H)6s$	^2H	$4\frac{1}{2}$	26158. 74		
$5d^5$	^4P	$2\frac{1}{2}$	26227. 00		1. 04
$5d^5(^3H)6s$	^2H	$5\frac{1}{2}$	26929. 34		
		$3\frac{1}{2}$	27273. 86		
		$2\frac{1}{2}$	28118. 90		
		$6\frac{1}{2}$	28187. 60		
		$5\frac{1}{2}$	28377. 80		
		$1\frac{1}{2}$	28491. 00		
		$3\frac{1}{2}$	28631. 86		
		$4\frac{1}{2}$	29341. 56		
		$4\frac{1}{2}$	30633. 02		
		$5\frac{1}{2}$	31100. 46		
		$5\frac{1}{2}$	33910. 56		1. 34
		$4\frac{1}{2}$	34091. 02		

TABLE 2. *Odd levels of* W II

Configuration	Designation	J	Level	Interval	Obs. g
$5d^4(^5D)6p$	$z\ ^6F°$	$0\frac{1}{2}$	*36165. 35*		0. 678
		$1\frac{1}{2}$	*39129. 41*	2964. 06	1. 147
		$2\frac{1}{2}$	*42049. 45*	2920. 04	1. 292
		$3\frac{1}{2}$	*44877. 18*	2827. 73	1. 277
		$4\frac{1}{2}$	*46493. 43*	1616. 25	1. 311
		$5\frac{1}{2}$	*51495. 00*	5001. 57	1. 054
$5d^4(^3P)6p$	$z\ ^2S°$	$0\frac{1}{2}$	*38576. 32*		1. 614
		$2\frac{1}{2}$	*39936. 81*		0. 889
		$1\frac{1}{2}$	*42298. 20*		1. 498
		$3\frac{1}{2}$	*42390. 27*		1. 161
		$2\frac{1}{2}$	*44354. 82*		1. 390
		$0\frac{1}{2}$	*44455. 18*		−0. 217
		$4\frac{1}{2}$	*44758. 10*		1. 270
		$1\frac{1}{2}$	*44911. 63*		1. 221
		$0\frac{1}{2}$	*45457. 02*		0. 519
		$1\frac{1}{2}$	*45553. 70*		1. 033
		$3\frac{1}{2}$	*46175. 42*		1. 452
		$2\frac{1}{2}$	*46355. 40*		1. 236
		$0\frac{1}{2}$	*46625. 27*		1. 70
		$1\frac{1}{2}$	*47179. 94*		1. 007
		$2\frac{1}{2}$	*47413. 33*		1. 111
		$1\frac{1}{2}$	*47588. 64*		2. 00
		$2\frac{1}{2}$	*48284. 48*		1. 366
		$5\frac{1}{2}$	*48332. 73*		
		$3\frac{1}{2}$	*48830. 70*		1. 008
		$1\frac{1}{2}$	*48982. 86*		1. 72
		$3\frac{1}{2}$	*49124. 52*		1. 499
		$0\frac{1}{2}$	*49154. 50*		2. 78
		$4\frac{1}{2}$	*49181. 04*		1. 409
		$2\frac{1}{2}$	*49242. 10*		1. 510
		$2\frac{1}{2}$	*50292. 33*		1. 334
		$1\frac{1}{2}$	*50430. 95*		0. 93
		$4\frac{1}{2}$	*50863. 05*		1. 194
		$3\frac{1}{2}$	*51045. 25*		
		$1\frac{1}{2}$	*51254. 40*		1. 58
		$2\frac{1}{2}$	*51438. 03*		1. 301
		$3\frac{1}{2}$	*51863. 03*		0. 937
		$2\frac{1}{2}$	*52087. 02*		
		$3\frac{1}{2}$	*52275. 28*		1. 297
		$0\frac{1}{2}$	*52355. 11*		0. 981
		$4\frac{1}{2}$	*52567. 15*		
		$0\frac{1}{2}$	*52593. 72*		1. 56 ?
		$1\frac{1}{2}$	*52803. 00*		
		$3\frac{1}{2}$	*52901. 74*		1. 374
		$2\frac{1}{2}$	*53113. 52*		1. 262
		$1\frac{1}{2}$	*53329. 71*		1. 357
		$3\frac{1}{2}$	*53338. 07*		0. 968
		$4\frac{1}{2}$	*53369. 97*		1. 086
		$1\frac{1}{2}$	*53422. 98*		0. 976
		$0\frac{1}{2}$	*53440. 17*		2. 038
		$2\frac{1}{2}$	*54026. 24*		
		$4\frac{1}{2}$	*54056. 54*		1. 123
		$1\frac{1}{2}$	*54137. 20*		1. 608
		$5\frac{1}{2}$	*54229. 06*		
		$2\frac{1}{2}$	*54375. 82*		1. 51
		$0\frac{1}{2}$	*54485. 60*		1. 46
		$3\frac{1}{2}$	*54498. 57*		
		$2\frac{1}{2}$	*54704. 61*		0. 623
		$0\frac{1}{2}$	*54760. 06*		
		$5\frac{1}{2}$	*54958. 58*		1. 141
		$3\frac{1}{2}$	*55022. 86*		
		$2\frac{1}{2}$	*55162. 30*		1. 00
		$4\frac{1}{2}$	*55392. 37*		1. 061
		$1\frac{1}{2}$	*55488. 01*		
		$1\frac{1}{2}$	*56084. 30*		1. 021
		$5\frac{1}{2}$	*56376. 45*		
		$4\frac{1}{2}$	*56413. 64*		
		$6\frac{1}{2}$	*56439. 60*		
		$2\frac{1}{2}$	*56544. 40*		

TABLE 2. *Odd levels of* W II—Continued

Configuration	Designation	J	Level	Interval	Obs. g
$5d^4(^3P)6p$	$z\,^2S^0$	$3\frac{1}{2}$	*56612. 74*		1. 22
		$3\frac{1}{2}$	*56768. 61*		1. 147
		$2\frac{1}{2}$	*56874. 99*		0. 815
		$1\frac{1}{2}$	*56932. 27*		1. 06
		$4\frac{1}{2}$	*57089. 46*		
		$2\frac{1}{2}$	*57252. 00*		
		$3\frac{1}{2}$	*57729. 92*		1. 184
		$2\frac{1}{2}$	*57856. 70*		1. 36
		$4\frac{1}{2}$	*57986. 92*		
		$1\frac{1}{2}$	*58007. 60*		1. 20
		$2\frac{1}{2}$	*58336. 98*		
		$4\frac{1}{2}$	*58687. 88*		
		$3\frac{1}{2}$	*58709. 56*		
		$1\frac{1}{2}$	*58747. 94*		0. 78
		$5\frac{1}{2}$	*58891. 74*		1. 144
		$3\frac{1}{2}$	*59276. 81*		1. 102
		$4\frac{1}{2}$	*59399. 34*		1. 179
		$1\frac{1}{2}$	*59816. 30*		
		$3\frac{1}{2}$	*59869. 14*		1. 125
		$3\frac{1}{2}$	*59933. 66*		
		$2\frac{1}{2}$	*59992. 20*		
		$5\frac{1}{2}$	*60218. 84*		1. 130
		$3\frac{1}{2}$	*60256. 45*		
		$4\frac{1}{2}$	*60278. 71*		
		$3\frac{1}{2}$	*60424. 14*		
		$2\frac{1}{2}$	*60474. 67*		
		$2\frac{1}{2}$	*60656. 51*		
		$2\frac{1}{2}$	*60900. 97*		0. 92
		$4\frac{1}{2}$	*61055. 80*		
		$5\frac{1}{2}$	*61240. 81*		1. 120
		$3\frac{1}{2}$	*61326. 29*		
		$4\frac{1}{2}$	*61360. 54*		
		$3\frac{1}{2}$	*61550. 60*		
		$2\frac{1}{2}$	*61566. 70*		1. 07
		$5\frac{1}{2}$	*61589. 46*		1. 149
		$6\frac{1}{2}$	*61602. 18*		
		$2\frac{1}{2}$	*62333. 20*		
		$4\frac{1}{2}$	*62437. 64*		
		$6\frac{1}{2}$	*62714. 56*		
		$4\frac{1}{2}$	*62715. 98*		
		$5\frac{1}{2}$	*62966. 56*		
		$2\frac{1}{2}$	*62989. 60*		
		$6\frac{1}{2}$	*63087. 90*		
		$3\frac{1}{2}$	*63266. 30*		
		$3\frac{1}{2}$	*63788. 20*		
		$2\frac{1}{2}$	*63880. 10*		
		$2\frac{1}{2}$	*64030. 34*		
		$4\frac{1}{2}$	*64207. 50*		
		$2\frac{1}{2}$	*64310. 00*		
		$3\frac{1}{2}$	*64356. 70*		
		$4\frac{1}{2}$	*64516. 37*		
		$3\frac{1}{2}$	*64896. 22*		
		$5\frac{1}{2}$	*64969. 10*		
		$2\frac{1}{2}$	*64990. 32*		
		$4\frac{1}{2}$	*65003. 20*		
		$2\frac{1}{2}$	*65141. 56*		
		$5\frac{1}{2}$	*65326. 40*		
		$3\frac{1}{2}$	*65644. 00*		
		$5\frac{1}{2}$	*65684. 80*		
		$4\frac{1}{2}$	*66270. 95*		
		$5\frac{1}{2}$	*66703. 50*		
		$5\frac{1}{2}$	*68012. 50*		
		$6\frac{1}{2}$	*68078. 98*		

TABLE 3. *Classified lines of* W II

Wavelength (Å)	Intensity		Wave number (cm^{-1})		Combination	Zeeman effect
	Arc	Spark	Observed	$O-C$		
Vac.						
1756. 604		8	56928. 0	−4. 3	$a\ ^6D_{0\frac{1}{2}}$—$59932^{1}_{1\frac{1}{2}}$	
1757. 789		3	56889. 6	0. 0	$a\ ^6S_{2\frac{1}{2}}$—$64310^{3}_{2\frac{1}{2}}$	
1759. 408		4	56837. 3	+3. 0	$a\ ^6D_{3\frac{1}{2}}$—$61550^{5}_{3\frac{1}{2}}$	
1760. 00		5	56818. 2	0. 0	$a\ ^6D_{1\frac{1}{2}}$—$58336^{3}_{2\frac{1}{2}}$	
1765. 514		20	56640. 7	−3. 1 −3. 5	$a\ ^6D_{2\frac{1}{2}}$—$59816^{1}_{1\frac{1}{2}}$ $a\ ^6D_{3\frac{1}{2}}$—$61360^{3}_{2\frac{1}{2}}$	
1766. 319		8	56614. 9	+4. 9 +5. 0	$a\ ^6D_{3\frac{1}{2}}$—$61326^{5}_{3\frac{1}{2}}$ $a\ ^6S_{2\frac{1}{2}}$—$64030^{3}_{2\frac{1}{2}}$	
1775. 023		3	56337. 3	−0. 6	$a\ ^6D_{1\frac{1}{2}}$—$57856^{3}_{2\frac{1}{2}}$	
1776. 834		4	56279. 9	+0. 8	$a\ ^4F_{1\frac{1}{2}}$—$64990^{3}_{2\frac{1}{2}}$	
1783. 050		10	56083. 7	−0. 6	$a\ ^6D_{0\frac{1}{2}}$—$56084^{1}_{1\frac{1}{2}}$	
1794. 166		4	55736. 2	+3. 0	$a\ ^6D_{1\frac{1}{2}}$—$57252^{3}_{2\frac{1}{2}}$	
1795. 131		20	55706. 2	−1. 6	$a\ ^6D_{3\frac{1}{2}}$—$60424^{5}_{3\frac{1}{2}}$	
1798. 60		3	55598. 8	+0. 1	$a\ ^4F_{1\frac{1}{2}}$—$64310^{3}_{2\frac{1}{2}}$	
1799. 558		4	55569. 2	0. 0	$a\ ^6S_{2\frac{1}{2}}$—$62989^{3}_{2\frac{1}{2}}$	
1800. 570		20	55538. 0	+1. 0 −2. 1	$a\ ^6D_{2\frac{1}{2}}$—$58709^{3}_{2\frac{1}{2}}$ $a\ ^6D_{3\frac{1}{2}}$—$60256^{5}_{3\frac{1}{2}}$	
1802. 211		8	55487. 4	−0. 6	$a\ ^6D_{0\frac{1}{2}}$—$55488^{1}_{1\frac{1}{2}}$	
1803. 840		8	55437. 3	−5. 0	$a\ ^6D_{4\frac{1}{2}}$—$61589^{5}_{3\frac{1}{2}}$	
1804. 51		6	55416. 7	+3. 2	$a\ ^6D_{1\frac{1}{2}}$—$59932^{1}_{1\frac{1}{2}}$	
1806. 437		3	55357. 6	+1. 4	$a\ ^6D_{1\frac{1}{2}}$—$56874^{2}_{2\frac{1}{2}}$	
1807. 645		2	55320. 5	+1. 4	$a\ ^4F_{1\frac{1}{2}}$—$64030^{3}_{2\frac{1}{2}}$	
1809. 082		2	55276. 6	+0. 7	$a\ ^6D_{3\frac{1}{2}}$—$59992^{3}_{2\frac{1}{2}}$	
1811. 021		5	55217. 5	+0. 2	$a\ ^6D_{3\frac{1}{2}}$—$59933^{3}_{2\frac{1}{2}}$	
1812. 161		40	55182. 7	+3. 6	$a\ ^6D_{4\frac{1}{2}}$—$61326^{5}_{3\frac{1}{2}}$	
1812. 765		6	55164. 4	−0. 1	$a\ ^6D_{2\frac{1}{2}}$—$58336^{3}_{2\frac{1}{2}}$	
1812. 977		5	55157. 9	+5. 1	$a\ ^6D_{3\frac{1}{2}}$—$59869^{3}_{2\frac{1}{2}}$	
1815. 073		2	55094. 2	+0. 6	$a\ ^6D_{4\frac{1}{2}}$—$61240^{5}_{3\frac{1}{2}}$	
1817. 347		10	55025. 2	−0. 4	$a\ ^6D_{1\frac{1}{2}}$—$56544^{3}_{2\frac{1}{2}}$	
1821. 062		30	54913. 0	+4. 4 +0. 2	$a\ ^6D_{4\frac{1}{2}}$—$61055^{4}_{3\frac{1}{2}}$ $a\ ^6S_{2\frac{1}{2}}$—$62333^{2}_{2\frac{1}{2}}$	
1823. 64		3	54835. 4	+0. 3	$a\ ^6D_{2\frac{1}{2}}$—$58007^{1}_{1\frac{1}{2}}$	
1826. 126		20	54760. 7	+0. 6	$a\ ^6D_{0\frac{1}{2}}$—$54760^{0}_{0\frac{1}{2}}$	
1828. 69		6	54684. 0	+1. 0 −0. 2	$a\ ^6D_{3\frac{1}{2}}$—$59399^{4}_{3\frac{1}{2}}$ $a\ ^6D_{2\frac{1}{2}}$—$57856^{3}_{2\frac{1}{2}}$	
1838. 338		25	54397. 0	−0. 8	$a\ ^4P_{1\frac{1}{2}}$—$64990^{3}_{2\frac{1}{2}}$	
1847. 041		5	54140. 6	+3. 4	$a\ ^6D_{0\frac{1}{2}}$—$54137^{1}_{1\frac{1}{2}}$	
1848. 104		30	54109. 7	+0. 4	$a\ ^6D_{4\frac{1}{2}}$—$60256^{5}_{3\frac{1}{2}}$	
1852. 110		15	53992. 5	−0. 7	$a\ ^6D_{3\frac{1}{2}}$—$58709^{3}_{2\frac{1}{2}}$	
1852. 917		20	53969. 0	−0. 2	$a\ ^6D_{1\frac{1}{2}}$—$55488^{1}_{1\frac{1}{2}}$	
1860. 069		4	53761. 4	+1. 6	$a\ ^6D_{2\frac{1}{2}}$—$56932^{1}_{1\frac{1}{2}}$	
1861. 26		6	53727. 0	+5. 0	$a\ ^6D_{4\frac{1}{2}}$—$59869^{3}_{2\frac{1}{2}}$	
1864. 976		15	53620. 0	−0. 7	$a\ ^6D_{3\frac{1}{2}}$—$58336^{2}_{2\frac{1}{2}}$	
1865. 818		8	53595. 8	−0. 3	$a\ ^6D_{2\frac{1}{2}}$—$56768^{3}_{2\frac{1}{2}}$	
1871. 261		6	53439. 9	−0. 3 −0. 3	$a\ ^6D_{0\frac{1}{2}}$—$53440^{0}_{0\frac{1}{2}}$ $a\ ^6D_{2\frac{1}{2}}$—$56612^{2}_{2\frac{1}{2}}$	
1871. 90		6	53421. 6	−1. 4	$a\ ^6D_{0\frac{1}{2}}$—$53422^{1}_{1\frac{1}{2}}$	
1873. 646		20	53371. 9	0. 0	$a\ ^6D_{2\frac{1}{2}}$—$56544^{3}_{2\frac{1}{2}}$	
1875. 156		12	53328. 9	−0. 8	$a\ ^6D_{0\frac{1}{2}}$—$53329^{1}_{1\frac{1}{2}}$	
1877. 33		2	53267. 2	−3. 4	$a\ ^6D_{3\frac{1}{2}}$—$57986^{3}_{2\frac{1}{2}}$	
1877. 869		20	53251. 8	−0. 4	$a\ ^6D_{4\frac{1}{2}}$—$59399^{4}_{3\frac{1}{2}}$	
1878. 54		4	53233. 0	−3. 1	$a\ ^6S_{2\frac{1}{2}}$—$60656^{3}_{2\frac{1}{2}}$	
1880. 216		8	53185. 4	−0. 4	$a\ ^6D_{1\frac{1}{2}}$—$54704^{2}_{2\frac{1}{2}}$	
1881. 798		15	53140. 6	+0. 2	$a\ ^6D_{3\frac{1}{2}}$—$57856^{3}_{2\frac{1}{2}}$	
1882. 185		8	53129. 7	+0. 1	$a\ ^6D_{4\frac{1}{2}}$—$59276^{4}_{3\frac{1}{2}}$	
1886. 304		6	53013. 7	+0. 1	$a\ ^6D_{3\frac{1}{2}}$—$57729^{3}_{2\frac{1}{2}}$	

TABLE 3. *Classified lines of* W II—Continued

Wavelength (Å)	Intensity		Wave number (cm^{-1})		Combination	Zeeman effect
	Arc	Spark	Observed	*O–C*		
Vac.						
1891. 908		6	52856. 7	−0. 3 +1. 3	$a\ {}^6D_{1\frac{1}{2}}$—*54375*$^{3}_{3\frac{1}{2}}$ $a\ {}^4F_{1\frac{1}{2}}$—*61566*$^{2}_{2\frac{1}{2}}$	
1892. 442		15	52841. 8	+5. 8	$a\ {}^6S_{2\frac{1}{2}}$—*60256*$^{3}_{3\frac{1}{2}}$	
1893. 80		4	52803. 9	+0. 9	$a\ {}^6D_{0\frac{1}{2}}$—*52803*$^{2}_{1\frac{1}{2}}$	
1895. 943		30	52744. 2	−0. 4	$a\ {}^6D_{4\frac{1}{2}}$—*58891*$^{3}_{3\frac{1}{2}}$	
1900. 503		12	52617. 6	−0. 8	$a\ {}^6D_{1\frac{1}{2}}$—*54137*$^{1}_{1\frac{1}{2}}$	
1901. 245		30	52597. 1	+3. 4	$a\ {}^6D_{0\frac{1}{2}}$—*52593*$^{3}_{0\frac{1}{2}}$	
1902. 51		20	52562. 1	−0. 3	$a\ {}^6D_{4\frac{1}{2}}$—*58709*$^{3}_{3\frac{1}{2}}$	
1906. 677		12	52447. 3	−1. 4	$a\ {}^6S_{2\frac{1}{2}}$—*59869*$^{3}_{3\frac{1}{2}}$	
1908. 750		10	52390. 3	−5. 6	$a\ {}^6S_{2\frac{1}{2}}$—*59816*$^{2}_{1\frac{1}{2}}$	
1909. 16		6	52379. 0	+5. 9	$a\ {}^6D_{3\frac{1}{2}}$—*57089*$^{4}_{4\frac{1}{2}}$	
1909. 80		4	52361. 4	+6. 3	$a\ {}^6D_{0\frac{1}{2}}$—*52355*$^{3}_{0\frac{1}{2}}$	
1911. 50		25	52314. 9	−0. 6	$a\ {}^6D_{2\frac{1}{2}}$—*55488*$^{1}_{1\frac{1}{2}}$	
1915. 38		8	52209. 0	−0. 9	$a\ {}^4P_{2\frac{1}{2}}$—*65644*$^{3}_{3\frac{1}{2}}$	
1925. 99		12	51921. 3	−0. 1	$a\ {}^6D_{1\frac{1}{2}}$—*53440*$^{3}_{0\frac{1}{2}}$	
1928. 61		20	51850. 8	+0. 5	$a\ {}^6D_{2\frac{1}{2}}$—*55022*$^{3}_{3\frac{1}{2}}$	
1929. 47		10	51827. 7	−0. 4	$a\ {}^6D_{3\frac{1}{2}}$—*56544*$^{3}_{2\frac{1}{2}}$	
1930. 10		6	51810. 8	−0. 1	$a\ {}^6D_{1\frac{1}{2}}$—*53329*$^{2}_{1\frac{1}{2}}$	
1931. 87		10	51763. 3	−0. 1	$a\ {}^4F_{1\frac{1}{2}}$—*60474*$^{3}_{2\frac{1}{2}}$	
1934. 345		10	51697. 1	−0. 2	$a\ {}^6D_{3\frac{1}{2}}$—*56413*$^{4}_{3\frac{1}{2}}$	
1934. 62		3	51689. 7	+1. 2	$a\ {}^4F_{2\frac{1}{2}}$—*62989*$^{2}_{2\frac{1}{2}}$	
1938. 21		25	51594. 0	−0. 7	$a\ {}^6D_{1\frac{1}{2}}$—*53113*$^{3}_{2\frac{1}{2}}$	
1938. 74		3	51579. 9	−2. 9 +1. 5	$a\ {}^6D_{4\frac{1}{2}}$—*57729*$^{3}_{3\frac{1}{2}}$ $a\ {}^4F_{3\frac{1}{2}}$—*64990*$^{3}_{3\frac{1}{2}}$	
1940. 54		8	51532. 0	−0. 1	$a\ {}^6D_{2\frac{1}{2}}$—*54704*$^{2}_{2\frac{1}{2}}$	
1943. 27		4	51459. 6	+0. 2	$a\ {}^4G_{4\frac{1}{2}}$—*68012*$^{3}_{3\frac{1}{2}}$	
1945. 02		10	51413. 5	−0. 2	$a\ {}^4F_{4\frac{1}{2}}$—*66270*$^{4}_{4\frac{1}{2}}$	
1948. 35		30	51325. 5	−0. 5	$a\ {}^6D_{2\frac{1}{2}}$—*54498*$^{3}_{3\frac{1}{2}}$	
1949. 55		40	51293. 9	+4. 8	$a\ {}^6S_{2\frac{1}{2}}$—*58709*$^{3}_{3\frac{1}{2}}$	
1949. 93		4	51283. 9	−0. 3	$a\ {}^6D_{1\frac{1}{2}}$—*52803*$^{1}_{1\frac{1}{2}}$	
1951. 06		40	51254. 2	−0. 2	$a\ {}^6D_{0\frac{1}{2}}$—*51254*$^{1}_{1\frac{1}{2}}$	
1953. 00		3	51203. 3	0. 0	$a\ {}^6D_{2\frac{1}{2}}$—*54375*$^{3}_{2\frac{1}{2}}$	
1957. 90		2	51075. 1	+0. 2	$a\ {}^6D_{1\frac{1}{2}}$—*52593*$^{3}_{0\frac{1}{2}}$	
1959. 54		5	51032. 3	+0. 2	$a\ {}^4F_{2\frac{1}{2}}$—*62333*$^{2}_{2\frac{1}{2}}$	
1961. 42		6	50983. 5	−0. 1	$a\ {}^4P_{0\frac{1}{2}}$—*59816*$^{1}_{1\frac{1}{2}}$	
1962. 14		40	50964. 7	0. 0	$a\ {}^6D_{2\frac{1}{2}}$—*54137*$^{1}_{1\frac{1}{2}}$	
1962. 92		20	50944. 4	−0. 3	$a\ {}^4F_{3\frac{1}{2}}$—*64356*$^{3}_{3\frac{1}{2}}$	
1963. 02		2	50941. 9	−0. 4	$a\ {}^6D_{4\frac{1}{2}}$—*57089*$^{4}_{4\frac{1}{2}}$	
1967. 09		2	50836. 5	+0. 2	$a\ {}^6D_{1\frac{1}{2}}$—*52355*$^{3}_{3\frac{1}{2}}$	
1967. 41		10	50828. 2	+0. 6	$a\ {}^4F_{4\frac{1}{2}}$—*65684*$^{4}_{3\frac{1}{2}}$	
1968. 67		8	50795. 6	+0. 1	$a\ {}^4F_{3\frac{1}{2}}$—*64207*$^{4}_{4\frac{1}{2}}$	
1973. 32		20	50676. 0	0. 0	$a\ {}^6D_{3\frac{1}{2}}$—*55392*$^{4}_{3\frac{1}{2}}$	
1974. 66		4	50641. 6	−0. 3	$a\ {}^4G_{5\frac{1}{2}}$—*68078*$^{4}_{4\frac{1}{2}}$	
1975. 48		15	50620. 7	−0. 7	$a\ {}^6D_{4\frac{1}{2}}$—*56768*$^{3}_{3\frac{1}{2}}$	
1976. 70		25	50589. 4	+2. 2	$a\ {}^6S_{2\frac{1}{2}}$—*58007*$^{1}_{1\frac{1}{2}}$	
1977. 24		12	50575. 6	+0. 1	$a\ {}^4G_{5\frac{1}{2}}$—*68012*$^{3}_{3\frac{1}{2}}$	
1977. 53		15	50568. 1	−0. 1	$a\ {}^6D_{1\frac{1}{2}}$—*52087*$^{2}_{1\frac{1}{2}}$	
1981. 42		20	50468. 8	+3. 2	$a\ {}^6D_{4\frac{1}{2}}$—*56612*$^{3}_{3\frac{1}{2}}$	
1982. 35		15	50445. 1	−0. 9	$a\ {}^6D_{3\frac{1}{2}}$—*55162*$^{3}_{2\frac{1}{2}}$	
1982. 73		1	50435. 5	−0. 8	$a\ {}^6S_{2\frac{1}{2}}$—*57856*$^{3}_{3\frac{1}{2}}$	
1982. 92		20	50430. 7	−0. 3	$a\ {}^6D_{0\frac{1}{2}}$—*50430*$^{1}_{1\frac{1}{2}}$	
1987. 80		25	50301. 9	−4. 6	$a\ {}^6D_{3\frac{1}{2}}$—*55022*$^{3}_{3\frac{1}{2}}$	
1989. 41		30	50266. 1	−0. 4	$a\ {}^6D_{4\frac{1}{2}}$—*56413*$^{4}_{4\frac{1}{2}}$	

TABLE 3. *Classified lines of* W II—Continued

Wavelength (Å)	Intensity		Wave number (cm^{-1})		Combination	Zeeman effect
	Arc	Spark	Observed	*O–C*		
Vac.						
1990. 07		15	50249. 4	−0. 1 −1. 1	$a\ ^4F_{2\frac{1}{2}}$—*61550*$^0_{3\frac{1}{2}}$ $a\ ^6D_{2\frac{1}{2}}$—*53423*$^0_{3\frac{1}{2}}$	
1990. 86		12	50229. 6	+0. 3	$a\ ^6D_{4\frac{1}{2}}$—*56376*$^0_{5\frac{1}{2}}$	
1993. 15		6	50171. 8	−1. 9	$a\ ^4D_{2\frac{1}{2}}$—*65141*$^0_{2\frac{1}{2}}$	
1993. 53		1	50162. 3	−3. 3	$a\ ^6D_{2\frac{1}{2}}$—*53338*$^0_{3\frac{1}{2}}$	
1993. 74		3	50156. 9	−0. 3	$a\ ^6D_{2\frac{1}{2}}$—*53329*$^0_{1\frac{1}{2}}$	
1994. 21		15	50145. 1	−0. 9	$a\ ^4F_{4\frac{1}{2}}$—*65003*$^0_{4\frac{1}{2}}$	
1995. 545		25	50111. 6	−0. 3	$a\ ^4F_{4\frac{1}{2}}$—*64969*$^0_{3\frac{1}{2}}$	
1997. 46		6	50063. 7	−0. 3	$a\ ^4P_{1\frac{1}{2}}$—*60656*$^0_{2\frac{1}{2}}$	
1998. 54		3	50036. 6	−0. 1	$a\ ^4F_{1\frac{1}{2}}$—*58747*$^0_{1\frac{1}{2}}$	
1998. 99		3	50025. 2	0. 0	$a\ ^4F_{2\frac{1}{2}}$—*61326*$^0_{3\frac{1}{2}}$	
Air						
1999. 83		12	49988. 1	−0. 2	$a\ ^6D_{3\frac{1}{2}}$—*54704*$^0_{2\frac{1}{2}}$	
2001. 70	3	30	49941. 4	+0. 4	$a\ ^6D_{2\frac{1}{2}}$—*53113*$^0_{1\frac{1}{2}}$	
2002. 59		2	49919. 2	0. 0	$a\ ^6D_{1\frac{1}{2}}$—*51438*$^0_{2\frac{1}{2}}$	
2002. 73	1	3	49915. 7	+0. 4	$a\ ^4P_{0\frac{1}{2}}$—*58747*$^0_{1\frac{1}{2}}$	
2005. 60		1	49844. 3	+1. 0	$a\ ^4D_{3\frac{1}{2}}$—*64990*$^0_{2\frac{1}{2}}$	
2006. 07		3	49832. 6	+0. 4	$a\ ^4P_{2\frac{1}{2}}$—*63266*$^0_{3\frac{1}{2}}$	
2008. 08	4	40	49782. 7	+0. 5	$a\ ^6D_{3\frac{1}{2}}$—*54498*$^0_{3\frac{1}{2}}$	
2009. 37		2	49750. 8	+1. 6	$a\ ^4D_{3\frac{1}{2}}$—*64896*$^0_{3\frac{1}{2}}$	
2009. 98	1	12	49735. 7	+0. 1	$a\ ^6D_{1\frac{1}{2}}$—*51254*$^0_{1\frac{1}{2}}$	
2010. 24	3	15	49729. 3	+0. 1	$a\ ^6D_{2\frac{1}{2}}$—*52901*$^0_{3\frac{1}{2}}$	
2010. 66	2	1	49718. 9	+1. 1	$a\ ^4G_{4\frac{1}{2}}$—*66270*$^0_{4\frac{1}{2}}$	
2012. 18		5	49681. 3	0. 0	$a\ ^4G_{3\frac{1}{2}}$—*66270*$^0_{4\frac{1}{2}}$	
2013. 06	4	4	49659. 6	+0. 1	$a\ ^6D_{3\frac{1}{2}}$—*54375*$^0_{3\frac{1}{2}}$	
2014. 23	3	15	49630. 7	+0. 2	$a\ ^6D_{2\frac{1}{2}}$—*52803*$^0_{1\frac{1}{2}}$	
2014. 43	3	10	49625. 8	+0. 1	$a\ ^4F_{1\frac{1}{2}}$—*58336*$^0_{2\frac{1}{2}}$	
2015. 44	2	8	49601. 0	+1. 1	$a\ ^4F_{2\frac{1}{2}}$—*60900*$^0_{2\frac{1}{2}}$	
2017. 26	—	2	49556. 2	+0. 7	$a\ ^4P_{2\frac{1}{2}}$—*62989*$^0_{2\frac{1}{2}}$	
2019. 08	—	1	49511. 6	−0. 2	$a\ ^6S_{2\frac{1}{2}}$—*56932*$^0_{1\frac{1}{2}}$	
2019. 55	2	5	49500. 0	+0. 5	$a\ ^4F_{4\frac{1}{2}}$—*64356*$^0_{3\frac{1}{2}}$	
2021. 43		3	49454. 0	−0. 6	$a\ ^6S_{2\frac{1}{2}}$—*56874*$^0_{2\frac{1}{2}}$	
2023. 25		1	49409. 5	+0. 1	$a\ ^4G_{2\frac{1}{2}}$—*65644*$^3_{3\frac{1}{2}}$	
2023. 63		3	49400. 3	+0. 6	$a\ ^4P_{1\frac{1}{2}}$—*59992*$^0_{2\frac{1}{2}}$	
2023. 79		3	49396. 4	+0. 4	$a\ ^4D_{1\frac{1}{2}}$—*64030*$^0_{2\frac{1}{2}}$	
2025. 45	1	4	49355. 9	+0. 5	$a\ ^4F_{2\frac{1}{2}}$—*60656*$^0_{2\frac{1}{2}}$	
2025. 62		2	49351. 7	+1. 4	$a\ ^4F_{4\frac{1}{2}}$—*64207*$^0_{4\frac{1}{2}}$	
2026. 07	8	30	49340. 8	+0. 6	$a\ ^6D_{3\frac{1}{2}}$—*54056*$^0_{4\frac{1}{2}}$	
2027. 30	1	12	49310. 8	+0. 9	$a\ ^6D_{3\frac{1}{2}}$—*54026*$^0_{2\frac{1}{2}}$	
2027. 55	2	3	49304. 8	+0. 8	$a\ ^4F_{3\frac{1}{2}}$—*62715*$^0_{4\frac{1}{2}}$	
2027. 87	2	5	49296. 9	+0. 6	$a\ ^4F_{1\frac{1}{2}}$—*58007*$^0_{1\frac{1}{2}}$	
2029. 12	1	15	49266. 6	+0. 1	$a\ ^4G_{3\frac{1}{2}}$—*66703*$^0_{3\frac{1}{2}}$	
2029. 99	5	50	49245. 5	+0. 3	$a\ ^6D_{4\frac{1}{2}}$—*55392*$^0_{4\frac{1}{2}}$	
2030. 87		3	49224. 2	+0. 4	$a\ ^4P_{1\frac{1}{2}}$—*59816*$^0_{1\frac{1}{2}}$	
2031. 44		12	49210. 4	+0. 7	$a\ ^4D_{3\frac{1}{2}}$—*64356*$^0_{3\frac{1}{2}}$	
2032. 16		3	49192. 9	+0. 6	$a\ ^6S_{2\frac{1}{2}}$—*56612*$^0_{2\frac{1}{2}}$	
2032. 92		12	49174. 5	−0. 4	$a\ ^4P_{0\frac{1}{2}}$—*58007*$^0_{1\frac{1}{2}}$	
2033. 38		10	49163. 4	+0. 4	$a\ ^4D_{3\frac{1}{2}}$—*64310*$^0_{2\frac{1}{2}}$	
2033. 73		8	49154. 9	+0. 4	$a\ ^6D_{0\frac{1}{2}}$—*49154*$^0_{0\frac{1}{2}}$	
2034. 19		3	49143. 8	−1. 6	$a\ ^4F_{1\frac{1}{2}}$—*57856*$^0_{2\frac{1}{2}}$	
2035. 02	5	25	49123. 8	−0. 2	$a\ ^6S_{2\frac{1}{2}}$—*56544*$^0_{2\frac{1}{2}}$	
2035. 87	5	40	49103. 3	+0. 5	$a\ ^6D_{2\frac{1}{2}}$—*52275*$^3_{3\frac{1}{2}}$	
2036. 40		2	49090. 5	−0. 4	$a\ ^4G_{4\frac{1}{2}}$—*65644*$^3_{3\frac{1}{2}}$	
2037. 58	3	40	49062. 1	−0. 4	$a\ ^4D_{2\frac{1}{2}}$—*64030*$^0_{2\frac{1}{2}}$	

TABLE 3. *Classified lines of* W II—Continued

Wavelength (Å)	Intensity		Wave number (cm^{-1})		Combination	Zeeman effect
	Arc	Spark	Observed	O–C		
Air						
2037.89	2	15	49054.6	+0.3	$a\ ^4G_{3\frac{1}{2}}$—$65644\frac{5}{3\frac{1}{2}}$	
2039.10	—	4	49025.5	+0.4	$a\ ^4F_{3\frac{1}{2}}$—$62437\frac{4}{4\frac{1}{2}}$	
2040.86	4	20	48983.3	+0.4	$a\ ^6D_{0\frac{1}{2}}$—$48982\frac{1}{1\frac{1}{2}}$	
2042.00	1	6	48956.0	+0.6	$a\ ^4F_{2\frac{1}{2}}$—$60256\frac{3}{3\frac{1}{2}}$	
2042.55		5	48942.7	+0.9	$19070_{4\frac{1}{2}}$—$68012\frac{5}{3\frac{1}{2}}$	
2043.02	2	8	48931.3	+0.3	$a\ ^4F_{4\frac{1}{2}}$—$63788\frac{3}{3\frac{1}{2}}$	
2043.52	5	30	48919.6	−1.6	$a\ ^4F_{3\frac{1}{2}}$—$62333\frac{5}{2\frac{1}{2}}$	
2043.72		15	48914.7	+0.2	$a\ ^6D_{2\frac{1}{2}}$—$52087\frac{3}{2\frac{1}{2}}$	
2043.82		3	48912.3	+0.1	$a\ ^6D_{1\frac{1}{2}}$—$50430\frac{1}{1\frac{1}{2}}$	
2044.33	2	10	48900.1	+1.0	$a\ ^4P_{2\frac{1}{2}}$—$62333\frac{5}{2\frac{1}{2}}$	
2045.05	3	3	48883.0	−0.3	$a\ ^4D_{3\frac{1}{2}}$—$64030\frac{2}{2\frac{1}{2}}$	
2045.32	2	15	48876.4	+0.7	$a\ ^6D_{4\frac{1}{2}}$—$55022\frac{5}{3\frac{1}{2}}$	
2047.07	2	20	48834.8	+0.9	$a\ ^4G_{3\frac{1}{2}}$—$66270\frac{4}{4\frac{1}{2}}$	
2047.76		2	48818.2	−2.2	$a\ ^4D_{2\frac{1}{2}}$—$63788\frac{3}{3\frac{1}{2}}$	
2048.03	5	30	48811.8	+0.4	$a\ ^6D_{4\frac{1}{2}}$—$54958\frac{5}{3\frac{1}{2}}$	
2049.62	8	25	48773.9	+0.3	$a\ ^6D_{1\frac{1}{2}}$—$50292\frac{2}{2\frac{1}{2}}$	
2050.36		12	48756.3	+0.8	$a\ ^4G_{2\frac{1}{2}}$—$64990\frac{3}{2\frac{1}{2}}$	
2051.32	1?	1	48733.5	+0.4	$a\ ^4D_{3\frac{1}{2}}$—$63880\frac{2}{2\frac{1}{2}}$	
2053.10	5	15	48691.3	+0.2 +0.8	$a\ ^4F_{2\frac{1}{2}}$—$59992\frac{3}{2\frac{1}{2}}$ $a\ ^6D_{2\frac{1}{2}}$—$51863\frac{3}{3\frac{1}{2}}$	
2053.35		3	48661.6	+0.2	$a\ ^4G_{2\frac{1}{2}}$—$64896\frac{1}{3\frac{1}{2}}$	
2054.67	10	50	48654.0	+0.4	$a\ ^6D_{3\frac{1}{2}}$—$53369\frac{4}{4\frac{1}{2}}$	
2055.19	2	3	48641.8	+0.6	$a\ ^4D_{3\frac{1}{2}}$—$63788\frac{3}{3\frac{1}{2}}$	
2055.54	1?	3	48633.5	+0.9	$a\ ^4F_{2\frac{1}{2}}$—$59933\frac{3}{3\frac{1}{2}}$	
2055.99	2	10	48622.8	+1.0	$a\ ^6D_{3\frac{1}{2}}$—$53338\frac{3}{3\frac{1}{2}}$	
2058.30	12	15	48568.3	+0.2	$a\ ^4F_{2\frac{1}{2}}$—$59869\frac{3}{3\frac{1}{2}}$	
2059.03	1	8	48550.9	−1.0	$a\ ^4G_{3\frac{1}{2}}$—$65141\frac{2}{2\frac{1}{2}}$	
2059.45	4	8	48541.1	+0.4	$a\ ^4F_{1\frac{1}{2}}$—$57252\frac{2}{2\frac{1}{2}}$	
2060.53	3	2	48515.7	+0.5	$a\ ^4F_{2\frac{1}{2}}$—$59816\frac{1}{1\frac{1}{2}}$	
2063.34		1	48449.7	−0.4	$a\ ^4G_{4\frac{1}{2}}$—$65003\frac{3}{4\frac{1}{2}}$	
2064.76	2	6	48416.3	+0.3	$a\ ^4G_{4\frac{1}{2}}$—$64969\frac{5}{5\frac{1}{2}}$	
2065.06	6*A*	3	48409.4	+0.3	$a\ ^4F_{4\frac{1}{2}}$—$63266\frac{3}{3\frac{1}{2}}$	
2065.57	3	30	48397.3	+0.1	$a\ ^6D_{3\frac{1}{2}}$—$53113\frac{2}{2\frac{1}{2}}$	
2067.52	—?	30	48351.7	+0.3	$a\ ^6D_{4\frac{1}{2}}$—$54498\frac{3}{3\frac{1}{2}}$	
2067.87	—?	10	48343.5	+0.4	$a\ ^4G_{4\frac{1}{2}}$—$64896\frac{3}{3\frac{1}{2}}$	
2069.36		10	48308.8	+2.2	$a\ ^4G_{3\frac{1}{2}}$—$64896\frac{3}{3\frac{1}{2}}$	
2069.77		3	48299.1	+0.6	$a\ ^4D_{2\frac{1}{2}}$—$63266\frac{3}{3\frac{1}{2}}$	
2071.19	2	40	48265.9	+0.4	$a\ ^6D_{2\frac{1}{2}}$—$51438\frac{2}{2\frac{1}{2}}$	
2071.95		3	48248.3	+0.5	$a\ ^4G_{5\frac{1}{2}}$—$65684\frac{5}{5\frac{1}{2}}$	
2074.63		15	48185.9	+0.5	$a\ ^6D_{3\frac{1}{2}}$—$52901\frac{3}{3\frac{1}{2}}$	
2075.59	2	30	48163.8	+0.1	$a\ ^4F_{1\frac{1}{2}}$—$56874\frac{2}{2\frac{1}{2}}$	
2075.93		10	48155.9	+0.5	$a\ ^4P_{1\frac{1}{2}}$—$58747\frac{1}{1\frac{1}{2}}$	
2076.92		2	48132.9	+0.3	$a\ ^4P_{2\frac{1}{2}}$—$61566\frac{3}{2\frac{1}{2}}$	
2077.36		5	48122.6	+0.7	$a\ ^4G_{2\frac{1}{2}}$—$64356\frac{3}{3\frac{1}{2}}$	
2077.61		6	48116.9	+0.4	$a\ ^4P_{2\frac{1}{2}}$—$61550\frac{3}{3\frac{1}{2}}$	
2077.92	1	10	48109.7	+0.4	$a\ ^4F_{4\frac{1}{2}}$—$62966\frac{5}{3\frac{1}{2}}$	
2078.32	1	40	48100.3	+0.7	$a\ ^4P_{0\frac{1}{2}}$—$56932\frac{1}{1\frac{1}{2}}$	
2079.11	20	80	48082.2	+0.3 +0.3	$a\ ^6D_{2\frac{1}{2}}$—$51254\frac{1}{1\frac{1}{2}}$ $a\ ^6D_{4\frac{1}{2}}$—$54229\frac{5}{3\frac{1}{2}}$	
2081.75		3	48021.2	−0.6	$a\ ^4D_{2\frac{1}{2}}$—$62989\frac{3}{2\frac{1}{2}}$	
2083.70	1	10	47976.4	+0.7	$a\ ^4F_{2\frac{1}{2}}$—$59276\frac{3}{3\frac{1}{2}}$	
2084.23		12	47964.1	+0.9	$a\ ^4G_{4\frac{1}{2}}$—$64516\frac{4}{4\frac{1}{2}}$	
2084.88		5	47949.1	+0.5	$a\ ^4F_{3\frac{1}{2}}$—$61360\frac{3}{4\frac{1}{2}}$	

TABLE 3. *Classified lines of* W II—Continued

Wavelength (Å)	Intensity		Wave number (cm^{-1})		Combination	Zeeman effect
	Arc	Spark	Observed	*O–C*		
Air						
2086. 37	2	3	47914. 9	+0. 6	$a\ ^4F_{3\frac{1}{2}}$—*61326*$^e_{3\frac{1}{2}}$	
2086. 58	5	4	47910. 0	+0. 6	$a\ ^6D_{4\frac{1}{2}}$—*54056*$^e_{4\frac{1}{2}}$	
2087. 34	2	2	47892. 6	+0. 4	$a\ ^4P_{2\frac{1}{2}}$—*61326*$^e_{3\frac{1}{2}}$	
2087. 46	5	4	47889. 9	+0. 5	$a\ ^4G_{5\frac{1}{2}}$—*65326*$^e_{5\frac{1}{2}}$	
2088. 18	60	30	47873. 4	+0. 7	$a\ ^6D_{2\frac{1}{2}}$—*51045*$^e_{3\frac{1}{2}}$	
2089. 13	40	20	47851. 6	+0. 8	$a\ ^6D_{3\frac{1}{2}}$—*52567*$^e_{4\frac{1}{2}}$	
2089. 49		4	47843. 4	+0. 8	$a\ ^4D_{3\frac{1}{2}}$—*62989*$^e_{2\frac{1}{2}}$	
2091. 23	2	4	47803. 5	−0. 1	$a\ ^4G_{4\frac{1}{2}}$—*64356*$^e_{3\frac{1}{2}}$	
2093. 79	20	20	47745. 1	+0. 6	$a\ ^4P_{1\frac{1}{2}}$—*58336*$^e_{2\frac{1}{2}}$	
2094. 72	50	25	47723. 9	+0. 6	$a\ ^6D_{1\frac{1}{2}}$—*49242*$^e_{2\frac{1}{2}}$	
2095. 78		1	47699. 8	+1. 0	$a\ ^4D_{1\frac{1}{2}}$—*62333*$^e_{2\frac{1}{2}}$	
2097. 76	2	3	47654. 6	+0. 2	$a\ ^4G_{4\frac{1}{2}}$—*64207*$^e_{4\frac{1}{2}}$	
2098. 22	60*A*	30	47644. 2	+0. 4	$a\ ^4F_{3\frac{1}{2}}$—*61055*$^e_{4\frac{1}{2}}$	
2098. 58	70	40	47636. 2	+0. 5	$a\ ^6D_{1\frac{1}{2}}$—*49154*$^e_{0\frac{1}{2}}$	
2098. 69	3	—	47633. 7	+0. 9	$19070_{4\frac{1}{2}}$—*66703*$^e_{5\frac{1}{2}}$	
2099. 37	2	1	47618. 3	+0. 5	$a\ ^4G_{3\frac{1}{2}}$—*64207*$^e_{4\frac{1}{2}}$	
2100. 06	—	1	47602. 6	+0. 2	$a\ ^6S_{2\frac{1}{2}}$—*55022*$^e_{3\frac{1}{2}}$	
2100. 66	50	20	47589. 0	+0. 4	$a\ ^6D_{0\frac{1}{2}}$—*47588*$^e_{1\frac{1}{2}}$	
2101. 05	—?	3	47580. 1	+0. 3	$a\ ^4F_{4\frac{1}{2}}$—*62437*$^e_{4\frac{1}{2}}$	
2101. 66		4	47566. 4	+0. 2	$a\ ^4G_{5\frac{1}{2}}$—*65003*$^e_{4\frac{1}{2}}$	
2101. 96	10	2	47559. 6	+0. 6	$a\ ^6D_{3\frac{1}{2}}$—*52275*$^e_{3\frac{1}{2}}$	
2102. 21	3	1	47553. 9	+0. 5	$a\ ^4G_{2\frac{1}{2}}$—*63788*$^e_{3\frac{1}{2}}$	
2103. 16	30	15	47532. 5	+0. 4	$a\ ^4G_{5\frac{1}{2}}$—*64969*$^e_{5\frac{1}{2}}$	
2105. 07		3	47489. 3	+0. 3	$a\ ^4F_{2\frac{1}{2}}$—*60900*$^e_{2\frac{1}{2}}$	
2106. 04	2		47467. 4	+0. 5	$a\ ^4P_{2\frac{1}{2}}$—*60900*$^e_{2\frac{1}{2}}$	
2106. 17	50	30	47464. 5	+0. 4	$a\ ^6D_{1\frac{1}{2}}$—*48982*$^e_{1\frac{1}{2}}$	
2107. 26		3	47440. 0	−0. 7	$a\ ^4G_{3\frac{1}{2}}$—*64030*$^e_{2\frac{1}{2}}$	
2108. 38	—?	25	47414. 8	−0. 3	$a\ ^4P_{1\frac{1}{2}}$—*58007*$^e_{1\frac{1}{2}}$	
2108. 65	—?	15	47408. 6	+0. 1	$a\ ^4F_{2\frac{1}{2}}$—*58709*$^e_{3\frac{1}{2}}$	
2110. 33	50	30	47371. 0	+0. 3	$a\ ^6D_{3\frac{1}{2}}$—*52087*$^e_{2\frac{1}{2}}$	
2113. 92	20	2	47290. 5	+0. 1 +0. 5	$a\ ^4G_{2\frac{1}{2}}$—*63880*$^e_{2\frac{1}{2}}$ $a\ ^4D_{3\frac{1}{2}}$—*62437*$^e_{4\frac{1}{2}}$	
2114. 16		1	47285. 1	+0. 9	$a\ ^6S_{2\frac{1}{2}}$—*54704*$^e_{2\frac{1}{2}}$	
2115. 08	10	2	47264. 5	+0. 3	$a\ ^4P_{1\frac{1}{2}}$—*57856*$^e_{2\frac{1}{2}}$	
2115. 35	20		47258. 6	+0. 2	$a\ ^6D_{2\frac{1}{2}}$—*50430*$^e_{1\frac{1}{2}}$	
2115. 65	2		47251. 8	+0. 2	$a\ ^4P_{0\frac{1}{2}}$—*56084*$^e_{1\frac{1}{2}}$	
2115. 91		2	47246. 1	+1. 5	$a\ ^4F_{3\frac{1}{2}}$—*60656*$^e_{2\frac{1}{2}}$	
2116. 94	25	2	47223. 1	+0. 3	$a\ ^6D_{4\frac{1}{2}}$—*53369*$^e_{4\frac{1}{2}}$	
2118. 03	15	5	47198. 8	+0. 3	$a\ ^4G_{3\frac{1}{2}}$—*63788*$^e_{3\frac{1}{2}}$	
2118. 34		2	47191. 8	+0. 9	$a\ ^6D_{4\frac{1}{2}}$—*53338*$^e_{3\frac{1}{2}}$	
2118. 87	40	20	47180. 1	+0. 2	$a\ ^6D_{0\frac{1}{2}}$—*47179*$^e_{1\frac{1}{2}}$	
2120. 38	1	1	47146. 4	−0. 3	$a\ ^6D_{2\frac{1}{2}}$—*51863*$^e_{3\frac{1}{2}}$	
2121. 60	100	25	47119. 3	−0. 5	$a\ ^6D_{2\frac{1}{2}}$—*50292*$^e_{2\frac{1}{2}}$	
2123. 42	15	20	47079. 0	−0. 4	$a\ ^4G_{5\frac{1}{2}}$—*64516*$^e_{4\frac{1}{2}}$	
2124. 14		1	47063. 0	+0. 3	$a\ ^4F_{3\frac{1}{2}}$—*60474*$^e_{2\frac{1}{2}}$	
2125. 58	4	10	47031. 1	−0. 4	$a\ ^4G_{2\frac{1}{2}}$—*63266*$^e_{3\frac{1}{2}}$	
2126. 86	2	4	47002. 8	+0. 3	$18000_{3\frac{1}{2}}$—*65003*$^e_{3\frac{1}{2}}$	
2127. 44	12	20	46990. 0	+0. 4 0. 0	$18000_{3\frac{1}{2}}$—*64990*$^e_{2\frac{1}{2}}$ $a\ ^4P_{2\frac{1}{2}}$—*60424*$^e_{3\frac{1}{2}}$	
2129. 00	10	2	46955. 6	+0. 2	$a\ ^6S_{2\frac{1}{2}}$—*54375*$^e_{2\frac{1}{2}}$	
2130. 05	20	2	46932. 4	+0. 1	$a\ ^4D_{1\frac{1}{2}}$—*61566*$^e_{2\frac{1}{2}}$	
2131. 73	4	3	46895. 5	0. 0	$18000_{3\frac{1}{2}}$—*64896*$^e_{3\frac{1}{2}}$	

TABLE 3. *Classified lines of* W II—Continued

Wavelength (Å)	Intensity		Wave number (cm^{-1})		Combination	Zeeman effect
	Arc	Spark	Observed	*O–C*		
Air						
2134.044	25	10	46844.61	+0.12	$a\,{}^4F_{2\frac{1}{2}}$—$60256^{\circ}_{3\frac{1}{2}}$	
2135.04	—	20	46822.8	+0.4	$a\,{}^4P_{2\frac{1}{2}}$—$60256^{\circ}_{3\frac{1}{2}}$	
2137.135	20A	10	46776.87	+0.12	$a\,{}^4F_{1\frac{1}{2}}$—$55488^{\circ}_{1\frac{1}{2}}$	
2137.636	25	6	46765.9	+0.2	$a\,{}^6D_{1\frac{1}{2}}$—$48284^{\circ}_{2\frac{1}{2}}$	
2138.133	40	30	46755.0	+0.4	$a\,{}^6D_{4\frac{1}{2}}$—$52901^{\circ}_{3\frac{1}{2}}$	
2139.16	30	12	46732.6	+0.4	$a\,{}^4F_{4\frac{1}{2}}$—$61589^{\circ}_{5\frac{1}{2}}$	
2139.646	12	6	46722.0	+0.3	$a\,{}^6D_{3\frac{1}{2}}$—$51438^{\circ}_{2\frac{1}{2}}$	
2139.86	1		46717.3	+0.5	$a\,{}^6S_{2\frac{1}{2}}$—$54137^{\circ}_{1\frac{1}{2}}$	
2140.03	5	6	46713.6	+0.4	$a\,{}^4G_{4\frac{1}{2}}$—$63266^{\circ}_{3\frac{1}{2}}$	
2140.94		2	46693.7	+0.3	$a\,{}^4F_{4\frac{1}{2}}$—$61550^{\circ}_{3\frac{1}{2}}$	
2142.49	15	4	46660.0	+0.5	$a\,{}^4P_{1\frac{1}{2}}$—$57252^{\circ}_{2\frac{1}{2}}$	
2142.736	3	1	46645.61	+0.26	$a\,{}^4P_{0\frac{1}{2}}$—$55488^{\circ}_{1\frac{1}{2}}$	
2143.257	15A	3	46643.27	+0.35	$a\,{}^4D_{0\frac{1}{2}}$—$59816^{\circ}_{1\frac{1}{2}}$	
2144.08	40	4	46625.4	+0.1	$a\,{}^6D_{0\frac{1}{2}}$—$46625^{\circ}_{0\frac{1}{2}}$	
2145.28	6		46599.3	+0.4	$a\,{}^4D_{2\frac{1}{2}}$—$61566^{\circ}_{2\frac{1}{2}}$	
2146.02	8	3	46583.1	+0.3	$a\,{}^4D_{2\frac{1}{2}}$—$61550^{\circ}_{3\frac{1}{2}}$	
2146.13	25	8	46580.8	+0.6	$a\,{}^4F_{3\frac{1}{2}}$—$59992^{\circ}_{2\frac{1}{2}}$	
2147.17	1		46558.3	+0.2	$a\,{}^4P_{2\frac{1}{2}}$—$59992^{\circ}_{2\frac{1}{2}}$	
2147.31	35A	3	46555.2	−0.4	$a\,{}^4F_{2\frac{1}{2}}$—$57856^{\circ}_{2\frac{1}{2}}$	
2148.84		8	46522.1	+0.4	$a\,{}^4F_{3\frac{1}{2}}$—$59933^{\circ}_{3\frac{1}{2}}$	
2149.136		12	46515.69	+0.02	$18000_{3\frac{1}{2}}$—$64516^{\circ}_{4\frac{1}{2}}$	
2149.69	3	3	46503.7	+0.4	$a\,{}^4F_{4\frac{1}{2}}$—$61360^{\circ}_{4\frac{1}{2}}$	
2151.28	—	3	46469.3	+0.2	$a\,{}^4F_{4\frac{1}{2}}$—$61326^{\circ}_{3\frac{1}{2}}$	
2151.83		4	46457.4	+0.2	$a\,{}^4F_{3\frac{1}{2}}$—$59869^{\circ}_{3\frac{1}{2}}$	
2152.126	20	25	46451.07	+0.03	$a\,{}^4F_{1\frac{1}{2}}$—$55162^{\circ}_{2\frac{1}{2}}$	
2152.85	5	—	46435.5	+0.5	$a\,{}^4P_{2\frac{1}{2}}$—$59869^{\circ}_{3\frac{1}{2}}$	
2153.15	8	1	46429.0	+0.2	$a\,{}^4F_{2\frac{1}{2}}$—$57729^{\circ}_{3\frac{1}{2}}$	
2153.550	40	20	46420.36	+0.37	$a\,{}^6D_{4\frac{1}{2}}$—$52567^{\circ}_{4\frac{1}{2}}$	
2153.870	4	20	46413.46	+0.10	$a\,{}^4G_{4\frac{1}{2}}$—$62966^{\circ}_{3\frac{1}{2}}$	
2154.31	4	3	46404.0	+0.4	$a\,{}^4D_{3\frac{1}{2}}$—$61550^{\circ}_{3\frac{1}{2}}$	
2155.25	3		46383.7	+0.1	$a\,{}^4F_{4\frac{1}{2}}$—$61240^{\circ}_{5\frac{1}{2}}$	
2155.31	4	2	46382.5	+0.3	$a\,{}^4P_{2\frac{1}{2}}$—$59816^{\circ}_{1\frac{1}{2}}$	
2156.00		4	46367.61	+0.13	$19276_{2\frac{1}{2}}$—$65644^{\circ}_{3\frac{1}{2}}$	
2156.42	4	20	46358.6	+0.1	$a\,{}^4D_{2\frac{1}{2}}$—$61326^{\circ}_{3\frac{1}{2}}$	
2157.798	4	20	46328.98	+0.05	$a\,{}^6D_{3\frac{1}{2}}$—$51045^{\circ}_{3\frac{1}{2}}$	
2159.96	4	8	46282.6	+0.1	$a\,{}^4P_{1\frac{1}{2}}$—$56874^{\circ}_{2\frac{1}{2}}$	
2160.69	2	—	46267.0	+0.4	$a\,{}^4D_{1\frac{1}{2}}$—$60900^{\circ}_{2\frac{1}{2}}$	
2161.83	2	3	46242.6	+0.3	$19442_{4\frac{1}{2}}$—$65684^{\circ}_{5\frac{1}{2}}$	
2162.36		5	46231.2	0.0	$20039_{3\frac{1}{2}}$—$66270^{\circ}_{4\frac{1}{2}}$	6
2163.49		3	46207.1	+0.3	$18000_{3\frac{1}{2}}$—$64207^{\circ}_{4\frac{1}{2}}$	
2163.880	6	30	46198.78	+0.20	$a\,{}^4F_{4\frac{1}{2}}$—$61055^{\circ}_{4\frac{1}{2}}$	
2164.800		5	46179.15	−0.12	$a\,{}^4D_{2\frac{1}{2}}$—$61326^{\circ}_{3\frac{1}{2}}$	
2165.264		6	46169.25	+0.10	$20534_{3\frac{1}{2}}$—$66703^{\circ}_{3\frac{1}{2}}$	
2165.56	3		46163.0	+0.2	$a\,{}^4G_{4\frac{1}{2}}$—$62715^{\circ}_{4\frac{1}{2}}$	
2166.316	40	80	46146.84	+0.11	$a\,{}^6D_{2\frac{1}{2}}$—$50863^{\circ}_{3\frac{1}{2}}$	
2167.185	10	20	46128.33	+0.21	$a\,{}^6D_{4\frac{1}{2}}$—$52275^{\circ}_{3\frac{1}{2}}$	
2167.276		1	46126.40	+0.09	$a\,{}^4G_{3\frac{1}{2}}$—$62715^{\circ}_{4\frac{1}{2}}$	
2168.590	4	10	46098.45	+0.09	$a\,{}^4G_{2\frac{1}{2}}$—$62333^{\circ}_{2\frac{1}{2}}$	
2169.936	15	40	46069.86	0.00 +0.28	$a\,{}^6D_{1\frac{1}{2}}$—$47588^{\circ}_{1\frac{1}{2}}$ $a\,{}^6D_{2\frac{1}{2}}$—$49242^{\circ}_{2\frac{1}{2}}$	
2172.206		12	46021.72	−0.43	$a\,{}^4D_{1\frac{1}{2}}$—$60656^{\circ}_{2\frac{1}{2}}$	
2172.926		6	46006.47	−0.15	$19637_{2\frac{1}{2}}$—$65644^{\circ}_{3\frac{1}{2}}$	
2173.26	1	2	45999.40	+0.04	$18990_{1\frac{1}{2}}$—$64990^{\circ}_{2\frac{1}{2}}$	
2173.55	25	50	45993.27	−0.08	$a\,{}^4F_{1\frac{1}{2}}$—$54704^{\circ}_{2\frac{1}{2}}$	
2173.825	5	15	45987.45	+0.07	$a\,{}^4F_{3\frac{1}{2}}$—$59399^{\circ}_{4\frac{1}{2}}$	
2175.494	12	8	45952.17	+0.17 +0.29	$a\,{}^6D_{2\frac{1}{2}}$—$49124^{\circ}_{3\frac{1}{2}}$ $a\,{}^4P_{1\frac{1}{2}}$—$56544^{\circ}_{2\frac{1}{2}}$	
2175.54		3	45951.1	+0.2	$a\,{}^4F_{2\frac{1}{2}}$—$57252^{\circ}_{2\frac{1}{2}}$	
2176.424	2	12	45932.54	+0.02	$19070_{4\frac{1}{2}}$—$65003^{\circ}_{4\frac{1}{2}}$	

TABLE 3. *Classified lines of* W II—Continued

Wavelength (Å)	Intensity		Wave number (cm^{-1})		Combination	Zeeman effect
	Arc	Spark	Observed	$O-C$		
Air						
2176.88	3	15	45922.9	−0.2	$20780_{4\frac{1}{2}}$—$66703^{5}_{5\frac{1}{2}}$	
2177.13	3	4	45917.65	+0.01	$a\ {}^{6}S_{2\frac{1}{2}}$—$53338^{3}_{3\frac{1}{2}}$	
2177.52	4	}	45909.42	+0.14	$a\ {}^{6}S_{2\frac{1}{2}}$—$53329^{2}_{1\frac{1}{2}}$	
2177.546		30	45908.88	+0.10	$a\ {}^{4}D_{3\frac{1}{2}}$—$61055^{4}_{4\frac{1}{2}}$	
2178.04	2		45898.46	+0.04	$19070_{4\frac{1}{2}}$—$64969^{5}_{5\frac{1}{2}}$	
2178.72	10	50	45884.14	+0.24	$a\ {}^{4}G_{4\frac{1}{2}}$—$62437^{5}_{4\frac{1}{2}}$	
2178.92	10	30	45879.9	+0.5	$18000_{3\frac{1}{2}}$—$63880^{3}_{3\frac{1}{2}}$	
2179.634		8	45864.9	{ +0.1	$a\ {}^{4}F_{3\frac{1}{2}}$—$59276^{3}_{3\frac{1}{2}}$	
				{ −0.1	$19276_{2\frac{1}{2}}$—$65141^{3}_{2\frac{1}{2}}$	
2180.46	20	40	45847.53	+0.16	$a\ {}^{4}G_{3\frac{1}{2}}$—$62437^{4}_{4\frac{1}{2}}$	
2180.68		8	45842.9	+0.2	$a\ {}^{4}P_{2\frac{1}{2}}$—$59276^{3}_{3\frac{1}{2}}$	
2181.49	15.1	3	45825.9	+0.4	$19070_{4\frac{1}{2}}$—$64896^{3}_{3\frac{1}{2}}$	
2182.225		40	45810.45	+0.11	$a\ {}^{6}D_{2\frac{1}{2}}$—$48982^{2}_{1\frac{1}{2}}$	
2183.32		40	45787.48	−0.02	$18000_{3\frac{1}{2}}$—$63788^{3}_{3\frac{1}{2}}$	
2183.94	2		45774.48	+0.14	$a\ {}^{4}F_{1\frac{1}{2}}$—$54485^{0}_{0\frac{1}{2}}$	
2185.42	—	50	45743.49	−0.04	$a\ {}^{4}G_{3\frac{1}{2}}$—$62333^{3}_{2\frac{1}{2}}$	
2185.75	5	40	45736.58	−0.02	$20534_{5\frac{1}{2}}$—$66270^{4}_{4\frac{1}{2}}$	
2186.738	30	40	45715.92	+0.05	$a\ {}^{6}D_{4\frac{1}{2}}$—$51863^{3}_{3\frac{1}{2}}$	
2186.835	4	10	45713.89	+0.09	$19276_{2\frac{1}{2}}$—$64990^{3}_{2\frac{1}{2}}$	
2187.82	3	1	45693.3	+0.2	$a\ {}^{6}S_{2\frac{1}{2}}$—$53113^{2}_{2\frac{1}{2}}$	
2188.06		2	45688.3	−0.4	$a\ {}^{4}D_{2\frac{1}{2}}$—$60656^{2}_{2\frac{1}{2}}$	
2189.19	30.1	30	45664.7	+0.1	$a\ {}^{4}F_{1\frac{1}{2}}$—$54375^{2}_{2\frac{1}{2}}$	
2189.364	40	40	45661.09	−0.07	$a\ {}^{6}D_{1\frac{1}{2}}$—$47179^{1}_{1\frac{1}{2}}$	
2189.494	50	50	45658.38	+0.20	$a\ {}^{6}D_{2\frac{1}{2}}$—$48830^{2}_{2\frac{1}{2}}$	
2189.740	6	10	45653.25	+0.31	$a\ {}^{4}P_{0\frac{1}{2}}$—$54485^{1}_{0\frac{1}{2}}$	
2189.850	40	80	45650.96	+0.08	$a\ {}^{4}G_{5\frac{1}{2}}$—$63087^{6}_{6\frac{1}{2}}$	
2190.80		6	45631.2	0.0	$a\ {}^{4}F_{2\frac{1}{2}}$—$56932^{2}_{1\frac{1}{2}}$	
2191.34	4	12	45619.9	+0.2	$19276_{2\frac{1}{2}}$—$64896^{3}_{3\frac{1}{2}}$	
2192.094	4	6	45604.23	−0.03	$20039_{3\frac{1}{2}}$—$65444^{3}_{3\frac{1}{2}}$	
2193.440	30	40	45576.25	+0.24	$a\ {}^{6}D_{3\frac{1}{2}}$—$50292^{2}_{2\frac{1}{2}}$	
2193.542	25	40	45574.13	+0.22	$a\ {}^{4}F_{2\frac{1}{2}}$—$56874^{2}_{2\frac{1}{2}}$	
2193.88		1	45567.1	+0.2	$a\ {}^{4}F_{4\frac{1}{2}}$—$60424^{3}_{3\frac{1}{2}}$	
2194.515	70	50	45593.92	+0.22	$a\ {}^{6}D_{0\frac{1}{2}}$—$45553^{1}_{1\frac{1}{2}}$	
2195.680		2	45529.76	+0.28	$a\ {}^{4}G_{5\frac{1}{2}}$—$62966^{5}_{5\frac{1}{2}}$	
2195.816		25	45526.94	+0.38	$19442_{6\frac{1}{2}}$—$64969^{5}_{5\frac{1}{2}}$	
2196.654		1	45509.57	+0.08	$a\ {}^{4}D_{3\frac{1}{2}}$—$60656^{2}_{2\frac{1}{2}}$	
2196.780	12	10	45506.96	+0.11	$a\ {}^{4}D_{2\frac{1}{2}}$—$60474^{2}_{2\frac{1}{2}}$	
2196.914		3	45504.18	0.00	$19637_{2\frac{1}{2}}$—$65141^{2}_{2\frac{1}{2}}$	
2197.504	8	10	45491.97	+0.19	$a\ {}^{4}P_{1\frac{1}{2}}$—$56084^{1}_{1\frac{1}{2}}$	
2197.585	1		45490.3	−0.3	$20780_{4\frac{1}{2}}$—$66270^{4}_{4\frac{1}{2}}$	
2198.008		6	45481.54	+0.23	$a\ {}^{6}S_{2\frac{1}{2}}$—$52901^{3}_{3\frac{1}{2}}$	
2198.676	40	60	45467.72	+0.19	$a\ {}^{4}F_{2\frac{1}{2}}$—$56768^{3}_{3\frac{1}{2}}$	
2199.166	40	20	45457.59	+0.57	$a\ {}^{6}D_{0\frac{1}{2}}$—$45457^{0}_{0\frac{1}{2}}$	
2199.742	2	8	45445.69	0.00	$19070_{4\frac{1}{2}}$—$64516^{4}_{4\frac{1}{2}}$	
2200.696	2		45426.0	+0.1	$a\ {}^{4}F_{1\frac{1}{2}}$—$54137^{1}_{1\frac{1}{2}}$	
2200.907		12	45421.64	+0.15	$a\ {}^{4}F_{4\frac{1}{2}}$—$60278^{4}_{4\frac{1}{2}}$	
2201.984		12	45399.42	+0.19	$a\ {}^{4}F_{4\frac{1}{2}}$—$60256^{3}_{3\frac{1}{2}}$	
2203.798	10	25	45362.06	+0.44	$a\ {}^{4}F_{4\frac{1}{2}}$—$60218^{3}_{3\frac{1}{2}}$	
2203.986	20	70	45358.19	+0.35	$a\ {}^{4}D_{1\frac{1}{2}}$—$59992^{2}_{2\frac{1}{2}}$	
2204.482	100	150	45347.98	+0.14	$a\ {}^{6}D_{4\frac{1}{2}}$—$z\ {}^{6}F^{5}_{3\frac{1}{2}}$	
2205.460	6	8	45327.88	+0.23	$a\ {}^{4}D_{3\frac{1}{2}}$—$60474^{2}_{2\frac{1}{2}}$	
2205.886	1	3	45319.12	+0.08	$18990_{1\frac{1}{2}}$—$64310^{2}_{2\frac{1}{2}}$	
2206.060	15	15	45315.55	−0.21	$a\ {}^{4}G_{2\frac{1}{2}}$—$61550^{3}_{3\frac{1}{2}}$	
2206.134	8	12	45314.03	+0.19	$a\ {}^{4}P_{2\frac{1}{2}}$—$58747^{3}_{1\frac{1}{2}}$	
2206.237	2	—	45311.91	+0.25	$a\ {}^{4}F_{2\frac{1}{2}}$—$56612^{2}_{3\frac{1}{2}}$	
2206.588	40	80	45304.71	+0.17	$a\ {}^{4}P_{0\frac{1}{2}}$—$54137^{1}_{1\frac{1}{2}}$	
2206.922	20	30	45297.85	+0.25	$a\ {}^{4}F_{3\frac{1}{2}}$—$58709^{3}_{3\frac{1}{2}}$	

TABLE 3. *Classified lines of* W II—Continued

Wavelength (Å)	Intensity		Wave number (cm^{-1})		Combination	Zeeman effect
	Arc	Spark	Observed	*O–C*		
Air						
2207. 435	—	5	45287. 33	+1. 31	$19070_{4\frac{1}{2}}$—*64356*$^{5}_{3\frac{1}{2}}$	
2207. 914	15	20	45277. 50	−0. 04	*a* $^{4}G_{5\frac{1}{2}}$—*62714*$^{6}_{5\frac{1}{2}}$	
2207. 986	30	40	45276. 02	+0. 10	*a* $^{4}F_{3\frac{1}{2}}$—*58687*$^{4}_{4\frac{1}{2}}$	
2208. 813		40	45259. 07	+0. 23	$19637_{2\frac{1}{2}}$—*64896*$^{3}_{3\frac{1}{2}}$	
2209. 564	12	6	45243. 69	+0. 37	*a* $^{4}F_{2\frac{1}{2}}$—*56544*$^{2}_{2\frac{1}{2}}$	
2216. 023	60	40	45111. 84	−0. 12	*a* $^{6}D_{2\frac{1}{2}}$—*48284*$^{5}_{2\frac{1}{2}}$	res
2216. 296	8	5	45106. 28	−0. 21	*a* $^{6}D_{3\frac{1}{2}}$—*46625*$^{6}_{3\frac{1}{2}}$	
2217. 582	4	3	45080. 13	−0. 05	$19276_{2\frac{1}{2}}$—*64356*$^{3}_{3\frac{1}{2}}$	
2217. 765	12	15	45076. 41	−0. 03	*a* $^{4}F_{4\frac{1}{2}}$—*59933*$^{3}_{3\frac{1}{2}}$	
2219. 588	6	12	45039. 39	+0. 01	$18990_{1\frac{1}{2}}$—*64030*$^{3}_{2\frac{1}{2}}$	
2219. 740	10	15	45036. 31	−0. 01	*a* $^{4}G_{4\frac{1}{2}}$—*61589*$^{5}_{5\frac{1}{2}}$	
2219. 882	2	2	45033. 42	−0. 06	$19276_{2\frac{1}{2}}$—*64310*$^{3}_{3\frac{1}{2}}$	
2220. 938	30	60	45012. 01	+0. 09	*a* $^{4}F_{4\frac{1}{2}}$—*59869*$^{3}_{3\frac{1}{2}}$	
2221. 525	10	15	45000. 12	+0. 10	*a* $^{4}G_{5\frac{1}{2}}$—*62437*$^{4}_{4\frac{1}{2}}$	
2221. 652	5	5	44997. 55	+0. 09	*a* $^{4}G_{4\frac{1}{2}}$—*61550*$^{3}_{3\frac{1}{2}}$	
2222. 070	10	30	44989. 08	+0. 18	$18000_{3\frac{1}{2}}$—*62989*$^{5}_{2\frac{1}{2}}$	
2223. 206	2	2	44966. 10	+0. 26	*a* $^{4}D_{2\frac{1}{2}}$—*59933*$^{3}_{3\frac{1}{2}}$	
2223. 326	4	6	44963. 67	+0. 21	$20039_{3\frac{1}{2}}$—*65003*$^{4}_{4\frac{1}{2}}$	
2223. 450	12	12	44961. 17	+0. 24	*a* $^{4}G_{3\frac{1}{2}}$—*61550*$^{3}_{3\frac{1}{2}}$	
2225. 230	15.4	5	44925. 20	+0. 18	*a* $^{4}F_{3\frac{1}{2}}$—*58336*$^{3}_{2\frac{1}{2}}$	
2225. 882	60	80	44912. 05	+0. 42	*a* $^{6}D_{0\frac{1}{2}}$—*44911*$^{1}_{1\frac{1}{2}}$	res
2226. 320	12	15	44903. 21	+0. 33	*a* $^{4}P_{2\frac{1}{2}}$—*58336*$^{3}_{2\frac{1}{2}}$	
2226. 40	8	15	44901. 6	+0. 3	*a* $^{4}D_{2\frac{1}{2}}$—*59869*$^{3}_{3\frac{1}{2}}$	
2226. 56	50	60	44898. 4	+0. 3	*a* $^{6}D_{4\frac{1}{2}}$—*51045*$^{5}_{3\frac{1}{2}}$	
2226. 68	20	25	44895. 95	+0. 46	*a* $^{4}P_{1\frac{1}{2}}$—*55488*$^{1}_{1\frac{1}{2}}$	
2226. 77	20	70	44894. 14			
2228. 29	1	3	44863. 5	−0. 1	$20780_{4\frac{1}{2}}$—*65644*$^{3}_{3\frac{1}{2}}$	
2228. 70	5	2	44855. 26	+0. 41	*a* $^{6}S_{2\frac{1}{2}}$—*52275*$^{3}_{3\frac{1}{2}}$	
2228. 88	12	80	44851. 64			
2229. 026	10	6	44848. 70	+0. 22	*a* $^{4}D_{2\frac{1}{2}}$—*59816*$^{2}_{1\frac{1}{2}}$	
2229. 620	75	100	44836. 76	+0. 14	*a* $^{6}D_{1\frac{1}{2}}$—*46355*$^{2}_{2\frac{1}{2}}$	
2229. 730	8	25	44834. 54	+0. 32	*a* $^{4}D_{0\frac{1}{2}}$—*58007*$^{1}_{1\frac{1}{2}}$	
2231. 080	12	30	44807. 42	+0. 02	*a* $^{4}G_{4\frac{1}{2}}$—*61360*$^{4}_{4\frac{1}{2}}$	
2231. 84	15	5	44792. 16	+0. 11	$20534_{3\frac{1}{2}}$—*65326*$^{3}_{3\frac{1}{2}}$	
2232. 11	3	3	44786. 74	+0. 10	*a* $^{4}D_{3\frac{1}{2}}$—*59933*$^{3}_{3\frac{1}{2}}$	
2232. 284	6	4	44783. 25	+0. 03	*a* $^{4}F_{2\frac{1}{2}}$—*56084*$^{1}_{1\frac{1}{2}}$	
2232. 56	4	8	44777. 72	+0. 09	$23234_{4\frac{1}{2}}$—*68012*$^{5}_{5\frac{1}{2}}$	
2232. 80	3	2	44772. 90	−0. 25	*a* $^{4}G_{4\frac{1}{2}}$—*61326*$^{3}_{3\frac{1}{2}}$	
2234. 63	5?	12	44736. 24	−0. 38	*a* $^{4}G_{3\frac{1}{2}}$—*61326*$^{3}_{3\frac{1}{2}}$	
2235. 00	4	2	44728. 84	−0. 07	*a* $^{4}F_{1\frac{1}{2}}$—*53440*$^{0}_{1\frac{1}{2}}$	
2235. 48	2		44719. 24	−0. 08	$19637_{2\frac{1}{2}}$—*64356*$^{3}_{3\frac{1}{2}}$	
2235. 64	20	30	44716. 03	+0. 14	*a* $^{6}D_{4\frac{1}{2}}$—*50863*$^{4}_{3\frac{1}{2}}$	
2235. 856	8	8	44711. 71	−0. 01	*a* $^{4}F_{1\frac{1}{2}}$—*53422*$^{1}_{1\frac{1}{2}}$	
2237. 06	15	100	44687. 65	−0. 02	*a* $^{4}G_{4\frac{1}{2}}$—*61240*$^{5}_{5\frac{1}{2}}$	
2237. 84	10	4	44672. 08	−0. 54	$19637_{2\frac{1}{2}}$—*64310*$^{3}_{3\frac{1}{2}}$	
2238. 10	2	1	44666. 8	+0. 2	*a* $^{6}S_{2\frac{1}{2}}$—*52087*$^{2}_{2\frac{1}{2}}$	
2240. 53	2?		44618. 4	0. 0	*a* $^{4}F_{1\frac{1}{2}}$—*53329*$^{1}_{1\frac{1}{2}}$	
2241. 080	30	50	44607. 5	0. 0	*a* $^{4}P_{0\frac{1}{2}}$—*53440*$^{1}_{1\frac{1}{2}}$	
2241. 282	50 1	10	44603. 48	−0. 10	$19276_{2\frac{1}{2}}$—*63880*$^{2}_{2\frac{1}{2}}$	6
2242. 71	7	7	44575. 08	+0. 12	*a* $^{4}F_{3\frac{1}{2}}$—*57986*$^{4}_{4\frac{1}{2}}$	
2242. 965	10	12	44570. 02	+0. 24	*a* $^{4}P_{1\frac{1}{2}}$—*55162*$^{2}_{2\frac{1}{2}}$	
2244. 15	10	25	44546. 48	+0. 46	$20780_{4\frac{1}{2}}$—*65326*$^{3}_{3\frac{1}{2}}$	
2244. 75	2	3	44534. 6	+0. 2	$20455_{1\frac{1}{2}}$—*64990*$^{3}_{3\frac{1}{2}}$	
2245. 19	25	40	44525. 8	0. 0	*a* $^{6}D_{3\frac{1}{2}}$—*49242*$^{2}_{2\frac{1}{2}}$	
2245. 90	5	3	44511. 8	+0. 1	$19276_{2\frac{1}{2}}$—*63788*$^{3}_{3\frac{1}{2}}$	

TABLE 3. *Classified lines of* W II—Continued

Wavelength (Å)	Intensity		Wave number (cm^{-1})		Combination	Zeeman effect
	Arc	Spark	Observed	$O-C$		
Air						
2246.35	8	10	44502.86	+0.20	$a\ ^4G_{4\frac{1}{2}}$—$61055^3_{4\frac{1}{2}}$	
2246.64	15	20	44497.12	+0.07	$a\ ^4P_{0\frac{1}{2}}$—$53329^1_{1\frac{1}{2}}$	
2247.67	6	40	44476.73	+0.10	$20039_{3\frac{1}{2}}$—$64516^3_{4\frac{1}{2}}$	
2248.27	25	40	44464.86	+0.14	$a\ ^6D_{3\frac{1}{2}}$—$49181^3_{4\frac{1}{2}}$	*d*
2248.75	60*A*	100	44455.37	+0.19	$a\ ^6D_{0\frac{1}{2}}$—$44455^1_{0\frac{1}{2}}$	
2249.28	6	5	44444.9	+0.2	$a\ ^4F_{3\frac{1}{2}}$—$57856^3_{2\frac{1}{2}}$	
2249.38	15	12	44442.9	+0.3	$a\ ^6S_{2\frac{1}{2}}$—$51863^3_{3\frac{1}{2}}$	
2249.702	5	5	44436.56	+0.22	$18000_{3\frac{1}{2}}$—$62437^3_{4\frac{1}{2}}$	
2249.804	20*A*	?	44434.54	−0.21	$20534_{3\frac{1}{2}}$—$64969^5_{3\frac{1}{2}}$	
2250.45	1	8	44421.79	+0.12	$a\ ^4G_{2\frac{1}{2}}$—$60656^3_{2\frac{1}{2}}$	
2250.560	3	3	44419.62	+0.03	$a\ ^4F_{4\frac{1}{2}}$—$59276^3_{3\frac{1}{2}}$	
2250.730	30	50	44416.26	+0.14	$a\ ^6D_{2\frac{1}{2}}$—$47588^1_{1\frac{1}{2}}$	res
2251.14	30	40	44408.17	−0.03	$a\ ^6D_{3\frac{1}{2}}$—$49124^3_{3\frac{1}{2}}$	6
2251.434	18	25	44402.38	+0.12	$a\ ^4F_{1\frac{1}{2}}$—$53113^3_{2\frac{1}{2}}$	
2251.924	5	25	44392.71	−0.25	$19637_{2\frac{1}{2}}$—$64030^3_{2\frac{1}{2}}$	
2254.98	10	20	44332.56	+0.06	$18000_{3\frac{1}{2}}$—$62333^3_{2\frac{1}{2}}$	
2255.715	10*A*	10	44318.12	+0.16	$a\ ^4F_{3\frac{1}{2}}$—$57729^3_{3\frac{1}{2}}$	
2255.770	1	1	44317.04	+0.08	$20039_{3\frac{1}{2}}$—$64356^3_{3\frac{1}{2}}$	
2256.18	2	6	44308.98	−0.01	$a\ ^4D_{2\frac{1}{2}}$—$59276^3_{3\frac{1}{2}}$	
2256.85	12	30	44295.8	0.0	$a\ ^4P_{2\frac{1}{2}}$—$57729^3_{3\frac{1}{2}}$	
2258.12	40	30	44270.9	+0.6	$20039_{3\frac{1}{2}}$—$64310^5_{3\frac{1}{2}}$	
2259.07	10	25	44252.3	0.0	$a\ ^4D_{3\frac{1}{2}}$—$59399^3_{4\frac{1}{2}}$	
2259.56	10?	15	44242.7	0.0	$19637_{2\frac{1}{2}}$—$63880^3_{2\frac{1}{2}}$	
2259.66	3	3	44240.8	0.0	$a\ ^6D_{2\frac{1}{2}}$—$47413^3_{2\frac{1}{2}}$	
2259.72	6	20	44239.6	−0.2	$a\ ^4G_{2\frac{1}{2}}$—$60474^3_{2\frac{1}{2}}$	
2260.58	4	6	44222.8	0.0	$20780_{4\frac{1}{2}}$—$65003^3_{4\frac{1}{2}}$	
2261.946	1	25	44196.04	+0.42	$19070_{4\frac{1}{2}}$—$63266^3_{3\frac{1}{2}}$	
2262.30	6	20	44189.13	−0.17	$a\ ^4G_{2\frac{1}{2}}$—$60424^3_{3\frac{1}{2}}$	
2262.406	4	4	44187.06	+0.13	$a\ ^4F_{2\frac{1}{2}}$—$55488^1_{1\frac{1}{2}}$	
2263.40	1	2?	44167.66	+0.12 −0.10	$a\ ^4P_{1\frac{1}{2}}$—$54760^1_{0\frac{1}{2}}$ $20039_{3\frac{1}{2}}$—$64207^3_{4\frac{1}{2}}$	
2263.53	15	80	44165.12	−0.04	$a\ ^4G_{5\frac{1}{2}}$—$61602^5_{4\frac{1}{2}}$	
2264.178	8	35	44152.48	+0.04	$a\ ^4G_{5\frac{1}{2}}$—$61589^5_{5\frac{1}{2}}$	
2265.338	7	35	44129.87	+0.08	$a\ ^4D_{3\frac{1}{2}}$—$59276^3_{3\frac{1}{2}}$	
2265.67	35	20	44123.4	−0.1	$23955_{5\frac{1}{2}}$—$68078^5_{4\frac{1}{2}}$	
2266.05	3	8?	44116.0	+0.2	$20780_{4\frac{1}{2}}$—$64896^3_{3\frac{1}{2}}$	
2266.12	15	80	44114.6	+0.2	$a\ ^6D_{3\frac{1}{2}}$—$48830_{2\frac{1}{2}}$	
2266.25	15	80	44112.1	0.0	$a\ ^4P_{1\frac{1}{2}}$—$54704^3_{2\frac{1}{2}}$	
2267.30	4	4	44091.69	+0.05	$a\ ^4F_{1\frac{1}{2}}$—$52803^3_{1\frac{1}{2}}$	
2268.064	2	2	44076.84	−0.03	$22194_{3\frac{1}{2}}$—$66270^3_{4\frac{1}{2}}$	
2269.08	2	4	44057.1	0.0	$23955_{5\frac{1}{2}}$—$68012^5_{5\frac{1}{2}}$	
2270.232	25	125	44034.75	−0.17 +0.23	$a\ ^6D_{1\frac{1}{2}}$—$45553^3_{1\frac{1}{2}}$ $a\ ^4F_{4\frac{1}{2}}$—$58891^5_{4\frac{1}{2}}$	
2270.905	6	6	44021.70	+0.1	$a\ ^4G_{2\frac{1}{2}}$—$60256^3_{3\frac{1}{2}}$	
2271.105	10	12	44017.82	+0.22	$a\ ^6S_{2\frac{1}{2}}$—$51438^3_{2\frac{1}{2}}$	
2271.64	2	—	44007.4	0.0	$a\ ^6D_{2\frac{1}{2}}$—$47179^1_{1\frac{1}{2}}$	
2272.09	—	3	43998.74	+0.10	$18990_{1\frac{1}{2}}$—$62989^3_{2\frac{1}{2}}$	
2272.510	8	25	43990.61	+0.01	$20039_{3\frac{1}{2}}$—$64030^3_{2\frac{1}{2}}$	
2272.96	5?	15	43981.9	−0.1	$20534_{3\frac{1}{2}}$—$64516^3_{4\frac{1}{2}}$	
2273.55	6	10	43970.49	+0.15	$a\ ^4P_{0\frac{1}{2}}$—$52803^3_{1\frac{1}{2}}$	
2275.22	5	?	43938.2	0.0	$a\ ^6D_{1\frac{1}{2}}$—$45457^1_{0\frac{1}{2}}$	
2275.98	3	2	43923.5	0.0	$a\ ^4G_{5\frac{1}{2}}$—$61360^3_{4\frac{1}{2}}$	
2277.416	3	4	43895.86	+0.04	$19070_{4\frac{1}{2}}$—$62966^5_{3\frac{1}{2}}$	
2277.583	60*A*	20	43892.64	−0.44	$a\ ^4P_{1\frac{1}{2}}$—$54485^1_{0\frac{1}{2}}$	
2277.977	10	35	43885.05	+0.05	$a\ ^4G_{3\frac{1}{2}}$—$60474^3_{2\frac{1}{2}}$	
2278.108	25	30	43882.52	+0.06	$a\ ^4F_{1\frac{1}{2}}$—$52593^3_{0\frac{1}{2}}$	
2278.704	10	12	43871.05	+0.05	$a\ ^4G_{4\frac{1}{2}}$—$60424^3_{3\frac{1}{2}}$	

TABLE 3. *Classified lines of* W II—Continued

Wavelength (Å)	Intensity		Wave number (cm^{-1})		Combination	Zeeman effect
	Arc	Spark	Observed	*O–C*		
Air						
2279.213	10	3	43861.25	+0.03	$a\,{}^4F_{2\frac{1}{2}}$—$55162\frac{2}{2\frac{1}{2}}$	
2279.672	1−	−?	43852.42	+0.08	$a\,{}^4F_{4\frac{1}{2}}$—$58709\frac{3}{3\frac{1}{2}}$	
2280.300	8	30	43840.34	−0.02	$20039_{3\frac{1}{2}}$—$63880\frac{2}{2\frac{1}{2}}$	
2280.621	30	12	43834.18	+0.21	$a\,{}^6S_{2\frac{1}{2}}$—$51254\frac{1}{1\frac{1}{2}}$	
2280.802	10?	10	43830.7	0.0	$a\,{}^4F_{4\frac{1}{2}}$—$58687\frac{4}{4\frac{1}{2}}$	
2282.202	25	75	43803.81	+0.02	$a\,{}^4G_{5\frac{1}{2}}$—$61240\frac{5}{5\frac{1}{2}}$	6
2283.266	25*A*	5	43783.40	+0.10	$a\,{}^4P_{1\frac{1}{2}}$—$54375\frac{2}{2\frac{1}{2}}$	
2283.437	4	3	43780.12	0.00	$a\,{}^4D_{2\frac{1}{2}}$—$58747\frac{1}{1\frac{1}{2}}$	
2284.436	20	18	43760.98	−0.08	$a\,{}^4P_{0\frac{1}{2}}$—$52593\frac{0}{1\frac{1}{2}}$	6
2284.619	10	40	43757.47	+0.11	$a\,{}^4G_{2\frac{1}{2}}$—$59992\frac{1}{2\frac{1}{2}}$	6
2285.09	—?	1	43748.45	−0.01	$20039_{3\frac{1}{2}}$—$63788\frac{3}{3\frac{1}{2}}$	
2285.75	1	3	43735.82	−0.17	$20780_{4\frac{1}{2}}$—$64516\frac{4}{4\frac{1}{2}}$	
2286.28	5?	8	43725.69	+0.12	$a\,{}^4G_{4\frac{1}{2}}$—$60278\frac{3}{4\frac{1}{2}}$	
2286.476	6	4	43721.94	+0.16	$a\,{}^4F_{2\frac{1}{2}}$—$55022\frac{3}{3\frac{1}{2}}$	
2286.94	1−	1	43713.07	−0.01	$19276_{2\frac{1}{2}}$—$62989\frac{2}{2\frac{1}{2}}$	
2287.46	8	5	43703.13	−0.18	$a\,{}^4G_{4\frac{1}{2}}$—$60256\frac{3}{4\frac{1}{2}}$	
2289.01	12*A*	8	43673.5	+0.3	$20534_{5\frac{1}{2}}$—$64207\frac{4}{5\frac{1}{2}}$	
2289.41	5	7	43665.9	+0.2	$a\,{}^4G_{4\frac{1}{2}}$—$60218\frac{5}{5\frac{1}{2}}$	
2290.48	2	2	43645.5	+0.1	$19442_{6\frac{1}{2}}$—$63087\frac{6}{6\frac{1}{2}}$	
2290.564	15	20	43643.92	+0.07	$a\,{}^4F_{1\frac{1}{2}}$—$52355\frac{0}{1\frac{1}{2}}$	
2291.376	4	7	43628.45	−0.47	$19637_{2\frac{1}{2}}$—$63266\frac{3}{3\frac{1}{2}}$	
2291.56	7	8	43625.0	+0.2	$a\,{}^6S_{2\frac{1}{2}}$—$51045\frac{2}{2\frac{1}{2}}$	
2294.20	—	3	43574.7	+0.3	$20455_{1\frac{1}{2}}$—$64030\frac{2}{2\frac{1}{2}}$	
2294.55	10?	35	43568.1	−0.1	$a\,{}^6D_{3\frac{1}{2}}$—$48384\frac{2}{3\frac{1}{2}}$	res
2294.84	10	20	43562.6	+0.1	$a\,{}^4D_{3\frac{1}{2}}$—$58709\frac{3}{3\frac{1}{2}}$	
2295.52	3	3	43549.7	−0.2	$18000_{3\frac{1}{2}}$—$61550\frac{3}{3\frac{1}{2}}$	
2295.78	15	20	43544.8	+0.1	$a\,{}^4P_{1\frac{1}{2}}$—$54137\frac{1}{1\frac{1}{2}}$	6
2295.985	15	25	43540.88	+0.02	$a\,{}^4D_{3\frac{1}{2}}$—$58687\frac{4}{4\frac{1}{2}}$	
2296.873	4	5	43524.05	+0.09	$19442_{6\frac{1}{2}}$—$62966\frac{5}{5\frac{1}{2}}$	
2296.956	8	6	43522.47	+0.02	$a\,{}^4P_{0\frac{1}{2}}$—$52355\frac{0}{1\frac{1}{2}}$	
2297.930	1	10	43504.03	0.00	$22140_{2\frac{1}{2}}$—$65644\frac{3}{4}$	
2298.23	8	20	43498.4	+0.2	$a\,{}^4P_{2\frac{1}{2}}$—$56932\frac{1}{1\frac{1}{2}}$	
2299.807	6	18	43468.53	−0.10	$23234_{4\frac{1}{2}}$—$66703\frac{5}{5\frac{1}{2}}$	
2300.078	1	5	43463.40	+0.37	$a\,{}^4F_{3\frac{1}{2}}$—$56874\frac{3}{3\frac{1}{2}}$	
2301.284	3	5	43440.63	−0.26	$a\,{}^4P_{2\frac{1}{2}}$—$56874\frac{3}{2\frac{1}{2}}$	
2301.642	20	30	43433.87	+0.15	$a\,{}^4P_{1\frac{1}{2}}$—$54026\frac{2}{1\frac{1}{2}}$	res
2302.139	—	1	43424.49	+0.32	$20455_{1\frac{1}{2}}$—$63880\frac{2}{2\frac{1}{2}}$	
2303.274	25	50	43403.10	+0.57	$a\,{}^4G_{3\frac{1}{2}}$—$59992\frac{3}{3\frac{1}{2}}$	
2303.819	25	75	43392.83	−0.02	$a\,{}^6D_{1\frac{1}{2}}$—$44911\frac{1}{1\frac{1}{2}}$	res
2304.474	—	2	43380.50	−0.02	$a\,{}^4G_{4\frac{1}{2}}$—$59933\frac{3}{4\frac{1}{2}}$	
2305.219	4	8	43366.48	+0.12	$19070_{4\frac{1}{2}}$—$62437\frac{4}{4\frac{1}{2}}$	
2305.553	—	1	43360.20	+0.36	$18000_{3\frac{1}{2}}$—$61360\frac{4}{3\frac{1}{2}}$	
2305.705	—	1	43357.34	+0.69	$a\,{}^4F_{3\frac{1}{2}}$—$56768\frac{3}{3\frac{1}{2}}$	
2305.972	1	1	43352.32	+0.10	$19637_{2\frac{1}{2}}$—$62989\frac{2}{2\frac{1}{2}}$	
2306.419	2	3	43343.92	−0.07	$a\,{}^4G_{3\frac{1}{2}}$—$59933\frac{3}{3\frac{1}{2}}$	
2306.511	—?	4	43342.19	−0.05	$18990_{1\frac{1}{2}}$—$62333\frac{2}{2\frac{1}{2}}$	
2306.918	15	40	43334.55	+0.04	$a\,{}^4P_{2\frac{1}{2}}$—$56768\frac{3}{2\frac{1}{2}}$	res
2307.392	2	3	43325.64	+0.05	$18000_{3\frac{1}{2}}$—$61326\frac{3}{3\frac{1}{2}}$	
2307.930	5	10	43315.54	−0.46	$a\,{}^4G_{4\frac{1}{2}}$—$59869\frac{3}{3\frac{1}{2}}$	
2309.850	8	25	43279.54	+0.07	$a\,{}^4G_{3\frac{1}{2}}$—$59869\frac{3}{3\frac{1}{2}}$	
2310.244	4	12	43272.16	+0.14	$19442_{6\frac{1}{2}}$—$62714\frac{6}{6\frac{1}{2}}$	
2312.800	—	4	43224.35	+0.20	$23046_{3\frac{1}{2}}$—$66270\frac{4}{3\frac{1}{2}}$	
2312.907	6	20	43222.35	+0.01	$a\,{}^4D_{1\frac{1}{2}}$—$57856\frac{2}{1\frac{1}{2}}$	
2314.084	—	6	43200.36	−0.42	$a\,{}^4F_{3\frac{1}{2}}$—$56612\frac{3}{3\frac{1}{2}}$	
2314.637	10	25	43190.04	+0.08	$a\,{}^4D_{3\frac{1}{2}}$—$58336\frac{2}{3\frac{1}{2}}$	
2315.022	20	50	43182.87	−0.01	$a\,{}^6D_{2\frac{1}{2}}$—$46355\frac{2}{2\frac{1}{2}}$	

TABLE 3. *Classified lines of* W II—Continued

Wavelength (Å)	Intensity		Wave number (cm^{-1})		Combination	Zeeman effect
	Arc	Spark	Observed	*O–C*		
Air						
2315.246	3	4	43178.69	+0.05	$a\ ^4P_{2\frac{1}{2}}$—$56612^3_{3\frac{1}{2}}$	
2317.722	4	6	43132.57	+0.13	$a\ ^4F_{3\frac{1}{2}}$—$56544^3_{2\frac{1}{2}}$	
2317.88	6	10	43129.62	−0.08	$a\ ^4F_{4\frac{1}{2}}$—$57986^5_{3\frac{1}{2}}$	
2318.916	3	6	43110.36	+0.06	$a\ ^4P_{2\frac{1}{2}}$—$56544^3_{2\frac{1}{2}}$	
2320.832	6	5	43074.76	+0.02	$a\ ^4F_{2\frac{1}{2}}$—$54375^3_{2\frac{1}{2}}$	
2321.807	—	1	43056.68	0.00	$19276_{2\frac{1}{2}}$—$62333^3_{2\frac{1}{2}}$	
2322.594	2	3	43042.10	+0.13	$a\ ^4G_{2\frac{1}{2}}$—$59276^3_{3\frac{1}{2}}$	
2322.720	5	8	43039.76	−0.02	$a\ ^4D_{2\frac{1}{2}}$—$58007^1_{1\frac{1}{2}}$	
2323.038	15	25	43033.87	−0.01	$a\ ^6D_{4\frac{1}{2}}$—$49181^1_{4\frac{1}{2}}$	6
2324.291	7	5	43010.67	+0.15	$a\ ^6S_{2\frac{1}{2}}$—$50430^1_{1\frac{1}{2}}$	
2324.714	1	1	43002.84	−0.06	$a\ ^6D_{2\frac{1}{2}}$—$46175^3_{3\frac{1}{2}}$	
2324.776	3	10	43001.70	+0.02 +0.11	$a\ ^4F_{3\frac{1}{2}}$—$56413^1_{4\frac{1}{2}}$ $22139_{2\frac{1}{2}}$—$65141^3_{2\frac{1}{2}}$	
2326.091	15	60	42977.38	+0.02	$a\ ^6D_{4\frac{1}{2}}$—$49124^3_{3\frac{1}{2}}$	
2327.592	8*A*	5	42949.67	−0.19	$20039_{3\frac{1}{2}}$—$62989^3_{3\frac{1}{2}}$	
2327.737	—	1	42947.0	−0.5	$22194_{3\frac{1}{2}}$—$65141^3_{2\frac{1}{2}}$	
2328.314	20	35	42936.35	−0.05	$a\ ^6D_{1\frac{1}{2}}$—$44455^5_{0\frac{1}{2}}$	res
2329.691	6	15	42910.98	+0.06	$a\ ^4D_{0\frac{1}{2}}$—$56084^1_{1\frac{1}{2}}$	
2330.89	5	8	42888.91	+0.03	$a\ ^4D_{2\frac{1}{2}}$—$57856^3_{3\frac{1}{2}}$	
2331.778	3	4	42872.57	−0.13	$a\ ^4F_{4\frac{1}{2}}$—$57729^3_{3\frac{1}{2}}$	
2331.816	1	1	42871.87	−0.03	$a\ ^6S_{2\frac{1}{2}}$—$50292^3_{2\frac{1}{2}}$	
2333.146	25*A*	12	42847.44	−0.21	$a\ ^4P_{1\frac{1}{2}}$—$53440^5_{0\frac{1}{2}}$	
2353.462	—	1	42841.64	−0.05	$a\ ^4G_{5\frac{1}{2}}$—$60278^1_{4\frac{1}{2}}$	
2333.57	3	8	42839.66	+0.24	$a\ ^4D_{3\frac{1}{2}}$—$57986^1_{4\frac{1}{2}}$	
2333.770	15	35	42835.98	−0.06	$a\ ^6D_{1\frac{1}{2}}$—$44354^3_{2\frac{1}{2}}$	res
2334.070	5	5	42830.48	+0.02	$a\ ^4P_{1\frac{1}{2}}$—$53422^1_{1\frac{1}{2}}$	
2335.205	6	25	42809.66	−0.01	$a\ ^4G_{3\frac{1}{2}}$—$59399^1_{4\frac{1}{2}}$	
2335.548		5	42803.38	+0.16	$25209_{4\frac{1}{2}}$—$68012^3_{3\frac{1}{2}}$	
2335.933	2	8	42796.32	+0.08	$22194_{3\frac{1}{2}}$—$64990^3_{2\frac{1}{2}}$	
2336.716	6	15	42781.98	+0.16	$a\ ^4G_{5\frac{1}{2}}$—$60218^3_{5\frac{1}{2}}$	
2337.799	6	20	42762.17	+0.07	$a\ ^4D_{2\frac{1}{2}}$—$57729^3_{3\frac{1}{2}}$	
2338.125	—?	2	42756.21	−0.04	$22139_{2\frac{1}{2}}$—$64896^3_{3\frac{1}{2}}$	
2338.582		1	42747.86	−0.24	$23955_{3\frac{1}{2}}$—$66703^3_{5\frac{1}{2}}$	
2339.16	15	30	42737.29	+0.10	$a\ ^4P_{1\frac{1}{2}}$—$53329^1_{1\frac{1}{2}}$	
2339.732	10	8	42726.84	+0.07	$a\ ^4F_{1\frac{1}{2}}$—$51438^3_{2\frac{1}{2}}$	
2339.817	1	?	42725.29	+0.13	$a\ ^4F_{2\frac{1}{2}}$—$54026^3_{2\frac{1}{2}}$	
2339.904	6	20	42723.70	+0.03	$a\ ^4G_{4\frac{1}{2}}$—$59276^3_{3\frac{1}{2}}$	
2340.668	4	6	42709.76	+0.08	$a\ ^4D_{3\frac{1}{2}}$—$57856^3_{2\frac{1}{2}}$	
2341.074	4	15	42702.35	+0.21	$22194_{3\frac{1}{2}}$—$64896^3_{3\frac{1}{2}}$	
2341.368	25	35	42696.99	−0.02	$a\ ^6D_{3\frac{1}{2}}$—$47413^3_{2\frac{1}{2}}$	res
2341.442	1−	2?	42695.64	−0.18	$19637_{2\frac{1}{2}}$—$62333^3_{2\frac{1}{2}}$	
2341.903	1	6	42687.24	+0.10	$a\ ^4G_{3\frac{1}{2}}$—$59276^3_{3\frac{1}{2}}$	
2346.864	1	5	42597.01	−0.15	$23046_{3\frac{1}{2}}$—$65644^3_{3\frac{1}{2}}$	
2347.644	1	3	42582.86	−0.04	$a\ ^4D_{3\frac{1}{2}}$—$57729^3_{3\frac{1}{2}}$	
2348.015		7	42576.13	+0.39	$18990_{1\frac{1}{2}}$—$61566^3_{2\frac{1}{2}}$	
2349.262	3	20	42553.53	−0.02	$20534_{3\frac{1}{2}}$—$63087^5_{4\frac{1}{2}}$	
2349.839	6	10	42543.09	−0.05	$a\ ^4F_{1\frac{1}{2}}$—$51254^1_{1\frac{1}{2}}$	6
2350.362	2	10	42533.62	−0.05	$20455_{1\frac{1}{2}}$—$62989^3_{2\frac{1}{2}}$	
2351.052	2	6	42521.14	+0.14	$a\ ^4P_{1\frac{1}{2}}$—$53113^3_{2\frac{1}{2}}$	
2351.168	1−	1	42519.04	+0.26	$19070_{4\frac{1}{2}}$—$61589^3_{3\frac{1}{2}}$	
2351.496	4	12	42513.11	+0.01	$a\ ^4G_{2\frac{1}{2}}$—$58747^5_{1\frac{1}{2}}$	
2352.924		4	42487.31	+0.07	$22503_{1\frac{1}{2}}$—$64990^3_{2\frac{1}{2}}$	
2353.334	2	8	42479.91	−0.01	$19070_{4\frac{1}{2}}$—$61550^3_{3\frac{1}{2}}$	
2353.667	1	5	42473.90	−0.07	$18000_{3\frac{1}{2}}$—$60474^3_{2\frac{1}{2}}$	
2354.018		2	42467.57	+0.46	$23803_{3\frac{1}{2}}$—$66270^5_{4\frac{1}{2}}$	
2355.019		4	42449.52	−0.41	$23234_{4\frac{1}{2}}$—$65684^5_{3\frac{1}{2}}$	
2356.469	1	2	42423.40	−0.04	$18000_{3\frac{1}{2}}$—$60424^3_{3\frac{1}{2}}$	

TABLE 3. *Classified lines of* W II—Continued

Wavelength (Å)	Intensity		Wave number (cm^{-1})		Combination	Zeeman effect
	Arc	Spark	Observed	$O-C$		
Air						
2357. 268	1	5	42409. 02	−0. 11	$23234_{4\frac{1}{2}}$—$65644^{?}_{3\frac{1}{2}}$	
2357. 931		1	42397. 10	−0. 20	$20039_{3\frac{1}{2}}$—$62437^{?}_{4\frac{1}{2}}$	
2358. 816	12	18	42381. 19	+0. 01	$a\ ^6D_{2\frac{1}{2}}$—$45553^{?}_{1\frac{1}{2}}$	res
2361. 194	12*A*	10	42338. 51	−0. 09	$a\ ^4G_{4\frac{1}{2}}$—$58891^{?}_{5\frac{1}{2}}$	
2362. 108	3	15	42322. 13	−0. 16	$22194_{3\frac{1}{2}}$—$64516^{?}_{4\frac{1}{2}}$	
2362. 484	1	10	42315. 40	−0. 15	$23955_{5\frac{1}{2}}$—$66270^{?}_{5\frac{1}{2}}$	
2362. 528	1	4?	42314. 61	−0. 02	$a\ ^4D_{0\frac{1}{2}}$—$55488^{?}_{1\frac{1}{2}}$	
2363. 464	8	14	42297. 85	−0. 06	$a\ ^4D_{1\frac{1}{2}}$—$56932^{?}_{1\frac{1}{2}}$	
2363. 721		1	42293. 25	−0. 21	$20039_{3\frac{1}{2}}$—$62333^{?}_{2\frac{1}{2}}$	
2363. 910	6	30	42289. 87	+0. 01	$19070_{4\frac{1}{2}}$—$61360^{?}_{4\frac{1}{2}}$	
2364. 225	10	50	42284. 24	+0. 06	$a\ ^4D_{2\frac{1}{2}}$—$57252^{?}_{2\frac{1}{2}}$	
2364. 577	3	1	42277. 94	−0. 07	$18000_{3\frac{1}{2}}$—$60278^{?}_{4\frac{1}{2}}$	
2365. 832		7	42255. 52	−0. 09	$19070_{4\frac{1}{2}}$—$61326^{?}_{3\frac{1}{2}}$	
2366. 684	4	6	42240. 31	−0. 32	$a\ ^4D_{1\frac{1}{2}}$—$56874^{?}_{2\frac{1}{2}}$	
2367. 132	1	3	42232. 32	+0. 08	$a\ ^4F_{4\frac{1}{2}}$—$57089^{?}_{4\frac{1}{2}}$	
2368. 021		2	42216. 46	−0. 27	$22139_{2\frac{1}{2}}$—$64356^{?}_{3\frac{1}{2}}$	
2368. 36	8	14	42210. 42	−0. 06	$a\ ^4P_{1\frac{1}{2}}$—$52803^{?}_{1\frac{1}{2}}$	
2369. 755	6	8	42185. 57	0. 00	$a\ ^6D_{4\frac{1}{2}}$—$48332^{?}_{3\frac{1}{2}}$	
2370. 056	10	45	42180. 22	+0. 01	$20534_{3\frac{1}{2}}$—$62714^{?}_{3\frac{1}{2}}$	
2370. 624	5	12	42170. 11	−0. 02	$19070_{4\frac{1}{2}}$—$61240^{?}_{3\frac{1}{2}}$	
2371. 058	1	7	42162. 40	−0. 22	$22194_{3\frac{1}{2}}$—$64356^{?}_{3\frac{1}{2}}$	
2371. 218	2	5	42159. 55	−0. 09	$19442_{6\frac{1}{2}}$—$61602^{?}_{6\frac{1}{2}}$	
2371. 936	5	20	42146. 79	−0. 13	$19442_{6\frac{1}{2}}$—$61589^{?}_{5\frac{1}{2}}$	
2372. 610	5	30	42134. 82	+0. 08	$a\ ^4G_{4\frac{1}{2}}$—$58687^{?}_{4\frac{1}{2}}$	
2373. 305		1	42122. 48	+0. 58	$a\ ^4F_{2\frac{1}{2}}$—$53422^{?}_{1\frac{1}{2}}$	
2373. 462		4	42119. 69	−0. 20	$a\ ^4G_{3\frac{1}{2}}$—$58709^{?}_{3\frac{1}{2}}$	
2373. 679	1	3	42115. 84	−0. 08	$22194_{3\frac{1}{2}}$—$64310^{?}_{2\frac{1}{2}}$	
2374. 454	5?	35	42102. 10	−0. 04	$a\ ^4G_{2\frac{1}{2}}$—$58336^{?}_{2\frac{1}{2}}$	
2375. 044	4	20	42091. 64	+0. 11	$23234_{4\frac{1}{2}}$—$65326^{?}_{3\frac{1}{2}}$	
2377. 172	6	12	42053. 96	+0. 05	$a\ ^4P_{2\frac{1}{2}}$—$55488^{?}_{1\frac{1}{2}}$	res
2377. 393	6	8	42050. 06	+0. 29	$19276_{2\frac{1}{2}}$—$61326^{?}_{3\frac{1}{2}}$	
2378. 130	8	15	42037. 02	+0. 03	$a\ ^4F_{2\frac{1}{2}}$—$53338^{?}_{3\frac{1}{2}}$	
2378. 603	10	15	42028. 67	+0. 04	$a\ ^4F_{2\frac{1}{2}}$—$53329^{?}_{1\frac{1}{2}}$	
2379. 466	1	2	42013. 42	0. 00	$22194_{3\frac{1}{2}}$—$64207^{?}_{3\frac{1}{2}}$	
2380. 159	4	9	42001. 19	−0. 01	$a\ ^4P_{1\frac{1}{2}}$—$52593^{?}_{0\frac{1}{2}}$	
2380. 708	3	5	41991. 51	+0. 01	$18000_{3\frac{1}{2}}$—$59992^{?}_{2\frac{1}{2}}$	
2381. 065	1	2	41985. 22	+0. 10	$19070_{4\frac{1}{2}}$—$61055^{?}_{1\frac{1}{2}}$	
2381. 333	6	8	41980. 47	+0. 06	$a\ ^4F_{3\frac{1}{2}}$—$55392^{?}_{4\frac{1}{2}}$	
2382. 243	2	2	41964. 45	0. 00	$a\ ^4D_{2\frac{1}{2}}$—$56932^{?}_{1\frac{1}{2}}$	
2382. 364	7	20	41962. 32	0. 00	$a\ ^4G_{3\frac{1}{2}}$—$59399^{?}_{4\frac{1}{2}}$	
2382. 700		25	41956. 40	0. 00	$23046_{3\frac{1}{2}}$—$65003^{?}_{4\frac{1}{2}}$	
2383. 500	2	3	41942. 32	−0. 12	$a\ ^4D_{3\frac{1}{2}}$—$57089^{?}_{4\frac{1}{2}}$	
2383. 884	1—	1	41935. 57	−0. 03	$20780_{4\frac{1}{2}}$—$62715^{?}_{4\frac{1}{2}}$	
2384. 033	3	6	41932. 95	−0. 01	$18000_{3\frac{1}{2}}$—$59933^{?}_{3\frac{1}{2}}$	
2385. 253	7	15	41911. 48	+0. 09	$a\ ^4F_{4\frac{1}{2}}$—$56768^{?}_{3\frac{1}{2}}$	
2385. 335	5	7	41910. 04	0. 00	$a\ ^4D_{1\frac{1}{2}}$—$56544^{?}_{2\frac{1}{2}}$	
2385. 500	8	12	41907. 14	−0. 03	$a\ ^4D_{2\frac{1}{2}}$—$56874^{?}_{2\frac{1}{2}}$	6
2386. 447	2	9	41890. 51	+0. 14	$22139_{2\frac{1}{2}}$—$64030^{?}_{2\frac{1}{2}}$	6
2387. 708	2	5	41868. 39	−0. 05	$18000_{3\frac{1}{2}}$—$59869^{?}_{3\frac{1}{2}}$	
2388. 536	2	8	41853. 88	+0. 12	$26158_{4\frac{1}{2}}$—$68012^{?}_{3\frac{1}{2}}$	
2388. 798	2	8	41849. 28	−0. 14	$23046_{3\frac{1}{2}}$—$64896^{?}_{3\frac{1}{2}}$	
2389. 541		1	41836. 28	+0. 02	$22194_{3\frac{1}{2}}$—$64030^{?}_{2\frac{1}{2}}$	
2390. 371	25	75	41821. 75	+0. 08	$a\ ^6S_{2\frac{1}{2}}$—$49242^{?}_{2\frac{1}{2}}$	
2390. 890	4	30	41812. 68	+0. 24	$a\ ^4F_{2\frac{1}{2}}$—$53113^{?}_{3\frac{1}{2}}$	
2391. 218	1	3	41806. 94	0. 00	$22503_{1\frac{1}{2}}$—$64310^{?}_{2\frac{1}{2}}$	
2391. 574	2	3	41800. 71	−0. 08	$a\ ^4D_{2\frac{1}{2}}$—$56768^{?}_{3\frac{1}{2}}$	

TABLE 3. *Classified lines of* W II—Continued

Wavelength (Å)	Intensity		Wave number (cm^{-1})		Combination	Zeeman effect
	Arc	Spark	Observed	*O–C*		
Air						
2391. 717	4	8	41798. 22	−0. 05	$19442_{6\frac{1}{2}}$—*61240*$^{8}_{5\frac{1}{2}}$	
2392. 932	20	60	41777. 00	−0. 11	*a* $^{6}D_{3\frac{1}{2}}$—*z* $^{6}F^{1}_{4\frac{1}{2}}$	res
2393. 171	4	10	41772. 83	+0. 07	*a* $^{4}G_{2\frac{1}{2}}$—*58007*$^{1}_{1\frac{1}{2}}$	
2393. 768	1	3	41762. 41	−0. 18	*a* $^{4}P_{1\frac{1}{2}}$—*52355*$^{0}_{0\frac{1}{2}}$	
2394. 162	7	25	41755. 54	+0. 02	*a* $^{4}F_{4\frac{1}{2}}$—*56612*$^{3}_{3\frac{1}{2}}$	
2394. 444	12	7	41750. 62	+0. 28	*a* $^{4}F_{3\frac{1}{2}}$—*55162*$^{2}_{2\frac{1}{2}}$	
2394. 636	1	7	41747. 27	−0. 04	*a* $^{4}G_{3\frac{1}{2}}$—*58336*$^{2}_{2\frac{1}{2}}$	
2395. 036	1	5	41740. 30	+0. 17	$22139_{2\frac{1}{2}}$—*63880*$^{3}_{2\frac{1}{2}}$	
2395. 104	9	10	41739. 12	+0. 01	*a* $^{6}D_{2\frac{1}{2}}$—*44911*$^{1}_{1\frac{1}{2}}$	
2395. 384	—	1	41734. 24	+0. 01	$23234_{4\frac{1}{2}}$—*64969*$^{3}_{3\frac{1}{2}}$	
2395. 664	1	3	41729. 36	−0. 04	$23955_{5\frac{1}{2}}$—*65684*$^{3}_{3\frac{1}{2}}$	
2395. 730	5	8	41728. 21	+0. 01 +0. 24	*a* $^{4}P_{2\frac{1}{2}}$—*55162*$^{2}_{2\frac{1}{2}}$ *a* $^{4}D_{3\frac{1}{2}}$—*56874*$^{2}_{2\frac{1}{2}}$	
2396. 221	7	10	41719. 66	−0. 03	*a* $^{4}F_{1\frac{1}{2}}$—*50430*$^{1}_{1\frac{1}{2}}$	res
2397. 097		200	41704. 42	−0. 24	*a* $^{6}D_{2\frac{1}{2}}$—*z* $^{6}F^{3}_{3\frac{1}{2}}$	res
2397. 997		15	41688. 77	−0. 14	$19637_{2\frac{1}{2}}$—*61326*$^{3}_{3\frac{1}{2}}$	
2398. 149		7	41686. 12	+0. 10	$22194_{3\frac{1}{2}}$—*63880*$^{3}_{2\frac{1}{2}}$	
2399. 332	4	12	41665. 57	+0. 02	$18990_{1\frac{1}{2}}$—*60656*$^{2}_{2\frac{1}{2}}$	
2399. 574	1	4	41661. 37	+0. 02	$23234_{4\frac{1}{2}}$—*64896*$^{3}_{3\frac{1}{2}}$	
2400. 358	1	6	41647. 76	−0. 47	$22139_{2\frac{1}{2}}$—*63788*$^{3}_{3\frac{1}{2}}$	
2400. 519	5	8	41644. 97	+0. 05	*a* $^{4}D_{2\frac{1}{2}}$—*56612*$^{3}_{3\frac{1}{2}}$	
2400. 866	4	2	41638. 95	−0. 13	*a* $^{6}D_{3\frac{1}{2}}$—*46355*$^{2}_{2\frac{1}{2}}$	
2401. 863	5	12	41621. 67	+0. 08	*a* $^{4}D_{3\frac{1}{2}}$—*56768*$^{3}_{3\frac{1}{2}}$	
2402. 480	2	7	41610. 98	+0. 08	*a* $^{4}F_{3\frac{1}{2}}$—*55022*$^{3}_{3\frac{1}{2}}$	
2403. 074	5	10	41600. 69	+0. 03	*a* $^{4}F_{2\frac{1}{2}}$—*52901*$^{3}_{3\frac{1}{2}}$	
2403. 222	10	15	41598. 13	−0. 16	*a* $^{4}P_{0\frac{1}{2}}$—*50430*$^{1}_{1\frac{1}{2}}$	
2403. 455	4	10	41594. 10	−0. 02	$22194_{3\frac{1}{2}}$—*63788*$^{3}_{3\frac{1}{2}}$	
2403. 762	1	2	41588. 79	+0. 03	*a* $^{4}P_{2\frac{1}{2}}$—*55022*$^{3}_{3\frac{1}{2}}$	
2405. 280		8	41562. 54	+0. 11	*a* $^{6}S_{2\frac{1}{2}}$—*48982*$^{1}_{1\frac{1}{2}}$	
2405. 631	—?	1	41556. 48	+0. 06	*a* $^{4}F_{4\frac{1}{2}}$—*56415*$^{3}_{3\frac{1}{2}}$	
2406. 576	1—	1	41540. 16	+0. 34	$23450_{2\frac{1}{2}}$—*64990*$^{3}_{3\frac{1}{2}}$	
2407. 286	1	6	41527. 92	+0. 64	$22503_{1\frac{1}{2}}$—*64030*$^{3}_{2\frac{1}{2}}$	
2407. 787	5	12	41519. 27	+0. 04	*a* $^{4}F_{4\frac{1}{2}}$—*56376*$^{3}_{3\frac{1}{2}}$	
2408. 282	12*A*	15	41510. 73	−0. 13	$20039_{3\frac{1}{2}}$—*61550*$^{3}_{3\frac{1}{2}}$	
2409. 226	5	20	41494. 48	−0. 02	*a* $^{4}P_{1\frac{1}{2}}$—*52087*$^{3}_{2\frac{1}{2}}$	res
2409. 474	3	18	41490. 21			
2409. 827		4	41484. 13	+0. 42	$18990_{1\frac{1}{2}}$—*60474*$^{3}_{2\frac{1}{2}}$	
2410. 694	—	2	41469. 21	−0. 36	$23046_{3\frac{1}{2}}$—*64516*$^{1}_{1\frac{1}{2}}$	
2410. 854	1	1	41466. 46	+0. 18	$24804_{3\frac{1}{2}}$—*66270*$^{3}_{3\frac{1}{2}}$	
2411. 287	7	3	41459. 01	−0. 09	*a* $^{6}D_{3\frac{1}{2}}$—*46175*$^{3}_{3\frac{1}{2}}$	
2411. 538	6	20	41454. 70	−0. 02	*a* $^{4}G_{3\frac{1}{2}}$—*58891*$^{3}_{3\frac{1}{2}}$	
2411. 820	10	25	41449. 86	−0. 08	*a* $^{4}D_{1\frac{1}{2}}$—*56084*$^{1}_{1\frac{1}{2}}$	
2412. 064	2	2	41445. 66	−0. 06	$23450_{2\frac{1}{2}}$—*64896*$^{3}_{3\frac{1}{2}}$	
2412. 76	5	8	41433. 72	−0. 06	*a* $^{4}G_{4\frac{1}{2}}$—*57986*$^{3}_{3\frac{1}{2}}$	
2414. 118	4	7	41410. 40	+0. 13	*a* $^{6}S_{2\frac{1}{2}}$—*48830*$^{3}_{3\frac{1}{2}}$	
2414. 806	6	25	41398. 60	−0. 04	$18000_{3\frac{1}{2}}$—*59399*$^{1}_{1\frac{1}{2}}$	4
2414. 888	3	3	41397. 20	−0. 05	*a* $^{4}G_{3\frac{1}{2}}$—*57986*$^{1}_{1\frac{1}{2}}$	
2416. 063	1	3	41377. 06	+0. 02	$22503_{1\frac{1}{2}}$—*63880*$^{3}_{2\frac{1}{2}}$	
2416. 416		1	41371. 02	+0. 02	$23955_{5\frac{1}{2}}$—*65326*$^{3}_{3\frac{1}{2}}$	
2417. 430	2	4	41353. 67	+0. 21	$19070_{4\frac{1}{2}}$—*60424*$^{3}_{3\frac{1}{2}}$	
2419. 350	8	35	41320. 85	+0. 05	$20039_{3\frac{1}{2}}$—*61360*$^{1}_{1\frac{1}{2}}$	
2419. 848	4	5	41312. 34	+0. 12	*a* $^{4}D_{0\frac{1}{2}}$—*54485*$^{0}_{0\frac{1}{2}}$	
2419. 987	3	8	41309. 98	+0. 08	$23046_{3\frac{1}{2}}$—*64356*$^{3}_{3\frac{1}{2}}$	
2420. 990	12	35	41292. 86	+0. 21	*a* $^{4}F_{3\frac{1}{2}}$—*54704*$^{3}_{3\frac{1}{2}}$	
2421. 358	1	3	41286. 59	+0. 04	$20039_{3\frac{1}{2}}$—*61326*$^{3}_{3\frac{1}{2}}$	
2421. 662	3	12	41281. 40	−0. 10	$23234_{4\frac{1}{2}}$—*64516*$^{1}_{1\frac{1}{2}}$	

TABLE 3. *Classified lines of* W II—Continued

Wavelength (Å)	Intensity		Wave number (cm^{-1})		Combination	Zeeman effect
	Arc	Spark	Observed	*O–C*		
Air						
2421. 974	5	12	41276. 09	−0. 02	$18000_{3\frac{1}{2}}$—*59276*$^{3}_{3\frac{1}{2}}$	
2422. 292	30*A*	20	41270. 67	+0. 16	*a* $^4P_{2\frac{1}{2}}$—*54704*$^{2}_{2\frac{1}{2}}$	
2422. 529	8	25	41266. 63	+0. 01	*a* $^4D_{1\frac{1}{2}}$—*56413*$^{3}_{4\frac{1}{2}}$	
2422. 726	1	4	41263. 28	+0. 08	$23046_{3\frac{1}{2}}$—*64310*$^{3}_{3\frac{1}{2}}$	
2425. 975	10*A*	6	41208. 02	−0. 01	$19070_{4\frac{1}{2}}$—*60278*$^{4}_{4\frac{1}{2}}$	
2426. 482	1	4	41199. 42	+0. 06	$23803_{3\frac{1}{2}}$—*65003*$^{3}_{4\frac{1}{2}}$	
2426. 558	4	10	41198. 13	−0. 02	$19276_{2\frac{1}{2}}$—*60474*$^{2}_{2\frac{1}{2}}$	6
2427. 493	10	40	41182. 26	−0. 04	*a* $^6D_{2\frac{1}{2}}$—*44354*$^{4}_{2\frac{1}{2}}$	6 res
2427. 807	4	6	41176. 93	+0. 15	*a* $^4G_{1\frac{1}{2}}$—*57729*$^{3}_{3\frac{1}{2}}$	
2428. 758	4	10	41160. 80	+0. 10	$23046_{2\frac{1}{2}}$—*64207*$^{4}_{4\frac{1}{2}}$	
2429. 396	4	10	41149. 99	+0. 43	$26929_{5\frac{1}{2}}$—*68078*$^{5}_{6\frac{1}{2}}$	
2429. 489	4	6	41148. 42	+0. 26	$19070_{4\frac{1}{2}}$—*60218*$^{4}_{5\frac{1}{2}}$	
2429. 528	3	8	41147. 76	+0. 14	$19276_{2\frac{1}{2}}$—*60424*$^{2}_{3\frac{1}{2}}$	
2429. 971	1	6	41140. 26	+0. 01	*a* $^4G_{3\frac{1}{2}}$—*57729*$^{3}_{3\frac{1}{2}}$	6
2430. 788	3	10	41126. 44	+0. 11	$22139_{2\frac{1}{2}}$—*63266*$^{3}_{3\frac{1}{2}}$	
2431. 373	5	18	41116. 54	+0. 06	*a* $^4D_{2\frac{1}{2}}$—*56084*$^{3}_{4\frac{1}{2}}$	
2431. 714	5	12	41110. 78	+0. 01	$20455_{1\frac{1}{2}}$—*61566*$^{2}_{2\frac{1}{2}}$	
2432. 797		6	41092. 47	+0. 09	$23803_{3\frac{1}{2}}$—*64896*$^{3}_{3\frac{1}{2}}$	
2433. 139	5	8	41086. 70	+0. 09	*a* $^4F_{3\frac{1}{2}}$—*54498*$^{3}_{3\frac{1}{2}}$	6 res
2433. 982	25*A*	20	41072. 47	+0. 25	$22194_{1\frac{1}{2}}$—*63266*$^{3}_{3\frac{1}{2}}$	
2434. 254	10*A*	12	41067. 88	+0. 05	$20534_{3\frac{1}{2}}$—*61602*$^{3}_{6\frac{1}{2}}$	
2434. 453	5	8	41064. 53	+0. 06	*a* $^4P_{2\frac{1}{2}}$—*54498*$^{3}_{3\frac{1}{2}}$	
2435. 008	10	50	41055. 17	+0. 06	$20534_{3\frac{1}{2}}$—*61589*$^{3}_{3\frac{1}{2}}$	
2435. 445	4	20	41047. 80	0. 00	$23955_{5\frac{1}{2}}$—*65003*$^{5}_{4\frac{1}{2}}$	
2437. 155	1—	1	41019. 00	−0. 13	$19637_{2\frac{1}{2}}$—*60656*$^{2}_{2\frac{1}{2}}$	
2437. 332	3	6	41016. 02	−0. 04	$20039_{3\frac{1}{2}}$—*61055*$^{3}_{4\frac{1}{2}}$	
2437. 471	4	15	41013. 68	−0. 02	$23955_{5\frac{1}{2}}$—*64969*$^{5}_{5\frac{1}{2}}$	6
2439. 473	4	12	40980. 03	+0. 10	$19276_{2\frac{1}{2}}$—*60256*$^{3}_{3\frac{1}{2}}$	
2439. 808	2	7	40974. 40	+0. 20	*a* $^4F_{2\frac{1}{2}}$—*52275*$^{3}_{3\frac{1}{2}}$	
2439. 913	2	7	40972. 64	+0. 01	$23234_{4\frac{1}{2}}$—*64207*$^{4}_{4\frac{1}{2}}$	
2440. 432	10	20	40963. 93	+0. 11	*a* $^4D_{0\frac{1}{2}}$—*54137*$^{2}_{1\frac{1}{2}}$	
2441. 612	7	12	40944. 13			6
2441. 790		7	40941. 14	−0. 58	*a* $^4P_{2\frac{1}{2}}$—*54375*$^{2}_{2\frac{1}{2}}$	
2443. 858		2	40906. 51	+0. 31	$23450_{2\frac{1}{2}}$—*64356*$^{3}_{3\frac{1}{2}}$	
2446. 394	25	120	40864. 10	+0. 05	*a* $^6S_{2\frac{1}{2}}$—*48284*$^{2}_{2\frac{1}{2}}$	6
2446. 570	1	1	40861. 16	−0. 07	$20039_{3\frac{1}{2}}$—*60900*$^{3}_{2\frac{1}{2}}$	
2447. 255	4	12	40849. 73	+0. 10	$22139_{2\frac{1}{2}}$—*62989*$^{3}_{2\frac{1}{2}}$	
2447. 52		1	40845. 3	−0. 2	*a* $^4P_{1\frac{1}{2}}$—*51438*$^{2}_{1\frac{1}{2}}$	
2448. 00	5	15	40837. 3	0. 0	$19637_{2\frac{1}{2}}$—*60474*$^{2}_{2\frac{1}{2}}$	
2448. 237	4	50	40833. 34	+0. 04	$23046_{3\frac{1}{2}}$—*63880*$^{3}_{2\frac{1}{2}}$	
2448. 662	4	8	40826. 26	+0. 07	$20534_{3\frac{1}{2}}$—*61360*$^{3}_{4\frac{1}{2}}$	
2448. 719	3	4	40825. 31	−0. 03	$18990_{1\frac{1}{2}}$—*59816*$^{1}_{1\frac{1}{2}}$	
2449. 694	4	20	40809. 06	−0. 02	$20780_{4\frac{1}{2}}$—*61589*$^{3}_{3\frac{1}{2}}$	
2450. 324	2	7	40798. 57	+0. 11	$19070_{4\frac{1}{2}}$—*59869*$^{3}_{3\frac{1}{2}}$	
2451. 032	3	7	40786. 78	+0. 02	$19637_{2\frac{1}{2}}$—*60424*$^{3}_{3\frac{1}{2}}$	
2451. 468		50	40779. 53	+0. 11	*a* $^6D_{1\frac{1}{2}}$—*43298*$^{4}_{1\frac{1}{2}}$	
2451. 660		1	40776. 33	+0. 03	$19442_{6\frac{1}{2}}$—*60218*$^{5}_{5\frac{1}{2}}$	
2453. 760	3	10	40741. 44	0. 04	$23046_{3\frac{1}{2}}$—*63788*$^{3}_{3\frac{1}{2}}$	
2455. 506	40*A*	10	40712. 48	−0. 05	$23803_{3\frac{1}{2}}$—*64516*$^{4}_{4\frac{1}{2}}$	
2455. 722	2	5	40708. 90	+0. 04	$18000_{3\frac{1}{2}}$—*58709*$^{3}_{3\frac{1}{2}}$	
2455. 866	6	35	40706. 51	+0. 05	$20534_{3\frac{1}{2}}$—*61240*$^{3}_{3\frac{1}{2}}$	6
2456. 072	4	8	40703. 09	−0. 01	*a* $^4P_{2\frac{1}{2}}$—*54137*$^{2}_{1\frac{1}{2}}$	
2457. 043	1	3	40687. 01	−0. 17	$18000_{3\frac{1}{2}}$—*58687*$^{4}_{4\frac{1}{2}}$	
2458. 529	3	4?	40662. 42	+0. 09	*a* $^4G_{3\frac{1}{2}}$—*57252*$^{3}_{2\frac{1}{2}}$	
2458. 564	5	30	40661. 84	−0. 04	*a* $^4P_{1\frac{1}{2}}$—*51254*$^{2}_{1\frac{1}{2}}$	

TABLE 3. *Classified lines of* W II—Continued

Wavelength (Å)	Intensity		Wave number (cm^{-1})		Combination	Zeeman effect
	Arc	Spark	Observed	*O–C*		
Air						
2458. 838	3	20	40657. 31	+0. 17	$19276_{2\frac{1}{2}}$—*59933*$^{3}_{3\frac{1}{2}}$	
2459. 602	20	10	40644. 68	+0. 10	*a* $^4F_{3\frac{1}{2}}$—*54056*$^{\circ}_{4\frac{1}{2}}$	
2459. 876	4	30	40640. 15	0. 00	*a* $^4G_{2\frac{1}{2}}$—*56874*$^{1}_{2\frac{1}{2}}$	6
2461. 148	5	20	40619. 15	+0. 08	$19637_{2\frac{1}{2}}$—*60256*$^{3}_{3\frac{1}{2}}$	
2461. 294	3	8	40616. 74	−0. 03	$20039_{3\frac{1}{2}}$—*60656*$^{\circ}_{2\frac{1}{2}}$	
2461. 442	5	15	40614. 30	+0. 02	*a* $^4F_{3\frac{1}{2}}$—*54026*$^{2}_{2\frac{1}{2}}$	
2464. 616	15	40	40562. 00	+0. 05	*a* $^4F_{2\frac{1}{2}}$—*51863*$^{3}_{3\frac{1}{2}}$	
2464. 70	1	4	40560. 6	−0. 4	$23955_{3\frac{1}{2}}$—*64516*$^{\circ}_{4\frac{1}{2}}$	
2465. 148		15	40553. 25	−0. 08	$23234_{4\frac{1}{2}}$—*63788*$^{3}_{3\frac{1}{2}}$	
2465. 598	2	7	40545. 85	−0. 06	$20780_{4\frac{1}{2}}$—*61326*$^{3}_{3\frac{1}{2}}$	
2465. 667	2	20	40544. 72	−0. 04	$26158_{4\frac{1}{2}}$—*66703*$^{3}_{3\frac{1}{2}}$	7
2465. 962	4	30	40539. 87	+0. 09	$19276_{2\frac{1}{2}}$—*59816*$^{\circ}_{1\frac{1}{2}}$	7
2466. 176	2	5	40536. 35	+0. 03	*a* $^4G_{4\frac{1}{2}}$—*57089*$^{4}_{4\frac{1}{2}}$	
2466. 330	5	10	40533. 82	+0. 05	*a* $^4G_{2\frac{1}{2}}$—*56768*$^{3}_{3\frac{1}{2}}$	
2466. 522	35	80	40530. 66	−0. 01 −0. 18	*a* $^6D_{1\frac{1}{2}}$—*z* $^6F^{3}_{3\frac{1}{2}}$ *a* $^4F_{1\frac{1}{2}}$—*49242*$^{2}_{2\frac{1}{2}}$	res
2467. 078	3	9	40521. 53	+0. 08	$20534_{3\frac{1}{2}}$—*61055*$^{4}_{4\frac{1}{2}}$	
2468. 006	2	10	40506. 29	+0. 13	$23803_{3\frac{1}{2}}$—*64310*$^{2}_{2\frac{1}{2}}$	
2468. 404	6	15	40499. 76	−0. 03	*a* $^4G_{3\frac{1}{2}}$—*57089*$^{4}_{4\frac{1}{2}}$	
2469. 206	2	6	40486. 61	+0. 07	$22503_{1\frac{1}{2}}$—*62989*$^{2}_{2\frac{1}{2}}$	
2469. 873	3	25	40475. 67	+0. 15	$25209_{4\frac{1}{2}}$—*65684*$^{3}_{3\frac{1}{2}}$	4
2470. 804	8	70	40460. 43	0. 00	$20780_{4\frac{1}{2}}$—*61240*$^{3}_{3\frac{1}{2}}$	
2471. 740	15	40	40445. 11	+0. 07	$20455_{1\frac{1}{2}}$—*60900*$^{2}_{2\frac{1}{2}}$	
2472. 380	1	3	40434. 64	−0. 29	$20039_{3\frac{1}{2}}$—*60474*$^{2}_{2\frac{1}{2}}$	res
2473. 752		1	40412. 21	−0. 01	$19404_{0\frac{1}{2}}$—*59816*$^{\circ}_{1\frac{1}{2}}$	
2474. 278		2	40403. 62	−0. 04	$23803_{3\frac{1}{2}}$—*64207*$^{\circ}_{1\frac{1}{2}}$	
2475. 474	1	3	40384. 43	+0. 03	$20039_{3\frac{1}{2}}$—*60424*$^{3}_{3\frac{1}{2}}$	
2475. 588	3	50	40382. 24			
2475. 844	4	10	40378. 07	+0. 17	*a* $^4G_{2\frac{1}{2}}$—*56612*$^{3}_{3\frac{1}{2}}$	
2477. 284	3	15	40354. 60	−0. 22	$19637_{2\frac{1}{2}}$—*59992*$^{2}_{2\frac{1}{2}}$	
2477. 796	30	200	40346. 26	−0. 01	*a* $^6D_{4\frac{1}{2}}$—*z* $^6F^{1}_{4\frac{1}{2}}$	6
2478. 313	2	20	40337. 84	+0. 14	$23450_{2\frac{1}{2}}$—*63788*$^{3}_{3\frac{1}{2}}$	
2478. 402	2	6	40336. 40	+0. 12	$18000_{3\frac{1}{2}}$—*58336*$^{2}_{2\frac{1}{2}}$	
2478. 874	4	10	40328. 72	+0. 06	$19070_{4\frac{1}{2}}$—*59399*$^{4}_{4\frac{1}{2}}$	
2480. 041	3	4	40309. 74	+0. 18	*a* $^4G_{2\frac{1}{2}}$—*56544*$^{3}_{2\frac{1}{2}}$	
2480. 867	3	6	40296. 32	+0. 04	$19637_{2\frac{1}{2}}$—*59933*$^{3}_{3\frac{1}{2}}$	
2481. 546	10	30	40285. 30	−0. 02	*a* $^4G_{3\frac{1}{2}}$—*56874*$^{3}_{2\frac{1}{2}}$	
2482. 154		3	40275. 43	+0. 01	$20780_{4\frac{1}{2}}$—*61055*$^{4}_{4\frac{1}{2}}$	
2482. 390	3	2	40271. 60	0. 00	*a* $^4F_{1\frac{1}{2}}$—*48982*$^{1}_{1\frac{1}{2}}$	
2482. 688	3	4	40266. 77	−0. 02	*a* $^4D_{0\frac{1}{2}}$—*53440*$^{0}_{0\frac{1}{2}}$	
2483. 592	4	12	40252. 11	+0. 01	$23955_{3\frac{1}{2}}$—*64207*$^{1}_{1\frac{1}{2}}$	
2483. 744	5	7	40249. 64	+0. 04	*a* $^4D_{0\frac{1}{2}}$—*53422*$^{1}_{1\frac{1}{2}}$	
2484. 008	7	20	40245. 37	+0. 02	*a* $^4D_{3\frac{1}{2}}$—*55392*$^{1}_{1\frac{1}{2}}$	
2484. 404	7	40	40238. 95	−0. 02	$20039_{3\frac{1}{2}}$—*60278*$^{1}_{1\frac{1}{2}}$	
2484. 848	2	4	40231. 76	0. 00	$19637_{2\frac{1}{2}}$—*59869*$^{3}_{3\frac{1}{2}}$	
2485. 160	1	2	40226. 71	+0. 21	$23803_{3\frac{1}{2}}$—*64030*$^{2}_{2\frac{1}{2}}$	
2485. 606	1	3	40219. 50	0. 00	$23046_{3\frac{1}{2}}$—*63266*$^{3}_{3\frac{1}{2}}$	
2485. 779	5	15	40216. 70	−0. 01	$20039_{3\frac{1}{2}}$—*60256*$^{3}_{3\frac{1}{2}}$	res
2486. 429	6	18	40206. 18	+0. 05	$19070_{4\frac{1}{2}}$—*59276*$^{3}_{3\frac{1}{2}}$	
2486. 776	3	6	40200. 57	−0. 01	$20455_{1\frac{1}{2}}$—*60656*$^{3}_{2\frac{1}{2}}$	
2487. 155	2	1	40194. 45	−0. 03	*a* $^4D_{2\frac{1}{2}}$—*55162*$^{2}_{2\frac{1}{2}}$	
2487. 231	3	5	40193. 22	−0. 01	$22139_{2\frac{1}{2}}$—*62333*$^{3}_{3\frac{1}{2}}$	
2488. 120	8	30	40178. 86	−0. 08 −0. 06	*a* $^4G_{3\frac{1}{2}}$—*56768*$^{3}_{3\frac{1}{2}}$ $19637_{2\frac{1}{2}}$—*59816*$^{1}_{1\frac{1}{2}}$	7
2488. 780	30	120	40168. 21	0. 00	*a* $^6S_{2\frac{1}{2}}$—*47588*$^{1}_{1\frac{1}{2}}$	4
2488. 932	15	7	40165. 76	+0. 12	*a* $^4F_{4\frac{1}{2}}$—*55022*$^{3}_{3\frac{1}{2}}$	
2489. 231	40	200	40160. 93	+0. 07	*a* $^6D_{3\frac{1}{2}}$—*z* $^6F^{3}_{3\frac{1}{2}}$	res

TABLE 3. *Classified lines of* W II—Continued

Wavelength (Å)	Intensity		Wave number (cm^{-1})		Combination	Zeeman effect
	Arc	Spark	Observed	*O–C*		
Air						
2489. 514	5	12	40156. 37	+0. 04	$a\ ^4D_{0\frac{1}{2}}$—*53329*$^{?}_{1\frac{1}{2}}$	
2489. 900	5	10	40150. 14	−0. 06	$a\ ^4P_{0\frac{1}{2}}$—*48982*$^{?}_{1\frac{1}{2}}$	
2490. 586	4	15	40139. 08	−0. 04	$22194_{3\frac{1}{2}}$—*62333*$^{?}_{2\frac{1}{2}}$	
2490. 718	12	25	40136. 95	0. 00	$a\ ^4F_{2\frac{1}{2}}$—*51438*$^{?}_{3\frac{1}{2}}$	
2492. 252	4	14	40112. 25	+0. 04	$26158_{4\frac{1}{2}}$—*66270*$^{?}_{4\frac{1}{2}}$	
2492. 928	8	80	40101. 38	+0. 02	$a\ ^4F_{4\frac{1}{2}}$—*54958*$^{?}_{5\frac{1}{2}}$	
2493. 54	3	7	40091. 54	−0. 01	$24804_{3\frac{1}{2}}$—*64896*$^{?}_{3\frac{1}{2}}$	
2494. 738		2	40072. 29	+0. 07	$24918_{1\frac{1}{2}}$—*64990*$^{?}_{2\frac{1}{2}}$	
2494. 872		7	40070. 14	−0. 11	$a\ ^4D_{1\frac{1}{2}}$—*54704*$^{?}_{2\frac{1}{2}}$	
2495. 522	5	10	40059. 70	+0. 10	$a\ ^4G_{4\frac{1}{2}}$—*56612*$^{?}_{5\frac{1}{2}}$	
2496. 648	50	120	40041. 63	−0. 15	$a\ ^6D_{3\frac{1}{2}}$—*44758*$^{?}_{4\frac{1}{2}}$	5
2497. 480	35	75	40028. 29	+0. 03	$a\ ^6D_{4\frac{1}{2}}$—*46175*$^{?}_{5\frac{1}{2}}$	5
2498. 076	2	3	40018. 74	0. 00	$20455_{1\frac{1}{2}}$—*60474*$^{?}_{2\frac{1}{2}}$	
2499. 223	8	16	40000. 38	+0. 09	$19276_{2\frac{1}{2}}$—*59276*$^{?}_{3\frac{1}{2}}$	
2499. 330	2	4	39998. 67	−0. 09	$24991_{1\frac{1}{2}}$—*64990*$^{?}_{2\frac{1}{2}}$	
2499. 692	15	100	39992. 88	−0. 02	$a\ ^6S_{2\frac{1}{2}}$—*47413*$^{?}_{3\frac{1}{2}}$	
2499. 934	3	4	39989. 00	+0. 12	$a\ ^4P_{2\frac{1}{2}}$—*53422*$^{?}_{1\frac{1}{2}}$	
2500. 11	12	30	39986. 19	−0. 03	$18000_{3\frac{1}{2}}$—*57986*$^{?}_{4\frac{1}{2}}$	
2500. 217	1	3	39984. 48	+0. 12	$23803_{3\frac{1}{2}}$—*63788*$^{?}_{3\frac{1}{2}}$	
2501. 020	1	10	39971. 64	−0. 05	$25169_{1\frac{1}{2}}$—*65141*$^{?}_{2\frac{1}{2}}$	res
2501. 877		10	39957. 95	−0. 06	$a\ ^4F_{3\frac{1}{2}}$—*53369*$^{?}_{4\frac{1}{2}}$	
2502. 072	2	10	39954. 84	+0. 11	$a\ ^4G_{3\frac{1}{2}}$—*56544*$^{?}_{3\frac{1}{2}}$	
2502. 162	3	4?	39953. 40	+0. 08	$a\ ^4F_{2\frac{1}{2}}$—*51254*$^{?}_{1\frac{1}{2}}$	
2502. 836	1	3	39942. 64	−0. 16	$23046_{3\frac{1}{2}}$—*62989*$^{?}_{2\frac{1}{2}}$	
2505. 264		1	39903. 93	−0. 04	$a\ ^4P_{2\frac{1}{2}}$—*53338*$^{?}_{3\frac{1}{2}}$	
2505. 790	3	5	39895. 56	−0. 05	$a\ ^4P_{2\frac{1}{2}}$—*53329*$^{?}_{1\frac{1}{2}}$	
2506. 048	—?	80	39891. 45	+0. 15	$28187_{6\frac{1}{2}}$—*68078*$^{?}_{6\frac{1}{2}}$	6
2507. 994	12	30	39860. 50	0. 00	$a\ ^4G_{4\frac{1}{2}}$—*56413*$^{?}_{4\frac{1}{2}}$	6
2508. 274	2	3	39856. 05	+0. 05	$18000_{3\frac{1}{2}}$—*57856*$^{?}_{3\frac{1}{2}}$	
2508. 582	1	3	39851. 16	−0. 08	$a\ ^4D_{1\frac{1}{2}}$—*54485*$^{?}_{0\frac{1}{2}}$	
2508. 690	—?	4	39849. 44	−0. 02	$a\ ^4G_{2\frac{1}{2}}$—*56084*$^{?}_{1\frac{1}{2}}$	
2509. 386	2	3	39838. 39	−0. 04	$a\ ^4P_{1\frac{1}{2}}$—*50430*$^{?}_{1\frac{1}{2}}$	
2509. 955	6	40	39829. 35	−0. 05	$20039_{3\frac{1}{2}}$—*59869*$^{?}_{3\frac{1}{2}}$	7
2510. 246		3	39824. 74	−0. 16	$28187_{6\frac{1}{2}}$—*68012*$^{?}_{5\frac{1}{2}}$	
2510. 348	—?	2	39823. 12	−0. 19	$a\ ^4G_{4\frac{1}{2}}$—*56376*$^{?}_{5\frac{1}{2}}$	
2510. 482	8	80	39821. 00	−0. 06	$19070_{4\frac{1}{2}}$—*58891*$^{?}_{5\frac{1}{2}}$	
2510. 799		3	39815. 97	+0. 17	$23450_{2\frac{1}{2}}$—*63266*$^{?}_{3\frac{1}{2}}$	
2512. 186	2	4	39793. 99	+0. 07	$25209_{4\frac{1}{2}}$—*65003*$^{?}_{4\frac{1}{2}}$	
2513. 435	1	30	39774. 22	+0. 06	$26929_{3\frac{1}{2}}$—*66703*$^{?}_{3\frac{1}{2}}$	6
2514. 358	2	4	39759. 62	+0. 11	$a\ ^6S_{2\frac{1}{2}}$—*47179*$^{?}_{1\frac{1}{2}}$	
2514. 526	3	20	39756. 96	−0. 02	$18990_{1\frac{1}{2}}$—*58747*$^{?}_{1\frac{1}{2}}$	res
2515. 324	3	30	39744. 35	+0. 18 −0. 01	$a\ ^4F_{2\frac{1}{2}}$—*51045*$^{?}_{3\frac{1}{2}}$ $20534_{5\frac{1}{2}}$—*60278*$^{?}_{4\frac{1}{2}}$	
2515. 508	5	8	39741. 44	−0. 02	$a\ ^4D_{1\frac{1}{2}}$—*54375*$^{?}_{2\frac{1}{2}}$	
2515. 806	2	10	39736. 73	−0. 06	$a\ ^4D_{2\frac{1}{2}}$—*54704*$^{?}_{2\frac{1}{2}}$	
2516. 138		10	39731. 49	−0. 14	$23234_{4\frac{1}{2}}$—*62966*$^{?}_{5\frac{1}{2}}$	
2516. 284	1	3	39729. 18	−0. 04	$18000_{3\frac{1}{2}}$—*57729*$^{?}_{3\frac{1}{2}}$	
2517. 406	1	25	39711. 48	−0. 22	$24804_{3\frac{1}{2}}$—*64516*$^{?}_{4\frac{1}{2}}$	5
2518. 144	6	50	39699. 84	+0. 03	$a\ ^4P_{1\frac{1}{2}}$—*50292*$^{?}_{2\frac{1}{2}}$	
2518. 973		4	39686. 78	−0. 16	$25209_{4\frac{1}{2}}$—*64896*$^{?}_{3\frac{1}{2}}$	
2519. 126	4	7	39684. 37	−0. 12	$20534_{5\frac{1}{2}}$—*60218*$^{?}_{3\frac{1}{2}}$	

TABLE 3. *Classified lines of* W II—Continued

Wavelength (Å)	Intensity		Wave number (cm^{-1})		Combination	Zeeman effect
	Arc	Spark	Observed	$O-C$		
Air						
2519.444	8	30	39679.36	−0.06	$a\ ^4P_{2\frac{1}{2}}$—$53113^{3}_{2\frac{1}{2}}$	res
2520.10	1	3	39669.0	−0.2	$23046_{3\frac{1}{2}}$—$62715^{4}_{4\frac{1}{2}}$	
2521.156	3	10	39652.42	−0.02	$a\ ^4G_{3\frac{1}{2}}$—$57089^{3}_{4\frac{1}{2}}$	
2521.686	3*A*	3	39644.09	+0.33	$20780_{4\frac{1}{2}}$—$60424^{3}_{3\frac{1}{2}}$	
2521.853	3	3	39641.46	+0.11	$a\ ^4F_{4\frac{1}{2}}$—$54498^{3}_{3\frac{1}{2}}$	
2522.039	30	60	39638.54	+0.04	$a\ ^6D_{3\frac{1}{2}}$—$44354^{3}_{2\frac{1}{2}}$	
2522.270	3	8	39634.91	+0.21	$28377_{5\frac{1}{2}}$—$68012^{3}_{3\frac{1}{2}}$	
2526.208	4	10	39573.12	−0.10	$a\ ^4F_{1\frac{1}{2}}$—$48284^{3}_{2\frac{1}{2}}$	res
2527.200	2	15	39557.59	0.00	$a\ ^4D_{3\frac{1}{2}}$—$54704^{3}_{3\frac{1}{2}}$	
2527.552	2	10	39552.08	+0.05	$24804_{3\frac{1}{2}}$—$64356^{3}_{3\frac{1}{2}}$	
2528.560	—?	8	39536.32	+0.05	$20455_{1\frac{1}{2}}$—$59992^{3}_{2\frac{1}{2}}$	
2528.913	5	20	39530.80	+0.05	$a\ ^4D_{2\frac{1}{2}}$—$54498^{3}_{3\frac{1}{2}}$	res
2529.209	2	8	39526.17	+0.11	$26158_{4\frac{1}{2}}$—$65684^{3}_{3\frac{1}{2}}$	
2530.54	1	4	39505.38	+0.05	$24804_{3\frac{1}{2}}$—$64310^{3}_{2\frac{1}{2}}$	
2530.70	10	8	39502.88	+0.04	$a\ ^4D_{1\frac{1}{2}}$—$54137^{3}_{1\frac{1}{2}}$	
2530.986	5	50	39498.42	+0.09	$20780_{4\frac{1}{2}}$—$60278^{4}_{4\frac{1}{2}}$	
2532.085	1	1	39481.28	+0.17	$23234_{4\frac{1}{2}}$—$62715^{4}_{4\frac{1}{2}}$	
2532.414	4	7	39476.15	+0.08	$20780_{4\frac{1}{2}}$—$60256^{3}_{3\frac{1}{2}}$	
2532.711	2	5	39471.52	+0.10	$19276_{2\frac{1}{2}}$—$58747^{3}_{1\frac{1}{2}}$	
2532.842	2	3	39469.48	+0.08	$25672_{2\frac{1}{2}}$—$65141^{3}_{2\frac{1}{2}}$	
2532.960	6	15	39467.64	0.00	$a\ ^4P_{2\frac{1}{2}}$—$52901^{3}_{3\frac{1}{2}}$	
2533.278	2	7	39462.69	+0.23	$23803_{3\frac{1}{2}}$—$63266^{3}_{3\frac{1}{2}}$	
2534.140	5	30	39449.27	+0.07	$19442_{2\frac{1}{2}}$—$58891^{3}_{3\frac{1}{2}}$	7
2534.829	5	50	39438.55	+0.09	$20780_{4\frac{1}{2}}$—$60218^{3}_{3\frac{1}{2}}$	7
2535.178		3	39433.12	+0.08	$19276_{2\frac{1}{2}}$—$58709^{3}_{3\frac{1}{2}}$	
2535.573	1	10	39426.98	+0.25	$22139_{2\frac{1}{2}}$—$61566^{3}_{2\frac{1}{2}}$	4
2536.000	6	40	39420.34	0.00	$a\ ^4D_{0\frac{1}{2}}$—$52593^{3}_{0\frac{1}{2}}$	
2536.622	2	25	39410.67	+0.04	$22139_{2\frac{1}{2}}$—$61550^{3}_{3\frac{1}{2}}$	
2536.789	1	1	39408.07	+0.07	$a\ ^4D_{2\frac{1}{2}}$—$54375^{3}_{2\frac{1}{2}}$	
2537.133	1	30	39402.73	−0.10	$24804_{3\frac{1}{2}}$—$64207^{4}_{4\frac{1}{2}}$	7
2539.313	7	35	39368.91	+0.01	$a\ ^4P_{2\frac{1}{2}}$—$52803^{3}_{1\frac{1}{2}}$	
2539.869	1	8	39360.29	−0.08	$20455_{1\frac{1}{2}}$—$59816^{3}_{1\frac{1}{2}}$	
2539.919	3	20	39359.52	−0.08	$20039_{3\frac{1}{2}}$—$59399^{3}_{4\frac{1}{2}}$	4
2540.101	1		39356.70	+0.18	$22194_{3\frac{1}{2}}$—$61550^{3}_{3\frac{1}{2}}$	
2540.431	1	4	39351.58	+0.03	$a\ ^4D_{3\frac{1}{2}}$—$54498^{3}_{3\frac{1}{2}}$	
2540.807		2	39345.76	−0.26	$18990_{1\frac{1}{2}}$—$58336^{3}_{2\frac{1}{2}}$	
2540.925	10*A*	4	39343.93	+0.07	$19404_{0\frac{1}{2}}$—$58747^{3}_{1\frac{1}{2}}$	
2541.063	6	20	39341.80	+0.19	$26929_{3\frac{1}{2}}$—$66270^{3}_{4\frac{1}{2}}$	
2542.598	1	30	39318.05	−0.11	$25672_{2\frac{1}{2}}$—$64990^{3}_{2\frac{1}{2}}$	6
2543.308	2	25	39307.07	−0.02	$25209_{4\frac{1}{2}}$—$64516^{3}_{4\frac{1}{2}}$	6
2544.658		1	39286.22	−0.18	$23046_{3\frac{1}{2}}$—$62333^{3}_{2\frac{1}{2}}$	
2546.283	3	30	39261.15			
2546.790	1	15	39253.33	+0.16	$a\ ^4G_{2\frac{1}{2}}$—$55488^{3}_{1\frac{1}{2}}$	res
2546.912	1	2	39251.45	+0.15	$18000_{3\frac{1}{2}}$—$57252^{3}_{2\frac{1}{2}}$	
2547.838		5	39237.19	+0.12	$20039_{3\frac{1}{2}}$—$59276^{3}_{3\frac{1}{2}}$	
2548.378	6	20	39228.88	+0.08	$a\ ^4D_{3\frac{1}{2}}$—$54375^{3}_{2\frac{1}{2}}$	
2548.690	1	6	39224.08	+0.02	$25672_{2\frac{1}{2}}$—$64896^{3}_{3\frac{1}{2}}$	
2549.096	5	15	39217.83	+0.08	$a\ ^6D_{2\frac{1}{2}}$—$42390^{3}_{3\frac{1}{2}}$	
2550.10		4	39202.38	+0.21	$23235_{4\frac{1}{2}}$—$62437^{3}_{4\frac{1}{2}}$	res
2550.295	5	8	39199.39	+0.07	$a\ ^4F_{4\frac{1}{2}}$—$54056^{3}_{4\frac{1}{2}}$	
2551.157	1	10	39186.15	−0.17	$22139_{2\frac{1}{2}}$—$61326^{3}_{3\frac{1}{2}}$	
2551.450		15	39181.65	−0.08	$a\ ^4D_{0\frac{1}{2}}$—$52355^{3}_{1\frac{1}{2}}$	res
2552.249	5	5	39169.38	0.00	$a\ ^4D_{2\frac{1}{2}}$—$54137^{3}_{1\frac{1}{2}}$	
2552.362	4	40	39167.65	−0.01	$26158_{4\frac{1}{2}}$—$65326^{3}_{3\frac{1}{2}}$	7
2553.168	70*A*	50	39155.29	+0.10	$a\ ^4F_{3\frac{1}{2}}$—$52567^{3}_{4\frac{1}{2}}$	res

TABLE 3. *Classified lines of* W II—Continued

Wavelength (Å)	Intensity		Wave number (cm^{-1})		Combination	Zeeman effect
	Arc	Spark	Observed	*O–C*		
Air						
2553.308	1	7	39153.14	−0.14	$20780_{4\frac{1}{2}}$—*59933*$^{\circ}_{3\frac{1}{2}}$	
2553.693		1	39147.24	−0.18	$25209_{4\frac{1}{2}}$—*64356*$^{\circ}_{3\frac{1}{2}}$	
2554.665	15	70	39132.34	−0.16	$23955_{3\frac{1}{2}}$—*63087*$^{\circ}_{6\frac{1}{2}}$	
				+0.13	$22194_{3\frac{1}{2}}$—*61326*$^{\circ}_{3\frac{1}{2}}$	
2554.864	40	60	39129.30	−0.11	$a\ ^6D_{0\frac{1}{2}}$—$z\ ^6F^{\circ}_{1\frac{1}{2}}$	
2555.106	40	100	39125.59	−0.09	$a\ ^6D_{2\frac{1}{2}}$—*42298*$^{\circ}_{1\frac{1}{2}}$	
2556.092		6	39110.50	−0.06	$19637_{2\frac{1}{2}}$—*58747*$^{\circ}_{1\frac{1}{2}}$	
2557.511		2	39088.80	+0.04	$18000_{3\frac{1}{2}}$—*57089*$^{\circ}_{4\frac{1}{2}}$	
2558.582		12	39072.44	+0.26	$19637_{2\frac{1}{2}}$—*58709*$^{\circ}_{3\frac{1}{2}}$	
2559.170		1	39063.46	−0.18	$22503_{1\frac{1}{2}}$—*61566*$^{\circ}_{2\frac{1}{2}}$	
2559.500	7	40	39058.43	+0.01	$a\ ^4D_{2\frac{1}{2}}$—*54026*$^{\circ}_{2\frac{1}{2}}$	6
2560.788		9	39038.78	0.00	$24991_{1\frac{1}{2}}$—*64030*$^{\circ}_{2\frac{1}{2}}$	
2562.244	1	9	39016.60	−0.04	$18990_{1\frac{1}{2}}$—*58007*$^{\circ}_{1\frac{1}{2}}$	6
2562.594	1	8	39011.27	+0.17	$23955_{3\frac{1}{2}}$—*62966*$^{\circ}_{3\frac{1}{2}}$	
2563.166	20	200	39002.57	−0.01	$a\ ^4G_{3\frac{1}{2}}$—*56439*$^{\circ}_{6\frac{1}{2}}$	4
2563.432		5	38998.52	+0.30	$25209_{4\frac{1}{2}}$—*64207*$^{\circ}_{4\frac{1}{2}}$	
2563.534	1	4	38996.97	−0.12	$27273_{3\frac{1}{2}}$—*66270*$^{\circ}_{4\frac{1}{2}}$	
2563.914	12	30	38991.19	−0.06	$a\ ^4F_{2\frac{1}{2}}$—*50292*$^{\circ}_{2\frac{1}{2}}$	6 res
2564.424		8	38983.43	−0.10	$24804_{3\frac{1}{2}}$—*63788*$^{\circ}_{3\frac{1}{2}}$	7
2565.834		7	38962.01	+0.01	$24918_{1\frac{1}{2}}$—*63880*$^{\circ}_{2\frac{1}{2}}$	
2567.320		1	38939.46	+0.03	$a\ ^4G_{5\frac{1}{2}}$—*56376*$^{\circ}_{5\frac{1}{2}}$	
2567.620	10	30	38934.92	−0.05	$a\ ^6S_{2\frac{1}{2}}$—*46355*$^{\circ}_{2\frac{1}{2}}$	6 res
2568.108	2	10	38927.52	+0.06	$a\ ^4G_{2\frac{1}{2}}$—*55162*$^{\circ}_{2\frac{1}{2}}$	
2568.850	10	30	38916.28	+0.03	$19070_{4\frac{1}{2}}$—*57986*$^{\circ}_{4\frac{1}{2}}$	6
2569.123	1	3	38912.14	0.00	$23803_{3\frac{1}{2}}$—*62715*$^{\circ}_{4\frac{1}{2}}$	
2569.298	8	80	38909.49	−0.03	$a\ ^4D_{3\frac{1}{2}}$—*54056*$^{\circ}_{4\frac{1}{2}}$	5
2570.701		2	38888.26	−0.28	$24991_{1\frac{1}{2}}$—*63880*$^{\circ}_{2\frac{1}{2}}$	
2571.459	50	150	38876.79	−0.14	$a\ ^6D_{2\frac{1}{2}}$—$z\ ^6F^{\circ}_{2\frac{1}{2}}$	res
2571.632	3	15	38874.18	−0.11	$18000_{3\frac{1}{2}}$—*56874*$^{\circ}_{2\frac{1}{2}}$	
2572.240	8	45	38864.99	0.00	$20534_{3\frac{1}{2}}$—*59399*$^{\circ}_{4\frac{1}{2}}$	
2572.366	8	30	38863.08	−0.24	$a\ ^4F_{3\frac{1}{2}}$—*52275*$^{\circ}_{3\frac{1}{2}}$	
2572.572		25	38859.97	−0.50	$25169_{1\frac{1}{2}}$—*64030*$^{\circ}_{2\frac{1}{2}}$	
2573.605		9	38844.38	−0.08	$26158_{4\frac{1}{2}}$—*65003*$^{\circ}_{4\frac{1}{2}}$	
2573.820	3	12	38841.13	−0.05	$a\ ^4P_{2\frac{1}{2}}$—*52275*$^{\circ}_{3\frac{1}{2}}$	
2573.952	15*A*	7	38839.14	−0.09	$a\ ^4G_{4\frac{1}{2}}$—*55392*$^{\circ}_{4\frac{1}{2}}$	
2576.168	7	30	38805.73	−0.08	$a\ ^4D_{1\frac{1}{2}}$—*53440*$^{\circ}_{0\frac{1}{2}}$	
2576.372	8	40	38802.66	−0.04	$a\ ^4G_{3\frac{1}{2}}$—*55392*$^{\circ}_{4\frac{1}{2}}$	
2577.308		5	38788.57	−0.05	$a\ ^4D_{1\frac{1}{2}}$—*53422*$^{\circ}_{1\frac{1}{2}}$	
2578.695	8	3	38767.71	−0.20	$18000_{3\frac{1}{2}}$—*56768*$^{\circ}_{3\frac{1}{2}}$	
2579.266	20	70	38759.13	−0.03	$23955_{3\frac{1}{2}}$—*62714*$^{\circ}_{3\frac{1}{2}}$	7
2579.497		20	38755.66	−0.32	$a\ ^4P_{0\frac{1}{2}}$—*47588*$^{\circ}_{1\frac{1}{2}}$	
				+0.20	$26929_{3\frac{1}{2}}$—*65684*$^{\circ}_{3\frac{1}{2}}$	
2579.542	20	100	38754.98	−0.01	$a\ ^6S_{2\frac{1}{2}}$—*46175*$^{\circ}_{3\frac{1}{2}}$	res
2581.140	2	8	38730.99	−0.09	$19276_{2\frac{1}{2}}$—*58007*$^{\circ}_{1\frac{1}{2}}$	
2581.206	18	30	38730.00	−0.02	$a\ ^6D_{4\frac{1}{2}}$—$z\ ^6F^{\circ}_{5\frac{1}{2}}$	
2582.527	1	5	38710.19	−0.04	$25169_{1\frac{1}{2}}$—*63880*$^{\circ}_{2\frac{1}{2}}$	
2582.746	1	4	38706.90	+0.01	$22194_{2\frac{1}{2}}$—*60900*$^{\circ}_{2\frac{1}{2}}$	
2583.520	3	5	38695.31	−0.04	$a\ ^4D_{1\frac{1}{2}}$—*53329*$^{\circ}_{1\frac{1}{2}}$	6
2584.236	12*A*	5	38684.59	+0.05	$25672_{2\frac{1}{2}}$—*64356*$^{\circ}_{3\frac{1}{2}}$	
2585.146		4	38670.97	+0.03	$29341_{4\frac{1}{2}}$—*68012*$^{\circ}_{5\frac{1}{2}}$	
2585.934	6	30	38659.18	−0.06	$19070_{4\frac{1}{2}}$—*57729*$^{\circ}_{3\frac{1}{2}}$	
2586.350	8	25	38652.97	+0.05	$a\ ^4P_{2\frac{1}{2}}$—*52087*$^{\circ}_{2\frac{1}{2}}$	6
2586.586	1	5	38649.44	−0.14	$a\ ^4P_{1\frac{1}{2}}$—*49242*$^{\circ}_{2\frac{1}{2}}$	
2587.367		6	38637.78	−0.06	$25672_{2\frac{1}{2}}$—*64310*$^{\circ}_{2\frac{1}{2}}$	
2587.676	2	9	38633.17	−0.03	$23803_{3\frac{1}{2}}$—*62437*$^{\circ}_{4\frac{1}{2}}$	
2589.171	30	90	38610.86	−0.08	$a\ ^6D_{4\frac{1}{2}}$—*44758*$^{\circ}_{3\frac{1}{2}}$	
2589.661	4	9	38603.56	+0.04	$19404_{0\frac{1}{2}}$—*58007*$^{\circ}_{1\frac{1}{2}}$	

TABLE 3. *Classified lines of* W II—Continued

Wavelength (Å)	Intensity		Wave number (cm^{-1})		Combination	Zeeman effect
	Arc	Spark	Observed	$O-C$		
Air						
2591. 229		2	38580. 20	+0. 02	$19276_{2\frac{1}{2}}$—$57856^{\circ}_{2\frac{1}{2}}$	
2591. 492	14	12	38576. 28	−0. 04	$a\ ^6D_{0\frac{1}{2}}$—$z\ ^2S^{\circ}_{0\frac{1}{2}}$	
2591. 738	1	4	38572. 62	−0. 01	$a\ ^4G_{3\frac{1}{2}}$—$55162^{\circ}_{2\frac{1}{2}}$	
2592. 458	3	3	38561. 91	−0. 07	$a\ ^4P_{1\frac{1}{2}}$—$49154^{\circ}_{0\frac{1}{2}}$	
2593. 686	1	2	38543. 65	−0. 05	$18000_{3\frac{1}{2}}$—$56544^{\circ}_{2\frac{1}{2}}$	
2594. 645		2	38529. 41	+0. 05	$23803_{3\frac{1}{2}}$—$62333^{\circ}_{2\frac{1}{2}}$	
2595. 506	2	7	38516. 63	+0. 09	$22139_{3\frac{1}{2}}$—$60656^{\circ}_{2\frac{1}{2}}$	7
2595. 580	5	5	38515. 53	−0. 37	$28187_{6\frac{1}{2}}$—$66703^{\circ}_{5\frac{1}{2}}$	
2595. 764	3	8	38512. 80	+0. 05	$a\ ^4F_{4\frac{1}{2}}$—$53369^{\circ}_{4\frac{1}{2}}$	6
2596. 867	3	15	38496. 44	+0. 01	$20780_{4\frac{1}{2}}$—$59276^{\circ}_{3\frac{1}{2}}$	7
2597. 866	2	25	38481. 64	0. 00	$23955_{5\frac{1}{2}}$—$62437^{\circ}_{4\frac{1}{2}}$	7
2598. 672	7A	7	38469. 71	−0. 06 −0. 01	$a\ ^4G_{2\frac{1}{2}}$—$54704^{\circ}_{2\frac{1}{2}}$ $a\ ^4G_{4\frac{1}{2}}$—$55022^{\circ}_{3\frac{1}{2}}$	
2598. 748	20	35	38468. 58	−0. 10	$a\ ^4F_{1\frac{1}{2}}$—$47179^{\circ}_{1\frac{1}{2}}$	
2599. 174	1−	1	38462. 27	−0. 16	$22194_{3\frac{1}{2}}$—$60656^{\circ}_{2\frac{1}{2}}$	
2599. 652	3	7	38455. 20	+0. 04	$a\ ^4D_{2\frac{1}{2}}$—$53422^{\circ}_{1\frac{1}{2}}$	
2599. 772	4	20	38453. 42	+0. 02	$19276_{2\frac{1}{2}}$—$57729^{\circ}_{3\frac{1}{2}}$	res
2601. 141	1	6	38433. 19	0. 00	$a\ ^4G_{3\frac{1}{2}}$—$55022^{\circ}_{3\frac{1}{2}}$	res
2601. 430	8	30	38428. 92	−0. 01	$a\ ^4P_{2\frac{1}{2}}$—$51863^{\circ}_{2\frac{1}{2}}$	
2602. 166	2	1	38418. 06	+0. 03	$a\ ^6D_{1\frac{1}{2}}$—$39936^{\circ}_{2\frac{1}{2}}$	
2602. 516	12	75	38412. 89	−0. 05	$18000_{3\frac{1}{2}}$—$56413^{\circ}_{4\frac{1}{2}}$	
2603. 018	20	120	38405. 48	+0. 04	$a\ ^4G_{4\frac{1}{2}}$—$54958^{\circ}_{5\frac{1}{2}}$	7
2603. 609		3	38396. 76	−0. 30	$26929_{3\frac{1}{2}}$—$65326^{\circ}_{3\frac{1}{2}}$	
2604. 042	2	6	38390. 38	+0. 04	$a\ ^4P_{1\frac{1}{2}}$—$48982^{\circ}_{1\frac{1}{2}}$	6
2605. 410	—?	5	38370. 23	−0. 02 +0. 01	$a\ ^4D_{2\frac{1}{2}}$—$53338^{\circ}_{3\frac{1}{2}}$ $19637_{2\frac{1}{2}}$—$58007^{\circ}_{1\frac{1}{2}}$	
2605. 973	7	15	38361. 94	+0. 05	$a\ ^4D_{2\frac{1}{2}}$—$53329^{\circ}_{1\frac{1}{2}}$	res
2606. 227		2?	38358. 20	+0. 02	$25672_{2\frac{1}{2}}$—$64030^{\circ}_{2\frac{1}{2}}$	
2606. 273	2	20	38357. 52	−0. 11 +0. 13	$26158_{4\frac{1}{2}}$—$64516^{\circ}_{4\frac{1}{2}}$ $20534_{5\frac{1}{2}}$—$58891^{\circ}_{5\frac{1}{2}}$	
2606. 472	4	40	38354. 59	0. 00	$23234_{4\frac{1}{2}}$—$61589^{\circ}_{5\frac{1}{2}}$	
2606. 974	4	12	38347. 21	−0. 07	$a\ ^4P_{0\frac{1}{2}}$—$47179^{\circ}_{1\frac{1}{2}}$	
2607. 822		20	38334. 74	+0. 04	$22139_{2\frac{1}{2}}$—$60474^{\circ}_{2\frac{1}{2}}$	7
2608. 440		5	38325. 66	−0. 04	$28377_{5\frac{1}{2}}$—$66703^{\circ}_{5\frac{1}{2}}$	
2609. 116	2	7	38315. 72	−0. 01	$23234_{4\frac{1}{2}}$—$61550^{\circ}_{3\frac{1}{2}}$	
2609. 250	4	40	38313. 76	+0. 02	$23046_{3\frac{1}{2}}$—$61360^{\circ}_{4\frac{1}{2}}$	5
2610. 370	1	3	38297. 32	−0. 08	$20039_{3\frac{1}{2}}$—$58356^{\circ}_{2\frac{1}{2}}$	
2611. 264	1	8	38284. 21	+0. 04	$22139_{2\frac{1}{2}}$—$60424^{\circ}_{3\frac{1}{2}}$	
2611. 510		1	38280. 60	+0. 01	$22194_{3\frac{1}{2}}$—$60474^{\circ}_{2\frac{1}{2}}$	
2611. 592	1	6	38279. 40	−0. 09	$23046_{3\frac{1}{2}}$—$61326^{\circ}_{3\frac{1}{2}}$	6
2612. 667	4	15	38263. 65	−0. 08	$a\ ^4G_{2\frac{1}{2}}$—$54498^{\circ}_{3\frac{1}{2}}$	
2612. 848		2	38261. 00	−0. 04	$18990_{1\frac{1}{2}}$—$57252^{\circ}_{2\frac{1}{2}}$	
2614. 956		2	38230. 16	+0. 10	$22194_{3\frac{1}{2}}$—$60424^{\circ}_{3\frac{1}{2}}$	
2615. 446	20	80	38223. 00	+0. 05	$a\ ^4D_{3\frac{1}{2}}$—$53369^{\circ}_{4\frac{1}{2}}$	
2615. 701	3	15	38219. 27	−0. 05	$19637_{2\frac{1}{2}}$—$57856^{\circ}_{2\frac{1}{2}}$	
2617. 162	1	2	38197. 94	−0. 02	$26158_{4\frac{1}{2}}$—$64356^{\circ}_{3\frac{1}{2}}$	
2617. 636		5	38191. 02	−0. 03	$a\ ^4D_{3\frac{1}{2}}$—$53338^{\circ}_{3\frac{1}{2}}$	6
2618. 072	1	7	38184. 66	−0. 27	$24804_{3\frac{1}{2}}$—$62989^{\circ}_{2\frac{1}{2}}$	
2619. 18	40A	15	38168. 50	−0. 14	$a\ ^4D_{1\frac{1}{2}}$—$52803^{\circ}_{1\frac{1}{2}}$	
2620. 215	50A	60	38153. 43	−0. 02	$22503_{1\frac{1}{2}}$—$60656^{\circ}_{2\frac{1}{2}}$	4
2620. 757	7	30	38145. 54	−0. 16	$a\ ^4D_{2\frac{1}{2}}$—$53113^{\circ}_{2\frac{1}{2}}$	res
2621. 074		2	38140. 93	−0. 05	$a\ ^4G_{2\frac{1}{2}}$—$54375^{\circ}_{2\frac{1}{2}}$	
2621. 601	5	12	38133. 26	−0. 01	$a\ ^6S_{2\frac{1}{2}}$—$45553^{\circ}_{1\frac{1}{2}}$	

TABLE 3. *Classified lines of* W II—Continued

Wavelength (Å)	Intensity		Wave number (cm^{-1})		Combination	Zeeman effect
	Arc	Spark	Observed	$O-C$		
Air						
2621.826		1	38129.99	+0.29	$26227_{2\frac{1}{2}}$—$64356^{3}_{3\frac{1}{2}}$	
2622.778	1	5	38116.15	−0.05	$23450_{2\frac{1}{2}}$—$61566^{2}_{2\frac{1}{2}}$	
2622.873	1	2	38114.77	−0.17	$a\ ^4G_{3\frac{1}{2}}$—$54704^{2}_{2\frac{1}{2}}$	
2623.114	6	50	38111.27	−0.09	$20780_{4\frac{1}{2}}$—$58891^{3}_{3\frac{1}{2}}$	
2623.890	2	8	38100.00	−0.10	$23450_{2\frac{1}{2}}$—$61550^{3}_{3\frac{1}{2}}$	res
2624.401		3	38092.58	+0.04	$19637_{2\frac{1}{2}}$—$57729^{3}_{3\frac{1}{2}}$	
2624.488	2	15	38091.32	−0.10	$23234_{4\frac{1}{2}}$—$61326^{3}_{3\frac{1}{2}}$	
2624.952		4	38084.59	−0.04	$22194_{3\frac{1}{2}}$—$60278^{4}_{3\frac{1}{2}}$	
2625.058		3	38083.05	+0.05	$26227_{2\frac{1}{2}}$—$64310^{2}_{2\frac{1}{2}}$	
2625.863		4	38071.38	−0.12	$24918_{1\frac{1}{2}}$—$62989^{2}_{2\frac{1}{2}}$	
2626.486		12	38062.35	−0.02	$22194_{3\frac{1}{2}}$—$60256^{3}_{3\frac{1}{2}}$	6
2626.851		3	38057.06	+0.04	$25209_{4\frac{1}{2}}$—$63266^{3}_{3\frac{1}{2}}$	
2627.722	4	10	38044.44	−0.08	$a\ ^4F_{4\frac{1}{2}}$—$52901^{3}_{3\frac{1}{2}}$	
2628.045	1	8	38039.76	0.00	$26929_{5\frac{1}{2}}$—$64969^{3}_{3\frac{1}{2}}$	
2628.996	7	35	38026.00	−0.07	$a\ ^4F_{3\frac{1}{2}}$—$51438^{2}_{2\frac{1}{2}}$	4
2629.496	1	5	38018.78	0.00	$19070_{4\frac{1}{2}}$—$57089^{3}_{4\frac{1}{2}}$	6
2630.177	3	7	38008.93	−0.07	$23046_{3\frac{1}{2}}$—$61055^{2}_{4\frac{1}{2}}$	7
2630.384	3	20	38005.94	0.00	$23234_{4\frac{1}{2}}$—$61240^{3}_{3\frac{1}{2}}$	
2630.534	6	9	38003.78	−0.15	$a\ ^4P_{2\frac{1}{2}}$—$51438^{2}_{2\frac{1}{2}}$	res
2630.946		2	37997.83	−0.21	$24991_{1\frac{1}{2}}$—$62989^{2}_{2\frac{1}{2}}$	
2632.485	35*A*	7	37975.61	+0.13	$19276_{2\frac{1}{2}}$—$57252^{3}_{2\frac{1}{2}}$	
2632.768	7?	7	37971.53	−0.08	$22503_{1\frac{1}{2}}$—$60474^{4}_{2\frac{1}{2}}$	
2633.886	4	25	37955.41	+0.06	$a\ ^4G_{3\frac{1}{2}}$—$55392^{4}_{4\frac{1}{2}}$	
2634.578	6	35	37945.45	+0.02	$a\ ^4G_{4\frac{1}{2}}$—$54498^{3}_{3\frac{1}{2}}$	
2635.379	6	30	37933.91	−0.01	$a\ ^4D_{2\frac{1}{2}}$—$52901^{3}_{3\frac{1}{2}}$	
2635.723		1	37928.96	−0.22	$20780_{4\frac{1}{2}}$—$58709^{3}_{3\frac{1}{2}}$	
2636.772	1	2	37913.87	−0.14	$a\ ^4F_{1\frac{1}{2}}$—$46625^{3}_{2\frac{1}{2}}$	
2636.953	1	20	37911.27	−0.04	$24804_{3\frac{1}{2}}$—$62715^{4}_{4\frac{1}{2}}$	
2637.209	—?	10	37907.59	+0.09	$20780_{4\frac{1}{2}}$—$58687^{3}_{4\frac{1}{2}}$	
2637.576	15*A*	25	37902.32	−0.04	$a\ ^4G_{2\frac{1}{2}}$—$54137^{1}_{1\frac{1}{2}}$	res
2638.220		7	37893.06	−0.09	$28377_{3\frac{1}{2}}$—$66270^{3}_{4\frac{1}{2}}$	
2638.870		1	37883.73	−0.30	$18990_{1\frac{1}{2}}$—$56874^{3}_{2\frac{1}{2}}$	
2639.052	1	3	37881.12	+0.07	$20455_{1\frac{1}{2}}$—$58336^{2}_{2\frac{1}{2}}$	
2639.432		1	37875.67	−0.12	$23450_{2\frac{1}{2}}$—$61326^{3}_{3\frac{1}{2}}$	
2641.076	2	8	37852.09	−0.14	$22139_{2\frac{1}{2}}$—$59992^{2}_{2\frac{1}{2}}$	6
2643.086	—?	10	37823.31	−0.13	$a\ ^4F_{2\frac{1}{2}}$—$49124^{3}_{3\frac{1}{2}}$	
2643.253	1	10	37820.92	−0.01	$23234_{4\frac{1}{2}}$—$61055^{2}_{4\frac{1}{2}}$	
2643.296	4	30	37820.31	+0.01	$a\ ^4P_{2\frac{1}{2}}$—$51254^{1}_{1\frac{1}{2}}$	
2645.692	25*A*	7	37786.06	−0.09	$a\ ^4G_{3\frac{1}{2}}$—$54375^{3}_{3\frac{1}{2}}$	
2647.309	1	4	37762.98	+0.12	$23803_{3\frac{1}{2}}$—$61566^{2}_{2\frac{1}{2}}$	
2647.726	7	70	37757.03	−0.19	$25209_{4\frac{1}{2}}$—$62966^{3}_{3\frac{1}{2}}$	4
2647.894	1	2	37754.63	−0.09	$a\ ^4D_{3\frac{1}{2}}$—$52901^{3}_{3\frac{1}{2}}$	
2648.453		2	37746.67	−0.09	$23803_{3\frac{1}{2}}$—$61550^{3}_{3\frac{1}{2}}$	
2648.958		2	37739.47	−0.11	$22194_{3\frac{1}{2}}$—$59933^{3}_{3\frac{1}{2}}$	
2649.682	1	10	37729.16	−0.01	$22139_{2\frac{1}{2}}$—$59869^{3}_{3\frac{1}{2}}$	
2650.276	3	7	37720.70	−0.05	$a\ ^4D_{1\frac{1}{2}}$—$52355^{0}_{1\frac{1}{2}}$	
2650.580	1	3	37716.38	−0.08	$27273_{3\frac{1}{2}}$—$64990^{2}_{2\frac{1}{2}}$	
2651.035	1	8	37709.90	−0.03	$a\ ^4F_{4\frac{1}{2}}$—$52567^{4}_{4\frac{1}{2}}$	6
2651.881	4	30	37697.87	−0.06	$19070_{4\frac{1}{2}}$—$56768^{3}_{3\frac{1}{2}}$	
2542.298	1	3	37691.95	−0.01	$a\ ^4P_{1\frac{1}{2}}$—$48284^{2}_{2\frac{1}{2}}$	
2652.433		4	37690.03	−0.15	$20039_{3\frac{1}{2}}$—$57729^{3}_{3\frac{1}{2}}$	
2653.015	10*A*	8	37681.76	−0.02	$a\ ^4F_{2\frac{1}{2}}$—$48982^{1}_{1\frac{1}{2}}$	
2653.424	7	35	37675.96	+0.04	$a\ ^4G_{4\frac{1}{2}}$—$54229^{3}_{3\frac{1}{2}}$	
2653.568	10	35	37673.91	−0.04	$a\ ^6D_{3\frac{1}{2}}$—$42390^{3}_{3\frac{1}{2}}$	
2654.841	1	5	37655.84	+0.09	$19276_{2\frac{1}{2}}$—$56932^{1}_{1\frac{1}{2}}$	

TABLE 3. *Classified lines of* W II—Continued

Wavelength (Å)	Intensity		Wave number (cm^{-1})		Combination	Zeeman effect
	Arc	Spark	Observed	$O-C$		
Air						
2655. 485	3	25	37646. 71	−0. 07	$23955_{5\frac{1}{2}}$—*61602*$^{\circ}_{3\frac{1}{2}}$	
2655. 667	15	20	37644. 13	−0. 01	*a* $^4F_{1\frac{1}{2}}$—*46355*$^{\circ}_{2\frac{1}{2}}$	
2656. 027		10	27639. 03	−0. 06	$28631_{3\frac{1}{2}}$—*66270*$^{\circ}_{4\frac{1}{2}}$	
2656. 435	—?	8	37633. 25	−0. 04	*a* $^4F_{3\frac{1}{2}}$—*51045*$^{\circ}_{3\frac{1}{2}}$	
2656. 706		10	37629. 41	−0. 05	$26158_{4\frac{1}{2}}$—*63788*$^{\circ}_{3\frac{1}{2}}$	
2657. 745	1	6	37614. 71	+0. 09	$19637_{2\frac{1}{2}}$—*57252*$^{\circ}_{3\frac{1}{2}}$	
2658. 036	25	100	37610. 59	−0. 04	*a* $^6D_{1\frac{1}{2}}$—*z* $^6F^{\circ}_{1\frac{1}{2}}$	res
2659. 171	1?	10	37594. 53	+0. 39	$25672_{3\frac{1}{2}}$—*63266*$^{\circ}_{3\frac{1}{2}}$	
2659. 703	1	15	37587. 02	−0. 01	$26929_{5\frac{1}{2}}$—*64516*$^{\circ}_{4\frac{1}{2}}$	
2661. 852	1	20	37556. 67	−0. 03	$23803_{3\frac{1}{2}}$—*61360*$^{\circ}_{4\frac{1}{2}}$	
2662. 214	3	30	37551. 57	−0. 10	$20455_{1\frac{1}{2}}$—*58007*$^{\circ}_{1\frac{1}{2}}$	res
2663. 874	2	15	37528. 17	−0. 02	$19404_{0\frac{1}{2}}$—*56932*$^{\circ}_{1\frac{1}{2}}$	
2664. 346	80	200	37521. 52	−0. 04	*a* $^4G_{3\frac{1}{2}}$—*54958*$^{\circ}_{3\frac{1}{2}}$	
2665. 644	2	8	27503. 25	−0. 15	*a* $^4G_{4\frac{1}{2}}$—*54056*$^{\circ}_{4\frac{1}{2}}$	
2666. 086	1	40	37497. 03	−0. 17	$28187_{6\frac{1}{2}}$—*65684*$^{\circ}_{5\frac{1}{2}}$	
2666. 446	8	?	37491. 97	−0. 12	$19276_{2\frac{1}{2}}$—*56768*$^{\circ}_{3\frac{1}{2}}$	
2666. 493	20	60	37491. 31	+0. 11	*a* $^6S_{2\frac{1}{2}}$—*44911*$^{\circ}_{1\frac{1}{2}}$	
2668. 245	1	5	37466. 69	−0. 18	*a* $^4G_{3\frac{1}{2}}$—*54056*$^{\circ}_{4\frac{1}{2}}$	
2668. 961	5	5	37456. 64	−0. 11	*a* $^6S_{2\frac{1}{2}}$—*z* $^6F^{\circ}_{3\frac{1}{2}}$	
2669. 250	10	25	37452. 59	−0. 07	*a* $^4D_{1\frac{1}{2}}$—*52087*$^{\circ}_{2\frac{1}{2}}$	
2669. 371	5	30	37450. 89	−0. 20	*a* $^4F_{3\frac{1}{2}}$—*50863*$^{\circ}_{4\frac{1}{2}}$	
2670. 395	10	50	37436. 52	−0. 04	*a* $^4G_{3\frac{1}{2}}$—*54026*$^{\circ}_{2\frac{1}{2}}$	
2671. 040		2	37427. 49	−0. 38	$23046_{3\frac{1}{2}}$—*60474*$^{\circ}_{2\frac{1}{2}}$	
2671. 580	8	18	37419. 92	−0. 21	*a* $^4D_{3\frac{1}{2}}$—*52567*$^{\circ}_{4\frac{1}{2}}$	
2672. 647		15	37404. 98	−0. 16	$23955_{5\frac{1}{2}}$—*61360*$^{\circ}_{4\frac{1}{2}}$	
2672. 956	1	3	37400. 66	−0. 11	$20455_{1\frac{1}{2}}$—*57856*$^{\circ}_{2\frac{1}{2}}$	
2673. 608	20	60	37391. 54	−0. 13	$18000_{3\frac{1}{2}}$—*55392*$^{\circ}_{4\frac{1}{2}}$	res
2674. 471		4	37379. 48	0. 00	$30633_{4\frac{1}{2}}$—*68012*$^{\circ}_{5\frac{1}{2}}$	
2674. 628		10	37377. 29	−0. 05	$23046_{3\frac{1}{2}}$—*60424*$^{\circ}_{3\frac{1}{2}}$	
2675. 734	1	20	37361. 84	−0. 10	$29341_{4\frac{1}{2}}$—*66703*$^{\circ}_{5\frac{1}{2}}$	
2677. 579	3	6	37336. 10	−0. 12	$19276_{2\frac{1}{2}}$—*56612*$^{\circ}_{3\frac{1}{2}}$	
2677. 796	20	60	37333. 07	−0. 06	*a* $^6D_{3\frac{1}{2}}$—*z* $^6F^{\circ}_{2\frac{1}{2}}$	
2679. 638	20	70	37307. 41	−0. 05	*a* $^4D_{2\frac{1}{2}}$—*52275*$^{\circ}_{3\frac{1}{2}}$	
2679. 758	3	18	37305. 74	−0. 03	$19070_{4\frac{1}{2}}$—*56376*$^{\circ}_{3\frac{1}{2}}$	
2680. 546		10	37294. 77	−0. 12	$19637_{2\frac{1}{2}}$—*56932*$^{\circ}_{1\frac{1}{2}}$	
2681. 568		2	37280. 55	+0. 05	$22535_{0\frac{1}{2}}$—*59816*$^{\circ}_{1\frac{1}{2}}$	
2681. 730		1	37278. 30	+0. 14	$26929_{5\frac{1}{2}}$—*64207*$^{\circ}_{4\frac{1}{2}}$	
2683. 226	8	80	37257. 52	−0. 05	*a* $^4D_{0\frac{1}{2}}$—*50430*$^{\circ}_{1\frac{1}{2}}$	
2683. 512	1	35	37253. 56			
2683. 632	4	30	37251. 89	−0. 07	$23803_{3\frac{1}{2}}$—*61055*$^{\circ}_{4\frac{1}{2}}$	
2684. 301	12	20	37242. 60	+0. 09	$27273_{3\frac{1}{2}}$—*64516*$^{\circ}_{4\frac{1}{2}}$	
2685. 068	12	25	37231. 96	+0. 05	$23046_{3\frac{1}{2}}$—*60278*$^{\circ}_{4\frac{1}{2}}$	
2685. 366	6	12	37227. 84	+0. 08	$25209_{4\frac{1}{2}}$—*62437*$^{\circ}_{4\frac{1}{2}}$	
2686. 946	4	100	37205. 95	−0. 06	$23450_{2\frac{1}{2}}$—*60656*$^{\circ}_{2\frac{1}{2}}$	res
2687. 000	5	70	37205. 20	−0. 06	$22194_{3\frac{1}{2}}$—*59399*$^{\circ}_{4\frac{1}{2}}$	
2688. 230	7	35	37188. 17	+0. 03	*a* $^4G_{2\frac{1}{2}}$—*53422*$^{\circ}_{1\frac{1}{2}}$	
2690. 036		2	37163. 21	−0. 12	$25169_{1\frac{1}{2}}$—*62333*$^{\circ}_{2\frac{1}{2}}$	
2690. 153	—?	1	37161. 59	−0. 01	$18000_{3\frac{1}{2}}$—*55162*$^{\circ}_{2\frac{1}{2}}$	
2690. 710	2	35	37153. 90			
2691. 952	2	5	37136. 74	−0. 10	$22139_{2\frac{1}{2}}$—*59276*$^{\circ}_{3\frac{1}{2}}$	
2692. 358	4	18	37131. 14	−0. 09	$19637_{2\frac{1}{2}}$—*56768*$^{\circ}_{3\frac{1}{2}}$	
2693. 228		1	37119. 14	−0. 06	*a* $^4D_{2\frac{1}{2}}$—*52087*$^{\circ}_{2\frac{1}{2}}$	
2694. 080		4?	37107. 40	−0. 16	$26158_{4\frac{1}{2}}$—*63266*$^{\circ}_{3\frac{1}{2}}$	
2694. 382	20	60	37103. 24	+0. 01	*a* $^4G_{2\frac{1}{2}}$—*53338*$^{\circ}_{3\frac{1}{2}}$	
2694. 594	6	70	37100. 32	−0. 08	$23955_{5\frac{1}{2}}$—*61055*$^{\circ}_{4\frac{1}{2}}$	

TABLE 3. *Classified lines of* W II—Continued

Wavelength (Å)	Intensity		Wave number (cm^{-1})		Combination	Zeeman effect
	Arc	Spark	Observed	*O–C*		
Air						
2694.828	2	6	37097.10	−0.03	$23803_{3\frac{1}{2}}$—*60900*$^{\circ}_{2\frac{1}{2}}$	
2694.994	6	30	37094.82	−0.05	*a* $^4G_{2\frac{1}{2}}$—*53329*$^{\circ}_{1\frac{1}{2}}$	
2695.111		1	37093.21	−0.13	$18990_{1\frac{1}{2}}$—*56084*$^{\circ}_{1\frac{1}{2}}$	
2695.874	3	10	37082.72	−0.01	$22194_{3\frac{1}{2}}$—*59276*$^{\circ}_{3\frac{1}{2}}$	
2696.914	2	35	37068.41			6
2697.714	80	160	37057.42	−0.12	*a* $^6D_{1\frac{1}{2}}$—*z* $^2S^{\circ}_{0\frac{1}{2}}$	res
2698.265	1	1?	37049.86	+0.14	$20039_{2\frac{1}{2}}$—*57089*$^{\circ}_{1\frac{1}{2}}$	
2698.706	1	3	37043.80	−0.04	$23234_{4\frac{1}{2}}$—*60278*$^{\circ}_{4\frac{1}{2}}$	
2699.041	8	12	37039.21	−0.09	$26227_{2\frac{1}{2}}$—*63266*$^{\circ}_{3\frac{1}{2}}$	
2699.270	1	10	37036.06	−0.08	$27273_{3\frac{1}{2}}$—*64310*$^{\circ}_{2\frac{1}{2}}$	
2700.320	3	50	37021.67	+0.09	$23234_{4\frac{1}{2}}$—*60256*$^{\circ}_{3\frac{1}{2}}$	res
2701.036	8*A*	10	37011.85	−0.29	$28631_{3\frac{1}{2}}$—*65644*$^{\circ}_{3\frac{1}{2}}$	
2701.485	20	60	37005.70	−0.11	*a* $^4F_{4\frac{1}{2}}$—*51863*$^{\circ}_{3\frac{1}{2}}$	
2702.115	25	250	36997.07	+0.01	$19442_{6\frac{1}{2}}$—*56439*$^{\circ}_{6\frac{1}{2}}$	6
2702.188	4	?	36996.07	−0.05	*a* $^4P_{1\frac{1}{2}}$—*47588*$^{\circ}_{1\frac{1}{2}}$	
2703.066	8	60	36984.05	+0.08	$23234_{4\frac{1}{2}}$—*60218*$^{\circ}_{5\frac{1}{2}}$	
2703.118	8	10	36983.36	−0.04	*a* $^4F_{2\frac{1}{2}}$—*48284*$^{\circ}_{3\frac{1}{2}}$	
2703.467	12	120	36978.57	+0.13	$31100_{5\frac{1}{2}}$—*68078*$^{\circ}_{6\frac{1}{2}}$	5
2703.698	1	5	36975.41	+0.05	$19637_{2\frac{1}{2}}$—*56612*$^{\circ}_{3\frac{1}{2}}$	
2703.829		1	36973.62	−0.02	$23450_{2\frac{1}{2}}$—*60424*$^{\circ}_{3\frac{1}{2}}$	
2705.599	10	35	36949.43	−0.11	$20780_{4\frac{1}{2}}$—*57729*$^{\circ}_{3\frac{1}{2}}$	
2705.895		12	36945.40	0.00	$23046_{3\frac{1}{2}}$—*59992*$^{\circ}_{3\frac{1}{2}}$	
2706.702	6	?	36934.38	−0.01	*a* $^6S_{2\frac{1}{2}}$—*44354*$^{\circ}_{2\frac{1}{2}}$	
2706.733		50	36933.95	+0.04	$19442_{6\frac{1}{2}}$—*56376*$^{\circ}_{5\frac{1}{2}}$	
2707.067		25	36929.40	+0.01	$29341_{4\frac{1}{2}}$—*66270*$^{\circ}_{4\frac{1}{2}}$	6
2708.360	4*A*	2	36911.77	−0.27	$31100_{5\frac{1}{2}}$—*68012*$^{\circ}_{5\frac{1}{2}}$	
2709.582	20	80	36895.12	−0.09	*a* $^4D_{2\frac{1}{2}}$—*51863*$^{\circ}_{3\frac{1}{2}}$	
2710.678	2	1	36880.20	−0.17	*a* $^4F_{3\frac{1}{2}}$—*50292*$^{\circ}_{2\frac{1}{2}}$	
2710.792	5	40	36878.65	−0.03	*a* $^4G_{2\frac{1}{2}}$—*53113*$^{\circ}_{2\frac{1}{2}}$	6 res
2711.336		3	36871.26	−0.16	$28118_{2\frac{1}{2}}$—*64990*$^{\circ}_{3\frac{1}{2}}$	
2712.704	5	50	36852.66	−0.01	$23803_{3\frac{1}{2}}$—*60656*$^{\circ}_{2\frac{1}{2}}$	
2713.478	4	2	36842.15	−0.29	*a* $^4F_{1\frac{1}{2}}$—*45553*$^{\circ}_{1\frac{1}{2}}$	
2714.016		1	36834.85	−0.40	$20039_{3\frac{1}{2}}$—*56874*$^{\circ}_{2\frac{1}{2}}$	
2714.950	1	5	36822.18	−0.16	$23046_{3\frac{1}{2}}$—*59869*$^{\circ}_{3\frac{1}{2}}$	
2715.346	25	80	36816.81	−0.02	*a* $^4G_{4\frac{1}{2}}$—*53369*$^{\circ}_{4\frac{1}{2}}$	6
2716.020	2	3	36807.67	−0.11 −0.09	$19276_{2\frac{1}{2}}$—*56084*$^{\circ}_{1\frac{1}{2}}$ $26158_{4\frac{1}{2}}$—*62966*$^{\circ}_{5\frac{1}{2}}$	
2716.147	3	15	36805.95	0.00	$23450_{2\frac{1}{2}}$—*60256*$^{\circ}_{3\frac{1}{2}}$	
2716.322	30	80	36803.58	−0.09	*a* $^4D_{1\frac{1}{2}}$—*51438*$^{\circ}_{2\frac{1}{2}}$	
2716.890	35*A*	35	36795.90	−0.17	$20455_{1\frac{1}{2}}$—*57252*$^{\circ}_{2\frac{1}{2}}$	
2717.180	10	40	36791.96	−0.08	*a* $^4G_{5\frac{1}{2}}$—*54229*$^{\circ}_{5\frac{1}{2}}$	6 res
2717.702	3	18	36784.90	−0.03	*a* $^4G_{4\frac{1}{2}}$—*53338*$^{\circ}_{3\frac{1}{2}}$	
2718.044	30	120	36780.26	−0.04	*a* $^4G_{3\frac{1}{2}}$—*53369*$^{\circ}_{4\frac{1}{2}}$	4
2718.257		2	36777.38	+0.06	$28118_{2\frac{1}{2}}$—*64896*$^{\circ}_{3\frac{1}{2}}$	
2719.232	8	3	36764.20	−0.09	*a* $^6D_{2\frac{1}{2}}$—*39936*$^{\circ}_{2\frac{1}{2}}$	
2719.392		10	36762.03	0.00	$24804_{3\frac{1}{2}}$—*61566*$^{\circ}_{2\frac{1}{2}}$	
2719.798		1	36756.54	+0.06	$27273_{3\frac{1}{2}}$—*64030*$^{\circ}_{2\frac{1}{2}}$	
2720.404	6	30	36748.36	−0.04	*a* $^4G_{3\frac{1}{2}}$—*53338*$^{\circ}_{3\frac{1}{2}}$	6
2720.594		40	36745.80	+0.04	*a* $^4F_{1\frac{1}{2}}$—*45457*$^{\circ}_{0\frac{1}{2}}$	
2721.850	4	15	36728.83	−0.04	$20039_{3\frac{1}{2}}$—*56768*$^{\circ}_{3\frac{1}{2}}$	
2722.805	20	70	36715.95	−0.06	*a* $^4D_{3\frac{1}{2}}$—*51863*$^{\circ}_{3\frac{1}{2}}$	6
2723.704	3	5	36703.84	−0.07	$18000_{3\frac{1}{2}}$—*54704*$^{\circ}_{2\frac{1}{2}}$	
2724.081	5	60	36698.75	−0.04	$23234_{4\frac{1}{2}}$—*59933*$^{\circ}_{3\frac{1}{2}}$	
2725.457		8	36680.23	+0.01	$19404_{0\frac{1}{2}}$—*56084*$^{\circ}_{1\frac{1}{2}}$	
2726.445	3	4	36666.94	+0.04	*a* $^4G_{2\frac{1}{2}}$—*52901*$^{\circ}_{3\frac{1}{2}}$	
2728.880	1	6	36634.22	−0.05	$23234_{4\frac{1}{2}}$—*59869*$^{\circ}_{3\frac{1}{2}}$	
2729.532	1	6	36625.48	+0.08	$28377_{5\frac{1}{2}}$—*65003*$^{\circ}_{3\frac{1}{2}}$	

TABLE 3. *Classified lines of* W II—Continued

Wavelength (Å)	Intensity		Wave number (cm^{-1})		Combination	Zeeman effect
	Arc	Spark	Observed	$O-C$		
Air						
2729.620	25	75	36624.30	−0.06	$a\ ^4P_{0\frac{1}{2}}$—$45457^{3}_{1\frac{1}{2}}$	res
2729.936	5	30	36620.06	+0.02	$a\ ^4D_{1\frac{1}{2}}$—$51254^{1}_{1\frac{1}{2}}$	
2730.846	3	8	36607.86	−0.11	$22139_{2\frac{1}{2}}$—$58747^{2}_{1\frac{1}{2}}$	
2732.078	2	8	36591.35	+0.05	$28377_{3\frac{1}{2}}$—$64969^{3}_{3\frac{1}{2}}$	6
2732.378	4	4	36587.33	−0.09	$a\ ^4P_{1\frac{1}{2}}$—$47179^{1}_{1\frac{1}{2}}$	6
2733.448	5	35	36573.01	+0.01	$20039_{3\frac{1}{2}}$—$56612^{2}_{3\frac{1}{2}}$	6
2733.704		3	36569.58	−0.01	$22139_{2\frac{1}{2}}$—$58709^{3}_{3\frac{1}{2}}$	
2734.627		3	36557.24	0.00	$26158_{4\frac{1}{2}}$—$62715^{4}_{3\frac{1}{2}}$	
2734.737	5	40	36555.77	−0.10	$24804_{3\frac{1}{2}}$—$61360^{4}_{4\frac{1}{2}}$	
2735.784	2	10	36541.78	+0.08	$23450_{2\frac{1}{2}}$—$59992^{3}_{2\frac{1}{2}}$	6
2737.135	1	3	36523.74	−0.11	$a\ ^4G_{3\frac{1}{2}}$—$53113^{2}_{3\frac{1}{2}}$	
2737.756	2	5	36515.46	−0.02	$22194_{3\frac{1}{2}}$—$58709^{3}_{3\frac{1}{2}}$	
2737.840		3	36514.34	0.00	$27273_{3\frac{1}{2}}$—$63788^{3}_{3\frac{1}{2}}$	
2738.962	1	5	36499.38	+0.06	$28491_{1\frac{1}{2}}$—$64990^{2}_{2\frac{1}{2}}$	7
2739.080	4	4	36497.81	−0.06	$18000_{3\frac{1}{2}}$—$54498^{3}_{3\frac{1}{2}}$	
2739.140	4	15	36497.01	−0.04	$18990_{1\frac{1}{2}}$—$55488^{1}_{1\frac{1}{2}}$	7
2739.384	6	30	36493.76	−0.04	$22194_{3\frac{1}{2}}$—$58687^{3}_{3\frac{1}{2}}$	
2740.187	6	20	36483.06	−0.10	$23450_{2\frac{1}{2}}$—$59933^{3}_{3\frac{1}{2}}$	
2740.801	20	200	36474.90	+0.03	$23803_{3\frac{1}{2}}$—$60278^{4}_{4\frac{1}{2}}$	4
2742.471	15	30	36452.68	+0.07	$23803_{3\frac{1}{2}}$—$60256^{3}_{3\frac{1}{2}}$	6 res
2742.903	8	40	36446.94	+0.02	$19637_{2\frac{1}{2}}$—$56084^{1}_{1\frac{1}{2}}$	
2745.036	2	30	36418.62	−0.02	$23450_{2\frac{1}{2}}$—$59869^{3}_{3\frac{1}{2}}$	4 res
2748.312	20	15	36375.21	+0.09	$18000_{3\frac{1}{2}}$—$54375^{2}_{2\frac{1}{2}}$	res
2748.418	2	12	36373.82	−0.08	$20039_{3\frac{1}{2}}$—$56413^{4}_{4\frac{1}{2}}$	
2750.023	1	9	36352.61	+0.07	$23046_{3\frac{1}{2}}$—$59399^{4}_{4\frac{1}{2}}$	
2750.325	10	20	36348.60	0.00	$a\ ^4G_{4\frac{1}{2}}$—$52901^{3}_{3\frac{1}{2}}$	res
2750.728	2	15	36343.28	+0.04	$29341_{4\frac{1}{2}}$—$65684^{3}_{3\frac{1}{2}}$	
2750.880	3	12	36341.28	−0.04	$25209_{4\frac{1}{2}}$—$61550^{3}_{3\frac{1}{2}}$	
2752.242	5	30	36323.28	−0.03	$23955_{3\frac{1}{2}}$—$60278^{4}_{4\frac{1}{2}}$	7
2752.360	1?	2	36321.72	+0.03	$19070_{4\frac{1}{2}}$—$55392^{4}_{4\frac{1}{2}}$	
2753.094		6	36312.03	−0.04	$a\ ^4G_{3\frac{1}{2}}$—$52901^{3}_{3\frac{1}{2}}$	
2753.320	6	25	36309.05	−0.03	$20780_{4\frac{1}{2}}$—$57089^{3}_{3\frac{1}{2}}$	7
2753.826		6	36302.37	−0.07	$29341_{4\frac{1}{2}}$—$65644^{3}_{4\frac{1}{2}}$	
2754.695	1	2	36290.93	−0.08	$a\ ^4D_{3\frac{1}{2}}$—$51438^{2}_{2\frac{1}{2}}$	
2755.036	1	3	36286.44	−0.14	$a\ ^4D_{2\frac{1}{2}}$—$51254^{1}_{1\frac{1}{2}}$	
2755.661		6	36278.21	−0.09	$26158_{4\frac{1}{2}}$—$62437^{3}_{4\frac{1}{2}}$	
2756.776	2	20	36263.54	+0.10	$23955_{3\frac{1}{2}}$—$60218^{3}_{3\frac{1}{2}}$	6
2757.710		6	36251.26	+0.13	$24804_{3\frac{1}{2}}$—$61055^{3}_{3\frac{1}{2}}$	
2758.182		4	36245.05	+0.17	$22503_{1\frac{1}{2}}$—$58747^{1}_{1\frac{1}{2}}$	
2758.333	18	20	36234.07	−0.04	$a\ ^6D_{4\frac{1}{2}}$—$42390^{3}_{3\frac{1}{2}}$	res
2759.338	1	10	36229.87	−0.14	$23046_{3\frac{1}{2}}$—$59276^{3}_{3\frac{1}{2}}$	7
2760.691	3	15	36212.11	−0.03	$22535_{0\frac{1}{2}}$—$58747^{1}_{1\frac{1}{2}}$	6
2760.742	12*A*	10	36211.44	−0.05	$19276_{2\frac{1}{2}}$—$55488^{1}_{1\frac{1}{2}}$	
2761.587	40	100	36200.37	0.00	$a\ ^4F_{1\frac{1}{2}}$—$44911^{1}_{1\frac{1}{2}}$	res
2761.837	2	6	36197.09	+0.08	$22139_{2\frac{1}{2}}$—$58336^{2}_{2\frac{1}{2}}$	
2762.499	6	15	36188.42	+0.06	$23803_{3\frac{1}{2}}$—$59992^{3}_{2\frac{1}{2}}$	
2764.263	200	400	36165.33	−0.02	$a\ ^6D_{0\frac{1}{2}}$—$z\ ^6F^{0}_{0\frac{1}{2}}$	
2764.768	8	50	36158.72	+0.16	$26929_{5\frac{1}{2}}$—$63087^{6}_{5\frac{1}{2}}$	5
2765.340	2	10	36151.24	−0.02	$25209_{4\frac{1}{2}}$—$61360^{4}_{4\frac{1}{2}}$	6
2765.986		1	36142.80	−0.10	$22194_{3\frac{1}{2}}$—$58336^{2}_{2\frac{1}{2}}$	
2766.318	1	35	36138.46	−0.11	$28377_{5\frac{1}{2}}$—$64516^{4}_{4\frac{1}{2}}$	7
2766.981	4	35	36129.80	−0.02	$23803_{3\frac{1}{2}}$—$59933^{3}_{3\frac{1}{2}}$	6
2767.967	4	25	36116.93	−0.08	$25209_{4\frac{1}{2}}$—$61326^{3}_{3\frac{1}{2}}$	
2768.326	30	50	36112.25	0.00	$a\ ^4F_{2\frac{1}{2}}$—$47413^{3}_{2\frac{1}{2}}$	6
2770.496	2	5	36083.96	+0.03	$19404_{0\frac{1}{2}}$—$55488^{1}_{1\frac{1}{2}}$	

TABLE 3. *Classified lines of* W II—Continued

Wavelength (Å)	Intensity		Wave number (cm^{-1})		Combination	Zeeman effect
	Arc	Spark	Observed	*O–C*		
Air						
2771.005	5	20	36077.34	−0.09	$a\ ^4D_{2\frac{1}{2}}$—$51045^{\circ}_{3\frac{1}{2}}$	
2771.531	5	3	36070.50	+0.02	$30633_{4\frac{1}{2}}$—$66703^{\circ}_{3\frac{1}{2}}$	
2771.927	2	6	36065.34	+0.04	$23803_{3\frac{1}{2}}$—$59869^{\circ}_{3\frac{1}{2}}$	
2772.658	2	8	36055.83	−0.01	$18000_{3\frac{1}{2}}$—$54056^{\circ}_{4\frac{1}{2}}$	
2773.849	5	25	36040.35	−0.09	$a\ ^4G_{2\frac{1}{2}}$—$52275^{\circ}_{3\frac{1}{2}}$	
2774.092	?	30	36037.20	+0.04	$26929_{5\frac{1}{2}}$—$62966^{\circ}_{5\frac{1}{2}}$	
2774.433		10?	36032.76	+0.01	$a\ ^4P_{1\frac{1}{2}}$—$46625^{\circ}_{0\frac{1}{2}}$	
2774.988	6	20	36025.56	+0.02	$18000_{3\frac{1}{2}}$—$54026^{\circ}_{2\frac{1}{2}}$	
2775.878	1	5	36014.01	0.00	$a\ ^4G_{4\frac{1}{2}}$—$52567^{\circ}_{4\frac{1}{2}}$	
2776.509	20	100	36005.84	+0.01	$a\ ^4F_{4\frac{1}{2}}$—$50863^{\circ}_{4\frac{1}{2}}$	6
2777.536	2	10	35992.51	+0.07	$27273_{3\frac{1}{2}}$—$63266^{\circ}_{3\frac{1}{2}}$	
2777.870	8	30	35988.18	−0.05	$20780_{4\frac{1}{2}}$—$56768^{\circ}_{3\frac{1}{2}}$	
2778.124		2	35984.90	+0.06	$29341_{4\frac{1}{2}}$—$65326^{\circ}_{3\frac{1}{2}}$	
2778.281		3	35982.86	−0.01	$24918_{1\frac{1}{2}}$—$60900^{\circ}_{2\frac{1}{2}}$	
2778.429	5	6	35980.95	−0.17	$a\ ^4D_{0\frac{1}{2}}$—$49154^{\circ}_{0\frac{1}{2}}$	
2778.694	20	80	35977.51	+0.03	$a\ ^4G_{3\frac{1}{2}}$—$52567^{\circ}_{4\frac{1}{2}}$	res
2780.285	60.*A*	40	35956.94	+0.05	$a\ ^6D_{2\frac{1}{2}}$—$z\ ^6F^{\circ}_{1\frac{1}{2}}$	res
2782.142	20	80	35932.93	−0.02	$a\ ^4G_{5\frac{1}{2}}$—$53369^{\circ}_{4\frac{1}{2}}$	
2783.979	2	6	35909.22	−0.19	$24991_{1\frac{1}{2}}$—$60900^{\circ}_{2\frac{1}{2}}$	
2784.290	2	15	35905.21	−0.04	$20534_{3\frac{1}{2}}$—$56439^{\circ}_{0\frac{1}{2}}$	
2785.126	1	3	35894.43	−0.11	$25672_{2\frac{1}{2}}$—$61566^{\circ}_{2\frac{1}{2}}$	
2785.634	12	50	35887.90	0.00	$19070_{4\frac{1}{2}}$—$54958^{\circ}_{3\frac{1}{2}}$	7
2786.300	4	20	35879.31	+0.02	$20534_{3\frac{1}{2}}$—$56413^{\circ}_{4\frac{1}{2}}$	
2786.340	3		35878.80	−0.06	$a\ ^4F_{2\frac{1}{2}}$—$47179^{\circ}_{1\frac{1}{2}}$	
2788.403		2	35852.25	+0.07	$a\ ^4G_{2\frac{1}{2}}$—$52087^{\circ}_{2\frac{1}{2}}$	
2788.536	4	6	35850.54	−0.09	$19637_{2\frac{1}{2}}$—$55488^{\circ}_{1\frac{1}{2}}$	
2789.197	10	20	35842.04	−0.06	$20534_{3\frac{1}{2}}$—$56376^{\circ}_{3\frac{1}{2}}$	7
2790.160	2	18	35829.67	−0.03	$28377_{3\frac{1}{2}}$—$64207^{\circ}_{4\frac{1}{2}}$	
2790.433	5	50	35826.17	−0.14	$23450_{2\frac{1}{2}}$—$59276^{\circ}_{3\frac{1}{2}}$	res
2790.998	3	3	35818.92	−0.08	$28491_{1\frac{1}{2}}$—$64310^{\circ}_{2\frac{1}{2}}$	
2791.740	2	5	35809.40	−0.08	$a\ ^4D_{0\frac{1}{2}}$—$48982^{\circ}_{1\frac{1}{2}}$	
2791.850	—?	1	35807.98	−0.02	$a\ ^4P_{2\frac{1}{2}}$—$49242^{\circ}_{2\frac{1}{2}}$	
2793.622	1	4	35785.28	+0.06	$26929_{5\frac{1}{2}}$—$62714^{\circ}_{6\frac{1}{2}}$	
2796.674	1	3	35746.23	−0.11	$19276_{2\frac{1}{2}}$—$55022^{\circ}_{3\frac{1}{2}}$	
2796.866	3	6	35743.77	−0.15	$a\ ^4F_{1\frac{1}{2}}$—$44455^{\circ}_{0\frac{1}{2}}$	res
2797.298		2	35738.25	−0.16	$24918_{1\frac{1}{2}}$—$60656^{\circ}_{2\frac{1}{2}}$	
2797.879		1	35730.83	−0.27	$25169_{1\frac{1}{2}}$—$60900^{\circ}_{2\frac{1}{2}}$	
2798.353		3	35724.78	−0.06	$28631_{3\frac{1}{2}}$—$64356^{\circ}_{3\frac{1}{2}}$	
2799.042	20	100	35715.98	−0.05	$a\ ^4D_{3\frac{1}{2}}$—$50863^{\circ}_{4\frac{1}{2}}$	5
2799.248	1		35713.36	−0.29	$18990_{1\frac{1}{2}}$—$54704^{\circ}_{2\frac{1}{2}}$	
2799.312	1		35712.54	−0.02	$a\ ^4F_{3\frac{1}{2}}$—$49124^{\circ}_{3\frac{1}{2}}$	
2801.058	4	30	35690.28	−0.14	$a\ ^4P_{2\frac{1}{2}}$—$49124^{\circ}_{3\frac{1}{2}}$	
2801.430		10	35685.54	−0.07	$a\ ^4G_{3\frac{1}{2}}$—$52275^{\circ}_{3\frac{1}{2}}$	6 res
3802.705		3	35669.31	+0.01	$28118_{2\frac{1}{2}}$—$63788^{\circ}_{3\frac{1}{2}}$	
2803.068		4	35664.70	−0.25	$24991_{1\frac{1}{2}}$—$60656^{\circ}_{2\frac{1}{2}}$	
2803.233	4	10	35662.60	−0.02	$22194_{3\frac{1}{2}}$—$57856^{\circ}_{2\frac{1}{2}}$	
2803.302	1	3	35661.71	+0.07	$29341_{4\frac{1}{2}}$—$65003^{\circ}_{3\frac{1}{2}}$	
2803.604	8	25	35657.87	−0.10	$a\ ^4D_{1\frac{1}{2}}$—$50292^{\circ}_{2\frac{1}{2}}$	res
2803.682		3	35656.88	+0.01	$23234_{4\frac{1}{2}}$—$58891^{\circ}_{3\frac{1}{2}}$	
2803.909		5	35654.00	−0.13	$25672_{2\frac{1}{2}}$—$61326^{\circ}_{3\frac{1}{2}}$	
2804.922	3	12	35641.12	+0.04	$23046_{3\frac{1}{2}}$—$58687^{\circ}_{4\frac{1}{2}}$	
2805.177	2	15	35637.88	−0.05	$30633_{4\frac{1}{2}}$—$66270^{\circ}_{4\frac{1}{2}}$	6
2805.546		7	35633.20	−0.06	$20780_{4\frac{1}{2}}$—$56415^{\circ}_{4\frac{1}{2}}$	6
2805.936	20	120	35628.24	−0.13	$20455_{1\frac{1}{2}}$—$56084^{\circ}_{1\frac{1}{2}}$	
				+0.05	$a\ ^4G_{2\frac{1}{2}}$—$51863^{\circ}_{3\frac{1}{2}}$	
2806.392	3	4	35622.45	−0.07	$a\ ^4P_{0\frac{1}{2}}$—$44455^{\circ}_{0\frac{1}{2}}$	

TABLE 3. *Classified lines of* W II—Continued

Wavelength (Å)	Intensity		Wave number (cm^{-1})		Combination	Zeeman effect
	Arc	Spark	Observed	*O–C*		
Air						
2806. 626	3	10	35619. 48	+0. 01	$24804_{3\frac{1}{2}}$—*60424*$^{\circ}_{3\frac{1}{2}}$	6
2808. 474	4	40	35596. 04	−0. 03	$20780_{4\frac{1}{2}}$—*56376*$^{\circ}_{3\frac{1}{2}}$	res
2808. 956	3	50	35589. 93	−0. 02	$22139_{2\frac{1}{2}}$—*57729*$^{\circ}_{3\frac{1}{2}}$	res
2810. 085		3	35575. 64	0. 00	$28631_{3\frac{1}{2}}$—*64207*$^{\circ}_{4\frac{1}{2}}$	
2811. 743	1	6	35554. 65	−0. 01	$29341_{4\frac{1}{2}}$—*64896*$^{\circ}_{3\frac{1}{2}}$	
2812. 210	8	50	35548. 76	0. 00	*a* $^4P_{2\frac{1}{2}}$—*48982*$^{\circ}_{1\frac{1}{2}}$	res
2813. 228	3	15	35535. 90	+0. 06	$22194_{3\frac{1}{2}}$—*57729*$^{\circ}_{3\frac{1}{2}}$	
2814. 106		2	35524. 81	−0. 11	$19637_{2\frac{1}{2}}$—*55162*$^{\circ}_{2\frac{1}{2}}$	
2814. 798	4	30	35516. 07	+0. 03	$19442_{0\frac{1}{2}}$—*54958*$^{\circ}_{1\frac{1}{2}}$	5
2815. 720		2	35504. 44	−0. 10	$22503_{1\frac{1}{2}}$—*58007*$^{\circ}_{1\frac{1}{2}}$	
2816. 283	6	10	35497. 35	0. 00	*a* $^4G_{3\frac{1}{2}}$—*52087*$^{\circ}_{2\frac{1}{2}}$	
2816. 478		2	35494. 90	+0. 26	$18990_{1\frac{1}{2}}$—*54485*$^{\circ}_{0\frac{1}{2}}$	
2817. 422	1	3	35483. 00	−0. 11	$24991_{1\frac{1}{2}}$—*60474*$^{\circ}_{2\frac{1}{2}}$	
2819. 002	4	12	35463. 11	−0. 02	*a* $^4D_{2\frac{1}{2}}$—*50430*$^{\circ}_{1\frac{1}{2}}$	7
2819. 897	4	20	35451. 85	+0. 07	$24804_{3\frac{1}{2}}$—*60256*$^{\circ}_{3\frac{1}{2}}$	res
2820. 532	3	8	35443. 87	−0. 07	$23955_{3\frac{1}{2}}$—*59399*$^{\circ}_{4\frac{1}{2}}$	
2821. 800	5	35	35427. 95	−0. 14	$19276_{2\frac{1}{2}}$—*54704*$^{\circ}_{2\frac{1}{2}}$	res
2822. 542	25	125	35418. 64	−0. 10	*a* $^4F_{3\frac{1}{2}}$—*48830*$^{\circ}_{3\frac{1}{2}}$	res
2824. 144		4	35398. 54	+0. 06	$28631_{3\frac{1}{2}}$—*64030*$^{\circ}_{2\frac{1}{2}}$	
2824. 306	4	4	35396. 52	−0. 08	*a* $^4P_{2\frac{1}{2}}$—*48830*$^{\circ}_{3\frac{1}{2}}$	
2824. 680	2	6	35391. 83	−0. 03	$26158_{4\frac{1}{2}}$—*61550*$^{\circ}_{3\frac{1}{2}}$	
2824. 896	1	7	35389. 12	+0. 02	$28491_{1\frac{1}{2}}$—*63880*$^{\circ}_{2\frac{1}{2}}$	
2825. 188	1	6	35385. 47	−0. 01	$19637_{2\frac{1}{2}}$—*55022*$^{\circ}_{3\frac{1}{2}}$	
2826. 482	3	15	35369. 27	0. 00	$18000_{3\frac{1}{2}}$—*53369*$^{\circ}_{4\frac{1}{2}}$	7
2827. 542		8	35356. 00	+0. 02	$19404_{0\frac{1}{2}}$—*54760*$^{\circ}_{0\frac{1}{2}}$	
2830. 064	12	80	35324. 50	−0. 01	*a* $^4D_{2\frac{1}{2}}$—*50292*$^{\circ}_{2\frac{1}{2}}$	6
2831. 236	7	35	35309. 88	−0. 01	*a* $^4G_{4\frac{1}{2}}$—*51863*$^{\circ}_{3\frac{1}{2}}$	
2831. 643	1	2	35304. 80	0. 00	$25169_{1\frac{1}{2}}$—*60474*$^{\circ}_{2\frac{1}{2}}$	
2832. 215		3	35297. 67	+0. 23	$23450_{2\frac{1}{2}}$—*58747*$^{\circ}_{1\frac{1}{2}}$	
2832. 848		1	35289. 80	−0. 38	$23046_{3\frac{1}{2}}$—*58336*$^{\circ}_{2\frac{1}{2}}$	
2834. 208		50	35272. 85	−0. 51	*a* $^4G_{3\frac{1}{2}}$—*51863*$^{\circ}_{3\frac{1}{2}}$	6
2835. 334	8*A*	5	35258. 85	−0. 21	$23450_{2\frac{1}{2}}$—*58709*$^{\circ}_{3\frac{1}{2}}$	
2838. 422	5	4	35220. 50	−0. 01	*a* $^6D_{3\frac{1}{2}}$—*39936*$^{\circ}_{2\frac{1}{2}}$	
2839. 820	3	10	35203. 15	−0. 04	*a* $^4G_{2\frac{1}{2}}$—*51438*$^{\circ}_{2\frac{1}{2}}$	
2839. 936	1	10	35201. 71	−0. 09	$26158_{4\frac{1}{2}}$—*61360*$^{\circ}_{4\frac{1}{2}}$	
2841. 080	2	6	35187. 54	+0. 01	$24804_{3\frac{1}{2}}$—*59992*$^{\circ}_{2\frac{1}{2}}$	
2842. 460		6	35170. 46	−0. 03	$31100_{3\frac{1}{2}}$—*66270*$^{\circ}_{4\frac{1}{2}}$	
2842. 700	2	15	35167. 50	−0. 05	$26158_{4\frac{1}{2}}$—*61326*$^{\circ}_{3\frac{1}{2}}$	
2843. 045	2	2	35163. 22	+0. 04	$27273_{2\frac{1}{2}}$—*62437*$^{\circ}_{4\frac{1}{2}}$	
2843. 449	2	5	35158. 23	−0. 15	$19070_{4\frac{1}{2}}$—*54229*$^{\circ}_{3\frac{1}{2}}$	
2843. 603	1	12	35156. 32	−0. 02	$28631_{3\frac{1}{2}}$—*63788*$^{\circ}_{3\frac{1}{2}}$	6
2844. 426		1	35146. 15	−0. 09	$18990_{1\frac{1}{2}}$—*54137*$^{\circ}_{1\frac{1}{2}}$	
2844. 500	2	8	35145. 24	−0. 07	*a* $^4D_{3\frac{1}{2}}$—*50292*$^{\circ}_{2\frac{1}{2}}$	res
2845. 725	3	10	35130. 11	−0. 02	*a* $^4G_{3\frac{1}{2}}$—*52567*$^{\circ}_{3\frac{1}{2}}$	res
2846. 357		1	35122. 31	−0. 25	$20039_{3\frac{1}{2}}$—*55162*$^{\circ}_{2\frac{1}{2}}$	
2847. 140	3	18	35112. 65	−0. 17	$18000_{3\frac{1}{2}}$—*53113*$^{\circ}_{2\frac{1}{2}}$	res
2848. 234	2	5	35099. 16	−0. 14 −0. 13	$19276_{2\frac{1}{2}}$—*54375*$^{\circ}_{3\frac{1}{2}}$ $26227_{2\frac{1}{2}}$—*61326*$^{\circ}_{3\frac{1}{2}}$	
2849. 678		1	35081. 38	−0. 04	$19404_{0\frac{1}{2}}$—*54485*$^{\circ}_{0\frac{1}{2}}$	
2850. 808	35*A*	8	35067. 48	+0. 25	$19637_{2\frac{1}{2}}$—*54704*$^{\circ}_{2\frac{1}{2}}$	
2851. 068		4	35064. 28	−0. 19	$24804_{3\frac{1}{2}}$—*59869*$^{\circ}_{3\frac{1}{2}}$	
2851. 554	3	3	35058. 30	+0. 38	$22194_{3\frac{1}{2}}$—*57252*$^{\circ}_{2\frac{1}{2}}$	
2852. 083	3	70	35051. 80	+0. 02	$30633_{4\frac{1}{2}}$—*65684*$^{\circ}_{3\frac{1}{2}}$	5
2852. 460		1	35047. 17	0. 00	$25209_{4\frac{1}{2}}$—*60256*$^{\circ}_{3\frac{1}{2}}$	
2853. 440	3	20	35035. 13	−0. 15	$18990_{1\frac{1}{2}}$—*54026*$^{\circ}_{2\frac{1}{2}}$	res
2853. 694		4	35032. 02	−0. 06	$20455_{1\frac{1}{2}}$—*55488*$^{\circ}_{1\frac{1}{2}}$	

TABLE 3. *Classified lines of* W II—Continued

Wavelength (Å)	Intensity		Wave number (cm^{-1})		Combination	Zeeman effect
	Arc	Spark	Observed	*O–C*		
Air						
2854.719	3	4	35019.44	−0.12	$a\ ^4G_{2\frac{1}{2}}$—$51254^{\circ}_{1\frac{1}{2}}$	
2855.524		25	35009.56	0.00	$25209_{4\frac{1}{2}}$—$60218^{\circ}_{3\frac{1}{2}}$	
2856.256		2	35000.60	−0.04	$24991_{1\frac{1}{2}}$—$59992^{\circ}_{2\frac{1}{2}}$	
2857.470		1	34985.72	−0.14	$19070_{4\frac{1}{2}}$—$54056^{\circ}_{4\frac{1}{2}}$	
2857.695	2	6	34982.97	−0.15	$20039_{3\frac{1}{2}}$—$55022^{\circ}_{3\frac{1}{2}}$	6
2859.484	8	30	34961.08	−0.10	$a\ ^4P_{1\frac{1}{2}}$—$45553^{\circ}_{1\frac{1}{2}}$	res
2860.898		12	34943.80			
2861.058	2	6	34941.85	−0.01	$a\ ^4G_{4\frac{1}{2}}$—$z\ ^6F^{\circ}_{5\frac{1}{2}}$	
2861.21	2	10	34939.99	−0.13	$23046_{3\frac{1}{2}}$—$57986^{\circ}_{4\frac{1}{2}}$	
2861.518		2	34936.23	−0.11	$23955_{3\frac{1}{2}}$—$58891^{\circ}_{3\frac{1}{2}}$	
2864.036		2	34905.52	−0.20	$23803_{3\frac{1}{2}}$—$58709^{\circ}_{3\frac{1}{2}}$	
2864.395	1		34901.14	+0.10	$18000_{3\frac{1}{2}}$—$52901^{\circ}_{3\frac{1}{2}}$	
2864.473	2	15	34900.20	−0.10	$28187_{6\frac{1}{2}}$—$63087^{\circ}_{6\frac{1}{2}}$	6
2864.744	1	8	34896.90	−0.16	$26158_{4\frac{1}{2}}$—$61055^{\circ}_{4\frac{1}{2}}$	7
2864.858	3	10	34895.51	+0.13	$22194_{3\frac{1}{2}}$—$57089^{\circ}_{4\frac{1}{2}}$	
2865.603		6	34886.43	−0.05	$23450_{2\frac{1}{2}}$—$58336^{\circ}_{2\frac{1}{2}}$	6
2865.804	3	20	34884.00	−0.04	$23803_{3\frac{1}{2}}$—$58687^{\circ}_{4\frac{1}{2}}$	
2866.322	8	10	34877.68	−0.09	$a\ ^6S_{2\frac{1}{2}}$—$42298^{\circ}_{1\frac{1}{2}}$	
2866.600	4	8	34874.30	−0.04	$a\ ^4F_{2\frac{1}{2}}$—$46175^{\circ}_{3\frac{1}{2}}$	
2866.751	6	20	34872.46	−0.06	$a\ ^4F_{3\frac{1}{2}}$—$48284^{\circ}_{2\frac{1}{2}}$	res
2866.910		1	34870.53	−0.17	$28118_{2\frac{1}{2}}$—$62989^{\circ}_{2\frac{1}{2}}$	
2867.409	6	15	34864.46	−0.04	$a\ ^4P_{1\frac{1}{2}}$—$45457^{\circ}_{0\frac{1}{2}}$	res
2867.697	4	3	34860.96	−0.23	$19637_{2\frac{1}{2}}$—$54498^{\circ}_{3\frac{1}{2}}$	
				+0.28	$19276_{2\frac{1}{2}}$—$54137^{\circ}_{1\frac{1}{2}}$	
2867.934	4	20	34858.08	+0.06	$20534_{3\frac{1}{2}}$—$55392^{\circ}_{4\frac{1}{2}}$	
2868.736	8	80	34848.33	−0.03	$a\ ^4G_{3\frac{1}{2}}$—$51438^{\circ}_{2\frac{1}{2}}$	
2870.906	18*A*	10	34822.00	−0.33	$25169_{1\frac{1}{2}}$—$59992^{\circ}_{2\frac{1}{2}}$	
2871.902	2	12	34809.92	+0.02	$23046_{3\frac{1}{2}}$—$57856^{\circ}_{2\frac{1}{2}}$	res
2873.352	2?	10	34792.35	+0.05	$22139_{2\frac{1}{2}}$—$56932^{\circ}_{1\frac{1}{2}}$	
2873.836	2	12	34786.50	−0.02	$19442_{6\frac{1}{2}}$—$54229^{\circ}_{5\frac{1}{2}}$	
2874.478		12	34778.72	−0.18	$28187_{6\frac{1}{2}}$—$62966^{\circ}_{5\frac{1}{2}}$	
2875.110		4	34771.08	−0.02	$25045_{0\frac{1}{2}}$—$59816^{\circ}_{1\frac{1}{2}}$	
2876.684	1−	2	34752.06	+0.08	$25672_{2\frac{1}{2}}$—$60424^{\circ}_{3\frac{1}{2}}$	
2876.934	20*A*	10	34749.01	+0.07	$22503_{1\frac{1}{2}}$—$57252^{\circ}_{2\frac{1}{2}}$	6
2877.827		2	34738.26	−0.18	$19637_{2\frac{1}{2}}$—$54375^{\circ}_{2\frac{1}{2}}$	
2878.083	10*A*	8	34735.16	+0.14	$22139_{2\frac{1}{2}}$—$56874^{\circ}_{2\frac{1}{2}}$	6
2878.316	2	40	34732.35	−0.13	$23955_{3\frac{1}{2}}$—$58687^{\circ}_{4\frac{1}{2}}$	
2880.164	1−	8	34710.07	−0.03	$28377_{5\frac{1}{2}}$—$63087^{\circ}_{6\frac{1}{2}}$	
2881.538		8	34693.52	+0.14	$30633_{4\frac{1}{2}}$—$65326^{\circ}_{3\frac{1}{2}}$	
2882.400	3	20	34683.14	+0.02	$23046_{3\frac{1}{2}}$—$57729^{\circ}_{3\frac{1}{2}}$	6
2883.152	3	3	34674.10	+0.13	$26227_{2\frac{1}{2}}$—$60900^{\circ}_{2\frac{1}{2}}$	
2883.247	6	4	34672.95	+0.11	$26929_{5\frac{1}{2}}$—$61602^{\circ}_{6\frac{1}{2}}$	
2883.915		2	34664.92	+0.05	$20039_{3\frac{1}{2}}$—$54704^{\circ}_{2\frac{1}{2}}$	
2884.310	2	20	34660.18	+0.06	$26929_{5\frac{1}{2}}$—$61589^{\circ}_{5\frac{1}{2}}$	6
2885.463	1	2	34646.33	−0.24	$a\ ^6D_{1\frac{1}{2}}$—$z\ ^6F^{\circ}_{2\frac{1}{2}}$	
2886.464		6	34634.31	−0.13	$28631_{3\frac{1}{2}}$—$63266^{\circ}_{3\frac{1}{2}}$	
2886.896	5		34629.13	+0.11	$a\ ^6S_{2\frac{1}{2}}$—$z\ ^6F^{\circ}_{3\frac{1}{2}}$	
2886.923		35	34628.81	+0.17	$22139_{2\frac{1}{2}}$—$56768^{\circ}_{3\frac{1}{2}}$	
2888.318	15*A*	8	34612.08	+0.09	$20780_{4\frac{1}{2}}$—$55392^{\circ}_{4\frac{1}{2}}$	*d*
2888.699		4	34607.52	−0.22	$a\ ^4D_{1\frac{1}{2}}$—$49242^{\circ}_{2\frac{1}{2}}$	
2889.780	4	50	34594.58	−0.09	$24804_{3\frac{1}{2}}$—$59399^{\circ}_{4\frac{1}{2}}$	
2890.634	2	25	34584.35	+0.01	$31100_{5\frac{1}{2}}$—$65684^{\circ}_{5\frac{1}{2}}$	6
2891.456	3	20	34574.52	−0.01	$22194_{3\frac{1}{2}}$—$56768^{\circ}_{3\frac{1}{2}}$	6
2892.912	2	10	34557.12	+0.02	$23450_{2\frac{1}{2}}$—$58007^{\circ}_{1\frac{1}{2}}$	res
2894.924	2	10	34533.10	−0.04	$23803_{3\frac{1}{2}}$—$58336^{\circ}_{2\frac{1}{2}}$	
2895.441	2	10	34526.94	−0.02	$28187_{6\frac{1}{2}}$—$62714^{\circ}_{5\frac{1}{2}}$	6

TABLE 3. *Classified lines of* W II—Continued

Wavelength (Å)	Intensity		Wave number (cm^{-1})		Combination	Zeeman effect
	Arc	Spark	Observed	*O–C*		
Air						
2897.726	2	3	34499.71	−0.11	$19637_{2\frac{1}{2}}$—*54137*$^{\circ}_{1\frac{1}{2}}$	
2898.102		2	34495.24	+0.19	$23234_{4\frac{1}{2}}$—*57729*$^{\circ}_{3\frac{1}{2}}$	
2898.360		1	34492.17	+0.06	*a* $^4G_{4\frac{1}{2}}$—*51045*$^{\circ}_{3\frac{1}{2}}$	
2901.174	2	25	34458.71	−0.12	$20039_{3\frac{1}{2}}$—*54498*$^{\circ}_{3\frac{1}{2}}$	
2901.448		3	34455.46	−0.12	*a* $^4G_{3\frac{1}{2}}$—*51045*$^{\circ}_{3\frac{1}{2}}$	
2902.201	30*A*	20	34446.52	−0.12	$29341_{4\frac{1}{2}}$—*63788*$^{\circ}_{3\frac{1}{2}}$	
2903.500		50	34431.11	−0.09	$26929_{3\frac{1}{2}}$—*61360*$^{\circ}_{4\frac{1}{2}}$	
2904.081	8	80	34424.22	−0.01	$20534_{3\frac{1}{2}}$—*54958*$^{\circ}_{3\frac{1}{2}}$	6
2904.556	2	8	34418.58	−0.08	$22194_{3\frac{1}{2}}$—*56612*$^{\circ}_{3\frac{1}{2}}$	6
2904.843	—?	5	34415.18	−0.08	*a* $^4D_{0\frac{1}{2}}$—*47588*$^{\circ}_{1\frac{1}{2}}$	
2905.602	8*A*	12	34406.20	0.00	$23450_{2\frac{1}{2}}$—*57856*$^{\circ}_{2\frac{1}{2}}$	6
2906.416	2	12	34396.57	+0.10	$22535_{0\frac{1}{2}}$—*56932*$^{\circ}_{1\frac{1}{2}}$	
2908.504	3	25	34371.87	−0.06	$22503_{1\frac{1}{2}}$—*56874*$^{\circ}_{2\frac{1}{2}}$	
2910.332	2	10	34350.30	−0.02	$22194_{3\frac{1}{2}}$—*56544*$^{\circ}_{2\frac{1}{2}}$	
2911.542	2	20	34336.01	−0.07 −0.07	$20039_{3\frac{1}{2}}$—*54375*$^{\circ}_{2\frac{1}{2}}$ $30633_{4\frac{1}{2}}$—*64969*$^{\circ}_{3\frac{1}{2}}$	
2912.464	2	25	34325.15			
2912.584	3	5	34323.73	−0.09	*a* $^4F_{4\frac{1}{2}}$—*49181*$^{\circ}_{4\frac{1}{2}}$	
2912.986	1		34319.00	−0.11	*a* $^4P_{1\frac{1}{2}}$—*44911*$^{\circ}_{1\frac{1}{2}}$	
2913.614		2	34311.60	+0.13	$26929_{3\frac{1}{2}}$—*61240*$^{\circ}_{3\frac{1}{2}}$	
2913.748	12	30	34310.02	+0.11	*a* $^4G_{4\frac{1}{2}}$—*50863*$^{\circ}_{4\frac{1}{2}}$	6
2914.272		30	34303.85	−0.28	$20455_{1\frac{1}{2}}$—*54760*$^{\circ}_{0\frac{1}{2}}$	
2914.655	2	15	34299.34	+0.05	$19070_{4\frac{1}{2}}$—*53369*$^{\circ}_{4\frac{1}{2}}$	6
2916.347		5	34279.44	+0.02	$23450_{2\frac{1}{2}}$—*57729*$^{\circ}_{3\frac{1}{2}}$	
2916.584	3	8	34276.66	−0.08	$27273_{3\frac{1}{2}}$—*61550*$^{\circ}_{3\frac{1}{2}}$	
2916.768	3	10	34274.50	+0.22 −0.08	*a* $^4D_{2\frac{1}{2}}$—*49242*$^{\circ}_{2\frac{1}{2}}$ $18000_{3\frac{1}{2}}$—*52275*$^{\circ}_{3\frac{1}{2}}$	
2916.896	2	12	34273.00	−0.38	*a* $^4G_{3\frac{1}{2}}$—*50863*$^{\circ}_{4\frac{1}{2}}$	
2917.389	3	5	34267.20	−0.10	*a* $^4F_{4\frac{1}{2}}$—*49124*$^{\circ}_{3\frac{1}{2}}$	
2917.540	1	5	34265.42	+0.02	$26158_{4\frac{1}{2}}$—*60424*$^{\circ}_{3\frac{1}{2}}$	
2917.895		3	34261.25	−0.25	$25672_{2\frac{1}{2}}$—*59933*$^{\circ}_{3\frac{1}{2}}$	
2918.633	25	100	34252.58	−0.04	*a* $^4F_{2\frac{1}{2}}$—*45553*$^{\circ}_{1\frac{1}{2}}$	7
2918.976	2	10	34248.57	−0.11	$20455_{1\frac{1}{2}}$—*54704*$^{\circ}_{2\frac{1}{2}}$	
2919.508	2	12	34242.33	−0.15	$20780_{4\frac{1}{2}}$—*55022*$^{\circ}_{3\frac{1}{2}}$	
2920.903	—	6	34225.98	+0.04	$31100_{5\frac{1}{2}}$—*65326*$^{\circ}_{5\frac{1}{2}}$	
2921.908	10*A*	12	34214.21	−0.09	$28118_{2\frac{1}{2}}$—*62333*$^{\circ}_{2\frac{1}{2}}$	*d*
2922.674	—	5	34205.24	+0.04	$23046_{3\frac{1}{2}}$—*57252*$^{\circ}_{2\frac{1}{2}}$	
2923.382	5*A*	10	34196.95	−0.03	$25672_{2\frac{1}{2}}$—*59869*$^{\circ}_{3\frac{1}{2}}$	
2923.451	1	10	34196.15	+0.04	*a* $^4G_{2\frac{1}{2}}$—*50430*$^{\circ}_{1\frac{1}{2}}$	
2923.980	3	12	34189.96	−0.10	$25209_{4\frac{1}{2}}$—*59399*$^{\circ}_{4\frac{1}{2}}$	6
2924.996	4	40	34178.08	−0.12	$20780_{4\frac{1}{2}}$—*54958*$^{\circ}_{3\frac{1}{2}}$	5
2925.834	5	125	34168.30	−0.04	$33910_{3\frac{1}{2}}$—*68078*$^{\circ}_{3\frac{1}{2}}$	5
2926.836	3	15	34156.60	−0.10	*a* $^4D_{2\frac{1}{2}}$—*49124*$^{\circ}_{3\frac{1}{2}}$	res
2926.990	40*A*	10	34154.80	+0.26	*a* $^4P_{2\frac{1}{2}}$—*47588*$^{\circ}_{1\frac{1}{2}}$	
2927.710	3	20	34146.40	−0.06	$19276_{2\frac{1}{2}}$—*53422*$^{\circ}_{1\frac{1}{2}}$	7
2929.984	3	20	34119.90	−0.07	$26158_{4\frac{1}{2}}$—*60278*$^{\circ}_{4\frac{1}{2}}$	6
2931.530	2	20	34101.90	−0.04	$33910_{3\frac{1}{2}}$—*68012*$^{\circ}_{3\frac{1}{2}}$	6
2931.895	5	35	34097.65	−0.06	$26158_{4\frac{1}{2}}$—*60256*$^{\circ}_{3\frac{1}{2}}$	res
2932.864	3	20	34086.39	+0.07	$18000_{3\frac{1}{2}}$—*52087*$^{\circ}_{2\frac{1}{2}}$	res
2933.068	1	1	34083.80	−0.32	$28631_{3\frac{1}{2}}$—*62715*$^{\circ}_{4\frac{1}{2}}$	
2935.201	2	6	34059.25	+0.01	$28377_{5\frac{1}{2}}$—*62437*$^{\circ}_{4\frac{1}{2}}$	
2935.358	8	25	34057.43	−0.06	*a* $^4G_{2\frac{1}{2}}$—*50292*$^{\circ}_{2\frac{1}{2}}$	6
2935.726	2	10	34053.16	−0.03	$19276_{2\frac{1}{2}}$—*53329*$^{\circ}_{1\frac{1}{2}}$	
2935.806	—	4	34052.23	−0.20	$27273_{3\frac{1}{2}}$—*61326*$^{\circ}_{3\frac{1}{2}}$	
2936.61	40*A*	125	34042.92	+0.26	$23046_{3\frac{1}{2}}$—*57089*$^{\circ}_{4\frac{1}{2}}$	
2937.200	8?	15	34036.07	−0.02	$19404_{0\frac{1}{2}}$—*53440*$^{\circ}_{0\frac{1}{2}}$	6
2937.61	10*A*	12	34031.33	−0.19	$23955_{5\frac{1}{2}}$—*57986*$^{\circ}_{4\frac{1}{2}}$	

TABLE 3. *Classified lines of* W II—Continued

Wavelength (Å)	Intensity		Wave number (cm^{-1})		Combination	Zeeman effect
	Arc	Spark	Observed	*O–C*		
Air						
2937.774	2	4	34029.42	−0.03	$26227_{2\frac{1}{2}}$—*60256*$^{3}_{3\frac{1}{2}}$	
2938.685	?	4	34018.87	−0.03	$19404_{0\frac{1}{2}}$—*53422*$^{1}_{1\frac{1}{2}}$	
2938.872	2	12	34016.71	−0.09	$20039_{3\frac{1}{2}}$—*54056*$^{4}_{4\frac{1}{2}}$	
2939.757	6	35	34006.47	−0.09	*a* $^4D_{0\frac{1}{2}}$—*47179*$^{0}_{1\frac{1}{2}}$	
2940.204	8	60	34001.30	−0.07	*a* $^4F_{3\frac{1}{2}}$—*47413*$^{3}_{2\frac{1}{2}}$	
2941.476	4	5	33986.60	+0.10	$20039_{3\frac{1}{2}}$—*54026*$^{2}_{2\frac{1}{2}}$	
2942.128	12*A*	10	33979.07	−0.16	*a* $^4P_{2\frac{1}{2}}$—*47413*$^{2}_{2\frac{1}{2}}$	
2942.263	2	10	33977.49	−0.01	*a* $^4D_{3\frac{1}{2}}$—*49124*$^{3}_{3\frac{1}{2}}$	
2942.618	3	10	33973.41	−0.07	*a* $^4F_{4\frac{1}{2}}$—*48830*$^{3}_{3\frac{1}{2}}$	
2945.137	—	6	33944.35	+0.02	$22139_{2\frac{1}{2}}$—*56084*$^{1}_{1\frac{1}{2}}$	
2946.454	—	25	33929.18			
2947.136	—?	2	33921.33	−0.15	$34091_{4\frac{1}{2}}$—*68012*$^{3}_{3\frac{1}{2}}$	
2950.453	4	40	33883.20	−0.01	$24804_{3\frac{1}{2}}$—*58687*$^{4}_{4\frac{1}{2}}$	res
2952.262	75*A*	100	33862.44	−0.22 +0.11	*a* $^4P_{1\frac{1}{2}}$—*44455*$^{0}_{0\frac{1}{2}}$ $18000_{3\frac{1}{2}}$—*51863*$^{3}_{3\frac{1}{2}}$	*d*
2952.974	4*A*	4	33854.27	−0.32	$23234_{4\frac{1}{2}}$—*57089*$^{4}_{4\frac{1}{2}}$	
2954.070	4*A*	3	33841.71	−0.49	$28491_{1\frac{1}{2}}$—*62333*$^{2}_{2\frac{1}{2}}$	
2954.482	4	15	33836.99	−0.01	$19276_{2\frac{1}{2}}$—*53113*$^{2}_{2\frac{1}{2}}$	6 res
2955.007	8	15	33830.98	−0.08	$19070_{4\frac{1}{2}}$—*52901*$^{4}_{3\frac{1}{2}}$	
2955.256	2	10	33828.13	−0.06	$23046_{3\frac{1}{2}}$—*56874*$^{3}_{2\frac{1}{2}}$	
2956.67	20*A*	10	33811.96	−0.08	$18990_{1\frac{1}{2}}$—*52803*$^{1}_{1\frac{1}{2}}$	
2957.266	1	12	33805.12	−0.06	$28631_{3\frac{1}{2}}$—*62437*$^{4}_{4\frac{1}{2}}$	
2957.590	1		33801.43	−0.07	$23450_{2\frac{1}{2}}$—*57252*$^{2}_{2\frac{1}{2}}$	
2958.972		4	33785.65	+0.05	$19637_{2\frac{1}{2}}$—*53422*$^{2}_{1\frac{1}{2}}$	
2959.312	—	2	33781.77	−0.17	$27273_{3\frac{1}{2}}$—*61055*$^{3}_{4\frac{1}{2}}$	
2959.910	—	10	33774.94	+0.02	$26158_{4\frac{1}{2}}$—*59933*$^{3}_{3\frac{1}{2}}$	
2960.771	—	1	33765.12	−0.08	$26227_{2\frac{1}{2}}$—*59992*$^{3}_{3\frac{1}{2}}$	
2961.020	12	50	33762.28	−0.02	*a* $^4P_{1\frac{1}{2}}$—*44354*$^{2}_{2\frac{1}{2}}$	
2961.558	—	2	33756.15	−0.23	$24991_{1\frac{1}{2}}$—*58747*$^{2}_{1\frac{1}{2}}$	
2964.412	—	1	33723.65	−0.03	$30633_{4\frac{1}{2}}$—*64356*$^{3}_{3\frac{1}{2}}$	
2964.898	2	20	33718.12	−0.07	$20780_{4\frac{1}{2}}$—*54498*$^{3}_{3\frac{1}{2}}$	res
2965.589	2	15	33710.27	−0.13	$26158_{4\frac{1}{2}}$—*59869*$^{3}_{3\frac{1}{2}}$	
2966.417	4*A*	2	33700.86	+0.17	$19637_{2\frac{1}{2}}$—*53338*$^{3}_{3\frac{1}{2}}$	
2967.926	4	20	33683.73	+0.05	*a* $^4D_{3\frac{1}{2}}$—*48830*$^{3}_{3\frac{1}{2}}$	6
2970.908	2	5	33649.92	−0.20	*a* $^4D_{1\frac{1}{2}}$—*48284*$^{2}_{2\frac{1}{2}}$	
2973.092	—	3	33625.24	+0.02	$19276_{2\frac{1}{2}}$—*52901*$^{3}_{3\frac{1}{2}}$	
2974.377	20	35	33610.67	+0.12	*a* $^4F_{2\frac{1}{2}}$—*44911*$^{1}_{1\frac{1}{2}}$	res
2975.078	3	10	33602.75	−0.01	$18990_{1\frac{1}{2}}$—*52593*$^{0}_{0\frac{1}{2}}$	
2976.476	15	50	33586.97	+0.03	*a* $^4F_{1\frac{1}{2}}$—*42298*$^{0}_{1\frac{1}{2}}$	res
2976.985	—	2	33581.23	−0.01	$22503_{1\frac{1}{2}}$—*56084*$^{1}_{1\frac{1}{2}}$	
2977.442		3	33576.08	−0.02	*a* $^4F_{2\frac{1}{2}}$—*z* $^6F^{\circ}_{3\frac{1}{2}}$	
2977.580	4	40	33574.52	+0.04	$30633_{4\frac{1}{2}}$—*64207*$^{4}_{4\frac{1}{2}}$	6
2977.950	3	20	33570.35	+0.04	$20445_{1\frac{1}{2}}$—*54026*$^{3}_{2\frac{1}{2}}$	
2978.332	1	6	33566.05	+0.11	$23046_{3\frac{1}{2}}$—*56612*$^{3}_{3\frac{1}{2}}$	
2981.319	1		33532.41	+0.10	$24804_{3\frac{1}{2}}$—*58336*$^{2}_{2\frac{1}{2}}$	
2982.219	2	25	33522.29	+0.10	$20534_{5\frac{1}{2}}$—*54056*$^{4}_{4\frac{1}{2}}$	
2984.426		6	33497.50	−0.10	$23046_{3\frac{1}{2}}$—*56544*$^{2}_{2\frac{1}{2}}$	
2985.830		6	33481.75	−0.02	$23450_{2\frac{1}{2}}$—*56932*$^{2}_{1\frac{1}{2}}$	
2986.103	5	25	33478.69	+0.09	$25209_{4\frac{1}{2}}$—*58687*$^{4}_{4\frac{1}{2}}$	6
2986.382	3	20	33475.57	+0.06	*a* $^4F_{4\frac{1}{2}}$—*48332*$^{3}_{3\frac{1}{2}}$	res
2987.294	15	60	33465.35	−0.19	*a* $^4P_{0\frac{1}{2}}$—*42298*$^{1}_{1\frac{1}{2}}$	res
2988.502	4	12	33451.82	−0.07	*a* $^4D_{0\frac{1}{2}}$—*46625*$^{0}_{0\frac{1}{2}}$	res
2988.771		12	33448.81	+0.13	$20780_{4\frac{1}{2}}$—*54229*$^{5}_{5\frac{1}{2}}$	
2990.850		12	33425.56	−0.47	*a* $^4G_{5\frac{1}{2}}$—*50863*$^{6}_{6\frac{1}{2}}$	
2991.470		4	33418.63	−0.25	$24918_{1\frac{1}{2}}$—*58336*$^{2}_{2\frac{1}{2}}$	
2991.855		3	33414.33	−0.25	$28187_{6\frac{1}{2}}$—*61602*$^{6}_{6\frac{1}{2}}$	

TABLE 3. *Classified lines of* W II—Continued

Wavelength (Å)	Intensity		Wave number (cm^{-1})		Combination	Zeeman effect
	Arc	Spark	Observed	$O-C$		
Air						
2992. 043		18	33412. 23			
2994. 700	3	60	33382. 59	−0. 06	$27273_{3\frac{1}{2}}$—*60656*$^{\circ}_{2\frac{1}{2}}$	
2995. 129		6	33377. 81	−0. 06	$23234_{4\frac{1}{2}}$—*56612*$^{\circ}_{3\frac{1}{2}}$	
2997. 685		8	33349. 35	−0. 02	$26929_{5\frac{1}{2}}$—*60278*$^{\circ}_{4\frac{1}{2}}$	
2998. 050		5	33345. 29	−0. 13	$24991_{1\frac{1}{2}}$—*58336*$^{\circ}_{2\frac{1}{2}}$	
2998. 693	15	50	33338. 14	−0. 05	*a* $^4F_{1\frac{1}{2}}$—*z* $^6F^{\circ}_{2\frac{1}{2}}$	res
3000. 499		3	33318. 07	−0. 04	$23450_{2\frac{1}{2}}$—*56768*$^{\circ}_{3\frac{1}{2}}$	
3000. 624	5	50	33316. 69	+0. 03	*a* $^4D_{2\frac{1}{2}}$—*48284*$^{\circ}_{2\frac{1}{2}}$	res
3002. 287	2	40	33298. 23	−0. 10	$20039_{3\frac{1}{2}}$—*53338*$^{\circ}_{3\frac{1}{2}}$	6 res
3003. 070	4	10	33289. 55	+0. 05	$26929_{5\frac{1}{2}}$—*60218*$^{\circ}_{5\frac{1}{2}}$	6
3003. 435		15	33285. 51	−0. 11	$23803_{3\frac{1}{2}}$—*57089*$^{\circ}_{4\frac{1}{2}}$	
3004. 284		5	33276. 10	−0. 06	$20780_{4\frac{1}{2}}$—*54056*$^{\circ}_{4\frac{1}{2}}$	
3007. 511		4?	33240. 40	−0. 20	$26158_{4\frac{1}{2}}$—*59399*$^{\circ}_{4\frac{1}{2}}$	
3008. 946	2	25	33224. 55	+0. 17	$28377_{5\frac{1}{2}}$—*61602*$^{\circ}_{6\frac{1}{2}}$	7
3010. 131		3	33211. 47	−0. 19	$28377_{5\frac{1}{2}}$—*61589*$^{\circ}_{5\frac{1}{2}}$	
3010. 750	4	80	33204. 64	+0. 04	$19070_{4\frac{1}{2}}$—*52275*$^{\circ}_{3\frac{1}{2}}$	res
3011. 102		2	33200. 76	−0. 05	$27273_{3\frac{1}{2}}$—*60474*$^{\circ}_{2\frac{1}{2}}$	
3011. 327		4	33198. 27	−0. 02	$22194_{3\frac{1}{2}}$—*55392*$^{\circ}_{4\frac{1}{2}}$	
3012. 102	2	15	33189. 74	+0. 10	$19404_{0\frac{1}{2}}$—*52593*$^{\circ}_{0\frac{1}{2}}$	res
3013. 093		1	33178. 82	+0. 05	$23234_{4\frac{1}{2}}$—*56413*$^{\circ}_{4\frac{1}{2}}$	
3014. 200	6*A*	3	33166. 63	−0. 48	$25169_{1\frac{1}{2}}$—*58336*$^{\circ}_{2\frac{1}{2}}$	
3014. 606	2	25	33162. 17	−0. 07	$23450_{2\frac{1}{2}}$—*56612*$^{\circ}_{3\frac{1}{2}}$	res
3015. 694	1	8	33150. 20	−0. 08	$27273_{3\frac{1}{2}}$—*60424*$^{\circ}_{3\frac{1}{2}}$	6
3017. 148	2	25	33134. 23	+0. 17	$23955_{5\frac{1}{2}}$—*57089*$^{\circ}_{4\frac{1}{2}}$	
3018. 624	1	20	33118. 03	−0. 04	$26158_{4\frac{1}{2}}$—*59276*$^{\circ}_{3\frac{1}{2}}$	5
3019. 628		3	33107. 08	+0. 04	$31100_{5\frac{1}{2}}$—*64207*$^{\circ}_{4\frac{1}{2}}$	
3020. 630	4	20	33096. 04	−0. 02	$18990_{1\frac{1}{2}}$—*52087*$^{\circ}_{2\frac{1}{2}}$	
3021. 982	20	80	33081. 23	−0. 24	*a* $^4F_{3\frac{1}{2}}$—*z* $^6F^{\circ}_{4\frac{1}{2}}$	
3022. 482		20	33075. 76	−0. 02 +0. 06	$25672_{2\frac{1}{2}}$—*58747*$^{\circ}_{1\frac{1}{2}}$ $28491_{1\frac{1}{2}}$—*61566*$^{\circ}_{1\frac{1}{2}}$	
3022. 672	3	30	33073. 68	−0. 10	$20039_{3\frac{1}{2}}$—*53113*$^{\circ}_{2\frac{1}{2}}$	
3022. 906	2	6	33071. 12	−0. 03	$23803_{3\frac{1}{2}}$—*56874*$^{\circ}_{2\frac{1}{2}}$	
3024. 502	25	250	33053. 67	−0. 07	*a* $^4F_{2\frac{1}{2}}$—*44354*$^{\circ}_{2\frac{1}{2}}$	res
3025. 993		1	33037. 38	−0. 02	$25672_{2\frac{1}{2}}$—*58709*$^{\circ}_{3\frac{1}{2}}$	
3027. 369		6	33022. 33	0. 00	$22139_{2\frac{1}{2}}$—*55162*$^{\circ}_{2\frac{1}{2}}$	
3028. 750		10	33007. 31	+0. 05	*a* $^4G_{2\frac{1}{2}}$—*49242*$^{\circ}_{2\frac{1}{2}}$	
3028. 975		8	33004. 86	+0. 01	$27273_{3\frac{1}{2}}$—*60278*$^{\circ}_{4\frac{1}{2}}$	
3029. 524		4	32998. 88	+0. 12	$19276_{2\frac{1}{2}}$—*52275*$^{\circ}_{3\frac{1}{2}}$	
3030. 793		2	32985. 06	+0. 11	$22503_{1\frac{1}{2}}$—*55488*$^{\circ}_{1\frac{1}{2}}$	
3031. 000		25	32982. 81	+0. 07	$28377_{5\frac{1}{2}}$—*61360*$^{\circ}_{4\frac{1}{2}}$	
3032. 450	3	15	32967. 04	−0. 01	$20455_{1\frac{1}{2}}$—*53422*$^{\circ}_{1\frac{1}{2}}$	res
3032. 660		8	32964. 76	−0. 01	$23803_{3\frac{1}{2}}$—*56768*$^{\circ}_{3\frac{1}{2}}$	
3033. 626		30	32954. 26	−0. 02	*a* $^4D_{1\frac{1}{2}}$—*47588*$^{\circ}_{1\frac{1}{2}}$	res
3033. 790		2	32952. 48	+0. 27	$22535_{0\frac{1}{2}}$—*55488*$^{\circ}_{1\frac{1}{2}}$	
3033. 913	4	20	32951. 14	+0. 11	$19404_{0\frac{1}{2}}$—*52355*$^{\circ}_{0\frac{1}{2}}$	
3036. 311		1	32925. 11	−0. 14	$24804_{3\frac{1}{2}}$—*57729*$^{\circ}_{3\frac{1}{2}}$	
3036. 670	5	50	32921. 23	−0. 07	*a* $^4P_{2\frac{1}{2}}$—*46355*$^{\circ}_{2\frac{1}{2}}$	
3039. 578	3	20	32889. 73	+0. 05	*a* $^4G_{2\frac{1}{2}}$—*49124*$^{\circ}_{3\frac{1}{2}}$	res
3044. 400		10	32837. 64	−0. 09	$25169_{1\frac{1}{2}}$—*58007*$^{\circ}_{1\frac{1}{2}}$	6
3044. 564		1	32835. 88	+0. 26	$20534_{5\frac{1}{2}}$—*53369*$^{\circ}_{4\frac{1}{2}}$	
3045. 216		15	32828. 85	+0. 07	$22194_{3\frac{1}{2}}$—*55022*$^{\circ}_{3\frac{1}{2}}$	
3046. 911	1	5	32810. 57	+0. 07	$19276_{2\frac{1}{2}}$—*52087*$^{\circ}_{2\frac{1}{2}}$	
3047. 060	1	15	32808. 97	+0. 07	$23803_{3\frac{1}{2}}$—*56612*$^{\circ}_{3\frac{1}{2}}$	6
3048. 604	4	40	32792. 36	+0. 01	$19070_{4\frac{1}{2}}$—*51863*$^{\circ}_{3\frac{1}{2}}$	res
3049. 563	—?	3	32782. 03	−0. 04	$28118_{2\frac{1}{2}}$—*60900*$^{\circ}_{2\frac{1}{2}}$	
3049. 850	5	50	32778. 96	−0. 01	*a* $^4D_{1\frac{1}{2}}$—*47413*$^{\circ}_{2\frac{1}{2}}$	

TABLE 3. *Classified lines of* W II—Continued

Wavelength (Å)	Intensity		Wave number (cm^{-1})		Combination	Zeeman effect
	Arc	Spark	Observed	*O–C*		
Air						
3051.29	25	250	32763.49	+0.03	$a\ ^4F_{3\frac{1}{2}}$—$46175\frac{5}{3\frac{1}{2}}$	res
3053.354	6	?)	32741.34	+0.02	$a\ ^4P_{2\frac{1}{2}}$—$46175\frac{3}{3\frac{1}{2}}$	
3053.420		20)	32740.64	+0.08	$23803_{3\frac{1}{2}}$—$56544\frac{2}{2\frac{1}{2}}$	
3054.129		1	32733.03	+0.03	$26158_{4\frac{1}{2}}$—$58891\frac{3}{3\frac{1}{2}}$	
3058.452	1	20	32686.79	−0.04	$25169_{1\frac{1}{2}}$—$57856\frac{3}{2\frac{1}{2}}$	res
3059.268		3	32678.06	+0.06	$28377_{5\frac{1}{2}}$—$61055\frac{1}{4\frac{1}{2}}$	
3061.027		10	32659.28	+0.04	$22503_{1\frac{1}{2}}$—$55162\frac{2}{2\frac{1}{2}}$	
3061.678	6	15	32652.35	−0.08	$a\ ^4G_{3\frac{1}{2}}$—$49242\frac{2}{2\frac{1}{2}}$	res
3063.422		8	32633.74	−0.06	$23450_{2\frac{1}{2}}$—$56084\frac{1}{3\frac{1}{2}}$	
3063.972	4	30	32627.89	−0.01	$a\ ^4G_{4\frac{1}{2}}$—$49181\frac{2}{4\frac{1}{2}}$	res
3064.635		3	32620.83	+0.01	$a\ ^4D_{2\frac{1}{2}}$—$47588\frac{1}{1\frac{1}{2}}$	
3066.976	6	60	32595.93	+0.07	$a\ ^4G_{2\frac{1}{2}}$—$48830\frac{3}{3\frac{1}{2}}$	7
3067.410	3	6	32591.32	−0.05	$a\ ^4G_{3\frac{1}{2}}$—$49181\frac{3}{3\frac{1}{2}}$	
3067.572	5	50	32589.61	+0.02	$20780_{4\frac{1}{2}}$—$53369\frac{1}{4\frac{1}{2}}$	6
3067.856	6	60	32586.59	+0.08	$19276_{2\frac{1}{2}}$—$51863\frac{3}{3\frac{1}{2}}$	7
3069.288	8	80	32571.38	0.00	$a\ ^4G_{4\frac{1}{2}}$—$49124\frac{3}{3\frac{1}{2}}$	res
3071.234	1	15	32550.74	−0.08	$26158_{4\frac{1}{2}}$—$58709\frac{3}{3\frac{1}{2}}$	res
3071.730	5	50	32545.48	−0.10	$a\ ^4D_{1\frac{1}{2}}$—$47179\frac{1}{1\frac{1}{2}}$	res
3072.740	4	30	32534.78	−0.07	$a\ ^4G_{3\frac{1}{2}}$—$49124\frac{3}{3\frac{1}{2}}$	res
3073.403		4	32527.77	+0.36	$20039_{3\frac{1}{2}}$—$52567\frac{1}{4\frac{1}{2}}$	
3075.963		8	32500.70			
3077.520	30	300	32484.26	+0.06	$23955_{3\frac{1}{2}}$—$56439\frac{3}{3\frac{1}{2}}$	5
3078.868	?	15	32470.03	+0.03	$26929_{5\frac{1}{2}}$—$59399\frac{1}{5\frac{1}{2}}$	res
3079.992		20	32458.19	−0.05	$23955_{3\frac{1}{2}}$—$56413\frac{1}{3\frac{1}{2}}$	4
3080.787		2	32449.81	+0.17	$19637_{2\frac{1}{2}}$—$52087\frac{2}{2\frac{1}{2}}$	
3081.042	4	40	32447.13	+0.06	$18990_{1\frac{1}{2}}$—$51438\frac{2}{2\frac{1}{2}}$	res
3081.215	1	3	32445.30	−0.21	$a\ ^4D_{2\frac{1}{2}}$—$47413\frac{2}{2\frac{1}{2}}$	
3083.520	2	20	32421.05	0.00	$23955_{3\frac{1}{2}}$—$56376\frac{3}{3\frac{1}{2}}$	6
3087.394	10	50	32380.37	+0.05	$a\ ^4D_{0\frac{1}{2}}$—$45553\frac{1}{1\frac{1}{2}}$	res
3089.742		6	32355.77	0.00	$28118_{2\frac{1}{2}}$—$60474\frac{2}{2\frac{1}{2}}$	
3090.712	2	2	32345.62	+0.07	$23046_{3\frac{1}{2}}$—$55392\frac{1}{3\frac{1}{2}}$	
3091.870		3	32333.49	+0.01	$30633_{4\frac{1}{2}}$—$62966\frac{1}{3\frac{1}{2}}$	
3094.629		4	32304.67	+0.18	$22194_{3\frac{1}{2}}$—$54498\frac{3}{3\frac{1}{2}}$	
3095.870	5	50	32291.73	+0.10	$18000_{2\frac{1}{2}}$—$50292\frac{3}{2\frac{1}{2}}$	res
3098.031		2	32269.20	+0.09	$28631_{3\frac{1}{2}}$—$60900\frac{2}{2\frac{1}{2}}$	
3098.300	2	12	32266.40	+0.09	$a\ ^4D_{3\frac{1}{2}}$—$47413\frac{2}{3\frac{1}{2}}$	
3098.580	—	12	32263.48	+0.04	$18990_{1\frac{1}{2}}$—$51254\frac{1}{1\frac{1}{2}}$	
3098.870	—	8	32260.47	+0.03	$24991_{1\frac{1}{2}}$—$57252\frac{2}{2\frac{1}{2}}$	
3100.074		5	32247.93	+0.03	$29341_{4\frac{1}{2}}$—$61589\frac{3}{3\frac{1}{2}}$	
3100.736	5	50	32241.05	+0.02	$a\ ^4G_{3\frac{1}{2}}$—$48830\frac{3}{3\frac{1}{2}}$	res
3101.224		4	32235.98	+0.13	$22139_{2\frac{1}{2}}$—$54375\frac{2}{2\frac{1}{2}}$	
3102.204	5	50	32225.79	+0.14	$19637_{2\frac{1}{2}}$—$51863\frac{3}{3\frac{1}{2}}$	res
3103.517	2	12	32212.16	+0.04	$a\ ^4D_{2\frac{1}{2}}$—$47179\frac{1}{1\frac{1}{2}}$	
3104.534		3	32201.61	+0.06	$22503_{1\frac{1}{2}}$—$54704\frac{2}{2\frac{1}{2}}$	
3106.180		8	32184.55	+0.01	$25672_{2\frac{1}{2}}$—$57856\frac{3}{2\frac{1}{2}}$	
3106.632		20	32179.86	−0.07	$34091_{4\frac{1}{2}}$—$66270\frac{1}{3\frac{1}{2}}$	
3108.386		3	32161.71	+0.20	$19404_{2\frac{1}{2}}$—$51438\frac{2}{2\frac{1}{2}}$	6
3108.778	6	60	32157.65	+0.15	$23234_{4\frac{1}{2}}$—$55392\frac{1}{4\frac{1}{2}}$	res
3110.690	4	40	32137.89	+0.10	$20455_{1\frac{1}{2}}$—$52593\frac{3}{2\frac{1}{2}}$	res
3111.887	1	4	32125.52	+0.04	$27273_{3\frac{1}{2}}$—$59399\frac{1}{4\frac{1}{2}}$	
3112.463	1	4	32119.58	−0.02	$a\ ^4P_{2\frac{1}{2}}$—$45553\frac{1}{1\frac{1}{2}}$	
3112.860	20	50	32115.48	−0.02	$23046_{3\frac{1}{2}}$—$55162\frac{2}{2\frac{1}{2}}$	res
3113.384		12	32110.08	+0.10	$26227_{2\frac{1}{2}}$—$58337\frac{2}{2\frac{1}{2}}$	6
3116.100		3	32082.09	−0.04	$25169_{1\frac{1}{2}}$—$57252\frac{2}{2\frac{1}{2}}$	
3117.263		1	32070.12	−0.20	$24804_{3\frac{1}{2}}$—$56874\frac{2}{2\frac{1}{2}}$	

TABLE 3. *Classified lines of* W II—Continued

Wavelength (Å)	Intensity		Wave number (cm^{-1})		Combination	Zeeman effect
	Arc	Spark	Observed	*O–C*		
Air						
3118.475		5	32057.66	−0.10	$25672_{2\frac{1}{2}}$—*57729*$^{3}_{3\frac{1}{2}}$	
3118.981		1	32052.46	0.00	$19442_{6\frac{1}{2}}$—*z* $^{6}F^{5}_{5\frac{1}{2}}$	
3119.237	5	12	32049.83	+0.19	*a* $^{4}G_{2\frac{1}{2}}$—*48284*$^{3}_{2\frac{1}{2}}$	
3121.032		10	32031.46	+0.16	$28187_{6\frac{1}{2}}$—*60218*$^{5}_{5\frac{1}{2}}$	
3125.700	1	2	31983.59	−0.08	$28491_{1\frac{1}{2}}$—*60474*$^{3}_{2\frac{1}{2}}$	
3125.790	1	8	31982.64	+0.10	$22503_{1\frac{1}{2}}$—*54485*$^{5}_{0\frac{1}{2}}$	
3126.420	4	40	31976.20	+0.14	$23046_{3\frac{1}{2}}$—*55022*$^{3}_{3\frac{1}{2}}$	6 res
3127.750	1	50	31962.60	+0.20	$26929_{5\frac{1}{2}}$—*58891*$^{3}_{3\frac{1}{2}}$	6 res
3128.982	2	40	31950.01	+0.21	$22535_{0\frac{1}{2}}$—*54485*$^{5}_{0\frac{1}{2}}$	res
3129.682	1	25	31942.87			
3129.907	3	2	31940.57	−0.14	$24991_{1\frac{1}{2}}$—*56932*$^{3}_{1\frac{1}{2}}$	
3133.780		3	31901.10	+0.19	$28377_{5\frac{1}{2}}$—*60278*$^{3}_{4\frac{1}{2}}$	
3133.965		20	31899.22	−0.03 +0.04	$29341_{4\frac{1}{2}}$—*61240*$^{5}_{3\frac{1}{2}}$ $20455_{1\frac{1}{2}}$—*52355*$^{5}_{0\frac{1}{2}}$	
3135.156		4	31887.10	+0.03	$25045_{0\frac{1}{2}}$—*56932*$^{3}_{1\frac{1}{2}}$	
3135.238		4	31886.27	0.00	$22139_{2\frac{1}{2}}$—*54026*$^{3}_{2\frac{1}{2}}$	
3135.838	1	12	31880.17	−0.01	$25209_{4\frac{1}{2}}$—*57089*$^{3}_{4\frac{1}{2}}$	6
3137.224	4	8	31866.08	+0.04	$31100_{5\frac{1}{2}}$—*62966*$^{3}_{3\frac{1}{2}}$	
3137.57		2	31862.56	+0.10	$22194_{3\frac{1}{2}}$—*54056*$^{3}_{4\frac{1}{2}}$	
3138.770		6	31850.39	+0.07	$19404_{0\frac{1}{2}}$—*51254*$^{1}_{1\frac{1}{2}}$	res
3139.517	1	12	31842.81	0.00	$28631_{3\frac{1}{2}}$—*60474*$^{3}_{2\frac{1}{2}}$	
3140.577	2	2	31832.06	−0.10	$22194_{3\frac{1}{2}}$—*54026*$^{3}_{2\frac{1}{2}}$	
3140.96		2	31828.18	0.00	$26158_{4\frac{1}{2}}$—*57986*$^{3}_{4\frac{1}{2}}$	
3142.928		3	31808.25	+0.18	$24804_{3\frac{1}{2}}$—*56612*$^{3}_{3\frac{1}{2}}$	
3143.348	4	20	31804.00	−0.02	$30633_{4\frac{1}{2}}$—*62437*$^{3}_{4\frac{1}{2}}$	6
3143.670		4	31800.74	+0.09	$19637_{2\frac{1}{2}}$—*51438*$^{3}_{2\frac{1}{2}}$	res
3144.493		25	31792.42	+0.05 +0.14	$19070_{4\frac{1}{2}}$—*50863*$^{1}_{4\frac{1}{2}}$ $28631_{3\frac{1}{2}}$—*60424*$^{3}_{3\frac{1}{2}}$	
3145.768	20	200	31779.53	−0.06	*a* $^{4}G_{4\frac{1}{2}}$—*48332*$^{3}_{3\frac{1}{2}}$	5
3146.292	—?	20	31774.24	0.00	$33910_{5\frac{1}{2}}$—*65684*$^{5}_{4\frac{1}{2}}$	7
3146.836	2	4	31768.75	+0.02	$19276_{2\frac{1}{2}}$—*51045*$^{3}_{3\frac{1}{2}}$	
3147.474	—	3	31762.31	−0.09	$25169_{1\frac{1}{2}}$—*56932*$^{3}_{1\frac{1}{2}}$	
3147.825		15	31758.77	+0.23	$26929_{5\frac{1}{2}}$—*58687*$^{3}_{4\frac{1}{2}}$	
3148.678	1	10	31750.17	−0.07	$28118_{2\frac{1}{2}}$—*59869*$^{3}_{3\frac{1}{2}}$	res
3149.856	30	300	31738.29	+0.04	*a* $^{4}D_{0\frac{1}{2}}$—*44911*$^{1}_{1\frac{1}{2}}$	res
3151.304	5	125	31723.71	0.00	$23234_{4\frac{1}{2}}$—*54958*$^{5}_{3\frac{1}{2}}$	5
3151.568	5	20	31721.05	+0.01	*a* $^{4}D_{1\frac{1}{2}}$—*46355*$^{3}_{2\frac{1}{2}}$	
3152.238		4	31714.31	+0.07	$29341_{4\frac{1}{2}}$—*61055*$^{3}_{4\frac{1}{2}}$	
3152.484	25	100	31711.84	+0.04	$23450_{2\frac{1}{2}}$—*55162*$^{3}_{2\frac{1}{2}}$	6
3152.749	5	6	31709.17	+0.19	*a* $^{6}S_{2\frac{1}{2}}$—*z* $^{6}F^{1}_{1\frac{1}{2}}$	
3153.134		2	31705.30	+0.18	$25169_{1\frac{1}{2}}$—*56874*$^{3}_{2\frac{1}{2}}$	
3153.934		2	31697.28	−0.12	$28118_{2\frac{1}{2}}$—*59816*$^{1}_{1\frac{1}{2}}$	
3154.172	5	10	31694.87	+0.06	*a* $^{4}G_{3\frac{1}{2}}$—*48284*$^{3}_{2\frac{1}{2}}$	
3158.925	1	2	31647.18	+0.33	$28631_{3\frac{1}{2}}$—*60278*$^{3}_{4\frac{1}{2}}$	
3160.026	20	200	31636.15	−0.06	*a* $^{4}F_{4\frac{1}{2}}$—*z* $^{6}F^{3}_{4\frac{1}{2}}$	6
3160.673	1	4	31629.68	−0.02	$26227_{2\frac{1}{2}}$—*57856*$^{3}_{3\frac{1}{2}}$	6
3161.942		10	31616.98	−0.04	$19637_{2\frac{1}{2}}$—*51254*$^{1}_{1\frac{1}{2}}$	res
3162.225		15	31614.15	+0.05	$31100_{5\frac{1}{2}}$—*62714*$^{5}_{4\frac{1}{2}}$	
3164.262		10	31593.80	+0.02	$34091_{4\frac{1}{2}}$—*65684*$^{5}_{4\frac{1}{2}}$	
3164.794	1	30	31588.49	−0.04	$23803_{3\frac{1}{2}}$—*55392*$^{1}_{1\frac{1}{2}}$	
3165.657		4	31579.88	+0.04	$25672_{2\frac{1}{2}}$—*57252*$^{3}_{2\frac{1}{2}}$	
3166.534		12	31571.13	−0.05	$26158_{4\frac{1}{2}}$—*57729*$^{3}_{3\frac{1}{2}}$	
3167.736	1	6	31559.16	−0.17	$25209_{4\frac{1}{2}}$—*56768*$^{3}_{3\frac{1}{2}}$	
3168.372		2	31552.82	−0.02	$24991_{1\frac{1}{2}}$—*56544*$^{3}_{2\frac{1}{2}}$	
3171.355	1	6	31523.14	−0.04	$22503_{1\frac{1}{2}}$—*54026*$^{3}_{2\frac{1}{2}}$	
3173.564		8	31501.20	0.00	$28491_{1\frac{1}{2}}$—*59992*$^{3}_{2\frac{1}{2}}$	7
3174.221		1	31494.68	−0.22	$20780_{4\frac{1}{2}}$—*52275*$^{3}_{3\frac{1}{2}}$	

TABLE 3. *Classified lines of* W II—Continued

Wavelength (Å)	Intensity		Wave number (cm^{-1})		Combination	Zeeman effect
	Arc	Spark	Observed	$O-C$		
Air						
3175.958	20	200	31477.46	−0.07	$a\ ^4P_{2\frac{1}{2}}$—$44911^\circ_{1\frac{1}{2}}$	res
3177.200	30	120	31465.15	−0.07	$a\ ^4F_{3\frac{1}{2}}$—$z\ ^6F^\circ_{3\frac{1}{2}}$	6
3178.036	6	60	31456.88	−0.05	$a\ ^4P_{1\frac{1}{2}}$—$z\ ^6F^\circ_{2\frac{1}{2}}$	res
3178.672		8	31450.58			
3179.436	15	120	31443.02	−0.06	$a\ ^4P_{2\frac{1}{2}}$—$z\ ^6F^\circ_{3\frac{1}{2}}$	res
3180.060	2	60	31436.85	−0.12	$23955_{5\frac{1}{2}}$—$55392^\circ_{4\frac{1}{2}}$	res
3182.194		30	31415.77	−0.07	$33910_{5\frac{1}{2}}$—$65326^\circ_{5\frac{1}{2}}$	
3183.000		2	31407.82	−0.05	$19637_{2\frac{1}{2}}$—$51045^\circ_{3\frac{1}{2}}$	
3183.441		12	31403.47	+0.01	$25209_{4\frac{1}{2}}$—$56612^\circ_{3\frac{1}{2}}$	
3183.965	3	10	31398.30	+0.01	$20039_{3\frac{1}{2}}$—$51438^\circ_{2\frac{1}{2}}$	
3185.057	2	20	31387.54	−0.04	$a\ ^4D_{2\frac{1}{2}}$—$46355^\circ_{2\frac{1}{2}}$	6
3186.396	2	15	31374.35	−0.18	$25169_{1\frac{1}{2}}$—$56544^\circ_{2\frac{1}{2}}$	7
3187.116	1	80	31367.26			
3188.016		6	31358.40	−0.06	$23803_{3\frac{1}{2}}$—$55162^\circ_{2\frac{1}{2}}$	
3188.495	1	10	31353.69	−0.11	$a\ ^4G_{2\frac{1}{2}}$—$47588^\circ_{1\frac{1}{2}}$	
3189.238	50*A*	100	31346.39	−0.02 +0.25	$a\ ^4D_{3\frac{1}{2}}$—$z\ ^6F^\circ_{4\frac{1}{2}}$ $a\ ^4F_{3\frac{1}{2}}$—$44758^\circ_{4\frac{1}{2}}$	
3191.016	2	20	31328.92	−0.10	$23046_{3\frac{1}{2}}$—$54375^\circ_{2\frac{1}{2}}$	res
3192.117		8	31318.12	−0.08	$a\ ^4F_{4\frac{1}{2}}$—$46175^\circ_{3\frac{1}{2}}$	
3193.825		25	31301.37	0.00	$18990_{1\frac{1}{2}}$—$50292^\circ_{2\frac{1}{2}}$	
3195.708	2	5	31282.93	−0.08	$22139_{2\frac{1}{2}}$—$53422^\circ_{1\frac{1}{2}}$	
3200.380		6	31237.26	−0.02	$28631_{2\frac{1}{2}}$—$59869^\circ_{3\frac{1}{2}}$	
3200.565		6	31235.46	+0.08	$34091_{4\frac{1}{2}}$—$65326^\circ_{5\frac{1}{2}}$	
3201.583	20	60	31225.53	−0.02	$a\ ^4F_{1\frac{1}{2}}$—$39936^\circ_{2\frac{1}{2}}$	res
3202.254		10	31218.98	−0.04	$23803_{3\frac{1}{2}}$—$55022^\circ_{3\frac{1}{2}}$	6
3203.343	12	60	31208.37	−0.01	$a\ ^4D_{3\frac{1}{2}}$—$46355^\circ_{2\frac{1}{2}}$	res
3203.433	6	30	31207.49	−0.11	$a\ ^4D_{2\frac{1}{2}}$—$46175^\circ_{3\frac{1}{2}}$	
3203.752		10	31204.39	+0.03	$25209_{4\frac{1}{2}}$—$56413^\circ_{4\frac{1}{2}}$	
3203.909	2		31202.86	+0.03	$25672_{2\frac{1}{2}}$—$56874^\circ_{2\frac{1}{2}}$	
3204.400	2	30	31198.07	−0.03	$22139_{2\frac{1}{2}}$—$53338^\circ_{3\frac{1}{2}}$	
3205.262		5	31189.69	−0.05	$22139_{2\frac{1}{2}}$—$53329^\circ_{1\frac{1}{2}}$	res
3206.420	6	60	31178.42	−0.07	$a\ ^4G_{2\frac{1}{2}}$—$47413^\circ_{3\frac{1}{2}}$	res
3206.680	—?	12	31175.89	0.00	$22194_{3\frac{1}{2}}$—$53369^\circ_{4\frac{1}{2}}$	
3207.580		8	31167.15	−0.02	$25209_{4\frac{1}{2}}$—$56376^\circ_{5\frac{1}{2}}$	
3207.671		6	31166.26	+0.06	$24918_{1\frac{1}{2}}$—$56084^\circ_{1\frac{1}{2}}$	
3209.968	4	80	31143.96	−0.03	$22194_{3\frac{1}{2}}$—$53338^\circ_{3\frac{1}{2}}$	res
3215.275	2	40	31092.56	−0.08 −0.18	$33910_{5\frac{1}{2}}$—$65003^\circ_{4\frac{1}{2}}$ $24991_{1\frac{1}{2}}$—$56084^\circ_{1\frac{1}{2}}$	
3215.648	?	30	31088.95	−0.24	$a\ ^4F_{2\frac{1}{2}}$—$42390^\circ_{3\frac{1}{2}}$	
3216.308	2	30	31082.57	−0.08 −0.01	$20780_{4\frac{1}{2}}$—$51863^\circ_{3\frac{1}{2}}$ $29341_{4\frac{1}{2}}$—$60424^\circ_{3\frac{1}{2}}$	
3218.806		6	31058.45	−0.09	$33910_{5\frac{1}{2}}$—$64969^\circ_{5\frac{1}{2}}$	
3219.890		5	31048.00	−0.07	$23450_{2\frac{1}{2}}$—$54498^\circ_{3\frac{1}{2}}$	
3221.914	60*A*	20	31028.49	+0.09	$a\ ^4D_{3\frac{1}{2}}$—$46175^\circ_{3\frac{1}{2}}$	
3222.274		3	31025.03	+0.03	$26227_{2\frac{1}{2}}$—$57252^\circ_{2\frac{1}{2}}$	
3222.646		20	31021.45	−0.09	$28377_{5\frac{1}{2}}$—$59399^\circ_{4\frac{1}{2}}$	
3223.22		2	31015.90	+0.09	$19276_{2\frac{1}{2}}$—$50292^\circ_{2\frac{1}{2}}$	
3223.900		8	31009.38	−0.36	$23046_{3\frac{1}{2}}$—$54056^\circ_{4\frac{1}{2}}$	
3224.320	3	4	31005.34	−0.17	$20039_{3\frac{1}{2}}$—$51045^\circ_{3\frac{1}{2}}$	
3224.550	6	15	31003.13	−0.05	$23955_{5\frac{1}{2}}$—$54958^\circ_{5\frac{1}{2}}$	6
3225.170	1	2	30997.17	+0.05	$a\ ^4F_{2\frac{1}{2}}$—$42298^\circ_{1\frac{1}{2}}$	
3225.480	2	20	30994.19	0.00	$23234_{4\frac{1}{2}}$—$54229^\circ_{5\frac{1}{2}}$	res
3226.750		5	30981.99	−0.11	$20455_{1\frac{1}{2}}$—$51438^\circ_{2\frac{1}{2}}$	
3227.020	1	6	30979.40	−0.04	$23046_{3\frac{1}{2}}$—$54026^\circ_{2\frac{1}{2}}$	
3228.990	3	15	30960.50	−0.15	$20534_{5\frac{1}{2}}$—$z\ ^6F^\circ_{4\frac{1}{2}}$	res
3229.422		8	30956.36	−0.08	$30633_{4\frac{1}{2}}$—$61589^\circ_{5\frac{1}{2}}$	
3230.604	4	20	30945.03	−0.07	$a\ ^4G_{2\frac{1}{2}}$—$47179^\circ_{1\frac{1}{2}}$	

TABLE 3. *Classified lines of* W II—Continued

Wavelength (Å)	Intensity		Wave number (cm^{-1})		Combination	Zeeman effect
	Arc	Spark	Observed	*O–C*		
Air						
3230.846	8	12	30942.71	−0.15	$a\ ^4F_{3\frac{1}{2}}$—$44354^{3}_{3\frac{1}{2}}$	res
3231.053		4	30940.73	+0.15	$25672_{2\frac{1}{2}}$—$56612^{3}_{3\frac{1}{2}}$	
3231.442		1	30937.01	−0.10	$22503_{1\frac{1}{2}}$—$53440^{6}_{1\frac{1}{2}}$	
3232.132	15*A*	6	30930.40	−0.32	$26158_{4\frac{1}{2}}$—$57089^{3}_{4\frac{1}{2}}$	
3233.140	3	8	30920.76	+0.04	$a\ ^4P_{2\frac{1}{2}}$—$44354^{3}_{2\frac{1}{2}}$	
3233.286		20	30919.36	−0.08 +0.02	$22194_{3\frac{1}{2}}$—$53113^{3}_{2\frac{1}{2}}$ $a\ ^4D_{1\frac{1}{2}}$—$45553^{1}_{1\frac{1}{2}}$	
3233.46		1	30917.70	+0.12	$30633_{4\frac{1}{2}}$—$61550^{3}_{3\frac{1}{2}}$	
3233.820		2	30914.25	−0.18	$25169_{1\frac{1}{2}}$—$56084^{1}_{1\frac{1}{2}}$	
3234.50		4	30904.40	+0.03	$22535_{0\frac{1}{2}}$—$53440^{6}_{1\frac{1}{2}}$	7
3235.774	1—	8	30895.59	−0.12	$a\ ^4G_{3\frac{1}{2}}$—$48332^{5}_{2\frac{1}{2}}$	6
3236.644	3	25	30887.29	+0.11	$22535_{0\frac{1}{2}}$—$53422^{1}_{1\frac{1}{2}}$	
3236.744		6	30886.33			
3237.684	1	30	30877.37	+0.09	$29341_{4\frac{1}{2}}$—$60218^{5}_{3\frac{1}{2}}$	
3238.220		2	30872.25	+0.01	$25672_{2\frac{1}{2}}$—$56544^{5}_{2\frac{1}{2}}$	
3243.008	5	40	30826.67	+0.02	$22503_{1\frac{1}{2}}$—$53329^{1}_{1\frac{1}{2}}$	res
3243.334	15	100	30823.58	−0.08	$a\ ^4G_{3\frac{1}{2}}$—$47413^{5}_{2\frac{1}{2}}$	5
3245.273		6	30805.16	−0.04	$34091_{4\frac{1}{2}}$—$64896^{3}_{3\frac{1}{2}}$	
3245.937		2	30798.86	+0.39	$20455_{1\frac{1}{2}}$—$51254^{1}_{1\frac{1}{2}}$	
3246.413		1	30794.35	+0.44	$22535_{0\frac{1}{2}}$—$53329^{1}_{1\frac{1}{2}}$	
3246.498	1	12	30793.54	−0.03	$19637_{2\frac{1}{2}}$—$50430^{1}_{1\frac{1}{2}}$	res
3249.848	10	30	30761.80	+0.03	$22139_{2\frac{1}{2}}$—$52901^{3}_{3\frac{1}{2}}$	res
3251.262	40*A*	40	30748.42	+0.05	$a\ ^4F_{2\frac{1}{2}}$—$z\ ^6F^{5}_{2\frac{1}{2}}$	res
3254.848	1	4	30714.54	−0.08	$20780_{4\frac{1}{2}}$—$z\ ^6F^{5}_{3\frac{1}{2}}$	
3255.012		30	30713.00	−0.05	$27273_{3\frac{1}{2}}$—$57986^{3}_{4\frac{1}{2}}$	5
3255.582		20	30707.62	−0.04	$22194_{3\frac{1}{2}}$—$52901^{3}_{3\frac{1}{2}}$	
3255.824		1	30705.33	+0.06	$26227_{2\frac{1}{2}}$—$56932^{1}_{1\frac{1}{2}}$	
3255.957	60*A*	20	30704.08	−0.06	$28187_{0\frac{1}{2}}$—$58891^{5}_{1\frac{1}{2}}$	
3257.815		12	30686.57	−0.13	$23450_{2\frac{1}{2}}$—$54137^{1}_{1\frac{1}{2}}$	
3260.32		3	30663.00	−0.03	$22139_{2\frac{1}{2}}$—$52803^{3}_{1\frac{1}{2}}$	
3261.937		8	30647.79	−0.20	$26227_{2\frac{1}{2}}$—$56874^{2}_{2\frac{1}{2}}$	
3262.244	3	60	30644.91	−0.04	$28631_{2\frac{1}{2}}$—$59276^{3}_{3\frac{1}{2}}$	6
3265.988	2	12	30609.78	−0.09	$26158_{4\frac{1}{2}}$—$56768^{3}_{3\frac{1}{2}}$	
3267.430		40	30596.27			
3268.353	—?	30	30587.63	−0.07	$24804_{3\frac{1}{2}}$—$55392^{3}_{4\frac{1}{2}}$	res
3268.882		4	30582.68	−0.16	$27273_{3\frac{1}{2}}$—$57856^{2}_{2\frac{1}{2}}$	
3269.622	50*A*	10	30575.76	+0.02	$23450_{2\frac{1}{2}}$—$54026^{2}_{2\frac{1}{2}}$	
3270.049		3	30571.77	−0.21	$23803_{3\frac{1}{2}}$—$54375^{2}_{2\frac{1}{2}}$	
3273.300	1	8	30541.41	−0.20	$26227_{2\frac{1}{2}}$—$56768^{3}_{3\frac{1}{2}}$	
3274.788	1	12	30527.53	−0.05	$29341_{4\frac{1}{2}}$—$59869^{3}_{3\frac{1}{2}}$	
3277.608	3	3	30501.27	−0.45	$31100_{5\frac{1}{2}}$—$61602^{3}_{6\frac{1}{2}}$	
3278.148		15	30496.24	−0.21	$24991_{1\frac{1}{2}}$—$55488^{1}_{1\frac{1}{2}}$	7
3278.924	12*A*	20	30489.02	+0.02	$31100_{5\frac{1}{2}}$—$61589^{5}_{5\frac{1}{2}}$	
3282.478		4	30456.01	−0.05	$27273_{3\frac{1}{2}}$—$57729^{5}_{3\frac{1}{2}}$	
3282.693	—?	5	30454.02	+0.02	$26158_{4\frac{1}{2}}$—$56612^{3}_{3\frac{1}{2}}$	
3283.765		20	30444.08			
3285.820	1	15	30425.04	−0.31	$34091_{4\frac{1}{2}}$—$64516^{3}_{4\frac{1}{2}}$	
3286.566	25	75	30418.13	−0.02	$a\ ^4F_{1\frac{1}{2}}$—$z\ ^6F^{3}_{1\frac{1}{2}}$	res
3290.10		1	30385.46	−0.28	$26227_{2\frac{1}{2}}$—$56612^{3}_{3\frac{1}{2}}$	
3291.45		3	30373.00	−0.07	$22194_{3\frac{1}{2}}$—$52567^{1}_{4\frac{1}{2}}$	
3293.138	2	25	30357.43	−0.20	$24804_{3\frac{1}{2}}$—$55162^{3}_{2\frac{1}{2}}$	
3297.418		4	30318.03	−0.11	$25169_{1\frac{1}{2}}$—$55488^{1}_{1\frac{1}{2}}$	
3297.497		4	30317.30	−0.10	$26227_{2\frac{1}{2}}$—$56544^{3}_{2\frac{1}{2}}$	
3298.284		40	30310.07	−0.01	$28377_{5\frac{1}{2}}$—$58687^{1}_{4\frac{1}{2}}$	
3299.39		4	30299.91	−0.03	$22503_{1\frac{1}{2}}$—$52803^{3}_{1\frac{1}{2}}$	
3299.741	6	25	30296.69	−0.06	$a\ ^4P_{0\frac{1}{2}}$—$z\ ^6F^{5}_{1\frac{1}{2}}$	

TABLE 3. *Classified lines of* W II—Continued

Wavelength (Å)	Intensity		Wave number (cm^{-1})		Combination	Zeeman effect
	Arc	Spark	Observed	$O-C$		
Air						
3300.344	5	12	30291.15	−0.12	$23046_{3\frac{1}{2}}$—*53338*$^{?}_{3\frac{1}{2}}$	6
3301.870		8	30277.15	−0.12	*a* $^4D_{1\frac{1}{2}}$—*44911*$^{?}_{1\frac{1}{2}}$	
3303.216		6	30264.81	−0.06	$20780_{4\frac{1}{2}}$—*51045*$^{?}_{3\frac{1}{2}}$	
3303.736		2	30260.05	−0.03	$31100_{5\frac{1}{2}}$—*61360*$^{?}_{4\frac{1}{2}}$	
3304.324	4*A*	3	30254.66	−0.24	$26158_{4\frac{1}{2}}$—*56413*$^{?}_{4\frac{1}{2}}$	
3304.548		80	30252.62	−0.08 +0.03	$23803_{3\frac{1}{2}}$—*54056*$^{?}_{3\frac{1}{2}}$ $20039_{3\frac{1}{2}}$—*50292*$^{?}_{2\frac{1}{2}}$	7
3305.46	1	1	30244.27	+0.07	$24918_{1\frac{1}{2}}$—*55162*$^{?}_{2\frac{1}{2}}$	
3308.358	3	60	30217.77	+0.06	$26158_{4\frac{1}{2}}$—*56376*$^{?}_{3\frac{1}{2}}$	5
3310.190		20	30201.05			
3312.163	1−	4	30183.06	−0.03	$25209_{4\frac{1}{2}}$—*55392*$^{?}_{4\frac{1}{2}}$	
3313.532		4	30170.59	−0.15	$24991_{1\frac{1}{2}}$—*55162*$^{?}_{2\frac{1}{2}}$	
3314.323		8	30163.39	−0.15	$18990_{1\frac{1}{2}}$—*49154*$^{?}_{0\frac{1}{2}}$	
3316.820		3	30140.68	+0.33	$31100_{5\frac{1}{2}}$—*61240*$^{?}_{5\frac{1}{2}}$	
3317.412	2	15	30135.31	0.00 +0.21	$22139_{2\frac{1}{2}}$—*52275*$^{?}_{3\frac{1}{2}}$ $23234_{4\frac{1}{2}}$—*53369*$^{?}_{4\frac{1}{2}}$	
3319.488	1	10	30116.47	−0.01	$34091_{4\frac{1}{2}}$—*64207*$^{?}_{4\frac{1}{2}}$	6
3320.944		10	30103.26	+0.06	$23234_{4\frac{1}{2}}$—*53338*$^{?}_{3\frac{1}{2}}$	
3322.345		6	30090.57	−0.09	$22503_{1\frac{1}{2}}$—*52593*$^{?}_{0\frac{1}{2}}$	
3323.414	15	10	30080.89	−0.31	$22194_{3\frac{1}{2}}$—*52275*$^{?}_{3\frac{1}{2}}$	6
3325.980	2	8	30057.68	−0.10	$29341_{4\frac{1}{2}}$—*59399*$^{?}_{4\frac{1}{2}}$	
3333.280	1	8	29991.85	−0.05	$18990_{1\frac{1}{2}}$—*48982*$^{?}_{1\frac{1}{2}}$	
3334.806		5	29978.13	−0.01	$27273_{3\frac{1}{2}}$—*57252*$^{?}_{3\frac{1}{2}}$	7
3335.404		3	29972.75	+0.27	$23450_{2\frac{1}{2}}$—*53422*$^{?}_{1\frac{1}{2}}$	
3336.170		2	29965.87	+0.29	$19276_{2\frac{1}{2}}$—*49242*$^{?}_{2\frac{1}{2}}$	
3337.352		3	29955.26	−0.08	$31100_{5\frac{1}{2}}$—*61055*$^{?}_{4\frac{1}{2}}$	
3338.276	1	12	29946.97	−0.08	$22139_{2\frac{1}{2}}$—*52087*$^{?}_{2\frac{1}{2}}$	
3338.632	5	25	29943.78	−0.03	*a* $^4D_{2\frac{1}{2}}$—*44911*$^{?}_{1\frac{1}{2}}$	res
3339.036	5	30	29940.15	−0.14	*a* $^4G_{4\frac{1}{2}}$—*z* $^6F^{?}_{4\frac{1}{2}}$	res
3339.590		8	29935.19	−0.06	$29341_{4\frac{1}{2}}$—*59276*$^{?}_{3\frac{1}{2}}$	
3342.468	25	120	29909.41	+0.05	*a* $^4D_{2\frac{1}{2}}$—*z* $^6F^{?}_{3\frac{1}{2}}$	res
3343.095	12	60	29903.80	+0.04	*a* $^4G_{3\frac{1}{2}}$—*z* $^6F^{?}_{3\frac{1}{2}}$	res
3343.410	15	80	29900.99	+0.11	*a* $^4F_{4\frac{1}{2}}$—*44758*$^{?}_{3\frac{1}{2}}$	6
3344.898	3	25	29887.69	+0.12	$23450_{2\frac{1}{2}}$—*53338*$^{?}_{3\frac{1}{2}}$	
3345.858	100*A*	80	29879.11	−0.10	$23450_{2\frac{1}{2}}$—*53329*$^{?}_{1\frac{1}{2}}$	7
3347.458	1	2	29864.83	−0.23	*a* $^4F_{1\frac{1}{2}}$—*z* $^2S^{?}_{0\frac{1}{2}}$	
3348.296	4	80	29857.36	+0.06	$26227_{2\frac{1}{2}}$—*56084*$^{?}_{1\frac{1}{2}}$	7
3348.876	4	40	29852.18	+0.13	$22503_{1\frac{1}{2}}$—*52355*$^{?}_{0\frac{1}{2}}$	6 res
3349.323	3	8	29848.20	+0.20	$19276_{2\frac{1}{2}}$—*49124*$^{?}_{3\frac{1}{2}}$	
3350.634	12	30	29836.52	+0.12	$20455_{1\frac{1}{2}}$—*50292*$^{?}_{2\frac{1}{2}}$	res
3352.388	3	10	29820.91	+0.09	*a* $^4D^{?}_{1\frac{1}{2}}$—*44455*$^{?}_{0\frac{1}{2}}$	
3352.954	20*A*	15	29815.88	+0.03	$25672_{2\frac{1}{2}}$—*55488*$^{?}_{1\frac{1}{2}}$	*d*
3356.241	4*A*	2	29786.68	+0.17	$24918_{1\frac{1}{2}}$—*54704*$^{?}_{2\frac{1}{2}}$	
3358.292		5	29768.49	−0.01	$24991_{1\frac{1}{2}}$—*54760*$^{?}_{0\frac{1}{2}}$	
3358.608	50	200	29765.69	−0.04	*a* $^4G_{3\frac{1}{2}}$—*46355*$^{?}_{2\frac{1}{2}}$	4
3359.274		10	29759.79	−0.23	$19070_{4\frac{1}{2}}$—*48830*$^{?}_{3\frac{1}{2}}$	
3360.326	3	30	29750.47	+0.05	$19404_{0\frac{1}{2}}$—*49154*$^{?}_{0\frac{1}{2}}$	res
3361.104	40*A*	100	29743.58	−0.08	*a* $^4P_{0\frac{1}{2}}$—*z* $^2S^{?}_{0\frac{1}{2}}$	res
3361.748		6	29737.89	+0.09	$28118_{2\frac{1}{2}}$—*57856*$^{?}_{2\frac{1}{2}}$	
3362.595		3	29730.39	+0.23	*a* $^4D_{3\frac{1}{2}}$—*z* $^6F^{?}_{3\frac{1}{2}}$	
3363.721	10	30	29720.44	−0.02	*a* $^4D_{1\frac{1}{2}}$—*44354*$^{?}_{2\frac{1}{2}}$	res
3364.351		4	29714.88	+0.02	$25045_{0\frac{1}{2}}$—*54760*$^{?}_{0\frac{1}{2}}$	
3364.588	1	3	29712.79	−0.26	$24991_{1\frac{1}{2}}$—*54704*$^{?}_{2\frac{1}{2}}$	
3366.718	2	30	29693.99	+0.09	$24804_{3\frac{1}{2}}$—*54498*$^{?}_{3\frac{1}{2}}$	res
3369.561		3	29668.93	−0.02	$22194_{3\frac{1}{2}}$—*51863*$^{?}_{3\frac{1}{2}}$	
3369.795	1	4	29666.87	0.00	$23234_{4\frac{1}{2}}$—*52901*$^{?}_{3\frac{1}{2}}$	
3370.240		3	29662.96	−0.06	$23450_{2\frac{1}{2}}$—*53113*$^{?}_{2\frac{1}{2}}$	

TABLE 3. *Classified lines of* W II—Continued

Wavelength (Å)	Intensity		Wave number (cm^{-1})		Combination	Zeeman effect
	Arc	Spark	Observed	$O-C$		
Air						
3372.202	2	15	29645.70	+0.01	$30633_{4\frac{1}{2}}$—$60278^{\circ}_{4\frac{1}{2}}$	6
3374.866	3	30	29622.30	+0.02	$a\ ^4G_{4\frac{1}{2}}$—$46175^{\circ}_{3\frac{1}{2}}$	res
3376.146	30	300	29611.07	−0.01	$a\ ^4D_{3\frac{1}{2}}$—$44758^{\circ}_{4\frac{1}{2}}$	res
3379.028	4	40	29585.81	+0.06	$a\ ^4G_{3\frac{1}{2}}$—$46175^{\circ}_{3\frac{1}{2}}$	res
3379.825		2	29578.84	+0.06	$19404_{0\frac{1}{2}}$—$48982^{\circ}_{1\frac{1}{2}}$	
3380.681	1	8	29571.35	+0.20	$24804_{3\frac{1}{2}}$—$54375^{\circ}_{2\frac{1}{2}}$	
3382.598	50*A*	40	29554.59	+0.41	$19276_{2\frac{1}{2}}$—$48830^{\circ}_{3\frac{1}{2}}$	
3383.091	2	50	29550.28	+0.10	$29341_{4\frac{1}{2}}$—$58891^{\circ}_{3\frac{1}{2}}$	
3384.888	25	20	29534.60	−0.14	$25169_{1\frac{1}{2}}$—$54704^{\circ}_{2\frac{1}{2}}$	
3386.502	4	20	29520.52	+0.17	$23046_{3\frac{1}{2}}$—$52567^{\circ}_{4\frac{1}{2}}$	
3386.933		3	29516.76	+0.16	$28491_{1\frac{1}{2}}$—$58007^{\circ}_{1\frac{1}{2}}$	
3387.634	1	15	29510.66	+0.40	$26929_{5\frac{1}{2}}$—$56439^{\circ}_{5\frac{1}{2}}$	
3389.544		2	29494.03	−0.01	$24991_{1\frac{1}{2}}$—$54485^{\circ}_{0\frac{1}{2}}$	
3389.985		1	29490.19	+0.05	$25672_{2\frac{1}{2}}$—$55162^{\circ}_{2\frac{1}{2}}$	
3390.324	1	20	29487.24	+0.10	$19637_{2\frac{1}{2}}$—$49124^{\circ}_{3\frac{1}{2}}$	res
3394.450	2	15	29451.40	+0.16	$23450_{2\frac{1}{2}}$—$52901^{\circ}_{3\frac{1}{2}}$	
3394.907	1	3	29447.44	+0.33	$26929_{5\frac{1}{2}}$—$56376^{\circ}_{5\frac{1}{2}}$	
3395.712		2	29440.45	+0.05	$25045_{0\frac{1}{2}}$—$54485^{\circ}_{0\frac{1}{2}}$	
3398.690		1	29414.66	+0.09	$23955_{5\frac{1}{2}}$—$53369^{\circ}_{4\frac{1}{2}}$	
3398.922	15	120	29412.65	+0.02	$18000_{3\frac{1}{2}}$—$47413^{\circ}_{2\frac{1}{2}}$	7
3401.884	30	300	29387.04	+0.04	$a\ ^4D_{2\frac{1}{2}}$—$44354^{\circ}_{2\frac{1}{2}}$	res
3402.194		40?	29384.37	+0.11	$24991_{1\frac{1}{2}}$—$54375^{\circ}_{2\frac{1}{2}}$	
3404.082		1	29368.07	+0.07	$29341_{4\frac{1}{2}}$—$58709^{\circ}_{3\frac{1}{2}}$	
3406.086	2	12	29350.79	+0.09	$25672_{2\frac{1}{2}}$—$55022^{\circ}_{3\frac{1}{2}}$	
3406.588	1	20	29346.47	+0.15	$29341_{4\frac{1}{2}}$—$58687^{\circ}_{4\frac{1}{2}}$	
3406.824	30*A*	40	29344.43	+0.14	$a\ ^4P_{1\frac{1}{2}}$—$39936^{\circ}_{2\frac{1}{2}}$	
3407.450	2	10	29339.04	+0.16	$27273_{3\frac{1}{2}}$—$56612^{\circ}_{3\frac{1}{2}}$	
3408.214	2	5	29332.47	+0.19	$23234_{4\frac{1}{2}}$—$52567^{\circ}_{4\frac{1}{2}}$	
3410.170	1	25	29315.64	−0.09	$25169_{1\frac{1}{2}}$—$54485^{\circ}_{0\frac{1}{2}}$	
3412.736	3	30	29293.60	+0.08	$18990_{1\frac{1}{2}}$—$48284^{\circ}_{2\frac{1}{2}}$	res
3415.406	4	6	29270.70	+0.16	$27273_{3\frac{1}{2}}$—$56544^{\circ}_{2\frac{1}{2}}$	
3416.370		2	29262.44	+0.39	$19070_{4\frac{1}{2}}$—$48332^{\circ}_{5\frac{1}{2}}$	
3416.623	20	100	29260.27			
3417.620		3	29251.74	−0.13	$24804_{3\frac{1}{2}}$—$54056^{\circ}_{4\frac{1}{2}}$	
3419.720		5	29233.77	+0.14	$26158_{4\frac{1}{2}}$—$55392^{\circ}_{4\frac{1}{2}}$	
3421.134	4	40	29221.69	+0.12	$24804_{3\frac{1}{2}}$—$54026^{\circ}_{3\frac{1}{2}}$	4
3421.430		5	29219.17	+0.07	$24918_{1\frac{1}{2}}$—$54137^{\circ}_{1\frac{1}{2}}$	
3422.742	1	6	29207.97	+0.17	$a\ ^4D_{3\frac{1}{2}}$—$44354^{\circ}_{2\frac{1}{2}}$	
3424.436	5	50	29193.52	+0.20	$19637_{2\frac{1}{2}}$—$48830^{\circ}_{3\frac{1}{2}}$	res
3426.20		4	29178.5	+0.3	$31100_{5\frac{1}{2}}$—$60278^{\circ}_{4\frac{1}{2}}$	
3430.558		1	29141.42	+0.12	$20039_{3\frac{1}{2}}$—$49181^{\circ}_{4\frac{1}{2}}$	
3430.739	1−	8	29139.89	+0.11	$27273_{3\frac{1}{2}}$—$56413^{\circ}_{4\frac{1}{2}}$	
3435.636		4	29098.35	+0.29	$28631_{3\frac{1}{2}}$—$57729^{\circ}_{3\frac{1}{2}}$	
3435.710	30*A*	6	29097.73	−0.17	$23803_{3\frac{1}{2}}$—$52901^{\circ}_{3\frac{1}{2}}$	*d*
3437.233	3	20?	29084.83	+0.05	$20039_{3\frac{1}{2}}$—$49124^{\circ}_{3\frac{1}{2}}$	res
3440.583	4	20	29056.51	+0.10	$a\ ^4G_{5\frac{1}{2}}$—$z\ ^6F^{\circ}_{4\frac{1}{2}}$	
3440.644		200	29056.00	+0.06	$33910_{5\frac{1}{2}}$—$62966^{\circ}_{5\frac{1}{2}}$	
3442.493	2	20	29040.40	+0.18	$23046_{3\frac{1}{2}}$—$52087^{\circ}_{2\frac{1}{2}}$	res
3443.167		2	29034.71	+0.03	$24991_{1\frac{1}{2}}$—$54026^{\circ}_{2\frac{1}{2}}$	
3444.934		2	29019.82	+0.04	$25209_{4\frac{1}{2}}$—$54229^{\circ}_{5\frac{1}{2}}$	
3449.862	10	100	28978.36	+0.05	$a\ ^4F_{3\frac{1}{2}}$—$42390^{\circ}_{3\frac{1}{2}}$	6
3451.166		10	28967.41	+0.08	$25169_{1\frac{1}{2}}$—$54137^{\circ}_{1\frac{1}{2}}$	7
3452.494	8	30	28956.27	+0.10	$a\ ^4P_{2\frac{1}{2}}$—$42390^{\circ}_{3\frac{1}{2}}$	res
3454.962	1*d*	30*d*	28935.54	+0.24	$26227_{2\frac{1}{2}}$—$55162^{\circ}_{2\frac{1}{2}}$	
3455.015			28935.14	+0.17	$22503_{1\frac{1}{2}}$—$51438^{\circ}_{2\frac{1}{2}}$	5

TABLE 3. *Classified lines of* W II—Continued

Wavelength (Å)	Intensity		Wave number (cm^{-1})		Combination	Zeeman effect
	Arc	Spark	Observed	*O–C*		
Air						
3460.377	1	10	28890.31	+0.12	$19442_{6\frac{1}{2}}$—*48332*$^{\circ}_{5\frac{1}{2}}$	
3463.510	20	150	28864.18	+0.08	*a* $^4P_{2\frac{1}{2}}$—*43298*$^{\circ}_{1\frac{1}{2}}$	7
3464.446	1	20	28856.38	+0.01	$25169_{1\frac{1}{2}}$—*54026*$^{\circ}_{2\frac{1}{2}}$	res
3465.062	1	10	28851.25	+0.08	$22194_{3\frac{1}{2}}$—*51045*$^{\circ}_{3\frac{1}{2}}$	6
3468.225	4	6	28824.94	+0.16	$23450_{2\frac{1}{2}}$—*52275*$^{\circ}_{3\frac{1}{2}}$	
3469.266	2	25	28816.29	+0.60	$23046_{3\frac{1}{2}}$—*51863*$^{\circ}_{3\frac{1}{2}}$	6
3470.746		1	28804.00	0.00	$33910_{5\frac{1}{2}}$—*62714*$^{\circ}_{6\frac{1}{2}}$	
3471.230	1	6	28799.99	+0.15	$26158_{4\frac{1}{2}}$—*54958*$^{\circ}_{5\frac{1}{2}}$	
3471.698		3	28796.10	+0.24	$26227_{2\frac{1}{2}}$—*55022*$^{\circ}_{3\frac{1}{2}}$	
3472.310	1	10	28791.03	+0.07	$20039_{3\frac{1}{2}}$—*48830*$^{\circ}_{3\frac{1}{2}}$	
3472.896		4	28786.17	0.00	$20455_{1\frac{1}{2}}$—*49242*$^{\circ}_{2\frac{1}{2}}$	
3475.288	2	80	28766.36	+0.04	$30633_{4\frac{1}{2}}$—*59399*$^{\circ}_{4\frac{1}{2}}$	res
3475.936	1	10	28761.00	0.00	$28491_{1\frac{1}{2}}$—*57252*$^{\circ}_{2\frac{1}{2}}$	
3476.496	30*A*	8	28756.36	+0.27	$28118_{2\frac{1}{2}}$—*56874*$^{\circ}_{2\frac{1}{2}}$	7
3477.092	1	4	28751.43	+0.09	$22503_{1\frac{1}{2}}$—*51254*$^{\circ}_{1\frac{1}{2}}$	6
3481.910	—?	10	28711.65	−0.01	$28377_{5\frac{1}{2}}$—*57089*$^{\circ}_{4\frac{1}{2}}$	
3483.490		3	28698.63	+0.06	$20455_{1\frac{1}{2}}$—*49154*$^{\circ}_{0\frac{1}{2}}$	
3486.122	10	50	28676.96	+0.17	*a* $^4G_{2\frac{1}{2}}$—*44911*$^{\circ}_{1\frac{1}{2}}$	res
3487.080		3	28669.08	+0.11	$22194_{3\frac{1}{2}}$—*50863*$^{\circ}_{4\frac{1}{2}}$	
3489.42		3	28649.86	+0.15	$28118_{2\frac{1}{2}}$—*56768*$^{\circ}_{3\frac{1}{2}}$	
3489.785	1	3	28646.86	+0.17	$20534_{5\frac{1}{2}}$—*49181*$^{\circ}_{4\frac{1}{2}}$	
3490.313	8	40	28642.53	+0.19	*a* $^4G_{2\frac{1}{2}}$—*z* $^6F^{\circ}_{3\frac{1}{2}}$	res
3490.912	12	50	28637.61	+0.12	*a* $^4F_{3\frac{1}{2}}$—*z* $^6F^{\circ}_{2\frac{1}{2}}$	4
3491.127	8	25	28635.85	+0.12	*a* $^4F_{2\frac{1}{2}}$—*39936*$^{\circ}_{2\frac{1}{2}}$	6 res
3492.056	3	40	28628.23	+0.07	$23234_{4\frac{1}{2}}$—*51863*$^{\circ}_{3\frac{1}{2}}$	
3492.46	1	3	28624.92	−0.04	$34091_{4\frac{1}{2}}$—*62715*$^{\circ}_{4\frac{1}{2}}$	
3493.62	1—		28615.42	+0.07	*a* $^4P_{2\frac{1}{2}}$—*z* $^6F^{\circ}_{2\frac{1}{2}}$	
3498.134	1	5	28578.49			
3503.22		3	28537.00	+0.11	*a* $^4P_{1\frac{1}{2}}$—*z* $^6F^{\circ}_{1\frac{1}{2}}$	
3503.656		30	28533.45	+0.05	$24804_{3\frac{1}{2}}$—*53338*$^{\circ}_{3\frac{1}{2}}$	
3505.05		2	28522.1	0.0	$24918_{1\frac{1}{2}}$—*53440*$^{\circ}_{0\frac{1}{2}}$	
3507.17		2	28504.87	−0.01	$24918_{1\frac{1}{2}}$—*53422*$^{\circ}_{1\frac{1}{2}}$	
3508.54	1	3	28493.73	−0.11	$28118_{2\frac{1}{2}}$—*56612*$^{\circ}_{3\frac{1}{2}}$	
3508.664		50	28492.73	0.00	$18000_{3\frac{1}{2}}$—*z* $^6F^{\circ}_{4\frac{1}{2}}$	
3511.269	2	15	28471.59	+0.15	$23803_{3\frac{1}{2}}$—*52275*$^{\circ}_{3\frac{1}{2}}$	
3512.077	1	20	28465.04	0.00	$25672_{2\frac{1}{2}}$—*54137*$^{\circ}_{1\frac{1}{2}}$	res
3512.98		3	28457.72	+0.12	$28631_{3\frac{1}{2}}$—*57089*$^{\circ}_{4\frac{1}{2}}$	
3514.106		20	28448.60	−0.01	$24991_{1\frac{1}{2}}$—*53440*$^{\circ}_{0\frac{1}{2}}$	
3514.990	1	4	28441.45	+0.18	$28491_{1\frac{1}{2}}$—*56932*$^{\circ}_{1\frac{1}{2}}$	
3516.234		15	28431.39	−0.03	$24991_{1\frac{1}{2}}$—*53422*$^{\circ}_{1\frac{1}{2}}$	
3517.39		3	28422.04	−0.33	$18990_{1\frac{1}{2}}$—*47413*$^{\circ}_{2\frac{1}{2}}$	
3518.56	1	2	28412.60	+0.07	$23450_{2\frac{1}{2}}$—*51863*$^{\circ}_{3\frac{1}{2}}$	
3521.57		2	28388.31	−0.05	$29341_{4\frac{1}{2}}$—*57729*$^{\circ}_{3\frac{1}{2}}$	
3522.102	1	10	28384.02	+0.03	$28491_{1\frac{1}{2}}$—*56874*$^{\circ}_{2\frac{1}{2}}$	
3523.133		8	28375.71			
3525.733	3	30	28354.79	+0.09	$18000_{3\frac{1}{2}}$—*46355*$^{\circ}_{2\frac{1}{2}}$	res
3526.817	—	50	28346.08	+0.06	$34091_{4\frac{1}{2}}$—*62437*$^{\circ}_{4\frac{1}{2}}$	6
3527.040	—?	30	28344.28	+0.14	$20780_{4\frac{1}{2}}$—*49124*$^{\circ}_{3\frac{1}{2}}$	
3529.546	10	100	28324.16	+0.12	*a* $^4G_{4\frac{1}{2}}$—*z* $^6F^{\circ}_{3\frac{1}{2}}$	res
3531.440	2	5	28308.97	+0.12	$24804_{3\frac{1}{2}}$—*53113*$^{\circ}_{2\frac{1}{2}}$	
3532.680		3	28299.03	+0.15	$31100_{5\frac{1}{2}}$—*59399*$^{\circ}_{4\frac{1}{2}}$	
3534.12		5	28287.50	−0.01	*a* $^4G_{3\frac{1}{2}}$—*z* $^6F^{\circ}_{3\frac{1}{2}}$	
3534.498	3	25	28284.48	−0.03	$25045_{0\frac{1}{2}}$—*53329*$^{\circ}_{1\frac{1}{2}}$	6?
3536.12		5	28271.50	−0.07	$26227_{2\frac{1}{2}}$—*54498*$^{\circ}_{3\frac{1}{2}}$	
3536.268	4	80	28270.32	+0.02	$25169_{1\frac{1}{2}}$—*53440*$^{\circ}_{0\frac{1}{2}}$	6?
3538.40		2	28253.29	+0.18	$25169_{1\frac{1}{2}}$—*53422*$^{\circ}_{1\frac{1}{2}}$	
3538.55	(—?)	3	28252.09	+0.09	$28187_{6\frac{1}{2}}$—*56439*$^{\circ}_{6\frac{1}{2}}$	

TABLE 3. *Classified lines of* W II—Continued

Wavelength (Å)	Intensity		Wave number (cm^{-1})		Combination	Zeeman effect
	Arc	Spark	Observed	*O–C*		
Air						
3539. 455	3*A*	4	28244. 87	+0. 13	$20039_{3\frac{1}{2}}$—*48284*$^{3}_{2\frac{1}{2}}$	res
3544. 460	5	25	28204. 98	+0. 02	*a* $^4G_{4\frac{1}{2}}$—*44758*$^{3}_{4\frac{1}{2}}$	res
3546. 474	3*A*	3	28188. 97	−0. 01	$18990_{1\frac{1}{2}}$—*47179*$^{3}_{1\frac{1}{2}}$	
3547. 00	1		28184. 79	+0. 23	$19404_{2\frac{1}{2}}$—*47588*$^{3}_{1\frac{1}{2}}$	
3548. 258	15*A*	12	28174. 79	+0. 07	$18000_{3\frac{1}{2}}$—*46175*$^{5}_{3\frac{1}{2}}$	*d*
3549. 052	25	150	28168. 49	+0. 06	*a* $^4G_{3\frac{1}{2}}$—*44758*$^{3}_{4\frac{1}{2}}$	res
3550. 14		3	28159. 86	+0. 02	$25169_{1\frac{1}{2}}$—*53329*$^{3}_{1\frac{1}{2}}$	
3551. 528		10	28148. 85	+0. 03	$26227_{2\frac{1}{2}}$—*54375*$^{3}_{2\frac{1}{2}}$	
3553. 020		5	28137. 03	+0. 22	$19276_{2\frac{1}{2}}$—*47413*$^{3}_{2\frac{1}{2}}$	
3554. 068	1	3	28128. 74	−0. 05	$25209_{4\frac{1}{2}}$—*53338*$^{3}_{3\frac{1}{2}}$	
3554. 93		2	28121. 92	−0. 04	$24991_{1\frac{1}{2}}$—*53113*$^{3}_{2\frac{1}{2}}$	
3555. 166	12	120	28120. 05	+0. 07	*a* $^4G_{2\frac{1}{2}}$—*44354*$^{5}_{2\frac{1}{2}}$	res
3557. 914	5	30	28098. 33	+0. 08	$22194_{3\frac{1}{2}}$—*50292*$^{3}_{2\frac{1}{2}}$	
3560. 67		2	28076. 58	+0. 04	$30633_{4\frac{1}{2}}$—*58709*$^{3}_{3\frac{1}{2}}$	
3561. 456		5	28070. 39	+0. 07	$26158_{4\frac{1}{2}}$—*54229*$^{3}_{3\frac{1}{2}}$	
3562. 508	1	5	28062. 10	+0. 30	$28377_{5\frac{1}{2}}$—*56439*$^{5}_{6\frac{1}{2}}$	4
3563. 59		3	28053. 6	+0. 2	$28491_{1\frac{1}{2}}$—*56544*$^{5}_{2\frac{1}{2}}$	
3563. 998	1	2	28050. 37	+0. 05	$20780_{4\frac{1}{2}}$—*48830*$^{3}_{3\frac{1}{2}}$	
3565. 834	1	3	28035. 92	+0. 08	$28377_{5\frac{1}{2}}$—*56413*$^{3}_{4\frac{1}{2}}$	
3566. 73		3	28028. 9	−0. 3	$26929_{3\frac{1}{2}}$—*54958*$^{3}_{3\frac{1}{2}}$	
3571. 972	3	8	27987. 75	+0. 22	$23450_{2\frac{1}{2}}$—*51438*$^{3}_{2\frac{1}{2}}$	
3572. 474	60	200	27983. 82	+0. 02	*a* $^4P_{1\frac{1}{2}}$—*z* $^2S^{5}_{0\frac{1}{2}}$	res
3572. 830	1	5	27981. 03	+0. 15	$28631_{3\frac{1}{2}}$—*56612*$^{5}_{3\frac{1}{2}}$	6
3574. 82		2	27965. 4	0. 0	$28118_{2\frac{1}{2}}$—*56084*$^{3}_{1\frac{1}{2}}$	
3577. 59		2	27943. 8	+0. 2	$25169_{1\frac{1}{2}}$—*53113*$^{5}_{2\frac{1}{2}}$	
3579. 64		3	27927. 8	−0. 1	$22503_{1\frac{1}{2}}$—*50430*$^{3}_{1\frac{1}{2}}$	
3581. 876	2	6	27910. 36	+0. 16	$26227_{2\frac{1}{2}}$—*54137*$^{3}_{1\frac{1}{2}}$	res
3582. 75	1	2	27903. 56	+0. 14	$19276_{2\frac{1}{2}}$—*47179*$^{3}_{1\frac{1}{2}}$	
3583. 458	1	8	27898. 04	+0. 24	$26158_{4\frac{1}{2}}$—*54056*$^{3}_{4\frac{1}{2}}$	6
3584. 68		3	27888. 53	+0. 09	$27273_{3\frac{1}{2}}$—*55162*$^{5}_{2\frac{1}{2}}$	
3592. 418	50	150	27828. 46	−0. 09 +0. 13	$20455_{1\frac{1}{2}}$—*48284*$^{5}_{2\frac{1}{2}}$ *a* $^4F_{2\frac{1}{2}}$—*z* $^6F^{5}_{1\frac{1}{2}}$	5 res 4
3596. 171	2	30	27799. 42	+0. 18	$26227_{2\frac{1}{2}}$—*54026*$^{5}_{2\frac{1}{2}}$	
3597. 48	—?	2	27789. 31	+0. 04	$22503_{1\frac{1}{2}}$—*50292*$^{3}_{2\frac{1}{2}}$	
3598. 45	2	20	27781. 8	0. 0	$28631_{3\frac{1}{2}}$—*56413*$^{3}_{4\frac{1}{2}}$	7
3600. 594		1	27765. 27	+0. 12	*a* $^4G_{3\frac{1}{2}}$—*44354*$^{5}_{2\frac{1}{2}}$	
3600. 933	1	6	27762. 66	+0. 18	$24804_{3\frac{1}{2}}$—*52567*$^{3}_{4\frac{1}{2}}$	
3601. 55		1	27757. 90	+0. 10	$25045_{0\frac{1}{2}}$—*52803*$^{3}_{1\frac{1}{2}}$	
3602. 455	3	8	27750. 93	+0. 11	$25672_{2\frac{1}{2}}$—*53422*$^{3}_{1\frac{1}{2}}$	
3602. 700	—?	1	27749. 04	+0. 04	$27273_{3\frac{1}{2}}$—*55022*$^{3}_{3\frac{1}{2}}$	
3608. 280		10	27706. 13			
3610. 044	1	20	27692. 59	+0. 13	$25209_{4\frac{1}{2}}$—*52901*$^{3}_{3\frac{1}{2}}$	res
3611. 826	1	20	27678. 92	+0. 02	$33910_{5\frac{1}{2}}$—*61589*$^{5}_{5\frac{1}{2}}$	6
3613. 530		4	27665. 88	−0. 03	$25672_{2\frac{1}{2}}$—*53338*$^{3}_{3\frac{1}{2}}$	
3613. 785	30	150	27663. 93	+0. 09	*a* $^4D_{1\frac{1}{2}}$—*42298*$^{3}_{1\frac{1}{2}}$	res
3614. 606	1	8	27657. 64	+0. 09	$25672_{2\frac{1}{2}}$—*53329*$^{3}_{1\frac{1}{2}}$	
3617. 652		4	27634. 36	+0. 05 +0. 17	$18990_{1\frac{1}{2}}$—*46625*$^{5}_{0\frac{1}{2}}$ $23803_{3\frac{1}{2}}$—*51438*$^{5}_{2\frac{1}{2}}$	
3618. 434	1	25	27628. 39	+0. 21	$23234_{4\frac{1}{2}}$—*50863*$^{3}_{3\frac{1}{2}}$	
3628. 413	3	30	27552. 40	+0. 05	$20780_{4\frac{1}{2}}$—*48332*$^{5}_{3\frac{1}{2}}$	res
3628. 924	2	25	27548. 52	0. 00	$25045_{0\frac{1}{2}}$—*52593*$^{3}_{0\frac{1}{2}}$	res
3630. 080	2	3	27539. 75	0. 15	$23955_{3\frac{1}{2}}$—*z* $^6F^{5}_{3\frac{1}{2}}$	
3630. 950		8	27533. 15	+0. 10	*a* $^4F_{4\frac{1}{2}}$—*42390*$^{3}_{3\frac{1}{2}}$	
3639. 213		1	27470. 64	+0. 03	$24804_{3\frac{1}{2}}$—*52275*$^{3}_{3\frac{1}{2}}$	
3641. 403	60	120	27454. 12	+0. 03	*a* $^4F_{1\frac{1}{2}}$—*z* $^6F^{5}_{0\frac{1}{2}}$	7
3645. 594	10	100	27422. 56	+0. 11	*a* $^4D_{2\frac{1}{2}}$—*42390*$^{3}_{3\frac{1}{2}}$	res
3646. 577	10	50	27415. 16	+0. 07	*a* $^4D_{1\frac{1}{2}}$—*z* $^6F^{3}_{2\frac{1}{2}}$	

TABLE 3. *Classified lines of* W II—Continued

Wavelength (Å)	Intensity		Wave number (cm^{-1})		Combination	Zeeman effect
	Arc	Spark	Observed	*O–C*		
Air						
3652.114	10	20	27373.60	+0.01	$20039_{3\frac{1}{2}}$—$47413^{\circ}_{2\frac{1}{2}}$	
3653.324	2	10	27364.54	+0.10	$18990_{1\frac{1}{2}}$—$46355^{\circ}_{2\frac{1}{2}}$	
3654.74		10	27353.94	+0.04	$30633_{4\frac{1}{2}}$—$57986^{\circ}_{4\frac{1}{2}}$	
3657.583	40	120	27332.67	−0.02	$a\ ^4P_{0\frac{1}{2}}$—$z\ ^6F^{\circ}_{0\frac{1}{2}}$	
3657.871	10	40	27330.52	+0.14	$a\ ^4D_{2\frac{1}{2}}$—$42298^{\circ}_{1\frac{1}{2}}$	res
3660.604	30*A*	8	27310.12	+0.21	$25045_{0\frac{1}{2}}$—$52355^{\circ}_{0\frac{1}{2}}$	
3670.65		1?	27235.37	+0.10	$34091_{4\frac{1}{2}}$—$61326^{\circ}_{3\frac{1}{2}}$	
3672.547	5	25	27221.31	+0.12	$19404_{0\frac{1}{2}}$—$46625^{\circ}_{0\frac{1}{2}}$	6
3677.405	1	8	27185.35	+0.11	$25169_{1\frac{1}{2}}$—$52355^{\circ}_{0\frac{1}{2}}$	
3678.210	1	10	27179.40	+0.07	$26158_{4\frac{1}{2}}$—$53338^{\circ}_{3\frac{1}{2}}$	res
3687.510		2	27110.85	−0.22	$26227_{2\frac{1}{2}}$—$53338^{\circ}_{3\frac{1}{2}}$	
3689.596		10	27095.52	+0.06	$24991_{1\frac{1}{2}}$—$52087^{\circ}_{2\frac{1}{2}}$	
3691.463	1	2	27081.82	+0.19	$a\ ^4D_{2\frac{1}{2}}$—$z\ ^6F^{\circ}_{2\frac{1}{2}}$	
3691.846	4	40	27079.01	+0.13	$19276_{2\frac{1}{2}}$—$46355^{\circ}_{2\frac{1}{2}}$	res
3692.864		2	27071.55	−0.53	$29341_{4\frac{1}{2}}$—$56413^{\circ}_{4\frac{1}{2}}$	
3694.525	40*A*	40	27059.38	+0.17	$23803_{3\frac{1}{2}}$—$50863^{\circ}_{3\frac{1}{2}}$	5
3705.310	1	4	26980.62	+0.17	$23450_{2\frac{1}{2}}$—$50430^{\circ}_{1\frac{1}{2}}$	
3707.478	3	2	26964.84	+0.06	$34091_{4\frac{1}{2}}$—$61055^{\circ}_{4\frac{1}{2}}$	
3708.494	8	60	26957.45	+0.05	$20455_{1\frac{1}{2}}$—$47413^{\circ}_{2\frac{1}{2}}$	
3712.202	3	12	26930.53	+0.09	$22194_{3\frac{1}{2}}$—$49124^{\circ}_{3\frac{1}{2}}$	
3714.033		2	26917.25	+0.10	$25169_{1\frac{1}{2}}$—$52087^{\circ}_{2\frac{1}{2}}$	
3715.832	3	8	26904.22	+0.26	$28118_{2\frac{1}{2}}$—$55022^{\circ}_{3\frac{1}{2}}$	
3716.062	10	50	26902.55	+0.12	$a\ ^4D_{3\frac{1}{2}}$—$z\ ^6F^{\circ}_{3\frac{1}{2}}$	res
3716.550	2	2	26899.02	+0.12	$19276_{2\frac{1}{2}}$—$46175^{\circ}_{3\frac{1}{2}}$	
3719.66		3	26876.53	+0.05	$18000_{3\frac{1}{2}}$—$z\ ^6F^{\circ}_{3\frac{1}{2}}$	
3721.102		10	26866.12			
3732.684	2	2	26782.76	+0.08	$27273_{3\frac{1}{2}}$—$54056^{\circ}_{3\frac{1}{2}}$	
3736.213	12	60	26757.46	+0.06	$18000_{3\frac{1}{2}}$—$44758^{\circ}_{4\frac{1}{2}}$	res
3736.91		2	26752.5	+0.1	$27273_{3\frac{1}{2}}$—$54026^{\circ}_{3\frac{1}{2}}$	
3741.706	30*A*	12	26718.18	+0.16	$19637_{2\frac{1}{2}}$—$46355^{\circ}_{2\frac{1}{2}}$	6
3745.530	4	40	26690.90	+0.17	$22139_{2\frac{1}{2}}$—$48830^{\circ}_{3\frac{1}{2}}$	7
3750.744	1	8	26653.80	+0.05	$25209_{4\frac{1}{2}}$—$51863^{\circ}_{3\frac{1}{2}}$	
3753.162		3	26636.63	+0.01	$22194_{3\frac{1}{2}}$—$48830^{\circ}_{3\frac{1}{2}}$	
3753.620		10	26633.38	+0.02	$24804_{3\frac{1}{2}}$—$51438^{\circ}_{3\frac{1}{2}}$	
3760.364	2	20	26585.61	−0.10	$28118_{2\frac{1}{2}}$—$54704^{\circ}_{2\frac{1}{2}}$	
3763.616	2	2	26562.64	−0.10	$18990_{1\frac{1}{2}}$—$45553^{\circ}_{1\frac{1}{2}}$	
3768.97		4	26524.91	+0.06	$a\ ^4F_{3\frac{1}{2}}$—$39936^{\circ}_{2\frac{1}{2}}$	
3772.05	8*A*	3	26503.25	+0.54	$a\ ^4P_{2\frac{1}{2}}$—$39936^{\circ}_{2\frac{1}{2}}$	
3774.14	—	20	26488.58	+0.09	$23803_{3\frac{1}{2}}$—$50292^{\circ}_{2\frac{1}{2}}$	
3777.35	1	10	26466.07	+0.01	$18990_{1\frac{1}{2}}$—$45457^{\circ}_{0\frac{1}{2}}$	
3778.686	30*A*	8	26456.71	+0.27	$30633_{4\frac{1}{2}}$—$57089^{\circ}_{3\frac{1}{2}}$	
3785.58		20	26408.5	+0.1	$26158_{4\frac{1}{2}}$—$52567^{\circ}_{4\frac{1}{2}}$	
3789.726		20	26379.64	−0.03	$28118_{2\frac{1}{2}}$—$54498^{\circ}_{3\frac{1}{2}}$	
3804.481	1	2	26277.3	+0.1	$19276_{2\frac{1}{2}}$—$45553^{\circ}_{1\frac{1}{2}}$	
3814.418	5	6	26208.88	−0.32	$25045_{0\frac{1}{2}}$—$51254^{\circ}_{1\frac{1}{2}}$	
3822.198	2	4	26155.53	+0.10	$a\ ^4G_{2\frac{1}{2}}$—$42390^{\circ}_{3\frac{1}{2}}$	
3823.062	3	10	26149.62	0.00	$19404_{0\frac{1}{2}}$—$45553^{\circ}_{1\frac{1}{2}}$	res
3827.89		4	26116.6	+0.1	$26158_{4\frac{1}{2}}$—$52275^{\circ}_{3\frac{1}{2}}$	
3833.61	2		26077.7	0.0	$23046_{2\frac{1}{2}}$—$49124^{\circ}_{3\frac{1}{2}}$	
3837.238	4	10	26053.02	+0.08	$19404_{0\frac{1}{2}}$—$45457^{\circ}_{0\frac{1}{2}}$	
3846.688	2		25989.02	+0.02	$31100_{5\frac{1}{2}}$—$57089^{\circ}_{4\frac{1}{2}}$	
3851.131	—?	2	25959.03	−0.05	$20534_{3\frac{1}{2}}$—$z\ ^6F^{\circ}_{4\frac{1}{2}}$	
3851.570	12	60	25956.07	+0.04	$a\ ^4D_{0\frac{1}{2}}$—$z\ ^6F^{\circ}_{1\frac{1}{2}}$	res
3856.828	3	6	25920.69	+0.02	$18990_{1\frac{1}{2}}$—$44911^{\circ}_{1\frac{1}{2}}$	6
3859.986	2	6	25899.48	+0.01	$20455_{1\frac{1}{2}}$—$46355^{\circ}_{2\frac{1}{2}}$	

TABLE 3. *Classified lines of* W II—Continued

Wavelength (Å)	Intensity		Wave number (cm^{-1})		Combination	Zeeman effect
	Arc	Spark	Observed	*O–C*		
Air						
3872. 656	4	10	25814. 75	+0. 14	$a\ ^4G_{2\frac{1}{2}}$—$z\ ^6F^\circ_{3\frac{1}{2}}$	
3877. 29	2	15	25783. 9	0. 0	$23046_{3\frac{1}{2}}$—$48830^\circ_{3\frac{1}{2}}$	6
3877. 65	1		25781. 5	+0. 1	$22503_{1\frac{1}{2}}$—$48284^\circ_{2\frac{1}{2}}$	
3883. 336	2	3	25743. 76	−0. 20	$28631_{3\frac{1}{2}}$—$54375^\circ_{2\frac{1}{2}}$	
3887. 951	1	3	25713. 20	+0. 15	$20780_{4\frac{1}{2}}$—$z\ ^6F^\circ_{4\frac{1}{2}}$	
3890. 658	—?	2	25695. 31	0. 00	$a\ ^4P_{2\frac{1}{2}}$—$z\ ^6F^\circ_{1\frac{1}{2}}$	
3891. 83	1	1	25687. 57	+0. 15	$19070_{4\frac{1}{2}}$—$44758^\circ_{3\frac{1}{2}}$	
3896. 930	3	20	25653. 95	+0. 18	$25209_{4\frac{1}{2}}$—$50863^\circ_{4\frac{1}{2}}$	6
3899. 782	2	3	25635. 19	+0. 08	$19276_{2\frac{1}{2}}$—$44911^\circ_{1\frac{1}{2}}$	
3900. 879	2	8	25627. 98	+0. 10	$27273_{3\frac{1}{2}}$—$52901^\circ_{3\frac{1}{2}}$	
3905. 79	1	3	25595. 8	0. 0	$23234_{4\frac{1}{2}}$—$48830^\circ_{3\frac{1}{2}}$	
3909. 276	2	2	25572. 94	+0. 11	$a\ ^4P_{1\frac{1}{2}}$—$z\ ^6F^\circ_{0\frac{1}{2}}$	
3915. 456	2	5	25532. 57	+0. 21	$23450_{2\frac{1}{2}}$—$48982^\circ_{1\frac{1}{2}}$	
3935. 43	4	10	25403. 0	+0. 1	$a\ ^4D_{0\frac{1}{2}}$—$z\ ^2S^\circ_{0\frac{1}{2}}$	
3936. 653	1	5	25395. 10	+0. 06	$20780_{4\frac{1}{2}}$—$46175^\circ_{3\frac{1}{2}}$	
3936. 782	1		25394. 27	−0. 11	$28631_{3\frac{1}{2}}$—$54026^\circ_{2\frac{1}{2}}$	
3938. 10		1	25385. 8	0. 0	$25045_{0\frac{1}{2}}$—$50430^\circ_{1\frac{1}{2}}$	
3939. 43	8	3	25377. 2	0. 0	$23803_{3\frac{1}{2}}$—$49181^\circ_{4\frac{1}{2}}$	
3951. 067	3	6	25302. 45	0. 00	$a\ ^4D_{1\frac{1}{2}}$—$39936^\circ_{2\frac{1}{2}}$	
3955. 606	1	1	25273. 42	+0. 06	$22139_{2\frac{1}{2}}$—$47413^\circ_{2\frac{1}{2}}$	
3960. 87	2	6	25239. 83	+0. 03	$19637_{2\frac{1}{2}}$—$z\ ^6F^\circ_{3\frac{1}{2}}$	
3691. 192	—?	3	25237. 78	+0. 10	$23046_{3\frac{1}{2}}$—$48284^\circ_{2\frac{1}{2}}$	
3964. 096	—?	6	25219. 29	+0. 04	$22194_{3\frac{1}{2}}$—$47413^\circ_{2\frac{1}{2}}$	
3983. 292	50*A*	5	25097. 76	−0. 01	$20455_{1\frac{1}{2}}$—$45553^\circ_{1\frac{1}{2}}$	6, *d*
3986. 38		1	25078. 3	0. 0	$19276_{2\frac{1}{2}}$—$44354^\circ_{2\frac{1}{2}}$	
3990. 42		2	25052. 9	+0. 1	$22535_{0\frac{1}{2}}$—$47588^\circ_{1\frac{1}{2}}$	
3994. 56	2		25027. 0	+0. 1	$23803_{3\frac{1}{2}}$—$48830^\circ_{3\frac{1}{2}}$	
4000. 10	1	1	24992. 3	+0. 1	$28377_{5\frac{1}{2}}$—$53369^\circ_{4\frac{1}{2}}$	
4001. 883	1	4	24981. 17	−0. 01	$33910_{5\frac{1}{2}}$—$58891^\circ_{5\frac{1}{2}}$	6
4060. 166	1	2	24622. 58	+0. 06	$28491_{1\frac{1}{2}}$—$53113^\circ_{2\frac{1}{2}}$	
4069. 61	1		24565. 4	−0. 3	$26929_{5\frac{1}{2}}$—$z\ ^6F^\circ_{5\frac{1}{2}}$	
4081. 294	4	10	24495. 12	+0. 07	$a\ ^4D_{1\frac{1}{2}}$—$z\ ^6F^\circ_{1\frac{1}{2}}$	6
4114. 19	1	2	24299. 3	−0. 08	$22194_{3\frac{1}{2}}$—$z\ ^6F^\circ_{4\frac{1}{2}}$	
4144. 41	1		24122. 1	−0. 1	$22503_{1\frac{1}{2}}$—$46625^\circ_{0\frac{1}{2}}$	
4146. 62	—?	1	24109. 2	−0. 1	$25045_{0\frac{1}{2}}$—$49154^\circ_{0\frac{1}{2}}$	
4157. 030	2	5	24048. 86	+0. 11	$18000_{3\frac{1}{2}}$—$z\ ^6F^\circ_{3\frac{1}{2}}$	
4165. 60	1	2	23999. 4	+0. 2	$20455_{1\frac{1}{2}}$—$44455^\circ_{0\frac{1}{2}}$	
4175. 58	5	5	23942. 0	0. 0	$a\ ^4D_{1\frac{1}{2}}$—$z\ ^2S^\circ_{0\frac{1}{2}}$	
4257. 82	1		23479. 6	−0. 2	$24804_{3\frac{1}{2}}$—$48284^\circ_{2\frac{1}{2}}$	
4262. 75	1		23452. 4	0. 0	$25672_{2\frac{1}{2}}$—$49124^\circ_{3\frac{1}{2}}$	
4263. 81	1		23446. 6	0. 0	$23046_{3\frac{1}{2}}$—$z\ ^6F^\circ_{4\frac{1}{2}}$	
4289. 28	2	2	23307. 4	0. 0 +0. 2	$28187_{6\frac{1}{2}}$—$z\ ^6F^\circ_{5\frac{1}{2}}$ $18990_{1\frac{1}{2}}$—$42298^\circ_{1\frac{1}{2}}$	
4298. 26	1		23258. 7	+0. 1	$23234_{4\frac{1}{2}}$—$z\ ^6F^\circ_{4\frac{1}{2}}$	
4323. 392	1	6	23123. 49	+0. 04	$25209_{4\frac{1}{2}}$—$48332^\circ_{5\frac{1}{2}}$	
4335. 58	1?	6	23058. 5	0. 0	$18990_{1\frac{1}{2}}$—$z\ ^6F^\circ_{2\frac{1}{2}}$	
4342. 40		2	23022. 3	0. 0	$26158_{4\frac{1}{2}}$—$49181^\circ_{4\frac{1}{2}}$	
4343. 20	2	5	23018. 0	+0. 1	$22535_{0\frac{1}{2}}$—$45553^\circ_{1\frac{1}{2}}$	res
4348. 108	20*A*	25	22992. 05	+0. 08	$a\ ^4D_{0\frac{1}{2}}$—$z\ ^6F^\circ_{0\frac{1}{2}}$	res
4361. 534	8*A*	3	22921. 28	+0. 06	$22535_{0\frac{1}{2}}$—$45457^\circ_{0\frac{1}{2}}$	
4393. 80	1	2	22753. 0	+0. 1	$19637_{2\frac{1}{2}}$—$42390^\circ_{3\frac{1}{2}}$	

TABLE 3. *Classified lines of* W II—Continued

Wavelength (Å)	Intensity		Wave number (cm^{-1})		Combination	Zeeman effect
	Arc	Spark	Observed	*O–C*		
Air						
4396.88	2	2	22737.0	−0.2 0.0	$22139_{2\frac{1}{2}}$—$z\,{}^6F^0_{3\frac{1}{2}}$ $30633_{4\frac{1}{2}}$—*53369*$^0_{4\frac{1}{2}}$
4421.836	15*A*	3	22608.69	+0.03	$24804_{3\frac{1}{2}}$—*47413*$^0_{2\frac{1}{2}}$
4438.92		2	22521.7	0.0	$34091_{4\frac{1}{2}}$—*56612*$^0_{3\frac{1}{2}}$
4468.72		1	22371.5	−0.1	$23803_{3\frac{1}{2}}$—*46175*$^0_{3\frac{1}{2}}$
4508.50		2	22174.1	+0.1	$26158_{4\frac{1}{2}}$—*48332*$^0_{3\frac{1}{2}}$
4542.144	1	2	22009.86	−0.21 +0.15	$25169_{1\frac{1}{2}}$—*47179*$^0_{1\frac{1}{2}}$ $20039_{3\frac{1}{2}}$—$z\,{}^6F^0_{3\frac{1}{2}}$
4554.045	1	2	21952.35	+0.23	$22503_{1\frac{1}{2}}$—*44455*$^0_{0\frac{1}{2}}$
4604.576	1	3	21711.44	+0.14	$23046_{3\frac{1}{2}}$—*44758*$^0_{4\frac{1}{2}}$
4658.24	2	2	21461.3	+0.19	$23450_{2\frac{1}{2}}$—*44911*$^0_{1\frac{1}{2}}$
4665.76	4*A*	3	21426.74	+0.06	$23450_{2\frac{1}{2}}$—$z\,{}^6F^0_{3\frac{1}{2}}$
4691.74	1	2	21308.1	+0.1	$23046_{3\frac{1}{2}}$—*44354*$^0_{2\frac{1}{2}}$
4718.91	1	3	21185.4	−0.1	$25169_{1\frac{1}{2}}$—*46355*$^0_{2\frac{1}{2}}$
4768.25	1	2	20966.2	+0.1	$25209_{4\frac{1}{2}}$—*46175*$^0_{3\frac{1}{2}}$
4782.35	1	1	20904.4	+0.1	$23450_{2\frac{1}{2}}$—*44354*$^0_{2\frac{1}{2}}$
4864.565	2	3	20551.08	+0.10	$23803_{3\frac{1}{2}}$—*44354*$^0_{2\frac{1}{2}}$
4959.33	3	2	20158.4	+0.2	$22139_{2\frac{1}{2}}$—*42298*$^0_{1\frac{1}{2}}$
5021.324	5	2	19909.51	+0.03	$22139_{2\frac{1}{2}}$—$z\,{}^6F^0_{2\frac{1}{2}}$
5104.427	6	6	19585.37	+0.01	$18990_{1\frac{1}{2}}$—$z\,{}^2S^0_{0\frac{1}{2}}$
5114.59	3	3	19546.46	+0.07	$22503_{1\frac{1}{2}}$—$z\,{}^6F^0_{2\frac{1}{2}}$
5131.83	2	2	19480.8	−0.1	$20455_{1\frac{1}{2}}$—*39936*$^0_{2\frac{1}{2}}$
5214.41	2	?	19172.3	+0.1	$19404_{0\frac{1}{2}}$—$z\,{}^2S^0_{0\frac{1}{2}}$
5219.04	3	?	19155.3	−0.1	$23234_{4\frac{1}{2}}$—*42390*$^0_{3\frac{1}{2}}$
5260.92	4	4	19002.8	+0.2	$23046_{3\frac{1}{2}}$—$z\,{}^6F^0_{3\frac{1}{2}}$
5278.38	8	2	18939.9	+0.1	$23450_{2\frac{1}{2}}$—*42390*$^0_{3\frac{1}{2}}$
5304.17	10	4	18847.8	+0.1	$23450_{2\frac{1}{2}}$—*42298*$^0_{1\frac{1}{2}}$
5353.677	5	3	18673.54	+0.06	$20455_{1\frac{1}{2}}$—$z\,{}^6F^0_{1\frac{1}{2}}$
5375.103	3	2	18599.12	−0.24 +0.17	$26158_{4\frac{1}{2}}$—*44758*$^0_{4\frac{1}{2}}$ $23450_{2\frac{1}{2}}$—$z\,{}^6F^0_{2\frac{1}{2}}$
5410.89	2		18476.12	−0.01	$34091_{4\frac{1}{2}}$—*52567*$^0_{4\frac{1}{2}}$
5597.056	3	3	17861.63	+0.06	$28631_{3\frac{1}{2}}$—$z\,{}^6F^0_{4\frac{1}{2}}$
5698.47	1	1	17543.7	+0.1	$28631_{3\frac{1}{2}}$—*46175*$^0_{3\frac{1}{2}}$
5821.00	4*A*	1	17174.42	+0.03	$18990_{1\frac{1}{2}}$—$z\,{}^6F^0_{0\frac{1}{2}}$
5884.32	2	2	16989.6	+0.2	$22139_{2\frac{1}{2}}$—$z\,{}^6F^0_{1\frac{1}{2}}$
5964.48	3	5	16761.28	+0.01	$19404_{0\frac{1}{2}}$—$z\,{}^6F^0_{0\frac{1}{2}}$
6024.64	2	5	16593.91	+0.30	$22535_{0\frac{1}{2}}$—$z\,{}^6F^0_{1\frac{1}{2}}$
6219.77	2	8	16073.32	+0.06	$22503_{1\frac{1}{2}}$—$z\,{}^2S^0_{0\frac{1}{2}}$

I gratefully acknowledge the assistance of Dr. C. C. Kiess, who supplied most of the spectrograms, and of Mrs. Isabel Murray, who carefully prepared press-copy of the tables.

4. References

[1] O. Laporte, Regelmässigkeiten im Bogenspektrum des Wolframs, Naturwissenschaften **13**, 627–628 (1925).

[2] O. Laporte and J. E. Mack, The spectrum of neutral tungsten, W I. Phys. Rev. **63**, 246–297 (1943).

[3] D. D. Laun, Preliminary lists of terms for the arc and spark spectra of tungsten, J. Res. NBS **21**, 207–224 (1938) RP 1125.

[4] D. D. Laun, Arc spectrum of tungsten; University of Chicago, Dissertation; University of Chicago Libraries, Chicago, Ill. (1934).

[5] C. D. Coleman, W. R. Bozman, and W. F. Meggers, Table of wavenumbers, NBS Mono. 3, U.S. Government Printing Office, Washington; 1960.

[6] Charlotte E. Moore, Atomic energy levels, NBS Cir. 467, vol. III, 161–163 (1958).

[7] E. Back and A. Landé, Zeemaneffekt und Multiplettstruktur der Spectrallinien, 168–169 (Julius Springer, Berlin, 1925).

[8] W. F. Meggers, C. H. Corliss, and B. F. Scribner, Tables of spectral-line intensities, NBS Mono. 32, pt. 1, 402–415 (U.S. Government Printing Office, Washington, 1961).

[9] C. C. Kiess, C. J. Humphreys, and D. D. Laun, Preliminary description and analysis of the first spectrum of uranium, J. Res. NBS 37, 57–72 (1946) RP 1729.

(Paper 68A2—270)

JOURNAL OF RESEARCH of the National Bureau of Standards—A. Physics and Chemistry
Vol. 68A, No. 2, March–April 1964

Publications of the National Bureau of Standards*

Selected Abstracts

Gaussian wave functions for polyatomic molecules: integral formulas, M. Krauss, *J. Res.* **68B** (*Math. and Math. Phys.*), *No. 1, 35–41 (Jan.–Mar. 1894).*
Explicit formulas are given for the molecular coulomb integrals that arise for all Gaussian basis functions. These results should expedite computational efforts with these basis functions.

A Fabry-Perot spectrometer for high-resolution spectroscopy and laser work, K. D. Mielenz, R. B. Stephens, and K. F. Nefflen, *J. Res.* **68C** (*Eng. and Instr.*), *No. 1, 1–6 (Jan.–Mar. 1964).*
A Fabry-Perot spectrometer with a piezoelectric spacer was constructed to record with a recorder, or display with an ocilloscope, the fine structure of the Haidinger fringes. The spectrometer is of the fixed spacer design, which provides great stability of adjustment. It was used to record the Zeeman splitting of the green line of Hg 198, as well as to exhibit, on the ocilloscope screen, the multimode output signal of a He-Ne gas laser.

A laser with a multihole diaphragm, T. Morokuma, *J. Res. NBS* **68C** (*Eng. and Instr.*), *No. 1, 25–34 (Jan.–Mar. 1964).*
The properties of a laser with a multihole diaphgram were both theoretically and experimentally examined. This laser may be called a multibeam laser. Laser action was observed in the optical paths which were defined by the position of the holes and the cavity configuration. Interference fringes were observed on one of the cavity mirrors. A wavelength dependent interaction among the beams was observed. It is believed that the wavelength of a beam can be stabilized by the intensities of the other beams. A possible method will be proposed for the stabilization.

Principles of cryometric impurity determination as applied to samples of small sizes, C. P. Saylor and G. S. Ross, *J. Res. NBS* **68C** (*Eng. and Instr.*), *No. 1, 35–39 (Jan.–Mar. 1964).*
A consideration of the factors that tend to prevent attainment of thermal and thermodynamic equilibrium during thermometric methods of purity analysis suggests that the problems largely originate from spontaneously introduced inequalities in composition. During either a freezing or melting cycle, the solid phase settles in the liquid. This results in a greater average purity in the bottom than in the upper part of the vessel. The effects would be particularly strong during a melting sequence where the liquid released by melting of the solid would provide the compositional environment for the establishemnt of final temperature. This hypothesis has been tested by the design of a new cell for small samples. The design incorporates use of small gold pans to hold solid and liquid in close contact. The results are comparable in precision to those from conventional time-temperature curves with much larger samples, a condition not ordinarily possible with small samples.

Reference tables for thermocouples of iridium-rhodium alloys versus iridium, G. F. Blackburn and F. R. Caldwell, *J. Res. NBS* **68C** (*Eng. and Instr.*), *No. 1, 41–59 (Jan.–Mar. 1964).*
The program at the National Bureau of Standards to establish reference tables of temperature versus emf for thermocouples of iridium-rhodium alloys versus iridium has been extended to cover all three of the currently used thermocouples of this type. In addition to the values published in 1962 for the 40 Ir-60 Rh versus Ir thermocouples, tables now are available for thermocouples of 60 Ir-40 Rh and 50 Ir-50 Rh versus Ir. These tables give emfs for temperatures in degrees Celsius from 0 to 2150 °C and in degrees Fahrenheit from 32 to 3900 °F, and temperatures in these units with emf in millivolts as the argument.
In addition to the reference tables for these thermocouples, temperature-emf relationships are presented for other alloys containing 10, 25, 75, and 90 percent iridium versus iridium. It appears from the information obtained on all of the alloy versus iridium combinations tested that the 50 Ir-50 Rh alloy versus iridium gives about the maximum thermal emf (12.2 mv at 2150 °C), and as a result may provide the optimum thermocouple combination of this type.

A simplified theory of diffraction at an interface separating two dielectrics, J. Kane and S. N. Karp, *Radio Sci. J. Res. NBS/USNC–URSI* **68D** *No. 3, 303–310 (Mar. 1964).*
Many electromagnetic problems involving more than one dielectric medium are not susceptible of an exact solution, when appropriate boundary conditions are considered. The purpose of the present paper is to formulate a new boundary condition, which is capable of leading to mathematically tractable problems, with limited sacrifices in accuracy.

Propagation of plasma waves in a "spoke-wheel" magnetic field, R. L. Liboff, *Radio Sci. J. Res. NBS/USNC–URSI* **68D** *No. 3, 325–331 (Mar. 1964).*
A study of the cold plasma cylindrical waves that may propagate in a specific type of two-dimensional magnetic field is initiated in this paper. The plasma is assumed to be of uniform density and collisionless, and a "spoke-wheel" magnetic field is considered which is both anisotropic and inhomogeneous (varying as the inverse radius), as defined in the text. Perturbation series solutions are obtained for the first Fourier component of the electric field for the four extreme cases: large and small magnetic field; large and small plasma densities.

Compilation of the melting points of the metal oxides, S. J. Schneider, *NBS Mono. 68 (Oct. 10, 1963), 25 cents.*
A compilation has been made of the melting points of 70 metal oxides published prior to January 1963. Both the original melting point and the equivalent value based on the International Practical Temperature Scale of 1948 are presented. Included in the survey is information on pertinent experimental details such as the method of temperature measurement, purity, furnace type, and environmental conditions.

Calibration and test services of the National Bureau of Standards, *NBS Misc. Publ. 250 (Nov. 22, 1963), 70 cents.*
This publication is a listing of the numerous calibration and testing services provided to science and industry by the National Bureau of Standards. The Bureau promotes accuracy and uniformity of measurement through its program of measurement services, including the calibration and testing of standards and standard instruments. An up-to-date listing of the Bureau's calibration and test fee schedules was printed in recent issues of the Federal Register, with a large proportion of the fees being changed at that time. This publication contains all of this material, but in larger, more legible type, and fully indexed. Besides listing all NBS calibration services and their cost, the publication includes a statement of the Bureau's statutory functions, testing policy, and routine for securing the Bureau's calibration and test services—from original request to the reporting and use of test results.

A comparison of two melting-pressure equations constrained to the triple point using data for eleven gases and three metals, R. D. Goodwin and L. A. Weber, *NBS Tech. Note 184 (Oct. 9, 1963), 25 cents.*

Parameters have been determined by a least-squares method for the reduced Simon equation and for a new, empirical melting equation using data for H_2, D_2, T_2, Ne, Ar, Kr, Xe, N_2, O_2, CO_2, H_2O, Na, K, and Hg. The new equation, $(P-P^3)/(T-T^3)=A\exp(-\alpha/T)+BT$, represents experimental data with essentially the same accuracy as the Simon equation. It provides a sensitive difference method for graphical examination of data.

Carbon resistors for cryogenic liquid level measurements, R. C. Muhlenhaupt and P. Smelser, *NBS Tech. Note 200 (Oct. 8, 1963), 25 cents.*
Data are shown in graphical form. One set of plots presents resistance ratio R_G/R_L as a function of "warming up" time at various levels of constant power dissipation. A second set of plots presents resistance ratio R_L/R_O as a function of nominal resistance at various levels of constant power dissipation.
The use of the data and the design of a practical liquid level indicator are discussed in the appendix.

Absolute calibration of the National Bureau of Standards photoneutron source: III. Absorption in a heavy water solution of manganous sulfate, R. H. Noyce, E. R. Mosburg, Jr., S. B. Garfinkel, and R. S. Caswell, *J. Nucl. Eng.* **17,** *No. 7, 313–318 (1963).*
The neutron emission rate for the National Bureau of Standards radium-beryllium (γ,n) standard source (NBS–I) has been redetermined by a relative comparison to an antimony-beryllium source which had been calibrated absolutely in a heavy water manganous sulfate solution through an indirect method involving $4\pi\beta-\gamma$ coincidence counting of the induced Mn^{56} activity. Correction was made for absorption of neutrons by other elements present in the bath. The emission rate of NBS–I was found to be $1.25_2\times10^6$ neutrons per second, as of June 1961 with an uncertainty of 1 percent. This measurement, when suitably averaged with previous determinations (DeJuren, Padgett, and Curtiss, 1955; and DeJuren and Chin, 1955), yields the best value $1.25_7\times10^6$ neutrons per second with an uncertainty of 1 percent.

Heating rate as a test of adiabatic calorimeters and the heat capacity of α alumina, E. D. West, *Trans. Faraday Soc.* **59,** *No. 489, pt. 9, 2200–2203 (Sept. 1963).*
The constancy of heat capacities measured in an adiabatic calorimeter at different heating rates does not demonstrate the absence of heat leak errors due to departures of the surface temperature from the "isothermal" condition. On the contrary, the total heat exchange between the calorimeter and its shield is virtually independent of the heating rate. The test tends to obscure a real source of error due to the variation in the total heat exchange between experiments with the empty and the full calorimeter.

A new standard of spectral irradiance, R. Stair, W. E. Schneider, and J. K. Jackson, *Appl. Opt.* **2,** *No. 11, 1151–1154 (Nov. 1963).*
The National Bureau of Standards has made available a new standard of spectral irradiance in the form of a 200-watt quartz-iodine lamp with a coiled-coil tungsten filament operating at about 3000° K and calibrated over the spectral range of 0.25 to 2.6 microns. The calibration of this standard is based upon the radiance of a blackbody as defined by the Planck law of radiation since it was done by comparisons with the NBS standards of spectral radiance, of luminous intensity, and of total irradiance, each of which was established through the use of blackbodies. This standard is used without auxiliary optics. Because of its small physical size and high operating temperature, relatively high spectral irradiances may be obtained through its use.

Intercomparisons of the standard thermal-neutron flux density of the National Bureau of Standards, W. M. Murphey and J. Chin, (*Proc. Symp. Neutron Detection, Dosimetry and Standardization, International Atomic Energy Agency, Atomic Energy Research Establishment, Harwell, England, Dec. 10–14, 1962*), *Book, Neutron Dosimetry* **II,** *513–521* (*International Atomic Energy Agency, Vienna, 1963*).
The standard thermal neutron flux maintained at the National Bureau of Standards since 1951 consists of two radium-beryllium (α,n) sources in a geometry of lead, paraffin and carbon. The flux has been absolutely measured twice by NBS; once in terms of the absorption cross section of boron, and once in terms of the absorption cross section of gold (1,2). A neutron flux with a cadmium ratio of about 7 (for 40 mg/cm² gold foils and 0.040 inch cadmium covers) and a conventional thermal neutron flux density of 4231 (Apr. 62) neutrons per cm² per second was obtained. It has also been absolutely measured twice through the intercomparison program; once by NPL, UK and once by PTB, Federal Republic of Germany.
The agreement between most laboratories at present is about 1.5%. This is in addition to the uncertainty in the absolute measurement which is about 1.5% or more for each laboratory. Intercomparisons of NBS with CEA, France; Oak Ridge National Laboratory, USA; Electrotechnical Laboratory, Japan; National Physical Laboratory, UK; and Physikalisch-Technische Bundesanstalt, Federal Republic of Germany will be shown.

Interpretation of *p*H measurements in alcohol-water solvents, R. G. Bates, M. Paabo, and R. A. Robinson, *J. Phys. Chem.* **67,** *1833–1838 (1963).*
The operational *p*H numbers for solutions in alcohol-water solvents obtained from the e.m.f. of the cell with hydrogen (or glass) electrode, salt bridge, and calomel reference electrode, standardized with aqueous buffer standards, are subject to no simple interpretation. Because of the indeterminate potential at the junction Soln. X (alc.$-H_2O$)|KCl bridge (aq.), they do not lie on a conventional scale of hydrogen ion activity referred either to the aqueous standard state (pa_H) or to the standard state in the alcoholic medium (pa_H^*). Values of $\overline{E}_j+\log {}_m\gamma_{Cl}$ (where $\overline{E}_j$ is the liquid-junction potential expressed in *p*H units and ${}_m\gamma_{Cl}$ is the primary medium effect of chloride ion) were found to be as constant for different buffer solutions in alcoholic solvents of fixed composition as for the strictly aqueous medium. Inasmuch as ${}_m\gamma_{Cl}$ at a given temperature is dependent only on solvent composition, the liquid-junction potential must therefore also be nearly constant for a given solvent medium. Correction terms $\overline{E}_j-\log {}_m\gamma_H=\delta$ have been calculated, and it is shown that $p\mathrm{H}-\delta$ closely approximates pa_H^* under optimum conditions of measurement. An operational scale of *p*H* (which is related to pa_H^* in the same way that *p*H is related to pa_H) is described. Values of pa_H^* were obtained for 12 solutions in methanol-water solvents (0 to 68.1 wt. % MeOH) and for 3 solutions in ethanol-water solvents (0 to 100 % EtOH).

Short-duration visible afterglow in helium, A. L. Schmeltekopf, Jr., and H. P. Broida, *J. Chem. Phys.* **39,** *1261–1268 (Sept. 1963).*
A bright, reproducible afterglow which consists of helium atomic and molecular emissions has been observed in the products of an electrical discharge in a deLaval nozzle clearly separated from the discharge. This afterglow has been observed at pressures from 0.4 to 20 mm Hg and with flows from 10 to 1000 cm³/sec NTP. At the low pressure the existence of the afterglow is extremely sensitive to small changes in pressure. Metastable He atom concentration decreases after the discharge and then increases in the region of afterglow emission. The afterglow is very sensitive to impurities greater than a few parts in 10^5 and emission intensity is reduced by the presence of an rf field, possibly because heating the electrons retards recombination.

Infrared transmission of the atmosphere to solar radiation, D. M. Gates and W. J. Harrop, *Appl. Opt.* **2,** *887–898 (Sept. 1963).*
Infrared solar spectrum observations taken on 12 January 1955 in Denver, Colorado, with a double pass NaCl prism spectrometer have been analyzed for transmission coefficients for the "selective" absorption and for the "continuum" extinction. The analysis was performed over the range 1.0 to 12.5μ. The goodness of fit for the average transmission for a random band model and for a regular band model is given for each of 203 data points distributed throughout the spectrum.

Some topics in quantum statistics. The Wigner function and transport theory, H. Mori, I. Oppenheim, and J. Ross, *Book, Studies in Statistical Mechanics, ed. DeBoer and Uhlenbeck*, **I,** *Pt. C, 218–298 (North Holland Publ. Co., Amsterdam, the Netherlands, 1962).*
This article is devoted to a discussion of Wigner functions and their application in quantal statistical mechanics, as well as some recent work in the theory of non-equilibrium systems. An analysis of these systems also requires the inclusion of some other topics: scattering theory, representative ensembles, and factors influencing the derivation of a transport equation for irreversible phenomena. We begin with the description of a quantum mechanical system. In Section I we first present some definitions and then discuss scattering theory. The description of equilibrium systems is given in Section II with primary emphasis on the construction of ensembles. A basis for the discussion of non-equilibrium systems is given in Section III and the construction of ensembles are treated in some detail. In Section IV, a derivation of a transport equation for non-uniform systems (the Maxwell-Boltzmann equation) is outlined. Section V is devoted to an alternative approach to transport theory for gases and liquids (the correlation function method).

Thermodynamic study of the thorium phosphide with a mass spectrometer, J. Efimenko and K. A. Gingerich, *Proc. Symp. Thermodynamics of Nuclear Materials, Vienna, May 21–25, 1963, pp. 477–486 (International Atomic Energy Agency, Vienna, Austria, Sept. 1962).*
For the thorium-phosphorous system the ion intensity variation with temperature over the range 1100°–2250°K and composition range $ThP_{1.3}$–$ThP_{0.8}$ has been obtained for the phosphorus vapor species. No molecules containing both thorium and phosphorus have been observed in the vapor below 2245°K. With the aid of a silver calibration the ion intensities have been related to the partial pressures of the effusing phosphorus vapor species, P, P_2, and P_4. From these data the "apparent" molar free energies of formation have been obtained with reference to gaseous P_2 for different compositions of the solid and the dissociation energy for P_2 has been computed. The vaporization of the thorium phosphides occurs incongruently by decomposition into gaseous phosphorus and a condensed phase of lower phosphorus content. The rate of phosphorus loss from the Th_3P_4 phase appears to be diffusion controlled. There is a marked increase of thermodynamic stability with decreasing phosphorus content within the homogeneity range of the lower phosphide. The phase boundaries of the lower phosphide have been estimated to correspond to $ThP_{0.7}$ and $ThP_{0.9}$. The thermodynamic stability of the thorium phosphides is compared with that of selected lower phosphides of transition metals.

Low energy levels of neutral cerium (Ce I), W. C. Martin, *J. Opt. Soc. Am.* **53,** *No. 9, 1047–1050 (Sept. 1963).*
The first results of a continuing analysis of the Ce I spectrum show the ground level to be $4f5d6s^2$ $^1G_4^0$, with g_J=0.945. Of twelve other low odd levels for which the energies, J- and g-values are given, six have been assigned to $4f5d6s^2$ and three to $4f5d^26s$.

A study of stress relaxation with finite strain, B. Bernstein, E. A. Kearsley, and L. J. Zapas, *Trans. Soc. Rheology* **VII,** *391–410 (1963).*
Two simple types of constitutive equations appropriate to materials exhibiting elasticity are presented, one of a basic solid nature and one of a basic fluid nature. The predictions of the equations for a stress relaxation experiment are worked out and compared to the data from some experiments on various elastomers. The fluid theory is shown to be most appropriate in a certain sense.

Measurement of weak magnetic fields by optical pumping methods, P. L. Bender, *Bull. Ampere* **9e,** *Pt. II, 261–628 (1960).*
Three new types of magnetometer, the dc alkali vapor magnetometer, the self-oscillating alkali vapor magnetometer, and the helium magnetometer, all based on optical pumping, are compared. Practical limitations and performance in various environmental circumstances are considered.

Three-body bound state in He^4, J. M. Blatt, J. N. Lyness, and S. Y. Larsen, *Phys. Rev.* **131,** *No. 5, 2131–2132 (Sept. 1, 1963).*
The binding energy of three He^4 atoms, subject to pair forces, is investigated numerically for a number of proposed intermolecular potentials and for a series of square wells. For some potentials a 3-body bound state is found, for others not. However, a direct correlation is found between 2-body and 3-body binding. The need for more accurate experimental data is discussed.

Momentum autocorrelation functions and energy transport in harmonic crystals containing isotopic defects, R. J. Rubin, *Phys. Rev.* **131,** *964 (1963).*
In this paper we review and extend the investigation of the effect of isotopic impurities on two statistical dynamical properties of harmonic crystals: the decay of the momentum autocorrelation function and the transport of energy. A spectral representation is obtained for the momentum autocorrelation functions. The spectral density is directly related to the normal mode frequency distribution of the crystal; the recent investigations of the classical momentum autocorrelation function in a perfect one-dimensional crystal and a one-defect crystal are discussed as special cases of this general Wiener-Khinchin formula. The corresponding quantum mechanical autocorrelation function is also treated. A formal relation involving the average momentum autocorrelation function of an isotopically disordered crystal and the frequency spectrum of the crystal is derived. The energy transport property is studied in terms of the time-dependent dispersion of the momentum of a lattice particle when the crystal is characterized initially by a spatially nonuniform temperature. The local temperature, which is related to the momentum dispersion, is studied analytically in the case of the perfect one-dimensional crystal and the one-defect one-dimensional crystal. The local temperature is studied numerically with the aid of an IBM 7090 for several isotopically disordered one-dimensional crystals.

Galvanostalametry, a new technique based on the negative pressure of liquids, for investigating electrochemical phenomena at an electrode, J. Sligh and A. Brenner, *J. Electrochem. Soc.* **110,** *No. 11, 1136–1142 (Nov. 1963).*
A procedure based on the negative pressure of water has been used as a sensitive indicator for the study of electrochemical phenomena. The apparatus consisted of a vertical glass tube, closed at the upper end, which was evacuated and filled with an electrolyte. The latter remained suspended in the column in a metastable state of tension. The column of electrolyte was dropped by producing a minute amount of electrolysis between an indicator electrode sealed in the top of the column and a companion electrode which could also be at the top or in the reservoir at the bottom of the column. The time or current required to drop the column was used for making the following experiments and/or observations: (*A*) The decomposition potential of water was determined by observing the lowest applied voltage required to drop the column. (*B*) The time required to drop the column (on passage of a constant current) was proportional to the concentration of iodide ion in the electrolyte. (*C*) The current required to drop the column was proportional to the area of the indicator electrode, regardless of the irregularity of its shape. (*D*) The formation of the gas required to drop the column occurred in less than 15 μsec after closing the circuit.

Electrical resistance-strain characteristics of thin evaporated metal films, R. L. Parker and A. Krinsky, *J. Appl. Phys.* **34,** *No. 9, 2700–2708 (Sept. 1963).*
The electrical resistance-strain coefficients of thin evaporated films of Aluminum, Gold, Cobalt, Nickel, Palladium, Platinum, Antimony, and Tellurium have been measured. The coefficients (strain-sensitivity coefficient or "gauge-factor" γ) depend on the specific resistance R_s of the films. For relatively thick films (small R_s), γ tends to approach the bulk value γ_b; for relatively thin films (large R_s), γ, may be many times greater than γ_b; for films of intermediate thickness γ has a minimum value. The resistance change was found to be proportional to strain for all the above films except those of Ni and Sb. Some possible mechanisms

for the observed behavior are discussed; it was found that free-path effects are predominant in films of intermediate thickness, and that the tunnelling conduction mechanism plays an important role in producing the high strain-sensitivity of very thin (high R_s) films of separated particles.

Other NBS Publications

J. Res. NBS 68B (Math. and Math. Phys.), No. 1 (Jan.–Mar. 1964) 75 cents.

A note on a generalized elliptic integral. G. H. Weiss.
An asymptotic expansion for the multivariate normal distribution and Mills' ratio. H. Ruben.
Calculation of certain multiple generating functions. G. H. Weiss.
Some infinite sums involving zeros of $J_0(x)$. L. F. Epstein.
Optimal matchings and degree-constrained subgraphs. A. J. Goldman.
Effects of a distribution on gap acceptance functions on pedestrian queues. G. H. Weiss.
Gaussian wave functions for polyatomic molecules: integral formulas. M. Krauss. (See above abstracts.)

J. Res. NBS 68C (Eng. and Instr.), No. 1 (Jan.–Mar. 1964) 75 cents.

A Fabry-Perot spectrometer for high-resolution spectroscopy and laser work. K. D. Mielenz, R. B. Stephens, and K. F. Nefflen.
Variable impedance power meter, and adjustable reflection coefficient standard. G. F. Engen.
A laser with a multihole diaphragm. T. Morokuma.
Principles of cryometric impurity determination as applied to samples of small sizes. C. P. Saylor and G. S. Ross.
Reference tables for thermocouples of iridium-rhodium alloys versus iridium. G. F. Blackburn and F. R. Caldwell.

Radio Sci. J. Res. NBS/USNC–URSI, Vol. 68D, No. 3 (Mar. 1964). $1.00.

An interpretation of rapid changes in the phase of horizontally polarized VLF waves recorded at night over a short path in the southwestern United States. E. E. Gossard and M. R. Paulson.
Precise phase and amplitude measurements on VLF signals propagated through the Arctic zone. F. H. Reder, C. J. Abom, and G. M. R. Winkler.
On the long term phase stability of the 19.8 kc/s signal transmitted from Hawaii, and received at Boulder, Colorado. A. H. Brady.
Oblique propagation of groundwaves across a coastline. Part III. J. R. Wait.
Impedance of a monopole antenna with a radial-wire ground system on an imperfectly conducting half space, Part III. S. W. Maley and R. J. King.
A simplified theory of diffraction at an interface separating two dielectrics. J. Kane and S. N. Karp. (See above abstract.)
Variational solution for the admittance of long cylindrical antenna. R. A. Hurd.
Admittance of annular slot antennas radiating into a plasma layer. J. Galejs.
Propagation of plasma waves in a "spoke-wheel" magnetic field. R. L. Liboff. (See above abstract.)
An experimental investigation of signal strength in the area around a transmitter's antipode. R. M. Pipp and J. B. Webster.
Relationship between simultaneous geomagnetic and ionospheric oscillations. H. Rishbeth and O. K. Garriott.

Bibliography on ignition and spark-ignition systems, G. F. Blackburn, NBS Misc. Publ. 251 (Nov. 22, 1963), 15 cents. (Supersedes NBS Circular 580.)
Recommended unit prefixes; Defined values and conversion factors; General physical constants, NBS Misc. Publ. 253 (Oct. 1963), 5 cents (wallet-size plastic card).
Lunar occultations of two discrete radio sources in 1963–1964, J. A. Eddy, NBS Tech. Note 184 (Oct. 11, 1963), 20 cents.
Expanded vinyl fabrics for apparel use, CS 258–63 (Sept. 19, 1963), 10 cents.
Steel spirals for reinforced concrete columns, SPR 53–63, (Oct. 1, 1963), 10 cents.
Determination of differential X-ray photon flux and total beam energy, H. W. Koch and J. S. Pruit, Ed. L. C. Yugan and C. Wu, Nuclear Physics, **5,** ch. 2.8.2, 508–553 (1963).
Metallurgical microanalysis with the electron probe, J. R. Cuthill, L. L. Wyman, and H. Yakowitz, J. Metals AIME **15,** No. 10, 763–768 (Oct. 1963).
Large longitudinal retarded elastic deformation of rubberlike network polymers. II. Application of a general formulation of nonlinear response, H. Leaderman, F. L. McCrackin, and O. Nakada, Trans. Soc. Rheology **VII,** 111–123 (1963).
The error rate in a multiple-frequency shift system and the output signal/noise ratio in a frequency modulation and a pulse-code-modulation/frequency-shift system, H. Akima, Intern. Conf. Satellite Communication, London, Nov. 22–28, 1963, pp. 305–309 (Programme and Conference Digest, London, England, 1963.)
Synoptic variations and vertical profiles of large-scale ionospheric irregularities, R. G. Merrill, R. S. Lawrence, and N. J. Roper, J. Geophys. Res. **68,** No. 19, 5453–5459 (Oct. 1, 1963).
Excitation of the red and green coronal lines, C. Pecker and R. N. Thomas, Ann. Astrophys. **25,** No. 2, 100–108 (1962).
Normal congruence subgroups of the $t \times t$ modular group, M. Newman, Bull. Am. Math. Soc. Res. Announcement **69,** No. 5, 719–720 (Sept. 1963).
Radiation impedance of a source near reflectors, R. V. Waterhouse, J. Acoust Soc. Am. **35,** No. 8, 1144–1151 (Aug. 1963).
The energy environment in which we live, D. M. Gates, Am. Scientist **51,** No. 3, 327–348 (Sept. 1963).
Evidence for field-aligned ionization irregularities between 400 to 100 km above the earth's surface, T. E. VanZandt, W. Calvert, R. W. Knecht and G. B. Goe, Third Intern. Space Sci. Symp. Proc., Wash., D.C., May 2–8, 1962, pp. 271–273 (John Wiley & Sons Inc., New York, N.Y., 1962).
Studies in the geomagnetic micropulsation frequency range. W. H. Campbell, IEEE Intern. Conv. Record **11,** Pt. 9, 25–28 (Mar. 25–28, 1963).
Determination of the electronic energy levels of molecules by low energy electron impact spectroscopy, J. A. Simpson and S. R. Mielczarek, J. Chem. Phys. Letter **39,** 1606 (1963).
Experimental evaluation of a thallium beam frequency standard, R. E. Beehler and D. J. Glaze, Proc. 17th Annual Frequency Control Symp. (1963).
Gas-phase radiolysis of *n*-butane, R. P. Borkowski and P. J. Ausloos, J. Chem. Phys. **39,** No. 3, 818–824 (Aug. 1, 1963).
Temperature control of the structure and variations of the quiet ionosphere, J. W. Wright, Proc. Intern. Conf. Ionosphere, July 1962, pp. 19–25 (Institute of Physics and the Physical Society, London, England, 1963).
Some factors affecting the creep behavior of an age-hardenable alloy, W. D. Jenkins and W. A. Willard, Trans. Quart. ASM **56,** No. 3, 427–441 (Sept. 1963).
A note on contingency tables involving zero frequencies and the 2I test, H. H. Ku, Technometrics **5,** No. 3, 398–400 (Aug. 1963).
Wilmer Souder, pioneer in dental research, G. C. Paffenbarger, N. Y. J. Dentistry **33,** No. 5, 191–192 (May 1963).
Equatorial electron density profiles to 5000 KM, Using the incoherent scatter technique, K. L. Bowls, Third Intern Space Sci. Symp. Proc. Washington, D.C., May 2–8, 1962, pp. 253–264 (John Wiley & Sons, Inc., New York, N.Y., 1963).
Physical measurements and experiment design, W. J. Youden, Scuola Azione No. 10, 181–200 (Scuola de Studi Sugli Idrocarburi, San Donato Milanese, Italy, 1961–1962).
Strain release in complete dentures, J. B. Woelfel, G. C. Paffenbarger, and W. T. Sweeney, J. Am. Dental Assoc. **67,** No. 2, 321 (Aug. 1963).
Questions of general background and methodology relating to aerodynamic phenomena in stellar atmosphere, J. C. Pecker and R. N. Thomas, Il Nuovo Cimento Suppl. **22,** No. X, Pt. I, 1–43 (1961).
Observation on reference electrodes for fused-salt systems, M. A. Reid and J. A. Lloyd, Rev. Sci. Instr. **34,** No. 8, 940–941 (Aug. 1963).

Primary processes in the photolysis of ethyl nitrate, R. E. Rebbert, J. Phys. Chem. **67,** No. 9, 1923–1925 (Sept. 1963).

High-field liquid H_2-cooled aluminum-wound magnet, J. R. Purcell and E. G. Payne, Rev. Sci Instr. **34,** 893–897 (Aug. 1963).

Complicating factors in the gas phase photolysis of azomethane, R. E. Rebbert and P. J. Ausloos, J. Phys. Chem. **67,** No. 9, 1925–1928 (Sept. 1963).

Use of transistors in Van de Graaff source leak controls, A. C. B. Richardson and L. Costrell, Nuclear Instr. Methods Letter to Editor **24,** No. 1, 129–130 (July 1963).

The formulation of F.D.I. specifications, G. C. Paffenbarger, Intern. Dental J. **13,** No. 1, 133–134 (Mar. 1963).

The *F*-region seasonal anomaly, J. W. Wright, J. Geophys. Res. **68,** No. 14, 4379–4381 (July 15, 1963).

Effect of hydrostatic pressures on the crystallization kinetics of natural rubber, G. M. Martin and L. Mandelkern, J. Appl. Phys. **34,** No. 8, 2312–2317 (Aug. 1963).

The redefinition of the second and the velocity of light, G. E. Hudson and W. Atkinson, Phys. Today **16,** No. 5, 30–32, 34, 36 (May 1963).

The shifts and widths of some stark broadened oxygen lines in an arc plasma, W. L. Wiese and P. W. Murphy, Phys. Rev. **131,** 2108–2115 (Sept. 1, 1963).

The ionization constants of *o*-nitrophenol and 4-nitro-*m*-cresol from 5 to 60°, R. A. Robinson and A. Peiperl, J. Phys. Chem. **67,** 1723 (1963).

Recent developments in neutron source standardization, R. S. Caswell, R. H. Noyce, S. B. Garfinkel, and E. R. Mosburg, Jr., (Proc. Symp. Neutron Detection, Dosimetry and Standardization, International Atomic Energy Agency, Atomic Energy Research Establishment, Harwell England, Dec. 10–14, 1962), Book, Neutron Dosimetry **II**, 547–555 (International Atomic Energy Agency, Vienna, 1963).

The following papers were published in Proc. Mountain States Navy Research and Development Clinic, Raton, N. M., Sept. 28–29, 1961, (Raton, Communications and Electronics Foundation, 1963).

Recent progress in cryogenic engineering, R. B. Scott, pp. D1–D4.

Remarks presented at panel discussion on modulation, J. L. Auterman, pp. A131–A132.

Predicting the performance of tropospheric communication links singly and in tandem, A. P. Barsis, K. A. Norton, and P. L. Rice, pp. A71–A104.

Required signal-to-noise ratios, carrier power, and bandwidth to achieve a given performance for multichannel radio communication systems, E. R. Florman and J. J. Tary, pp. A135–A140.

VLF propagation, W. L. Taylor and A. G. Jean, pp. A45–A66.

Millimeter wave research at the National Bureau of Standards, R. W. Zimmerer, pp. A109–A112.

Some low temperature properties of materials, R. H. Kropschot, pp. D5–D6.

Aspects of radio meteorology, J. D. Horn, pp. C51–C56.

Problems and prospects in electrical properties of materials, J. L. Dalke, pp. D7–D14.

Noise in VLF to HF bands and prediction of communication reliability, W. Q. Crichlow, pp. A67–A70.

Signal-to-noise characteristics of some typical systems and their comparisons, H. Akima, pp. A125–A130.

Cyclotron resonances in slightly ionized gases, F. Fehsenfeld, J. Chem. Phys. **39,** No. 7, 1653–1661 (Oct. 1, 1963).

Some physical properties of organic denture base materials, J. B. Woelfel, G. C. Paffenbarger, and W. T. Sweeney, J. Am. Dental Assoc. **67,** 489–504 (Oct. 1963).

Dependence of power output of a gas laser on the length and rate of excitation of the discharge, J. A. White, Appl. Phys. Letters **3,** No. 7, 107–109 (Oct. 1, 1963).

Shifts and widths of some stark-broadened oxygen lines in an arc plasma, W. L. Wiese and P. W. Murphy, Phys. Rev. **131,** No. 5, 2108–2115 (Sept. 1963).

The adsorption of methane and nitrogen on silica gel, synthetic zeolite and charcoal, A. J. Kidnay and J. M. Hiza, J Phys. Chem. **67,** 1725–1727 (1963).

Studying the lunar tidal variations in the *D* region of the ionosphere by means of very-low-frequency phase observations, A. H. Brady and D. D. Crombie, J. Geophys. Res. **68,** No. 19, 5437–5442 (Oct. 1, 1963).

Natural electromagnetic field fluctuations in the 3.0 to 0.02 cps range, W. H. Campbell, Proc. IEEE **51,** 1337–1342 (Oct. 1963).

Current development in an electronically scanned antenna, H. V. Cottony, Proc. Symp. Electromagnetic Theory and Antennas, Copenhagen, June 25–30, 1962, pp. 1289–1294 (Pergamon Press, Oxford, London, 1963).

Airglow research, F. E. Roach, Trans. Am. Geophys. Union **44,** No. 2, 431–432 (June 1963).

Velocity-depth relationship in microelectrophoresis cell for asphaltenes in nitromethane, J. R. Wright and R. R. Minesinger, J. Colloid Sci. **18,** 802–804 (Oct. 1963).

Some results of a new method for obtaining ionospheric N(h) profiles and their bearing on the structure of the lower *F* region, A. K. Paul and J. W. Wright, J. Geophys. Res. **68,** No. 19, 5413–5420 (Oct. 1, 1963).

A 100 megapulse per second binary counter with impedance steering, S. B. Geller and P. A. Mantek, IEEE Trans. Electronic Computers **EC–12,** No. 5, 568 (Oct. 1963).

Mathematics and experimental science, W. J. Youden, Sci. Teacher **30,** No. 5, 23–26 (Sept. 1963).

Line shapes, saturation behavior, and temperature studies in the nuclear resonance of nickel, R. L. Streever and L. H. Bennett, Phys. Rev. **131,** No. 5, 2000–2009 (Sept. 1, 1963).

Impedance of Leclanche cells and batteries, R. J. Brodd and H. J. DeWane, J. Electrochem. Soc. **110,** No. 11, 1091–1097 (Nov. 1963).

Hyperfine structure and isotope shifts in the 2537–A line of mercury by a new interferometric method, W. G. Schweitzer, Jr., J. Opt. Soc. Am. **53,** No. 9, 1055–1072 (Sept. 1963).

Absolute scale of oscillator strenghts, C. W. Allen and C. H. Corliss, Monthly Notices Roy. Astron. Soc. **126,** No. 1, 37–40 (1963).

Stable 6300 A auroral arcs in mid-latitudes, F. E. Roach and J. R. Roach, Planet. Space Sci. **11,** 523–545 (1963).

Relation of partial (110) pole figures to thickness and microstructure of electrodeposited copper, F. Ogburn and C. J. Newton, J. Electrochem. Soc. **110,** No. 11, 1148–1150 (Nov. 1963).

Regulation of ionization gauge emission current to better than 0.05%, K. W. Yee and R. J. Carpenter, Rev. Sci. Instr. **34,** No. 10, 1101–1103 (Oct. 1963).

Errors in "drop" calorimetry due to sample container transitions, D. C. Ginnings, J. Phys. Chem. **67,** 1917–1918 (1963).

A theory of incoherent scattering of radio waves by a plasma. III Scattering in a partially ionized gas, J. P. Dougherty and D. T. Farley, Jr., J. Geophys. Res. **68,** 5473–5486 (Oct. 1, 1963).

Energy dependence of proportional-counter fast-neutron dosimeters, R. S. Caswell, W. B. Beverly and V. Speigel, Jr., (Proc. Symp. Neutron Detection, Dosimetry and Standardization, Atomic Energy, Atomic Energy Research Establishment, Harwell, England, Dec. 10–14, 1962), Book, Neutron Dosimetry **II,** 227–237 (July 1963).

Projection X-ray microscopy of roofing materials, S. B. Newman and S. H. Greenfeld, Mater. Res. Std. **3,** No. 11, 893–898 (Nov. 1963).

Normal congruence subgroups of the $t \times t$ modular group, M. Newman, Bull. Am. Math. Soc. **69,** No. 5, 719–720 (Sept. 1963).

Growth and evaporation kinetics and surface diffusion of K and Hg crystal whiskers, R. L. Parker, R. L. Anderson, and S. C. Hardy, Applied Phys. Letters **3,** No. 6, 93–95 (Sept. 15, 1963).

Very-low-frequency phase observations of solar flare ionization in the *D* region of the ionosphere, C. J. Chilton, F. K. Steele, and R. B. Norton, J. Geophys. Res. **68,** No. 19, 5421–5435 (Oct. 1, 1963).

Generalized variational principles for electromagnetic vibrations; application to the theory of waveguide junctions, D. M. Kerns, Proc. Symp. Electromagnetic Theory and Antennas, Copenhagen, June 25–30, 1962, pp. 253–259 (Pergamon Press, Oxford, London, 1963).

The following papers were published in Advances in Cryogenic Engineering, Volume 8 (1963).

Some idealized solutions for choking, two-phase flow of hydrogen, nitrogen, and oxygen, R. V. Smith, Paper J–10, pp. 563–573.

P-ρ-T values for neon from 27° to 300° K for pressures to 200 atm using corresponding states theory, R. D. McCarty, R. B. Stewart, and K. D. Timmerhaus, Paper C–3, pp. 135–145.

An apparatus to determine the solid-vapor equilibria of binary cryogenic systems, M. J. Hiza and R. N. Herring, Paper C–5, pp. 158–161.

A comparison of the low-temperature adsorption of nitrogen and methane from hydrogen gas on three different adsorbents, M. J. Hiza and A. J. Kidnay, Paper C–7, pp. 174–182.

A refrigeration system incorporating a low-capacity, high-speed, gas-bearing-supported expansion turbine, D. B. Mann, H. Sixsmith, W. A. Wilson, and B. W. Birmingham, Paper D–5, pp. 221–227.

Experimental determination of the bulk density of boiling liquid oxygen, R. W. Arnett, D. R. Millhiser, and W. H. Probert, Paper E–4, pp. 256–262.

Thermal conductivity of solid H_2O and D_2O at low temperatures, J. W. Dean and K. D. Timmerhaus, Paper E–5, pp. 263–267.

Linear thermal expansion of elastomers in the range 300° to 76° K, R. F. Robbins, Y. Ohori, and D. H. Weitzel, Paper E–8, pp. 287–299 (1963).

Solid formation in flowing cryogenic fluids, D. B. Chelton, B. W. Birmingham, and J. W. Dean, Paper E–11, pp. 311–314.

Temperature measurements in cryogenic engineering, R. J. Corruccini, Paper F–1, pp. 315–333.

Pressure measurements in cryogenic systems, P. Smelser, Paper F–7, pp. 378–386.

Perlite for cryogenic insulation, R. H. Kropschot and R. W. Burgess, Paper G–7, pp. 425–436.

Force and seal evaluation of elastomeric O-rings, P. R. Ludtke and D. H. Weitzel, Paper H–6, pp. 467–477.

Experimental investigation of liquid-hydrogen cooling by helium gas injection, A. F. Schmidt, Paper J–5, pp. 521–528.

Liquid requirements for the cool-down of cryogenic equipment, R. B. Jacobs, Paper J–6, pp. 529–535.

Cool-down and warm-up of large powder-insulated dewars, F. Kreith, J. W. Dean, and L. Brooks, Paper J–7, pp. 536–543.

**Publications for which a price is indicated are available by purchase from the Superintendent of Documents, Government Printing Office, Washington, D.C. 20402 (foreign postage, one-fourth additional). Reprints from outside journals and the NBS Journal of Research may often be obtained directly from the authors.*

UNIVERSITY MICROFILMS
313 NORTH FIRST STREET
ANN ARBOR, MICHIGAN
SJR-A-OCT

GOVERNMENT PRINTING OFFICE
DIVISION OF PUBLIC DOCUMENTS
WASHINGTON, D.C. 20402
OFFICIAL BUSINESS

PENALTY FOR PRIVATE USE TO AVOID
PAYMENT OF POSTAGE, $300
(GPO)

JOURNAL OF RESEARCH of the National Bureau of Standards
A. Physics and Chemistry

Vol. 68A, No. 2 March–April 1964

Contents

	Page
Tritium-labeled compounds X. Isotope effects in the oxidation of aldoses-*1-t* with bromine. Horace S. Isbell and Lorna T. Sniegoski.	145
Thermal degradation of fractionated high and low molecular weight polyisobutylene. D. McIntyre, J. H. O'Mara, and S. Straus.	153
Ionization constants of the six dichloroanilines and the six dichlorophenols in aqueous solution at 25 °C. R. A. Robinson.	159
Stereoregularity in ionic polymerization of acenaphthylene. V. M. Story and G. Canty.	165
Dielectric behavior of the film formed on mica cleaved in moist air. S. Ruthberg and L. Frenkel.	173
On the measurement of dielectric losses and surface conductivity of dielectrics in parallel plane test capacitors. Lothar Frenkel.	185
Polymorphism of bismuth sesquioxide. I. Pure Bi_2O_3. Ernest M. Levin and Robert S. Roth.	189
Polymorphism of bismuth sesquioxide. II. Effect of oxide additions on the polymorphism of Bi_2O_3. Ernest M. Levin and Robert S. Roth.	197
Second spectrum of tungsten (W II). Donald D. Laun.	207
Publications of the National Bureau of Standards.	253

Library of Congress Catalog Card Number: 62–37059

For sale by the Superintendent of Documents, U.S. Government Printing Office, Washington, D.C., 20402. Price 70 cents (single copy)
Subscription price: $4 a year; 75 cents additional for foreign mailing.
UNITED STATES GOVERNMENT PRINTING OFFICE, WASHINGTON : 1964